Multi-isotopic tracing of historical mining pollution in European environmental archives and their impact on the population

Carlos Rodrigo Heredia Aguilar

THÈSE

Pour obtenir le grade de

DOCTEUR DE L'UNIVERSITÉ GRENOBLE ALPES

École doctorale : STEP - Sciences de la Terre de l'Environnement et des Planètes
Spécialité : Sciences de la Terre et de l'Environnement
Unité de recherche : Institut des Sciences de la Terre

Traçage multi-isotopique des pollutions minières historiques dans des archives environnementales Européennes et de leur impact sur les population

Multi-isotopic tracing of historical mining pollution in European environmental archives and their impact on the population

Présentée par :

Carlos HEREDIA

Direction de thèse :

Alexandra GOURLAN MAITRE DE CONFERENCES, Université Grenoble Alpes	Directrice de thèse
Stephane GUEDRON DIRECTEUR DE RECHERCHE, IRD	Co-directeur de thèse
Laurence AUDIN DIRECTRICE DE RECHERCHE, IRD	Co-directrice de thèse

Rapporteurs :

Olalla LOPEZ-COSTAS
SCIENTIST, Universidad de Santiago de Compostela
Nathalie VIGIER
DIRECTRICE DE RECHERCHE, CNRS

Thèse soutenue publiquement le **13 septembre 2024**, devant le jury composé de :

Alexandra GOURLAN, MAITRESSE DE CONFERENCES, Université Grenoble Alpes	Directrice de thèse
Stéphane GUEDRON, DIRECTEUR DE RECHERCHE, IRD	Co-directeur de thèse
Laurence AUDIN, DIRECTRICE DE RECHERCHE, IRD	Co-directrice de thèse
Olalla LOPEZ-COSTAS, SCIENTIST, Universidad de Santiago de Compostela	Rapporteure
Nathalie VIGIER, DIRECTRICE DE RECHERCHE, CNRS	Rapporteure
Pascale HUYGHE, PROFESSEURE DES UNIVERSITES, UGA	Président
Sandrine BARON, CHARGEE DE RECHERCHE, CNRS	Examinatrice
Sophia HANSSON, CHARGEE DE RECHERCHE, CNRS	Examinatrice

Invités :

Daniel Veres
DIRECTEUR DE RECHERCHE, Romanian Academy

Multi-isotopic (Pb and Cu) tracing of historical mining pollution in European environmental archives and their impact on the populations

Carlos Heredia

Supervisors: Alexandra Gourlan

Co-supervisors: Stéphane Guédron

Laurence Audin

“When one reads of lead, it is rarely long before the Roman world is mentioned. Their two stories are closely intertwined in a tale of necessity, progress, and the enticing vices of civilization that has left the world a deadly legacy.”

- Publius Cornelius Tacitus

Some important lessons that I have learned this past year and for which I am grateful…

« Γνώθι σεαυτόν »

« Το παθός μαθός »

« Ὁποιος δεν έχει νου, έχει πόδια »

Acknowledgments

This PhD has been quite a journey!

Despite all the side effects, the coffee addiction, the muscle cramps, the laboratory accidents, the mental breakdowns, and a broken bone, I sincerely enjoyed every part of this process. Therefore, I would like to thank everyone that made it possible.

First, I would like to thank **Stéphane**. You have been a constant source of support, advice, and inspiration since we met in Bolivia. You have always been available and willing to help and guide me in my professional and academic journey. Your energy and enthusiasm for knowledge are contagious and materialize in the outstanding research you do. Thank you for your tireless support, genuine care, and infinite patience, and for being such a kind supervisor and human being.

I would like to give a special thanks to **Alexandra**. Thank you for giving me the opportunity to work with you on this exciting intersection of geochemistry, archaeology, and health. Thank you for always being available, no matter the day or the hour, and for reacting quickly and patiently to my requests and mistakes. I admire the efficiency with which you solve any problem and the way you react to unforeseen events. Thank you for all the teachings in and out of the lab.

Thanks to the jury members (**Olalla Lopez Costas, Nathalie Vigier, Sandrine Baron, and Sophia Hansson**) for reading this manuscript and making this PhD possible. Thanks to the members of my PhD committee (**Francis Albarede, Hugo Delile, and Daniel Veres**) for their valuable advice, which significantly improved this work.

Thanks to **Sylvain**, le “Chef” of the lab. You have saved my samples and analyses so many times that I would not have good-quality results if not for you. Thank you for the

good company, the good humor, the good food, the patience, and, above all, the willingness to teach. Thank you for making the clean room a safe and comfortable place to work, even though it was not your responsibility. You are an amazing "Chef"!

Thanks to **Sarah**, who taught me with patience and good humor how to manage myself in a clean room and handle this interesting element called lead and its tedious purifications. Thanks to **Sabine** for the enthusiasm, the fast analyses, the accuracy and quality of the results, and for always being kind to me.

I would like to thank all my colleagues on the Geochemistry team at ISTerre for creating such a pleasant work environment. **Aya**, you are the best officemate anyone could ever wish for. Thank you for your infinite kindness, for putting up with my disorganization, my love of spiders and their webs, and my general temper. You have supported, fed, encouraged, cheered up, and cared for me as only family can. And for that, I am infinitely grateful. **Ahmed**, you work harder than anyone I know. Thanks for being a wise officemate and an inspiration for working hard.

Laura, my dear *mattone*, thanks for always being there! You bring kindness, joy, laughs, and funny anecdotes to my life in and out of the lab. With you, I share this passion for cinema, art, and old stuff (a.k.a. cultural heritage). Thank you for your support, for being a refuge in difficult moments, and for showing me the true meaning of "overexposure to awesomeness".

Μαριεύη, thank you for giving me the privilege of experiencing the Socratic method and all its unforeseen outputs, as well as teaching me the meaning of "εὐδαιμονία." Thanks for fostering big and small conversations with me and for making me discover a new way of drinking coffee. Ευχαριστώ.

Carlos, thank you for being a friend I can always count on. Thanks for all the lessons, in science but also in life. Thanks for putting up with my character and for being the voice of reason on different occasions. I am grateful for the endless hours of play, fun, alcoholism, and, above all, very good food that we shared together. Thank you for adopting me as your brother and being my family in Grenoble. And, of course, thank you for introducing me to the rich and vast world of fountain pens and their amazing inks.

Juliette, thank you for bearing up with me through the tedious process of being myself during stressful moments. Thank you also for being the kind soul who improved the quality and the logic of my messy French-redacted emails. **Jafar**, my army man who is always willing to help. Thank you for taking care of me after my accident and implanting the seed of madness for climbing that I bear with me now. **Luca**, thanks for bringing your humor to the coffee and lunch breaks and for sharing your vast knowledge of Italy. **Robin**, you are the target of so many of my jokes (all with good intentions). Thanks for being the pal with whom I do our 5 pm reminder (that we are, in fact, not a complete failure). **Hester**, thank you for the company and the laughs in the clean room and for making the tedious tasks (like purification and cleaning) more bearable. **Rémy**, thank you for the crazy activities, the coffee machine, poking Aya, and above all for Milky.

Finally, a big thanks to my family. **Tatis, Mama, Geral, Pachini, Tia Cu and Pepe**. Without you and your neverending support in all aspects of life, this PhD or any of my professional dreams would not be possible. I have not enough words to express my gratitude to you.

Summary

Metal pollution is a major health problem whose origins predate industrialization. Environmental and physiological levels of lead (Pb) exposure in the population are a global public health concern because exposure, even at low levels, can have complex and serious effects on health, including developmental delays, cancers, metabolic disorders, and even death. Lead (Pb) had considerable industrial importance in the Roman world and was used for the development of urban centers, particularly in the production of lead pipes (i.e., fistulae) for urban freshwater supply. Other applications included the manufacture of ordinary objects like household and cooking utensils and their use as an ingredient in food, cosmetics, and medicine. Once processed and transformed into ingots, Pb was shipped to several metallurgical centers in the Roman world, such as the city of Vienna (Vienne, France), for the manufacture of Pb artifacts.

First, we studied the provenance of the lead used for the production of Pb artifacts at the Roman capital of Vienna. We analyzed the Pb isotope composition of twenty-two Roman artifacts as well as twenty-nine galena ores collected from 9 local mining areas and compared them to end-members (ores) derived from a new database using a newly developed algorithm that takes into account the three-dimensional space of Pb isotope compositions. Our results suggest that most of the lead used by the manufacturers at Vienna was of distant origin, with the most probable source attributed to the mines in the Rhenish massif, with local and regional mines appearing to be secondary in the composition of Pb production.

Second, we studied the historical environmental exposure and health degradation of Vienna's human population related to its Pb manufacturing industry. We innovatively combined the analysis of both the Pb (pollution) and Cu (health status) isotope compositions and multi-elemental concentrations of ancient human bones. Our results

show negligible diagenetic perturbation on the bones and higher Pb and Hg concentrations in the bones of Romans compared to post-Roman individuals, in agreement with historical chronology. The lack of correlations with sex and age suggests a widespread Pb contamination, likely linked to the use of lead artifacts (especially pipes) and high background atmospheric Hg levels. We report for the first time the use of Cu isotope ratios to explore the potential physiological consequences of Pb exposure in ancient skeletal remains, and show evidence of health degradation related to chronic lead exposure.

Diagenesis is a major issue when reconstructing past human exposure from the osteoarcheological record. Thus, we studied the reliability of archaeological human remains as archives of past environmental conditions in a highly contaminated medieval graveyard. We analyzed the multi-elemental composition of ancient human bones recovered from the medieval mining town of Brandes (Oisans, France) and from two towns (Huez & La Garde) that were not involved in any mining activity. Our results show elevated concentrations of Pb, As, Sb, and Cu, suggesting environmental exposure and diagenetic incorporation. The combination of conventional and unconventional diagenetic proxies revealed complex diagenetic alterations that are element-specific and independent of the type of bone.

This study supports the use of archaeological bones as environmental archives to reconstruct the metallic exposure of ancient human populations when metal pollution and the environmental background are low. Diagenesis must be systematically evaluated with multiproxy approaches before any past reconstruction is attempted.

Résumé

La pollution par les métaux est un problème de santé majeur dont les origines sont antérieures à l'industrialisation. L'exposition au plomb (Pb) des populations constitue un problème mondial de santé publique, car l'exposition, même à de faibles niveaux, peut avoir des effets complexes et graves sur la santé, notamment des retards de développement, des cancers, des troubles métaboliques et même la mort.

Le plomb (Pb) avait une importance industrielle considérable dans le monde romain et était utilisé pour le développement des centres urbains, en particulier dans la production de tuyaux en plomb (fistules) pour l'approvisionnement en eau douce des villes. D'autres applications comprenaient la fabrication d'objets ordinaires tels que des ustensiles ménagers et de cuisine et leur utilisation comme ingrédient dans l'alimentation, les cosmétiques et la médecine. Une fois traités et transformés en lingots, le Pb était expédié vers plusieurs centres métallurgiques du monde romain, comme la ville de Vienne (France), pour la fabrication d'objets en Pb.

Afin de déterminer la provenance du plomb utilisé pour la production d'artefacts à Vienne, les compositions isotopiques en Pb de vingt-deux artefacts romains ainsi que de vingt-neuf minerais de galène collectés dans neuf zones minières locales ont été analysées puis comparées aux valeurs des minerais d'une nouvelle base de données à l'aide d'un algorithme nouvellement développé qui prend en compte l'espace tridimensionnel des compositions isotopiques en Pb. Nos résultats suggèrent que la plupart du plomb utilisé par les fabricants de Vienne provenait de sources éloignées, les mines du massif rhénan étant les plus probables. Les mines locales et régionales semblent avoir joué un rôle secondaire dans la composition de la production de Pb.

Nous avons ensuite étudié l'exposition environnementale historique liée à l'industrie manufacturière du plomb et son impact sur la santé des habitants viennois. Pour cela, nous avons combiné de manière innovante l'analyse de la composition isotopique du Pb (pollution) et du Cu (état de santé) et des concentrations multiélémentaires d'anciens ossements humains. Nos résultats montrent des perturbations diagénétiques négligeables sur les os et des concentrations de Pb et de Hg plus élevées dans les os des Romains que dans ceux des post-romains, en accord avec la

chronologie historique. L'absence de corrélation aussi bien avec le sexe qu'avec l'âge suggère une contamination généralisée par le Pb, probablement liée à l'utilisation d'artefacts en plomb (en particulier des tuyaux) avec des niveaux élevés de Hg dans l'atmosphère. Nous présentons pour la première fois l'utilisation des rapports isotopiques de Cu pour explorer les conséquences physiologiques potentielles de l'exposition au Pb dans les restes squelettiques anciens.

La diagenèse est un problème majeur lorsqu'il s'agit de reconstituer l'exposition humaine passée à partir des archives ostéo-archéologiques. Nous avons donc étudié la fiabilité des restes humains archéologiques en tant qu'archives des conditions environnementales passées dans le cimetière d'une comunauté minière médiévale. Nous avons analysé la composition multiélémentaire d'ossements humains anciens provenant de la ville minière médiévale de Brandes (Oisans, France) et de deux villes (Huez et La Garde) qui n'étaient pas impliquées dans une activité minière. Nos résultats révèlent des concentrations élevées en Pb, As, Sb et Cu, suggérant une exposition environnementale et une incorporation diagénétique. La combinaison d'outils diagénétiques conventionnels et non conventionnels a mis en évidence des altérations diagénétiques complexes qui sont spécifiques à l'élément et indépendantes du type d'os.

Cette étude confirme que les vestiges osseux peuvent servir d'archives environnementales pour reconstituer l'exposition métallique des populations humaines anciennes lorsque la pollution métallique et le milieu ambiant sont faibles. Cependant, il est essentiel d'évaluer systématiquement la diagenèse à l'aide d'approches multi-proxy avant toute tentative de reconstitution historique.

Table of contents

Context and objectives

Metal pollution is a major health problem whose origins predate industrialization. Environmental and physiological levels of lead (Pb) exposure in the population are a global public health concern. Recently, the structural fire of Notre Dame de Paris (April 2019) has put the spotlight back on this contamination issue, as hundreds of tons of Pb contained in the roof and the spire's framework have been released into the atmosphere and deposited on the ground in particulate form, exposing and endangering the population of Paris, especially children.

This work was set up to improve the understanding of the sources and pathways of human exposure of historical populations related to mining and metallurgical pollution through the study of archaeological human remains. The addressed main questions of this study are:

- What is the source of Pb used for the manufacturing of Gallo-Roman artifacts in Vienna?
- What was the extent of Pb contamination and the route of exposure related to metallurgical activity at Vienna?
- Is it possible to detect a degraded state of health associated with mining/metallurgical pollution?
- What is the effect of diagenesis in highly contaminated archaeological settings? Are bones still reliable archives for investigating health status?

Combined with multi-elemental proxies, we developed a new methodology using a **multi-isotopic** approach to identify the sources, routes of exposure, and health impacts of lead (Pb) exposure in historical human populations involved in mining and metallurgical activities. This approach also allowed us to evaluate the reliability of archaeological

human remains in reconstructing paleoenvironmental conditions from archaeological sites in mining contexts, with different degrees of contamination and diagenetic alteration.

This PhD thesis will be declined into three research chapters presented as scientific articles that are or have been submitted to scientific journals, plus an introductory and a concluding chapter. The first chapter reviews the current knowledge regarding Pb in the first place, including its biogeochemical cycle, as well as the paths of exposure and its impact on human health. Then, a focus is made on the current knowledge regarding Cu and its metabolic role, as well as its use as a tracer of metabolic alterations. Finally, the chapter ends with a review on the current knowledge regarding bones, their potential as archives, and the effect of diagenesis.

Chapter two is the first experimental work in this thesis dissertation. It elucidates the source of the Pb supply used for the fabrication of Pb artifacts in Vienna. Chapter three extends the work performed in Vienna by studying the source and exposure pathways of Pb for the inhabitants of Vienna. Additionally, we also aimed to elucidate a potential degradation of their health status linked to the metallurgical industry of the city. In Chapter 4, we assessed the use of human remains in paleoenvironmental studies from the highly contaminated medieval graveyard of Brandes. Furthermore, we also evaluate the limits of traditional methods for evaluating diagenesis. `

To complement these three studies, three annexes are presented at the end of the manuscript. The first three annexes complement each chapter (supplementary information). Two other annexes, numbered four and five, present complementary studies that use multiple isotope systems (including Pb) for tracking anthropogenic contributions in:

i) the context of ancient mining and smelting operations in eastern Europe (Annex 4). In this study, we aimed to reconstruct the past anthropogenic pollution associated with mineral exploitation in Central-eastern Europe. This work covers the analysis of several high-resolution records in Europe, and due to its extension, it is still preliminary (in progress).

ii) the context of modern urban anthropogenic organic contamination in a high-altitude Lake ecosystem (Annex 5). Here, we present published work regarding the use of stable nitrogen and carbon isotopes ($\delta^{15}N$, $\delta^{13}C$) for the monitoring of the dissemination and amplitude of anthropogenic discharges (wastewaters) in Lake Titicaca (Bolivia).

Finally, Chapter 5 ends the manuscript by summarizing the main findings of these works, and provides perspectives and recommendations for future research.

Chapter 1: Introduction

1.1. Part A: Fundamentals of isotope geochemistry

An atom is composed of a nucleus made up of protons (positive charge) and neutrons (neutral charge), with electrons (negative charge) orbiting around it. An equal number of protons and electrons maintains the neutrality of each atom. Each atom of any chemical element is characterized by its atomic mass (i.e., the sum of protons and neutrons) and its atomic number (Z), which represents the number of protons/electrons in the atom (Sulzman, 2007). Isotopes are nuclear species of the same chemical element, meaning that they have the same number of protons but a different number of neutrons, resulting in different atomic masses between them (Sulzman, 2007; Wiederhold, 2015). Isotopes can be defined as stable or radioactive (i.e., producing decay), with atomic stability found when the number of neutrons (*N*) and the number of protons (*Z*) are quite similar [$N/Z <$ 1.5 (Faure, 1986)].

Isotopes are reported in relative values because the isotopic difference between different matrices (i.e., plant, mineral, water) is very small. Hence, the isotopic composition of an element of any material is reported relative to an international standard and is expressed in parts per thousand (i.e., ‰, referred to as per mil) following the delta notation:

$$\delta = \left(\frac{R_{sample}}{R_{standard}} - 1\right) * 1000$$

Where *R* is the ratio of heavy-to-light isotope of the sample (R_{sample}) over the one of the standard ($R_{standard}$) (Sulzman, 2007). In this notation, a positive δ value indicates the sample has more of the heavy isotope than the standard, whereas a negative δ value indicates the contrary (i.e., the sample has less of the heavy isotope) (Sulzman, 2007).

The chemical behavior between two isotopes is qualitatively similar, while their physical behavior is quantitatively different because the difference in mass between the two will

produce differences in both the reaction rates and the strength of chemical bonds, leading to an uneven distribution between different phases, known as fractionation (Sulzman, 2007; Wiederhold, 2015).

Isotopic fractionation can be divided into mass-dependent (MDF) and mass-independent (MIF). MDF follows a smooth, predictable variation that is governed by the mass difference between the isotopes, with both equilibrium and kinetic processes known to account for MDF (Albarède, 2011; Clark and Fritz, 1997; Wiederhold, 2015). MIF does not follow the mass difference rules described for MDF and is associated with quantum mechanical effects or physicochemical processes like photochemistry or nuclear field shifts (Thiemens, 2006). Almost all processes producing stable isotope fractionation in natural samples are mass-dependent, but there are a few exceptions where MIF has been observed (Thiemens, 2013; Thiemens et al., 2012; Wiederhold, 2015).

However, isotope variations for some elements can also be generated by radiogenic processes, i.e., the radioactive decay of unstable isotopes to stable ones (Wiederhold, 2015). A classic example of this is lead (Pb). Pb is present in the environment as four main isotopes: ^{204}Pb (1%), ^{206}Pb (24%), ^{207}Pb (23%), and ^{208}Pb (52%) (Komárek et al., 2008). Only ^{204}Pb has a constant abundance on Earth over time (i.e., primordial), while the rest (^{206}Pb, ^{207}Pb, ^{208}Pb) are radiogenic products of the radioactive decay of ^{238}U, ^{235}U, and ^{232}Th, respectively, known as the radioactive U-Th decay series (Wiederhold, 2015). Hence, the abundance of Pb isotopes in a sample is not only dependent on the concentrations of primordial Pb but also depends on the concentration of U, Th (i.e., parent isotopes) and the length of their decay processes (i.e., the half-lives = $t_{1/2}$) (Komárek et al., 2008). Therefore, Pb isotopes cannot be reported following the delta notation (δ) because of the influence of the radiogenic processes, and thus, the isotopic composition of Pb is expressed as ratios between the four isotopes (e.g., ^{206}Pb/^{204}Pb,

$^{206}Pb/^{207}Pb$, $^{208}Pb/^{206}Pb$) (Wiederhold, 2015). Normalization to ^{204}Pb ($^{206}Pb/^{204}Pb$, $^{207}Pb/^{204}Pb$, $^{208}Pb/^{204}Pb$) is commonly used to observe the largest variabilities between different reservoirs (Komárek et al., 2008).

1.2. Part B: Lead (Pb)

1.2.1. Biogeochemical cycle

1.2.1.1.Chemical properties and abundance in the continental crust.

Lead (Pb, from the Latin *plumbum*; Z = 82, atomic weight 207.19) is an element of the IVa Group of the periodic table; it is remarkably dense (11.35 g .cm^{-1}), poor conductor of electricity, ductile, soft, highly malleable, and gray in appearance (Marshall and Fairbridge, 1998). Lead is one of Earth's most abundant heavy metals on earth, with approximately 3:1 x 10^{14} tons found within the continental crust, from which ores represent around 9.3 x 10^{7} tons (Reuer and Weiss, 2002). This is due to its radiogenic nature: Pb is partially derived from the radioactive decay of ^{238}U, ^{235}U, and ^{232}Th (Table 1.1), meaning that around half of the ^{206}Pb, one-third of the ^{207}Pb, and one-fifth of the ^{208}Pb originate from the respective uranium and thorium isotopes since Earth's differentiation into crust and mantle [i.e., 4.5 billion years ago, (Marshall and Fairbridge, 1998)]. Pb is enriched in crustal rocks because it can substitute potassium (K) in potassium feldspars and micas partly due to its ionic radius being closely similar to that of K, and it can also substitute smaller ions such as Sr^{2+}, Ba^{2+}, Ca^{2+}, and Na^{+} in other silicates (Shotyk and Le Roux, 2005). This also explains lead's enrichment in high-temperature fluids associated with ore deposits and volcanic activity and its presence in soils resulting from feldspar weathering (Reuer and Weiss, 2002).

Like other chalcophile elements (i.e., Cu, Ni, Cd, Ag, and Zn), terrestrial Pb is primarily associated with massive sulfide deposits, with its primary and predominant mineral form

being galena (PbS). However, it is also present in sulfide alteration products like plattnerite (PbO2), cerussite ($PbCO_3$), and anglesite ($PbSO_4$) (Reuer and Weiss, 2002). While approximately 240 lead minerals are known, economically significant ones are galena (PbS), cerussite ($PbCO_3$), and anglesite ($PbSO_4$). Other significant lead sulfides include boulangerite ($5PbS.2Sb_2S_3$), bournonite ($PbCuSbS_3$), and jamesonite ($Pb_4FeSb_6S_{14}$) (Shotyk and Le Roux, 2005). A summary of the typical concentrations of Pb in various geological materials is presented in Table 1.2.

Table 1.1 *Lead (Pb) stable and radioactive isotopes along with their half-lives and natural abundances [Taken and modified from Cullen and MacAlister (2017)].*

Isotope (mass number)	Natural abundance (%)[a]	Half-life[b]	Decay mode	Decay series from	Half-life of parent isotope (yr.)	λ (yr^{-1})
^{204}Pb	1	stable	--	--	--	--
^{206}Pb	24	stable	--	^{238}U	4.5×10^9	1.5×10^{-10}
^{207}Pb	23	stable	--	^{235}U	0.7×10^9	9.8×10^{-10}
^{208}Pb	52	stable	--	^{232}Th	1.4×10^9	4.9×10^{-11}
^{210}Pb	--	22.2 yr.	β^-, α^-	^{238}U	4.5×10^9	1.5×10^{-10}
^{212}Pb	--	10.64 h	β^-	^{232}Th	1.4×10^9	4.9×10^{-11}
^{214}Pb	--	26.8 min	β^-	^{238}U	4.5×10^9	1.5×10^{-10}

Lambda (λ) : parent isotope decay constant
[a]Taken from Audi et al., (2003)
[b]Taken from Berglund and Wieser (2011)

Table 1.2. *Lead (Pb) concentrations in Earth's crustal materials [adapted from Cullen and MacAlister (2017); Rauch and Pacyna (2009)].*

Material	Lead content ($\mu g.g^{-1}$)	References
Continental crust	11	Rudnick and Gao (2003)
Upper	17	Rudnick and Gao (2003)
Middle	15.2	Rudnick and Gao (2003)
Lower	12.5	Rudnick and Gao (2003)
Oceanic crust	0.49	McDonough and Sun (1995)
Mantle	0.03	Salters and Stracke (2004); Workman and Hart (2005)
Core	0.4	Allègre et al., (1995)
Granite	18, 17	Adriano (1986)
Basalt	8, 6	Adriano (1986)
Shale	23, 20	Adriano (1986)
Sandstone	10, 7	Adriano (1986)
Limestone	9	Adriano (1986)

K feldspar	25-30	Shotyk and Le Roux (2005)
Loess	13	McLennan (1995)
Soil	27	Han et al., (2002)

Lead displays three primary oxidation states: (IV), (II), and (0). Still, under Earth's surface conditions, it exists predominantly in the oxidation state of Pb^{2+} (Marshall and Fairbridge, 1998), which is the prevalent inorganic species across a wide range of pH and Eh values under low dissolved carbon (C) and sulfur (S) conditions [Fig. 1.1, Brookins (1988)]. While the formation of sulfate, carbonate, chloride, and phosphate complexes of Pb can also be significant in natural waters (Bodek et al., 1988), $PbCO_3$ largely determines the solubility of Pb in oxic environments above pH 6 [Fig. 1.1, Shotyk and Le Roux (2005)]. In neutral to alkaline, reducing conditions (i.e., anoxic sediments and active bacterial sulfate reduction), Pb solubility is regulated through the formation of Pb sulfides, therefore highly restricting its mobility. In acidic conditions, Pb^{2+} can form stable complexes with natural organic ligands and then be adsorbed onto the surfaces of manganese and iron hydroxides (Lindsay, 1979).

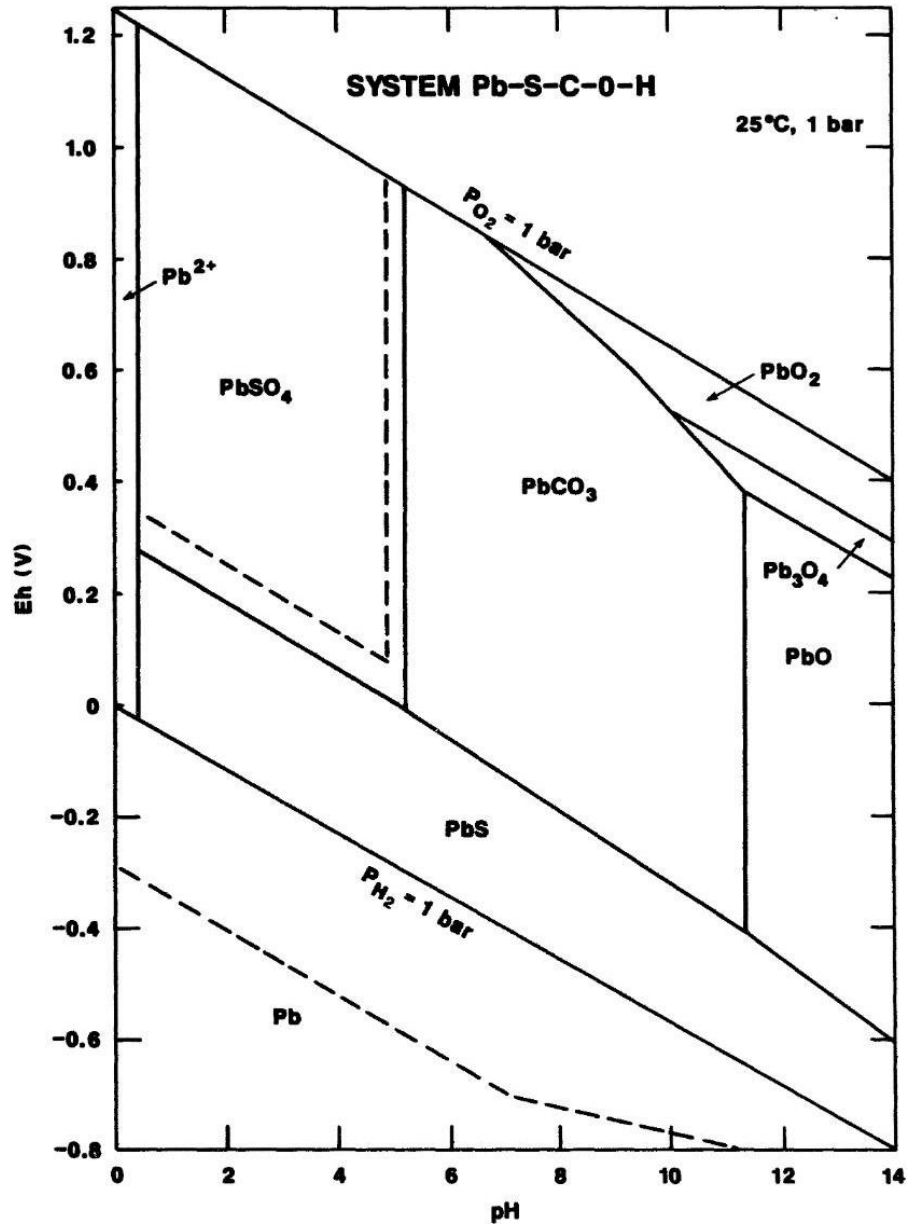

Figure 1.1. *Eh – pH diagram for the inorganic speciation of Pb [taken from Brookins (1988)].*

1.2.1.2.Mobilization: natural and anthropogenic sources

Due to its malleability, ductility, resistance to corrosion, and relatively low melting point (327 °C), Pb is an easy metal to work with, proving to be extremely useful for humans since the Neolithic (i.e., as early as 6400 BCE), continuing through Antiquity and the Roman Republic and Empire, and peaking in the 20th century due to industrialization and the use of leaded gasoline (Acharya, 2013; Nriagu, 1996, 1983). Consequently, natural sources of Pb towards the biosphere have been largely overshadowed by anthropogenic

sources, and global estimates of natural Pb fluxes must be carefully interpreted (Cullen and McAlister, 2017).

Moreover, there are significant disparities in the characteristics of the Pb emitted by natural and anthropogenic sources. In pre-anthropogenic times (i.e., before the Neolithic), the majority of the Pb originated from rock weathering, mainly in the form of soil dust particles [i.e., between 5 to 50 µm (Leinen and Sarnthein, 1989)], and mirrored the Pb concentrations in the crustal rocks (Shotyk et al., 2001). The bioavailability of this Pb remained relatively limited because the hosting particles were silicate minerals (i.e., K feldspar), characterized by its very low solubility in aqueous solutions under normal conditions of temperature and pressure (Heinrichs et al., 1980). In contrast, most of the anthropogenic Pb originates directly or indirectly from high-temperature combustion processes (see following section), which emit sub-micron particles [i.e., ~ 0.5 µm in diameter, (Rahn, 1976)] that have higher solubility (i.e., due to the increased relative surface) and are easily transported to long-range atmospheric dispersion (Shotyk and Le Roux, 2005).

1.2.1.3.Natural sources

The natural mobilization of lead from the continental crust and mantle to the atmosphere and the ocean arises from various processes, including windborne particles and runoff (i.e., released through physical and chemical weathering of rocks and soils), volcanic eruptions and outgassing, forest fires, sea salt spray, extraterrestrial particles, and radioactive decay (Marshall and Fairbridge, 1998; Nriagu, 1996, 1978; Nriagu and Davidson, 1985; Patterson and Settle, 1987; Rauch and Pacyna, 2009). Estimations of the global natural Pb emissions released per year to the atmosphere are between 970 and 23,000 tons (average: 13,000 $t.y^{-1}$, table 1.3) (Nriagu, 1990, 1989; Nriagu and Pacyna,

1988; Pacyna and Pacyna, 2001). From these, windborne particles account for roughly 30% (~3900 $t.y^{-1}$), volcanic emissions around 25 % (~ 3300 $t.y^{-1}$), forest fires around 15 % (~ 1900 $t.y^{-1}$), and the remaining flux (30 %) comes from biogenic sources (~ 1700 $t.y^{-1}$) and sea salt spray (~ 1400 $t.y^{-1}$) (Nriagu, 1990, 1989, 1978). The input to the oceans from continental runoff is approximately 295,000 tons per year, i.e., ~ 23 times greater than the natural atmospheric flux (Duce et al., 1991; Holland and Turekian, 2013).

Table 1.3. *Global natural and anthropogenic emissions of Pb to the atmosphere and continental runoff [adapted from Cullen and McAlister (2017)].*

Natural		**Anthropogenic**		
Source	**Pb (tons per year) 1995[a]**	**Source**	**Pb (tons per year)**	
			1995[a]	**1983[b]**
Wind-borne particles	3,900	Vehicular transportation	88,700	248,000
Volcanic activity	3,300	Non-ferrous mining (Pb, Cu, Zn)	14,800	49,800
Forest fires	1,900	Fossil fuel combustion	11,700	18,400
Biogenic	1,700	Iron and steel production	2900	7,600
Sea-salt spray	1,400	Waste disposal	820	2,100
		Cement production	280	7,100
Total emissions	12,200	Total emissions	119,200	333,000
Total continental runoff[c]	295,000			

[a]*adapted from Pacyna and Pacyna (2001)*
[b]*adapted from Nriagu and Pacyna (1988)*
[c]*Duce et al., (1991)*

1.2.1.4.Anthropogenic sources

The biogeochemical cycle of Pb has been substantially disrupted by the increasing human activity that exerts a predominant influence on the global distribution of this metal (Boutron and Patterson, 1987; Cheema et al., 2020; Holland and Turekian, 2013; Hong et al., 1994; Murozumi et al., 1969; Settle and Patterson, 1982). Global Pb production has increased since Antiquity, with estimations of the Romans producing between 80,000 and

100,000 $t.y^{-1}$ (Hong et al., 1994; Nriagu, 1996) to 1,000,000 $t.y^{-1}$ at the beginning of the 20th century and 5,500,000 tons/year by 2013 (Cullen and McAlister, 2017), with a significant portion originating from China (2,300,000 tons), and smaller contributions from Australia (633,000 tons), and the USA (385,000 tons) (Flegal et al., 2013).

The modern anthropogenic mobilization of Pb occurs through mining and smelting of ores [90% of the world's primary lead is extracted from galena (Shotyk and Le Roux, 2005)], burning fossil fuels, and the utilization, recycling, and disposal of products containing Pb [i.e., Pb-acid batteries, ammunition/ballistics, oxides for glass and ceramic strengthening, piping, metal casting, metal coating, weights, leaded-gasoline, and radiation shielding (Cullen and McAlister, 2017)]. Over the past two decades, around 80 % of the Pb consumed worldwide has been utilized in manufacturing lead-acid batteries, which are extensively employed in starting-ignition systems for automobiles and heavy industrial vehicles (Cullen and McAlister, 2017).

In 1983, the Pb emissions to the atmosphere were 333,000 $t.y^{-1}$ (Nriagu and Pacyna, 1988), with the highest sources being vehicular transport (248,000 $t.y^{-1}$), non-ferrous metal production (46,500 $t.y^{-1}$), and fossil fuel combustion (i.e., for heat and electricity generation, 18,400 $t.y^{-1}$), all of them significantly surpassing the total natural emissions (i.e., 12,200 $t.y^{-1}$, Table 1.3). During the mid-1990s, the total atmospheric emissions decreased to 119,200 $t.y^{-1}$, with Europe and Asia as the major anthropogenic emitters (Pacyna and Pacyna, 2001). This three-fold decrease in Pb emissions reflects the implementation of stricter regulations on the use of Pb, enhanced capture at emission sources, improved recycling practices, and most importantly, the progressive abandonment of leaded gasoline worldwide (Shotyk and Le Roux, 2005).

1.2.1.5.Distribution in the environment: behavior, speciation, and fate.

Compared to other metals (i.e., Cd, Zn, Ni, Cu, and Cr), Pb exhibits a notable tendency to react with particles and remains relatively immobile in soils and freshwater systems, resulting in lower dissolved concentrations in river and ocean waters relative to its abundance in the Earth's crust (Holland and Turekian, 2013; Viers et al., 2009). However, due to the predominant influence of anthropogenic contributions worldwide, particulate Pb emitted to the atmosphere can be easily dispersed by prevailing winds and deposited into terrestrial and aquatic environments through wet and dry deposition (Nriagu, 1996, 1978). Soils, freshwater systems, and their sediments constitute complex systems where chemical reactions can influence the flow of both natural and anthropogenic Pb from land to rivers and groundwater. Pb from both natural and anthropogenic sources is ultimately transferred to the ocean [i.e., primarily via wet deposition and riverine transport (Duce et al., 1991)], where it accumulates and serves as a final burial for Pb (Cullen and McAlister, 2017).

Table 1.4. *Global lead (Pb) concentrations in different Earth's compartments [adapted from Rauch and Pacyna (2009)].*

Material	Lead content ($ng.g^{-1}$)	References
Soil	400	Han et al., (2002)
Rivers (particulate)	35000	Martin et al., (1993); Martin and Whitfield (1983)
Rivers (dissolved)	0.08	Martin et al., (1993); Martin and Whitfield (1983)
Freshwater lakes (dissolved)	0.036	Rossmann and Barres (1988); Sterner et al., (2004)
Groundwater (dissolved)	1	Page (1981); Sañudo-Wilhelmy et al., (2002)
Oceanic sediment	20000	Plank and Langmuir, (1998)
Greenland ice	0.028	Hong et al., (1996, 1994)
Antarctic ice	0.005	Boutron and Patterson (1987); Planchon et al., (2002)
Ocean (dissolved)	0.002	Li (1991)
Terrestrial biomass (dry weight)	9400	Adriano (2001); Kabata-Pendias (2010)
Agricultural crops (dry weight)	1100	Adriano (2001); Kabata-Pendias (2010)
Marine organisms (dry weight)	8700	Li (1991)

Atmosphere	0.001	Rauch and Pacyna (2009)
Dissolved Riverine Flux (tons/yr)	3,000	Viers et al., (2009)
Particulate Riverine Flux(tons/yr)	916,000	Viers et al., (2009)

1.2.1.6. Lead in the atmosphere

The atmosphere represents a relatively minor lead reservoir (Table 1.4), but it efficiently facilitates lead transportation between continents and oceans (Reuer and Weiss, 2002). Natural Pb aerosols have short residence times (~ 10 days) and rapid deposition rates due to their large particle size. In contrast, anthropogenic Pb exists as submicron-sized particles (Rahn, 1976), able to disperse thousands of kilometers with prevailing winds and reach remote, pristine environments (Cullen and McAlister, 2017). In remote areas, wet deposition removes a significant fraction of Pb from the atmosphere through the solubilization of aerosols in water droplets or the leaching of particles associated with precipitation, contributing to almost 83% of the depositional flux of Pb to the surface ocean (Heintzenberg et al., 2000). Moreover, the Pb associated with these aerosols is highly soluble, with a considerable fraction dissolving within hours of exposure to seawater (Duce et al., 1991).

The concentration of lead in rainwater, snow, and ice exhibits a latitudinal gradient in deposition and is mainly influenced by the trajectory of air masses and the proximity to sources of anthropogenic activity (Bertinetti et al., 2020; Lee et al., 2008; Liu et al., 2011; Planchon et al., 2002; Rosman et al., 1993; Veysseyre et al., 2001). For example, Pb levels in rainwater across Europe and the North Atlantic have mirrored the temporal variability of continental emissions, whereas remote areas in the South Pacific exhibited much lower values (Arimoto et al., 1987; Halstead et al., 2000). Moreover, snow records from central Greenland have shown that anthropogenic sources at lower latitudes from Europe

dominate deposition in this remote area, allowing for the reconstruction of pollution history through time (Rosman et al., 1997; Sherrell et al., 2000).

1.2.1.7.Lead in soils

Soil formation occurs through chemical and physical weathering processes from parent rocks; hence, the composition of Pb in soils typically reflects the Pb content of these rocks [Table 1.2, (Holland and Turekian, 2013)]. The mobility and uptake of Pb by organisms in freshwater and soil environments depend on its physical and chemical forms, which are influenced by factors such as redox potential, pH, and the presence of inorganic and organic compounds and ions in solution (Degryse et al., 2009). However, as previously discussed, substantial anthropogenic inputs of Pb into the atmosphere and natural water bodies have likely altered the Pb content of soils (Cheema et al., 2020; Pacyna and Pacyna, 2001).

Upon introduction to soils, Pb tends to form progressively less soluble forms through reactions with soil components. Reactive Pb can become integrated into minerals or bind to soil surfaces through processes like absorption, co-precipitation, ion exchange, and complexation reactions (Bradl, 2004; Degryse et al., 2009). Carbonates play a significant role in controlling Pb distribution, as $PbCO_3$ can readily form in soils under oxidizing and slightly acidic to alkaline pH conditions [Fig. 1.1, (Bradl, 2004)]. Additionally, the solubility of lead phosphates is remarkably low (Lindsay, 1979), which further affects the migration of lead, especially in agricultural soils with phosphorus addition (Shotyk and Le Roux, 2005). The organic matter content of soils also influences Pb mobility, either through surface adsorption to particles or through solubilization via coordination and complexation in solution (Pinheiro et al., 1999; Strawn and Sparks, 2000). Overall, Pb mobilization in soils is very limited, with vertical migration between 1 to 8 $mm.y^{-1}$

(Steinmann and Stille, 1997; Whitehead et al., 1997). However, under low pH conditions, Pb mobilization may become significant (Brännvall et al., 2001) due to reversible adsorption to mineral surfaces (Nelson and Campbell, 1991).

1.2.1.8.Lead in freshwater

Suspended particulate Pb concentrations among rivers are highly variable and can be attributed to some extent to disparities in the Pb content in soils and rocks within river catchments, but inputs from the anthropogenic mobilization of Pb play a significant role in the average Pb concentration observed in rivers worldwide [i.e., 0.08 $\mu g.L^{-1}$, Table 1.4, Holland and Turekian (2013); Viers et al., (2009)].

The fate of Pb in freshwater ecosystems is closely linked to its chemical speciation (Filella et al., 2001). Under normal conditions (i.e., oxic and neutral pH), Pb primarily exists as carbonate [$Pb(CO_3)$], with sulfate (SO_4^{2-}) and hydroxide (OH^-) complexes becoming more significant at lower and higher pH levels, respectively [Fig. 1.1, Morel and Hering (1993); Turner (1987); Vuceta and Morgan (1978)]. The complexation of Pb by natural organic matter is also possible under these conditions, but it is highly variable and depends on the pH, the concentration and binding characteristics of dissolved organic carbon (DOC), and the competition with other cations (Abate and Masini, 2002; Hettiarachchi and Pierzynski, 2004; Morel and Hering, 1993; Mylon et al., 2003; Pinheiro et al., 1999; Sigel, 2014; Taillefert et al., 2000).

Similar to complexation reactions in solution, the adsorption of Pb to suspended particles or aquatic sediments is an important factor controlling Pb mobilization (Erel et al., 1991; Holland and Turekian, 2013; Laxen, 1985) and is influenced by pH, ionic strength, the concentration of competing cations, and the presence of organic and inorganic ligands (Morel and Hering, 1993). The greatest predictors of the partitioning of Pb between

dissolved and suspended phases in freshwater (i.e., the distribution coefficient, Kd) are total Pb concentration and pH (Holland and Turekian, 2013; Laxen, 1985; Sauvé et al., 2000), with global estimations of 3,000 $t.y^{-1}$ and 916,000 $t.y^{-1}$ of dissolved and particulate Pb riverine fluxes to the ocean, respectively [Table 1.4, Holland and Turekian (2013); Viers et al., (2009)].

Before reaching the ocean, the flux of particulate and dissolved Pb from rivers experiences mixing with more saline water in estuaries, which alters the speciation of Pb, leading to a significant decrease in concentrations as salinity increases (Fu et al., 2013; Waeles et al., 2008). During winter, particulate Pb is remobilized due to erosion and resuspension, causing estuaries to behave as both sinks and sources of Pb (Holland and Turekian, 2013).

1.2.1.9.Lead in the ocean

The behavior and fate of dissolved lead in the marine environment, similar to freshwater, depend on the chemical speciation of Pb and particle reactivity and ultimately reflect its atmospheric origin (Reuer and Weiss, 2002). Lead is present in trace amounts in the ocean, typically at ~ 2 $pg.g^{-1}$ [Table 1.4, Flegal et al., (2013); Kelly et al., (2009); Noble et al., (2015); Schaule and Patterson (1981); Weiss et al., Weiss et al., (2003); Wu and Boyle (1997)]. The distribution of lead in the ocean and its primary removal from the system through burial in marine sediments are driven by particle scavenging reactions, where lead is adsorbed to or complexed by particle surfaces (Boyle et al., 2014; Holland and Turekian, 2013).

In estuarine systems, lead is mostly complexed with the particulate or colloidal phase, whereas the speciation in the remaining soluble fraction is predominantly associated with Cl^- (46–75%), CO_3^{2-} (11–42%), and OH^- (8–9%) (Powell et al., 2009; Turner, 1987;

Woosley and Millero, 2013). In environments with higher dissolved organic carbon concentrations, such as coastal areas, dissolved lead comprises approximately 90% of the total concentration (Shen and Boyle, 1987), with roughly 50 to 70% of dissolved lead complexed with organic ligands, thus reducing the concentration of inorganic lead complexes (Buffle et al., 1988; Kozelka et al., 1997; Muller, 1996). The rest of the inorganic fraction is represented as $PbCO_3$ (55 %), $PbCl_2$ (11 %), $Pb(CO_3,Cl_3)^-$ (10%), and $PbCl^+$ (7 %) (Whitfield and Turner, 1980). The remaining 17% encompasses other chloride, sulfate, and hydroxide complexes, which are rapidly scavenged by biological particles in the open ocean, resulting in a surface ocean residence time of approximately two years (Bacon et al., 1976). The result of the atmospheric deposition and particle scavenging in open waters is the formation of the upper-ocean lead seasonality, which is characterized by summer aerosol lead accumulation within a warm, stratified mixed layer and subsequent Pb dilution during deep winter mixing (Boyle et al., 1986).

Although lead has no known biological function, organisms can concentrate intracellular lead from the seawater they inhabit through various non-selective uptake mechanisms (Holland and Turekian, 2013; Morel and Hering, 1993; Sunda, 1994). Phytoplankton, in particular, can impact lead distributions by internalizing lead through surface adsorption (Fisher et al., 1988). Zones of high productivity in the ocean margins and areas of active upwelling are significant sites of lead removal in the ocean (Buesseler et al., 2008). Passive trapping and biological uptake in the ocean's surface waters are likely to be important sinks for dissolved lead, while passive scavenging of the particle surface and sinking are the main mechanisms for removing lead from the ocean interior to the sediments. Organisms interacting with ocean sediments, such as filter-feeding organisms and polychaete worms, can influence the biogeochemical cycling of lead in the ocean by mobilizing or concentrating lead. However, biomagnification of lead is not believed to

occur in marine food webs (Rainbow et al., 2006; Reinfelder et al., 1998; Suedel et al., 1994).

1.2.2. Impact on Human Health

1.2.2.1.Pathways of exposure

Human exposure to lead (Pb) occurs through various sources such as contaminated food, water, air, house dust, and various industrial activities, including metallurgy, recycling, construction, and battery manufacturing (Barbosa et al., 2005). Pb's pathways depend on its source and bioavailability, with the absorbed fraction influenced by physical and chemical attributes like particle size and compound solubility (Barbosa et al., 2005). Additionally, individual-specific factors such as age, gender, nutritional status, and potentially genetic background play a crucial role in this complex process (ATSDR, 2020).

During the last century, millions of tons of Pb (in the form of tetraethyl lead) have been added to gasoline and other motor fuels and released into the atmosphere during combustion (Fewtrell et al., 2004; Rosner and Markowitz, 1985). This has produced a global pandemic of Pb poisoning, with main consequences for children’s health (Landrigan et al., 1975; Needleman et al., 1979; Needleman and Gatsonis, 1990). The progressive removal of Pb from gasoline since the '60s was closely followed by a parallel year-to-year reduction in blood lead levels (Angrand et al., 2022; Centers for Disease Control and Prevention (CDC), 2005; Thomas, 1995). In contemporary settings, adult lead poisoning is predominantly linked to occupational exposure; however, acute cases can also arise from everyday items like leaded dishware, moonshine liquor, cosmetics, traditional or folk remedies (Needleman, 2004), lead-based paints (O’Connor et al., 2018), but also drinking water (Ericson et al., 2021).

1.2.2.2.Human exposure during Roman and Medieval times

The Roman period is considered to have provoked the highest Pb metal pollution during Antiquity due to its large-scale mining and metallurgical operations (Hong et al., 1994; McConnell et al., 2018; Nriagu, 1983; Silva-Sánchez and Armada, 2023). The use of Pb by the Romans was extensive and included both public and domestic applications, such as household and cooking utensils (crafted from pure lead or other alloys like pewter), as an ingredient in cosmetics, medicine, paints (Needleman and Needleman, 1985; Nriagu, 1983), and in water distribution systems (i.e., pipes, pipe seals, and aqueduct lining), which lead to Pb-contaminated waters of ancient urban centers (Delile et al., 2017, 2014; Flaux et al., 2023; Véron et al., 2013).

An important and particular source of human exposure to Pb during Roman times was the use and consumption of Pb-laced sweeteners prepared in Pb-containing cooking containers (Reddy and Braun, 2010). These sweeteners were made from unfermented grape juice (*must*) that was boiled down and reduced (i.e., to concentrate the sugars) to produce *sapa*, *defrutum*, or *carenum*, each with varying degrees of water content to yield different degrees of sweetness (Apicius, 1984; Nriagu, 1983; Waldron, 1973). These grape syrups were used as sweeteners due to the presence of lead acetate ("sugar of lead") that was formed during the boiling process and as wine and food preservatives (i.e., the lethal effect of Pb on bacteria prevented any spoiling) (Eisinger, 1982; Montgomery et al., 2010).

In medieval times, the use of Pb was also extensive and included several Pb-containing products like coins, glass windows, and roof tiles. Additionally, Pb pipes for water distribution were still being used in many European capitals following Roman tradition (Nriagu, 1983; Rasmussen et al., 2015). In northern urban centers, plates, cups, and other kitchenware, alongside lead-glazed ceramics and pewter, were commonly used (Nriagu,

1983). It is assumed that in contact with acidic or salty foods, the Pb^{2+} of the glazing kitchenware was leached into the food (Rasmussen et al., 2015), thus representing an important source of exposure. Additionally, workers in mining, smelting, metalworking, and glassmaking were particularly exposed to toxic fumes and airborne particles (Montgomery et al., 2010).

1.2.2.3.Distribution in the body

Lead (Pb) concentration within the body exhibits distinctive patterns, with bones containing higher concentrations than soft tissues, with the majority of the total body burden of Pb in adults found in bone, constituting over 90% of the total, of which approximately 70% is located in cortical bone (Barry, 1975). In addition to bone, Pb concentrations are also observable in hair and nails, surpassing levels found in soft tissues. However, it's important to note that Pb concentrations in hair may not be reliable for assessing Pb absorption. Male adult bones show a 30% higher Pb content than females, particularly in cortical bone, with this discrepancy being even more pronounced among male adults occupationally exposed to Pb, where concentrations exceed 2 to 3 times those of unexposed male adults (Barry, 1975). However, this difference might be related to different turnover rates.

Children are particularly susceptible to the deleterious effects of Pb due to physiological differences, like higher absorption rates by the gut, lower Pb-bone body burden (94% in adults compared to only 70% in children), and the ongoing bone remodeling associated with constant growth (Needleman, 2004). Clinical symptoms in children (i.e., abdominal pain, arthralgia, clumsiness, staggering, headache, and behavioral changes) typically manifest at blood Pb concentrations of 60 $\mu g.dl^{-1}$ or higher. As exposure increases, these symptoms can progress to more severe outcomes, including alterations of consciousness,

stupor, and convulsions (Needleman, 2004). Remarkably, neurodevelopmental toxic effects associated with lead exposure show a lack of a clear threshold (Bellinger et al., 1987) because blood Pb concentrations below 10 $\mu g.dl^{-1}$ in children exhibit an inverse correlation with IQ scores, with a more pronounced decline observed at lower concentrations rather than at higher levels (Canfield et al., 2003).

The residence time of Pb in the bloodstream is approximately 40 days, whereas it ranges from 10 to 40 years in bone (Oflaherty, 1995; Rabinowitz, 1991), although these may vary in pregnant women and children due to increased bone remodeling (Gulson et al., 1995). The slow but continuous release of Pb from bone back to blood during this process is known as endogenous contamination, and turnover rates depend on factors like bone type (i.e., slow rates in cortical bone vs fast rates in trabecular bone), intensity of exposure, and the individual's age (Brito et al., 2002).

1.2.2.4. Symptoms and toxicity

Clinical manifestations of high blood Pb levels are diverse and severe and are mostly dependent on chronic or acute cases. They encompass intractable colic, motor clumsiness, clouded consciousness, general weakness, paralysis, peripheral neuropathy, hypertension, kidney dysfunction, and renal failure (Needleman, 2004). Additionally, Pb exposure is fetotoxic and associated with a heightened incidence of stillbirths, neonatal deaths, decreased fertility rates in women (Oliver, 1911), and decreased sperm count and teratospermia in men (Lancranjan et al., 1975).

Lead (Pb) exerts its toxic effects predominantly through its capacity to mimic or compete with calcium (Ca) and its strong binding affinity with sulfhydryl groups. Thus, it alters the structural integrity of enzymes and proteins (Needleman, 2004). This has far-reaching

consequences on various physiological processes, with the central nervous system (CNS) being the most affected organ (Needleman, 2004).

While Pb toxicity research began with high-dose effects and symptomatic individuals, now the focus has changed towards a broader consideration of low-dose asymptomatic exposure. For example, Pb competes with Ca at picomolar concentrations for binding sites on cerebellar phosphokinase C, influencing neuronal signaling and neurotransmitter release (Bressler and Goldstein, 1991; Markovac and Goldstein, 1988). This interference inhibits Ca entrance into cells (Simons, 1993) and induces swelling in the mitochondria, leading to the inhibition of cellular respiration and altered Ca kinetics (Holtzman et al., 1984). Pb also interferes with myelin formation (Krigman, 1978) and collagen synthesis, affecting vascular permeability and resulting in brain edema and hemorrhage (Pentschew, 1965). Even at lower doses, Pb disrupts synaptogenesis (Alfano and Petit, 1982), interferes with brain development (Wilson et al., 2000), and can induce apoptosis (Adhikari et al., 2001; Fox et al., 1997; He et al., 2000; Iavicoli et al., 2001; Shabani and Rabbani, 2000; Tavakoli-Nezhad et al., 2001).

Besides the physiological alterations, Pb also produces behavioral alterations in mammals, including reduced learning capabilities and impaired social function (Bushnell and Bowman, 1979). Exposure to Pb at levels below those leading to clinically diagnosable symptoms is linked with IQ deficits in children (Needleman and Gatsonis, 1990; Pocock et al., 1994) and with cognitive decline in adults (Muldoon et al., 1996), but also with an elevated risk of engaging in antisocial and delinquent behavior (Needleman et al., 2002, 1996), violent crimes (Stretesky and Lynch, 2001), and neuropsychological impairments affecting academic performance (Fergusson et al., 1997; Needleman et al., 1990, 1979). Overall, high blood Pb levels have been associated with dementia (Schwartz et al., 2000) and increased mortality (Lustberg and Silbergeld, 2002).

1.2.2.5.Pb toxicity in Antiquity: Paleopathology

While Greco-Roman writers observed and were aware of the harmful effects of lead toxicity, Roman society continued mining, smelting, and using this metal without hesitation (Montgomery et al., 2010). It is only in the 7th century CE that the classic chronic symptoms of lead poisoning (i.e., saturnism) were comprehensively documented (Burstein and Finch, 2022; Hodge, 1981; Retief and Cilliers, 2006).

Paleopathology is a subdiscipline of physical anthropology that targets archaeological human remains to identify diseases and reconstruct their effects and impacts on ancient human populations (Buikstra, 2010). In this sense, paleopathology integrates historical, social, biomedical, and geochemical approaches to reconstruct the life of ancient human groups (Buikstra and DeWitte, 2019).

In the case of Pb poisoning, the diagnostic limitations of paleopathological research are related to the absence of visible effects on the skeleton. Even if these were present (i.e., dense metaphyseal lines in long bones), the impact of this condition on the individual's ability to continue living and function effectively is not completely clear and can only be inferred either from the present knowledge of symptoms and toxicity (Ortner, 2003) or historical accounts (Jacques, 1955; Waldron, 1973). However, recent studies on the application of isotope geochemistry in the medical field have demonstrated its potential to enhance understanding of health issues; these findings will be discussed in the following section.

1.3. PART C: Copper (Cu)

1.3.1. An essential element (metabolic cycle)

Cu serves as a potent catalyst for oxidation-reduction reactions and readily participates in ionic bonds. Within biological systems, copper in solution can bind up to four anions, facilitating easy covalent bonding with protein amino acids (Holm et al., 1996). As an essential trace element (Linder, 2001; Lutsenko, 2010), Cu is vital in low concentrations (humans require 8 $mg.d^{-1}$) and is primarily found predominantly in vegetables and in lower proportion in starchy foods and animal proteins (Sandstead, 1982). Following ingestion, copper enters the bloodstream through the stomach and intestine. Initially, it is taken up in its oxidized form by transcurrent and albumin (Tapiero et al., 2003), but it is rapidly transported by ceruloplasmin (>90%), a protein secreted by hepatocytes (Harris, 1991; Kosman, 2002). Subsequently, copper is stored in the liver by metallothioneins (Terada et al., 1999; Turnlund, 1998). Furthermore, copper is distributed to various organs.

Before entering cells, Cu undergoes reduction (Cu^{2+} => Cu^{+}) by reductases from the STEAP protein family (Kidane et al., 2012) and is then imported into cells by hCtr1p proteins (Hasan and Lutsenko, 2012; Lee et al., 2002). Inside cells, copper does not remain in a free form (which would be toxic to the cell) and instead becomes complexed to metallochaperones, such as ATOX1 or COX17 (Lutsenko, 2016). These chaperones transport copper to organelles where it binds once again to functional proteins, such as cytochrome c oxidase in the mitochondrial respiratory chain or Superoxide Dismutase 1 (SOD1), regulating oxidative stress by detoxifying oxygen free radicals from cellular respiration. Finally, copper is exported to the extracellular environment, including the blood, bile, or cerebrospinal fluid, via the hAtp7a or hAtp7b proteins (Ohgami et al., 2006).

Copper is an indispensable trace element in the metabolism of numerous cellular enzymes, some of which are crucial to the organism. Alterations in its metabolism can lead to the development of diseases such as Wilson's or Menkes' disease (Bandmann et al., 2015; Kaler, 2011). Excessive accumulation of copper in the liver, brain, or eyes can induce cirrhosis or neurological problems, triggering Wilson's disease. Conversely, deficiency can lead to Menkes disease, characterized by hair loss, neuronal deficits, and stunted growth. In both these diseases, an over-concentration of oxygen free radicals occurs within the cell. The cause lies in a gene mutation affecting intra-membrane copper transport proteins, specifically the absence of the cellular copper exporter hATp7a (in the case of Menkes disease) and hepatic cells hATp7b (in Wilson's disease) (Chelly et al., 1993; Tanzi et al., 1993; Vulpe et al., 1993).

1.3.2. Isotopy of Cu and its use as a tracer of metabolic alteration

Copper has two stable isotopes, ^{63}Cu and ^{65}Cu, with natural abundances of 69.7% and 30.8%, respectively (Wiederhold, 2015). Both isotopes have the same number of protons (29), but they differ in the number of neutrons (34 for ^{63}Cu and 36 for ^{65}Cu). More neutrons lead to a higher atomic mass, making ^{65}Cu (M = 64.9278 $g.mol^{-1}$) "heavier" than ^{63}Cu (M = 62.9296 $g.mol^{-1}$) (Wiederhold, 2015).

During biochemical processes and metabolic reactions, isotopes with different masses and, therefore, distinct physicochemical properties are incorporated variably into biological reservoirs (e.g., blood or cerebrospinal fluid) and compounds (proteins, molecules). This differential incorporation results in variability in isotopic abundances, known as "isotopic fractionation." The degree of isotopic fractionation is quantified by measuring isotopic composition (‰), which represents the ratio of two isotopes of the same chemical element normalized to a reference standard. For copper, the reference

standard is a pure copper solution (NIST 97), and the isotopic composition of a sample is calculated using the following formula:

$$\delta^{65}Cu = \left[\frac{\left(\frac{^{65}Cu}{^{63}Cu}\right)_{sple}}{\left(\frac{^{65}Cu}{^{63}Cu}\right)_{std}} - 1 \right] * 1000$$

With sple = the ratio of the sample and std = the ratio of the reference standard. By definition, the isotopic composition of the Cu reference standard is zero. δ^{65}Cu is positive when the isotopic compositions of the analyzed sample are heavier than the reference standard and negative when they are lighter. In biological contexts, isotopic fractionation is primarily influenced by two factors: (1) the oxidation state of the metal ion and (2) the nature of the ligands binding the metal (Schauble, 2004). Recent *ab initio* calculations have demonstrated that species (such as molecules, proteins, and enzymes) binding metals with highly electronegative ligands like oxygen (O, e.g., lactate) or nitrogen (N, e.g., histidine) tend to be enriched in heavy isotopes (e.g., ^{65}Cu). Conversely, metals bound to species with lower electronegativity, such as sulfur (S, e.g., cysteine and metallothionein), are enriched in light isotopes (e.g., ^{63}Cu) (Albarede et al., 2016). Additionally, oxidized species (which bind oxidized ions like Cu^{2+}) typically have heavier isotopic compositions compared to reduced species (which bind reduced ions like Cu^{+}) (Albarede et al., 2016; Balter et al., 2013).

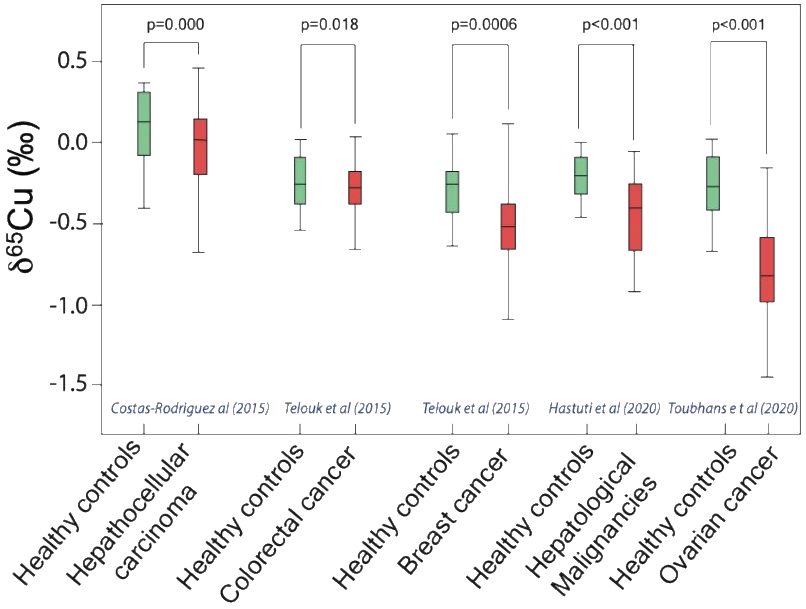

Figure 1.2. *Cu isotope compositions of serum from patients with various cancers compared with control values (Costas-Rodríguez et al., 2016; Hastuti et al., 2020; Télouk et al., 2015; Toubhans et al., 2020).*

The use of conventional stable isotopes (C, H, O, N, and S) in medicine is limited because these elements are not specific to particular biological processes. However, they are extensively used in archaeological human remains (Ambrose and Krigbaum, 2003) to explore questions related to mobility and diet (Bogaard and Outram, 2013; Pederzani and Britton, 2019; van Der Merwe, 1982). In contrast, elements like alkali metals (Ca, Mg) and transition metals (Cu, Zn, Fe) are more promising as diagnostic tools because they are often more specific to biological functions and have a relatively short turnover time in the body (Albarède, 2015). Copper (Cu), with a turnover time of about 4 to 6 weeks (Linder, 1991; Milne, 1998), is particularly relevant for studying rapidly progressing diseases (i.e., between a month and a year) like cancer. For this latter, medical research has shown a systematic enrichment in light Cu isotopes (^{63}Cu) in the blood of patients with different types of cancer compared to controls (healthy individuals), resulting in a decrease in the ^{65}Cu/^{63}Cu isotopic ratio (Kazi Tani et al., 2021; Télouk et al., 2015; Toubhans et al., 2020). This decrease was observed across various cancers: -0.25 ‰ for

breast cancer, -0.14 ‰ for colorectal cancer, -0.15 ‰ for liver cancer, and -0.3 ‰ in the red blood cells of hepatocarcinoma patients (Fig. 1.2.) (Costas-Rodríguez et al., 2016; Télouk et al., 2015).

Furthermore, a study on dogs diagnosed with multicentric lymphoma showed that Cu levels in cancerous dogs were significantly lower than in healthy controls ($P < 0.0001$) but not significantly different from dogs with non-oncological diseases, suggesting inflammatory diseases also affect Cu isotopic composition (Chamel et al., 2017). Thus, Cu isotopes could be a potential tool for tracing metabolic changes related to cancer or inflammatory diseases.

1.4. PART D: Bones as archives of the past

1.4.1. Bone characteristics

Besides the most evident, like protection of vital organs, support, and enabling motion, bones also serve as a mineral (calcium and phosphate) and energy storage (i.e., lipids stored in the yellow bone marrow), and as a metabolic regulator, being the reservoir of blood-forming cells (i.e., red and white blood cells and platelets) (Monier-Faugere et al., 1998; Nikita, 2017a). Understanding the categorization of human bones based on their shape, structure, and composition is a basic aspect with important implications for this study. Therefore, a brief summary is presented below.

1.4.1.1.Structure

Bones can be divided into long, short, flat, and irregular, each with its unique characteristics and functions. Long bones, the archetype of skeletal structure, consist of a central shaft known as the diaphysis, two epiphyses at the extremities, and two metaphyses in-between containing the epiphyseal plate (Fig. 1.3, top), which remain

active until maturity when it becomes fully ossified (Nikita, 2017a). In contrast, short, flat, and irregular bones have a simpler structure compared to long ones (Fig. 1.3, bottom). All bones share an external coating named the periosteum, which is crucial for both thickness growth and osseous protection but also as an anchor surface for ligaments and tendons, underscoring its importance in structural integrity and movement (Monier-Faugere et al., 1998). Central to the bone's anatomy is the medullary cavity, filled during the lifetime with the yellow bone marrow, which is encased by the endosteum, a cell-rich membrane critical for bone development and remodeling (Monier-Faugere et al., 1998; Nikita, 2017b).

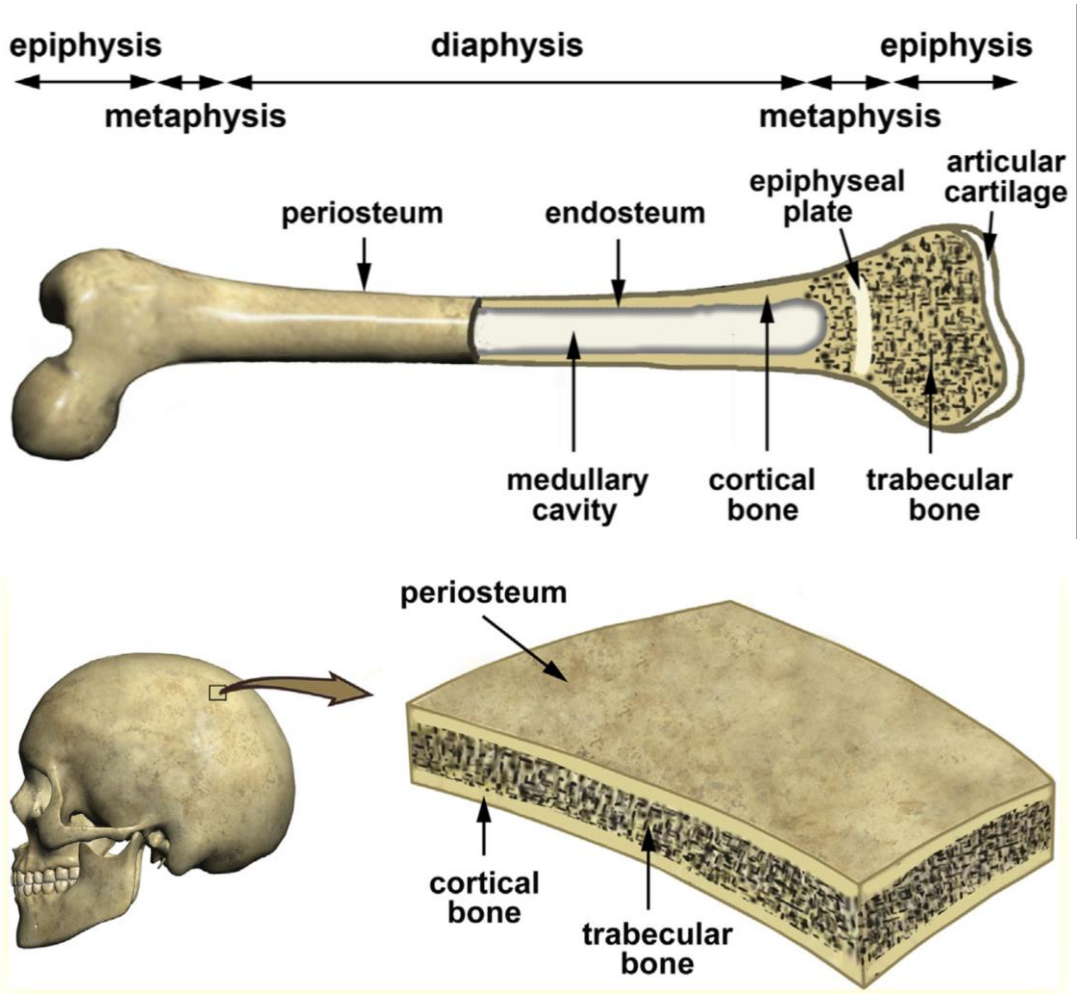

Figure 1.3. *Structure of a long bone, archetype of skeletal structure (top) and a flat bone, similar to short and irregular bones (bottom) [taken from Nikita (2017a)].*

During bone growth, repair (i.e., bone remodeling and fracture healing), or with specific pathologies, the initial bone tissue yielded by the body is woven bone (i.e., primary bone) characterized by an irregular, random, and disorganized pattern of collagen arrangement (Fuchs et al., 2009; Nikita, 2017b). While this formation is an effective response to the immediate structural needs, its disarray hinders it from serving as a long-term structural support. As such, during late childhood and early adulthood, it is substituted by lamellar bone (i.e., mature bone), consisting of organized layers of mineral crystals and collagen fibers known as lamellae (Nikita, 2017a).

There are two structural types of lamellar bone: cortical (also named compact) and trabecular (also named cancellous) (Nikita, 2017a). The cortical bone is located underneath the periosteum and is characterized by its compactness and density (i.e., low porosity), which confers its high tolerance against compressive stress, thus forming up to 80% of the total skeletal mass, predominantly distributed within the long bones of the appendicular skeleton (Fuchs et al., 2009). Osteons (200 - 250 μm in diameter) are the basic structural unit (BSU) of cortical bone (Fig. 1.3), each one consisting of organized layers of osseous lamellae (70 - 100 μm thick) concentrically arranged around Haversian canals (22 - 110 μm in diameter, containing blood vessels and nerve fibers), which are transversely connected between each other and to the periosteum and bone marrow through Volkmann's canals, ensuring metabolic communication throughout the bone matrix (Hollinger et al., 2011).

By contrast, trabecular bone is irregularly arranged and forms a honeycomb-like structure (Fig. 1.3) characterized by its low density and large porosity (i.e., between 50 to 90 % of its total volume), conferring it with a very low compressive strength but higher capacities for load distribution and energy transfer (Foldes et al., 1991; Fuchs et al., 2009). Its basic structural unit (BSU) is the trabeculae (i.e., thin spicules consisting of a few stacked layers

of lamellae), which is a hotbed for metabolic activity that hosts the red marrow (i.e., during lifetime), crucial for nutrient exchange, metabolic regulation, and blood cell formation (Hollinger et al., 2011). It represents up to 20 % of total skeletal mass and is predominantly located within the short and flat bones of the axial skeleton (Fuchs et al., 2009). The dynamic nature of bone is reflected in its turnover rates, with cortical bone undergoing 2 – 10 % renewal (i.e., osteonal remodeling) and trabecular bone 25 % renewal (i.e., hemiosteonal remodeling) annually, highlighting a continuous cycle of regeneration and maintenance (Fahy et al., 2017; Hollinger et al., 2011; Parfitt, 2013; Quinn, 2024).

1.4.1.2.Composition

The bone tissue is primarily a composite matrix, with an organic phase and an inorganic phase, as well as water, corresponding to 30%, 60%, and 10% by weight and 35%, 45%, and 25% by volume, respectively, for each phase (Morgan et al., 2013). The organic component is predominantly composed of collagen fibers, constituting 90 % of the phase, with the remaining 10 % composed of non-collagenous proteins and proteoglycans. Collagen is crucial for cellular differentiation, mineralization, and bone remodeling (Gordon et al., 2007; Hunter and Goldberg, 1993; Roach, 1994). From the nineteen genetically different collagens found in the body, type I collagen is the predominant type in bone (90 %), with types III, V, X, and XII making up the remainder (Ayad et al., 1998; Buckwalter et al., 1995; Vuorio and Crombrugghe, 1990). Type I collagen is a relatively small (300 nm long, 1.5 nm wide), fibrous protein with very low solubility, composed of three polypeptide chains (i.e., two identical α1 and one unique α2 chain, 1000 amino acids each, cross-linked by hydrogen bondings) and arranged in a triple-helical structure (Fuchs et al., 2009; Morgan et al., 2013). They are organized in parallel with a one-quarter

staggered displacement with respect to each other, forming a fibril that, in turn, twists around other fibrils in opposite directions to form a fiber (Gross and Berndt, 2002).

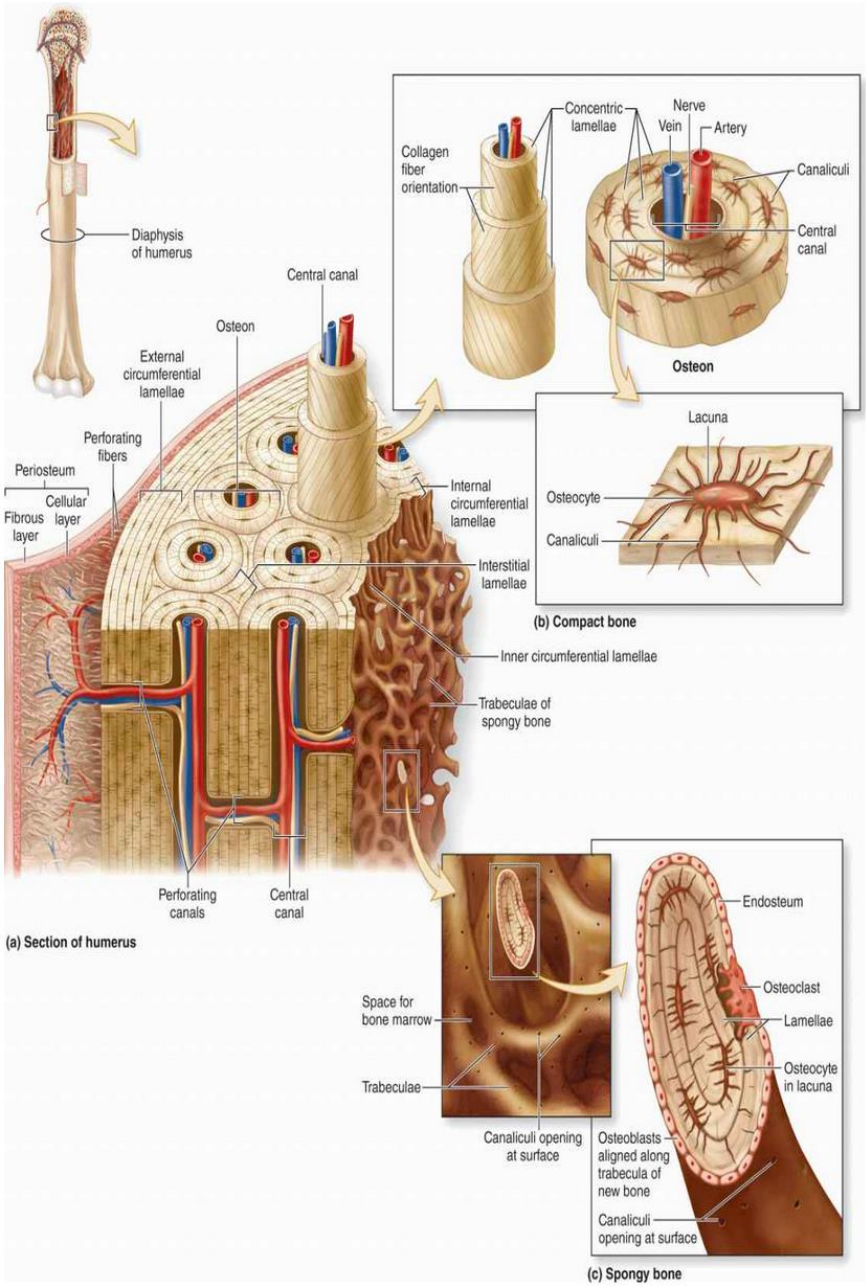

Figure 1.4. *Schematic representation of the microscopic composition of bone, including cortical and trabecular tissues [(taken and adapted from Fuchs et al.* (2009)*].*

The inorganic portion of bone primarily consists of a carbonated calcium-phosphate mineral akin to other apatite minerals and structurally resembles hydroxylapatite [HA: $Ca_{10}(PO_4)_6(OH)_2$; (Hollinger et al., 2011; Trueman and Tuross, 2002)]. However, bone apatite (BA) differs spectroscopically from geological and synthetic variants of HA

(Boskey, 2007; Wopenka and Pasteris, 2005), mostly due to impurities that arrive in the form of elemental substitutions (Morgan et al., 2013), which can arise from various sources, including environmental and biological processes (Tuross, 2003). Substitutions include chlorine (Cl^-) and fluor (F^-) ions replacing hydroxyl (OH^-) groups and trace elements like Na^+, Mg^{2+}, K^+, Sr^{2+}, Zn^{2+}, As^{3+}, Pb^{2+}, Cd^{2+} replacing Ca^{2+} ions (Driessens and Verbeeck, 1990; Elliott, 2002; Gross and Berndt, 2002; McConnell, 1962; Skinner, 2013; Trueman and Tuross, 2002). The most common substitution in BA is carbonate (CO_3^-, approximately seven wt. %) replacing phosphate (PO_4^{3-}) groups [B-type substitution (Wopenka and Pasteris, 2005)], and, to a lesser degree, the OH^- group [A-type substitution (Madupalli et al., 2017)]. These substituent species produce large lattice strains on the BA, reducing its crystallinity and increasing its rates of solubility (Driessens, 1988; Elliott, 2002; Ou-Yang et al., 2001). The BA crystals are smaller (20 - 50 nm long, 15 nm wide, 2 - 5 nm) than those of other calcified tissues like enamel (Morgan et al., 2013) and are organized as plate-shaped crystals found within and around the collagen fibers, following its same orientation, which is also the morphological axis of the bone (Elliott, 2002; Sasaki and Sudoh, 1997). Alone, the inorganic phase is brittle but offers stiffness, whereas the organic phase is flexible but lacks resistance to bending. By intercalating between and around the collagen fibers, the BA crystals can offer structural resistance and remain protected during loading by energy absorption and reversible deformation of the collagen fibers (Seeman, 2008).

1.4.1.3.Homeostasis

Bone homeostasis is the result of a dynamic equilibrium where bones undergo continual microstructural adjustments and mass distributions in response to the body's needs for repair, growth, modeling, and remodeling (Fuchs et al., 2009; Hollinger et al., 2011) (Fig.

1.5.). These actions derive from two fundamental processes: resorption, which mobilizes Ca^{2+} and PO_4^{3-} from bone, and deposition, where these minerals form new bone (Nikita, 2017a). These processes are controlled by the coordinated action of the basic multicellular unit (BMU), which consists of osteoblasts, osteocytes, bone lining cells, and osteoclasts (Andersen et al., 2009; Hauge et al., 2001; Ortner and Turner-walker, 2003). The three first cellular types derive from the mesenchymal stem cell lineage (i.e., osteoprogenitor cells) in the bone marrow and the periosteum, while osteoclasts derive from the hematopoietic lineage (i.e., monocytic-macrophage stem cells) (Hollinger et al., 2011; Morgan et al., 2013).

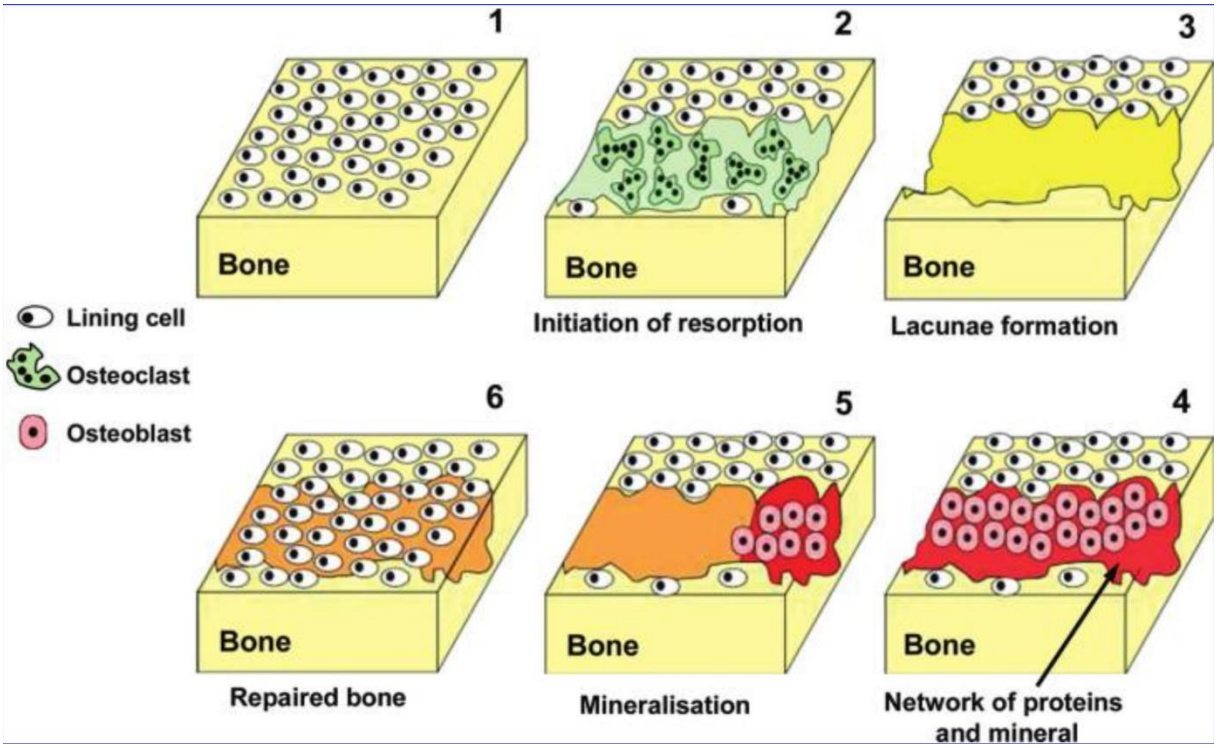

Figure 1.5. *Schematic representation of bone remodeling. (1) Bone lining cells covering intact bone, (2) bone resorption mediated by osteoclast, (3) lacunae formation, (4) Osteoblast division and synthesis of new bone matrix, (5) Secondary mineralization, and (6) osteoblast turn into new bone lining cells [Taken from Vidaud et al. (2012)].*

Osteoblasts are the architects of bone formation, mostly found under the periosteum and near the medullary cavity, where metabolic bone rates are higher (Nikita, 2017a). They are responsible for the synthesis of new bone matrix, a task that is performed in two steps: deposition of the organic matrix (i.e., osteoid) and its subsequent mineralization

(Florencio-Silva et al., 2015; Ortner and Turner-walker, 2003). Once bone synthesis is complete, osteoblasts may either turn into a bone-lining cell (i.e., coating of the bone surface) or undergo apoptosis (i.e., programmed death cell) (Jilka et al., 1998; Manolagas, 2000). However, if osteoblasts get surrounded and encapsulated by the calcified bone matrix, they sustain differentiation into osteocytes, which represent the most abundant and long-lived cellular component in mature mammalian bone (Franz-Odendaal et al., 2006). Osteocytes do not synthesize new bone matrix but perform various vital functions, including mechanical stress sensing, calcium regulation, and cellular communication (Bonewald, 2011; Dallas et al., 2013). Conversely, osteoclasts are tasked with bone resorption by lowering the pH (i.e., through H+ pumping) and secreting lysosomal enzymes (i.e., proteases) for BA dissolution and organic protein digestion, respectively (Morgan et al., 2013; Ortner and Turner-walker, 2003). Bone homeostasis, therefore, depends on the delicate and coordinated balance between the osteoblast-mediated formation and osteoclast-mediated removal (i.e., osteoblast-osteoclast coupling) of bone tissue, a process responsible for the renewal of approximately 4-10% of bone mass annually in humans (Morgan et al., 2013). Imbalances in bone homeostasis lead to pathologies with low bone density, like osteoporosis (Vidaud et al., 2012).

In summary, bone formation is fundamentally an inorganic geochemical process analogous to geological mineralization (Boskey, 2003) but strongly regulated by biological factors (Molenda and Kolmas, 2023; Rey and Combes, 2016; Yamaguchi, 2007).

1.4.1.4.Major and trace element composition

Bone is an essential reservoir of many trace elements, such as calcium (Ca), phosphorus (P), iron (Fe), and zinc (Zn), as well as non-essential elements like strontium (Sr), barium

(Ba), rubidium (Rb) and toxic ones like lead (Pb, Fig. 1.6) (Confavreux, 2011; Copp and Shim, 1963; Harkness and Darrah, 2019). Ca comprises 96% of bone cation content, which is one order of magnitude greater than sodium (Na), two orders of magnitude greater than magnesium (Mg) and potassium (K), and four orders of magnitude greater than Zn and Fe (Harkness and Darrah, 2019).

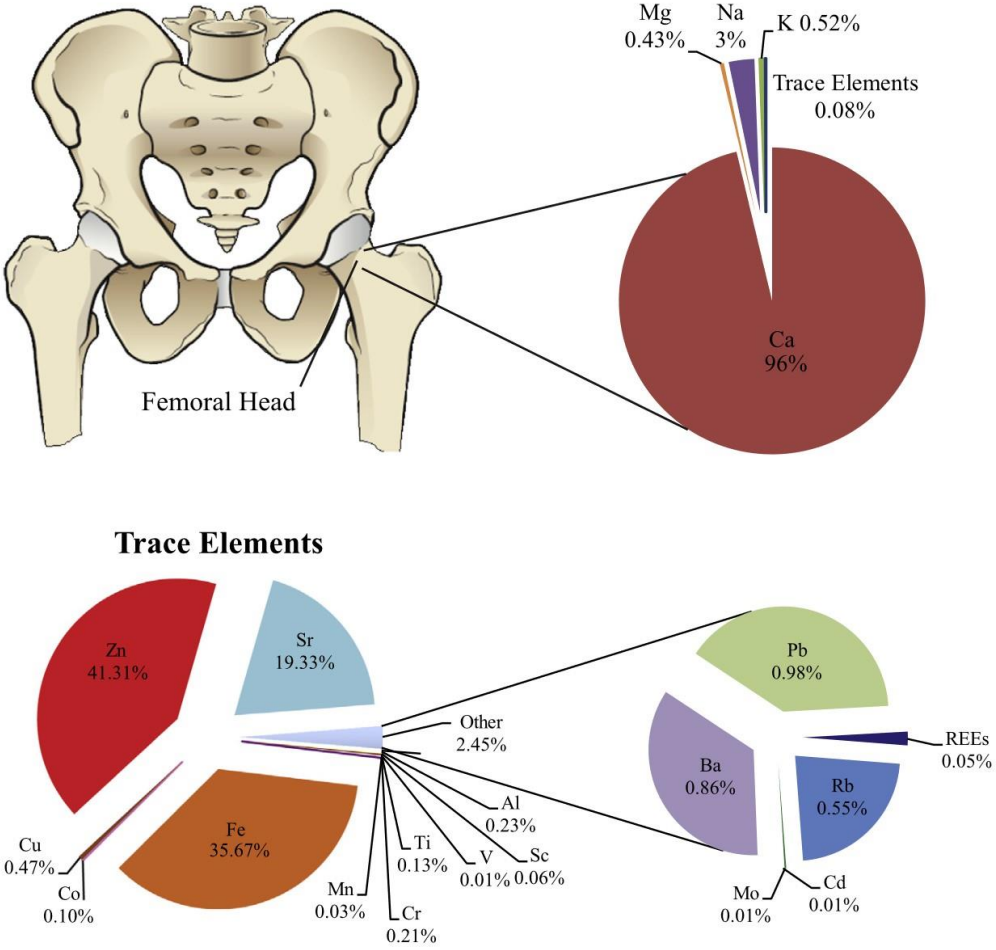

Figure 1.6. *Major and trace element composition in cortical bone. Taken from Harkness & Darrah (2019).*

As a living organ, the skeleton is in constant exchange, incorporating and releasing elements. The trace element incorporation into the human body and, by extension, into bones depends on dietary (food and water), geological, cultural, and environmental inputs

(Harkness and Darrah, 2019). Bio-essential elements are absorbed through the gut and actively transported by divalent metal transporters (Blaby-Haas and Merchant, 2012; Iolascon and De Falco, 2009; Mims and Prchal, 2005), whereas non-essential and rare earth elements (REE) are passively transported along the biological pathway of an essential element with which they share similar chemical properties (Reynard and Balter, 2014). Although significantly reduced from dietary and environmental inputs due to biopurification, the absorption of trace and REE suggests complex biological pathways of incorporation during the life of the individual (Darrah, 2009; Darrah et al., 2009; Harkness and Darrah, 2019).

At normal environmental levels, the body demonstrates a remarkable ability to manage toxic or non-essential element accumulation. It does so through the excretion or the retention of the elements in biochemically inactive forms (Vidaud et al., 2012). Once metals reach the bloodstream, they are either eliminated by filtration in the kidneys or deposited into the skeleton, thus limiting their bioavailability and deleterious effects on the body (Vidaud et al., 2012). The skeleton is the preferential organ for trace element deposition because bones have the remarkable ability to incorporate these in the form of ions into their mineral matrix (Pasteris, 2016). This is due to the crystallographic structure of apatite, which allows the incorporation of a wide variety of elements at relatively high concentrations (> 100 ppm), independently of factors like ionic radius and charge, suggesting that trace element incorporation into BA is not controlled primarily by crystal-chemical effects but rather by enzymatic processes (Reynard and Balter, 2014). In consequence, the chemical composition found in bones is a complex combination of diet (i.e., food and water), exposure (i.e., geogenic and anthropogenic), biopurification, and metabolic processes within the body (Harkness and Darrah, 2019; López-Costas et al., 2016).

1.4.2. Bone in Paleoenvironmental Studies

While the study of archaeological artifacts offers features of how people lived during specific times, skeletal remains from archaeological contexts can provide a wider and sometimes deeper range of information (Weston, 2020) about paleoenvironments (Tütken and Vennemann, 2011). The chemical (Simpson et al., 2021) and isotopic (Bogaard and Outram, 2013) compositions of both the organic and inorganic phases of bone and teeth (i.e., collagen and bioapatite, respectively) can offer important clues about human evolution (Green et al., 2010), life stories (Ericson et al., 1991), habitats (Knudson and Price, 2007), migration (Schweissing and Grupe, 2003) and diet (Richards, 2015) of ancient humans, as well as the environmental conditions in which they lived (López-Costas et al., 2020; Rasmussen et al., 2015). A non-exhaustive summary of the elemental and isotopic tracers in bone and teeth for bioarchaeological and paleoenvironmental studies is presented in Fig. 1.7 and can be found in Schoeninger and Moore (1992), Tütken & Vennemann (2011), Price (2014), and Simpson et al. (2021).

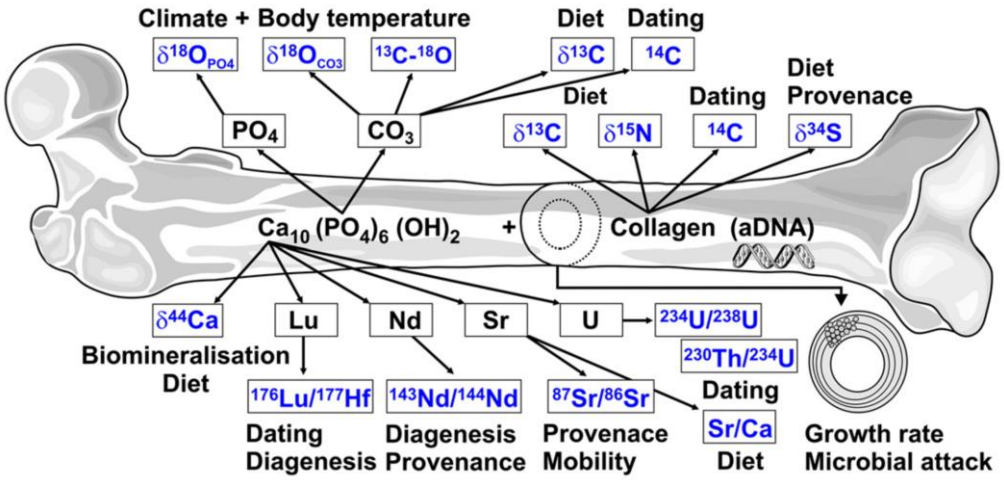

Figure 1.7. *Chemical elements and their isotopes found in bone with potential applications in paleoenvironmental studies [taken from Tütken and Vennemann (2011)].*

1.4.3. Bone diagenesis

One of the most critical questions when working with archaeological bones is whether the biogenic substrate is intact enough to reconstruct paleoenvironments, paleodiets, paleoclimates, and paleopollution (Balter and Zazzo, 2014). After death and once the soft tissues have decomposed, the skeleton undergoes modifications in its structure and composition that are largely dependent on the environment (Christensen et al., 2014). In the context of osteoarcheology, **diagenesis** is any post-depositional (i.e., chemical, physical, or biological) alteration to the bones due to contact with the soil (Price et al., 1992). In essence, diagenesis is a process of stabilization between bone and the soil, which can result in the complete destruction or fossilization of the skeletal remains (Lee-Thorp and Sealy, 2008; Trueman and Martill, 2002).

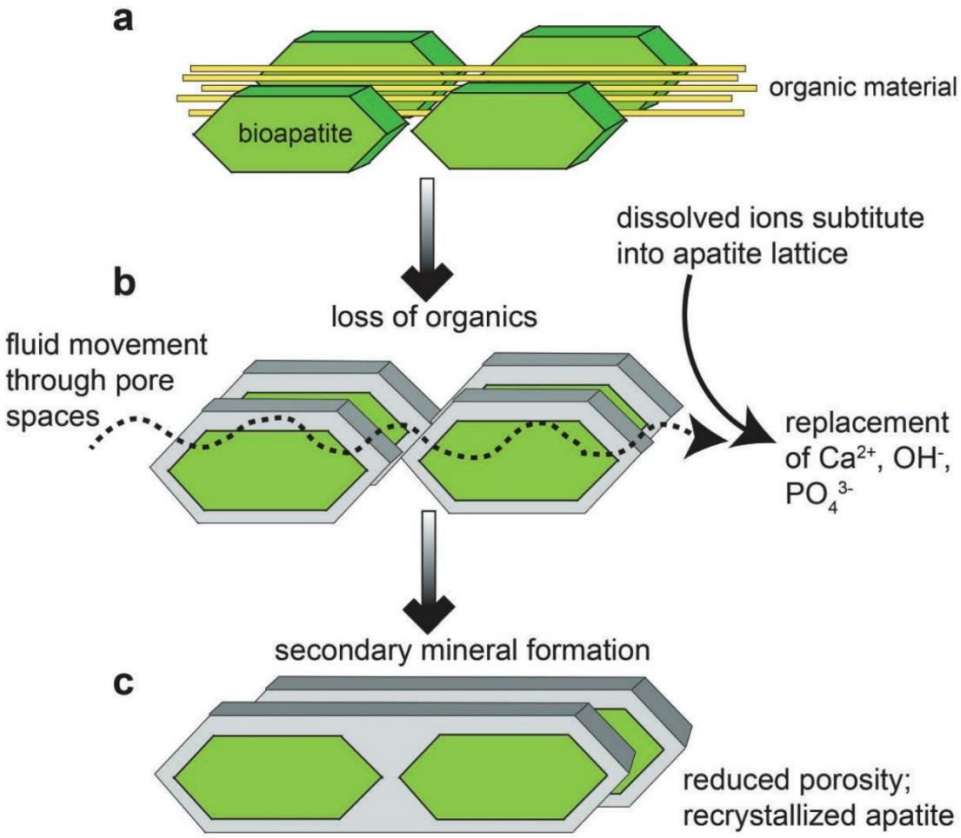

Figure. 1.8. *Schematic representation of diagenetic alteration of bioapatite (BA). [Taken from Keenan (2016)]*

The degree of diagenesis is determined by intrinsic and extrinsic factors. Intrinsic factors (i.e., the pre-mortem configuration) include the initial state of bone preservation, the bone type (i.e., shape, size, structure, and density), and any processing and treatment before burial (Buckberry, 2000; Nielsen-Marsh et al., 2007; Smith et al., 2007; Von Endt and Ortner, 1984). Extrinsic factors include the burial environment, the soil conditions (pH, oxygen, temperature, and groundwater), and bioperturbation [bacteria, fungi, plants, animals (Dal Sasso et al., 2014; Galloway et al., 1997; Nielsen-Marsh et al., 2007; Reiche et al., 2003; Smith et al., 2007; Von Endt and Ortner, 1984)]. Due to both intrinsic and extrinsic factors, diagenesis involves complex, highly variable bone-soil interactions that are site-specific and bone-specific (Dal Sasso et al., 2014; Fabig and Herrmann, 2002; Reiche et al., 2003).

The critical step during diagenesis is the movement of solutes and ions to, from, and within the bone, which is determined by the pore-size distribution and the interaction between bone and groundwater. In consequence, the most important parameters of diagenetic alteration are the hydrology (Kendall et al., 2018; López-Costas et al., 2016; Nielsen-Marsh and Hedges, 2000) and the geochemical composition of the soil (Reiche et al., 2003). The post-mortem uptake of trace and REE can occur in three ways: i) adsorption onto the crystal lattice, ii) direct ion substitution into the crystal lattice, and iii) growth of metal-phosphate phases within the bone (Trueman and Tuross, 2002). In consequence, the major and trace element composition of buried bones can vary within a single bone and between bones buried in the same site (i.e., intra and inter-skeletal variability (Keenan, 2016).

Early diagenesis may begin with the microbial attack and the removal of the collagen, which ensures bone matrix stability (Caruso et al., 2020; Hedges, 2002). The loss of the organic matter can lead to shifts in pore size distribution (i.e., an increase in the

microporosity), leaving the bioapatite exposed to interactions with exogenous fluid (Fig. 1.8) (Hedges et al., 1995; Keenan, 2016). Due to all the vacancies in its crystal structure, bioapatite is relatively unstable and has great flexibility for ionic substitutions, leading to the dissolution of biogenic apatite (Berna et al., 2004) and recrystallization of more stable components, i.e., authigenic apatite and other mineral phases with lower carbonate content (Asscher et al., 2011; Keenan, 2016; Keenan et al., 2015; Kendall et al., 2018; King et al., 2011; Salesse et al., 2014; Trueman, 2013; Trueman and Tuross, 2002). This produces a reduction of the organic and carbonate fractions, accompanied by a reduction of the macroporosity (i.e., Haversian canals and vascular porosity) and an increase in the crystal size and overall crystallinity (Fig. 1.8) (Caruso et al., 2020; Hedges, 2002; Hedges et al., 1995; Nielsen-Marsh and Hedges, 2000).

Considering all this, some diagenetic parameters can be analyzed to estimate the degree of post-mortem alteration. These are histological preservation (microbial damage, internal structure, presence of lamellae or osteocytes), protein content, changes in the overall (micro and macro) porosity, crystallinity of bioapatite, carbonate content, and trace and REE element content and ratios (Fabig and Herrmann, 2002; Hedges et al., 1995; Nielsen-Marsh and Hedges, 2000; Reiche et al., 2003; Trueman and Tuross, 2002).

1.4.4. Ethical considerations of destructive analysis in archaeological remains

The health status and lifestyles of ancient individuals can be elucidated through biogeochemical and molecular analyses performed on skeletal or dental samples (Makarewicz and Sealy, 2015), which can provide considerable and important data for radiocarbon dating (Piotrowska and Goslar, 2002), dietary reconstruction (Schoeninger, 2010), demographic changes (Schweissing and Grupe, 2003), migration (Knudson and Price, 2007), disease (Bos et al., 2011), and genetic variations within and among

populations (Pääbo et al., 2004). However, these analyses require the extraction and destruction of an individual's skeletal remains. Hence, it is critical to evaluate the cost-benefit between the destruction required and the loss of material against the amount of information that can be potentially obtained (Lewis Jr and Tung, 2013). However, the rise in the use of destructive analyses on archaeological remains is somehow followed by improvements and newly developed techniques. As the methods continue to evolve, the required sample amount has progressively decreased, reducing the amount of destruction on archeological remains and supporting their preservation for future research (Squires et al., 2019).

In light of the ethical concerns surrounding the destructive analyses of human skeletal remains (Larsen and Walker, 2012), it is essential to carefully consider several key factors before any data collection and analysis is performed (Lewis Jr and Tung, 2013; Squires et al., 2019):

- Clear, focused research questions that can be specifically addressed by the planned analyses.
- Encouraging interdisciplinary collaboration to maximize the amount of information obtained from different studies on the same sample, including well-established protocols with quality controls that can assure reliable data and qualified personnel experienced in these samples.
- A pilot project on a limited number of individuals to assess feasibility, including collecting complementary samples (i.e., soil, flora, fauna) to better contextualize and interpret the data.
- Obtaining the proper permissions from institutions, agencies, archaeologists, and curators involved in the excavation and conservation of the remains.

- All remnants of samples taken from skeletal remains should be returned and stored with the rest of the skeleton(s) from which the sample(s) were taken.

1.5. PART E: Ancient Metallurgy

1.5.1. Historical use of metals

Mining and metallurgy have been major factors in the development of human civilizations, driving the exploration and long-distance trade of metals (Killick and Fenn, 2012). Among the metals of Antiquity [i.e., copper (Cu), lead (Pb), gold (Au), iron (Fe), mercury (Hg), silver (Ag), and tin (Sn)], all except tin can be found in native form near the surface of the ground, but in limited quantities (Haynes, 2014). The historical progression in the use of metals is related to the free energy of the formation of each metal oxide. Gold is usually found in its native form; Ag, Pb, and Cu are mostly found in the form of sulfides, whereas Fe is mostly in the form of oxides (Killick and Fenn, 2012). Hence, the discovery of a new smelted metal in the archaeological record marks an improvement in the understanding and use of new technologies to reach higher temperatures and lower partial pressures inside the furnace (Killick and Fenn, 2012).

The first metal to be found in the archaeological record is native Cu [around the 12th to the 11th millennia BCE in Iran and the Near East (Solecki, 1969)], whereas the earliest known evidence for the use of native Cu dates back to 9th millennia BCE in Anatolia (Stech, 1999). The next native element to be found in the archaeological record is Au, but much later, i.e., around the mid-fifth millennium BCE, near the Black Sea (Chernykh, 1992). The first evidence of smelting (of Cu) dates back to the 5th millennium BCE in both Iran (Frame, 2012) and Serbia (Radivojević et al., 2010). Hg has been used since the 9th millennium BCE (Goren et al., 2001), but the earliest documented use of it in Europe (i.e., as decorative pigments in ceramics) probably dates back to the 6th millennium BCE

by the Vinča culture of the middle Danube basin (Gajić-Kvaščev et al., 2012). Ag and Pb were smelted and separated through cupellation throughout Southwest Asia as early as the 4th millennium BCE (Pernicka, 2020). Cupellation is a refining technique used for the purification of silver and gold from other base metals (i.e., Pb, Cu, Zn, Sb) present in Au and Ag-bearing ores (Forbes, 1950).

Tin smelting started around the 3rd millennium BCE in Anatolia and the Fertile Crescent and gave way to the discovery and widespread use of bronze in Central Europe (Roberts et al., 2009). Bronze is harder and more durable than copper and thus is superior for tools and weapons manufacturing (Kristiansen and Larsson, 2005). Iron is even harder and tougher than bronze, but more importantly, iron ores were more abundant and more evenly distributed in comparison to tin and copper deposits, which were fairly rare and more expensive to extract during the Bronze Age (Bloch-Smith and Nakhai, 1999). With the achievement of higher temperatures and low partial pressures, iron was obtained around the 2nd millennium BCE and started to replace bronze as the dominant material (Sykes et al., 2016).

The Romans extensively used all these seven metals and advanced metallurgy through large-scale mining, but they also improved the existing smelting techniques (Craddock, 1991; Jouttijärvi, 2017; Lang, 2017). After the fall of the Western Roman Empire, mining and metallurgical activities in Europe declined due to the lack of a centralized organized power. However, much of the metallurgical knowledge was preserved and expanded in the Byzantine Empire and the Islamic Caliphates (Verhoeven et al., 2018; Wertime and Muhly, 1980). One example of this is the production of Damascus steel, which has a high reputation for its high quality and characteristic surface patterns (Wadsworth and Sherby, 1982). Finally, mining and metallurgical activities in central and eastern Europe increased during the High and Late Middle Ages, with notable centers like Saxony, Bohemia, and

the Hartz Mountains (Tylecote, 1992), and other regional mining and metallurgical centers in southeastern Europe (Longman et al., 2024).

1.5.2. Pb use and production in Roman times

Lead (Pb) held significant importance during Antiquity, and especially in ancient Rome, contributing to the development of urban infrastructure, including the construction of lead pipes for freshwater distribution from aqueducts to buildings, as well as being widely utilized in various public and domestic applications (Boulakia, 1972; Delile et al., 2017, 2014; Deming, 2020; Needleman and Needleman, 1985; Nriagu, 1983).

The primary mineral of interest in lead (Pb) production is galena, a lead sulfide ore. The outcrops of mineralized beds or veins also featured cerussite and anglesite, which are galena alteration products. This ore, however, was often found in a mixed state with other sulfides, leading to ores containing zinc, iron, copper, arsenic, antimony, and bismuth (Anthony et al., 2005).

The metallurgical techniques employed during the Bronze and Iron Ages involved a sequence of processes to extract lead from galena. Modern lead metallurgy, in comparison, follows a roasting process of galena, which entails heating it in an oxidizing atmosphere to produce lead oxide (PbO) and sulfur dioxide (SO_2), followed by a reduction step (Cochet, 2000).

In the techniques employed by the ancients, partial roasting at moderate temperatures was a key method. This involved the reaction of lead sulfide (PbS) with oxygen to form lead sulfate ($PbSO_4$, eq. 1). The process, starting around 425 degrees °C, resulted in a mixture of PbO, $PbSO_4$, and PbS (eq. 2 and 3). Subsequent reactions at higher temperatures, such as the reactions between PbS and PbO, produced lead (Pb) and sulfur dioxide (SO_2).

However, these reactions were not complete, leaving a residue containing a significant amount of lead (Cochet, 2000).

$PbS + 2O^{2-} => PbSO_4^{4-}$ (eq. 1)

$PbS + 2PbO => 3Pb + SO_2$ (eq. 2)

$PbS + PbSO_4 => 2Pb + SO_2$ (eq. 3)

In Laurium, an ancient Greek mining region, a different approach was taken. A mixture of cerussite (carbonate) and lead sulfide was treated in cylindrical furnaces, bypassing the roasting phase. The hot carbonate decomposes, leading to the formation of lead oxide (PbO) and carbon dioxide (CO_2)(eq. 4). The subsequent reactions between PbS and PbO then produced lead and sulfur dioxide (Cochet, 2000).

$PbCO_3 => PbO + CO_2$ then $PbS + 2PbO => 3Pb + SO_2$ (eq. 4)

The main aim of these techniques was to oxidize the lead and separate it from the silver. The metal was to be heated only by the gases in the furnace or the radiation from the vault, as contact with a reducing fuel would have prevented oxidation. A current of air blown over the bath's surface induced oxidation, forming litharge (PbO) that floated on the bath and could be carefully removed. The temperature had to be sufficiently high for the litharge to be liquid and, towards the end of the operation, for the silver to also be in a liquid state (Cochet, 2000).

References

Abate, G., Masini, J.C., 2002. Complexation of Cd(II) and Pb(II) with humic acids studied by anodic stripping voltammetry using differential equilibrium functions and discrete site models. Organic Geochemistry 33, 1171–1182. https://doi.org/10.1016/S0146-6380(02)00087-6

Acharya, S., 2013. Lead between the lines. Nature Chem 5, 894–894. https://doi.org/10.1038/nchem.1761

Adhikari, N., Sinha, N., Narayan, R., Saxena, D.K., 2001. Lead-induced cell death in testes of young rats. Journal of Applied Toxicology 21, 275–277. https://doi.org/10.1002/jat.754

Adriano, D.C., 2001. Trace Elements in Terrestrial Environments. Springer, New York, NY. https://doi.org/10.1007/978-0-387-21510-5

Adriano, D.C., 1986. Trace Elements in the Terrestrial Environment. Springer, New York, NY. https://doi.org/10.1007/978-1-4757-1907-9

Albarède, F., 2015. Metal Stable Isotopes in the Human Body: A Tribute of Geochemistry to Medicine. Elements 11, 265–269. https://doi.org/10.2113/gselements.11.4.265

Albarède, F., 2011. Fractionation, Mass Independent and Dependent, in: Gargaud, M., Amils, R., Quintanilla, J.C., Cleaves, H.J. (Jim), Irvine, W.M., Pinti, D.L., Viso, M. (Eds.), Encyclopedia of Astrobiology. Springer, Berlin, Heidelberg, pp. 611–612. https://doi.org/10.1007/978-3-642-11274-4_597

Albarede, F., Télouk, P., Balter, V., Bondanese, V.P., Albalat, E., Oger, P., Bonaventura, P., Miossec, P., Fujii, T., 2016. Medical applications of Cu, Zn, and S isotope effects. Metallomics 8, 1056–1070. https://doi.org/10.1039/C5MT00316D

Alfano, D.P., Petit, T.L., 1982. Neonatal lead exposure alters the dendritic development of hippocampal dentate granule cells. Experimental Neurology 75, 275–288. https://doi.org/10.1016/0014-4886(82)90160-1

Allègre, C.J., Poirier, J.-P., Humler, E., Hofmann, A.W., 1995. The chemical composition of the Earth. Earth and Planetary Science Letters 134, 515–526. https://doi.org/10.1016/0012-821X(95)00123-T

Ambrose, S.H., Krigbaum, J., 2003. Bone chemistry and bioarchaeology. Journal of Anthropological Archaeology, Bone Chemistry and Bioarchaeology 22, 193–199. https://doi.org/10.1016/S0278-4165(03)00033-3

Andersen, T.L., Sondergaard, T.E., Skorzynska, K.E., Dagnaes-Hansen, F., Plesner, T.L., Hauge, E.M., Plesner, T., Delaisse, J.-M., 2009. A Physical Mechanism for Coupling Bone Resorption and Formation in Adult Human Bone. The American Journal of Pathology 174, 239–247. https://doi.org/10.2353/ajpath.2009.080627

Angrand, R.C., Collins, G., Landrigan, P.J., Thomas, V.M., 2022. Relation of blood lead levels and lead in gasoline: an updated systematic review. Environmental Health 21, 138. https://doi.org/10.1186/s12940-022-00936-x

Anthony, J.W., Bideaux, R.A., Bladh, K.W., Nichols, M.C. (Eds.), 2005. Handbook of Mineralogy. Mineralogical Society of America, Chantilly, VA.

Apicius, 1984. The Roman Cookery of Apicius: A Treasury of Gourmet Recipes & Herbal Cookery. Hartley & Marks.

Arimoto, R., Duce, R.A., Ray, B.J., Hewitt, A.D., Williams, J., 1987. Trace elements in the atmosphere of American Samoa: Concentrations and deposition to the tropical South Pacific. Journal of Geophysical Research: Atmospheres 92, 8465–8479. https://doi.org/10.1029/JD092iD07p08465

Asscher, Y., Weiner, S., Boaretto, E., 2011. Variations in Atomic Disorder in Biogenic Carbonate Hydroxyapatite Using the Infrared Spectrum Grinding Curve Method. Advanced Functional Materials 21, 3308–3313. https://doi.org/10.1002/adfm.201100266

ATSDR, 2020. Toxicological profile for lead. CDC.

Audi, G., Bersillon, O., Blachot, J., Wapstra, A.H., 2003. The Nubase evaluation of nuclear and decay properties. Nuclear Physics A, The 2003 NUBASE and Atomic Mass Evaluations 729, 3–128. https://doi.org/10.1016/j.nuclphysa.2003.11.001

Ayad, S., Boot-Handford, R., Humphries, M., Kadler, K., Shuttleworth, A., 1998. The Extracellular Matrix Factsbook, 2nd ed. Academic Press.

Bacon, M.P., Spencer, D.W., Brewer, P.G., 1976. 210Pb/226Ra and 210Po/210Pb disequilibria in seawater and suspended particulate matter. Earth and Planetary Science Letters 32, 277–296. https://doi.org/10.1016/0012-821X(76)90068-6

Balter, V., Lamboux, A., Zazzo, A., Télouk, P., Leverrier, Y., Marvel, J., Moloney, A.P., Monahan, F.J., Schmidt, O., Albarède, F., 2013. Contrasting Cu, Fe, and Zn isotopic patterns in organs and body fluids of mice and sheep, with emphasis on cellular fractionation. Metallomics 5, 1470–1482. https://doi.org/10.1039/c3mt00151b

Balter, V., Zazzo, A., 2014. Bone and enamel diagenesis: From the crystal to the environment — A tribute to Jean-François Saliège. Palaeogeography, Palaeoclimatology, Palaeoecology, Bone and enamel diagenesis: From the crystal to the environment - A tribute to Jean-François Saliège 416, 1–3. https://doi.org/10.1016/j.palaeo.2014.09.017

Bandmann, O., Weiss, K.H., Kaler, S.G., 2015. Wilson's disease and other neurological copper disorders. The Lancet Neurology 14, 103–113. https://doi.org/10.1016/S1474-4422(14)70190-5

Barbosa, F., Tanus-Santos, J.E., Gerlach, R.F., Parsons, P.J., 2005. A critical review of biomarkers used for monitoring human exposure to lead: advantages, limitations, and future needs. Environ Health Perspect 113, 1669–1674. https://doi.org/10.1289/ehp.7917

Barry, P.S.I., 1975. A Comparison of Concentrations of Lead in Human Tissues. British Journal of Industrial Medicine 32, 119–139.

Bellinger, D., Leviton, A., Waternaux, C., Needleman, H., Rabinowitz, M., 1987. Longitudinal Analyses of Prenatal and Postnatal Lead Exposure and Early Cognitive Development. New England Journal of Medicine 316, 1037–1043. https://doi.org/10.1056/NEJM198704233161701

Berglund, M., Wieser, M.E., 2011. Isotopic compositions of the elements 2009 (IUPAC Technical Report). Pure and Applied Chemistry 83, 397–410. https://doi.org/10.1351/PAC-REP-10-06-02

Berna, F., Matthews, A., Weiner, S., 2004. Solubilities of bone mineral from archaeological sites: the recrystallization window. Journal of Archaeological Science 31, 867–882. https://doi.org/10.1016/j.jas.2003.12.003

Bertinetti, S., Ardini, F., Vecchio, M.A., Caiazzo, L., Grotti, M., 2020. Isotopic analysis of snow from Dome C indicates changes in the source of atmospheric lead over the last fifty years in East Antarctica. Chemosphere 255, 126858. https://doi.org/10.1016/j.chemosphere.2020.126858

Blaby-Haas, C.E., Merchant, S.S., 2012. The ins and outs of algal metal transport. Biochimica et Biophysica Acta (BBA) - Molecular Cell Research, Cell Biology of Metals 1823, 1531–1552. https://doi.org/10.1016/j.bbamcr.2012.04.010

Bloch-Smith, E., Nakhai, B.A., 1999. A Landscape Comes to Life: The Iron Age I. Near Eastern Archaeology 62, 62–127. https://doi.org/10.2307/3210703

Bodek, I., Lyman, W.J., Reehl, W.F., Rosenblatt, D.H., 1988. Environmental inorganic chemistry: properties, processes, and estimation methods, SETAC special publications series. Pergamon Press, New York.

Bogaard, A., Outram, A.K., 2013. Palaeodiet and beyond: stable isotopes in bioarchaeology. World Archaeology 45, 333–337. https://doi.org/10.1080/00438243.2013.829272

Bonewald, L.F., 2011. The amazing osteocyte. Journal of Bone and Mineral Research 26, 229–238. https://doi.org/10.1002/jbmr.320

Bos, K.I., Schuenemann, V.J., Golding, G.B., Burbano, H.A., Waglechner, N., Coombes, B.K., McPhee, J.B., DeWitte, S.N., Meyer, M., Schmedes, S., Wood, J., Earn, D.J.D., Herring, D.A., Bauer, P., Poinar, H.N., Krause, J., 2011. A draft genome of Yersinia pestis from victims of the Black Death. Nature 478, 506–510. https://doi.org/10.1038/nature10549

Boskey, A.L., 2007. Mineralization of Bones and Teeth. Elements 3, 385–391. https://doi.org/10.2113/GSELEMENTS.3.6.385

Boskey, A.L., 2003. Biomineralization: An Overview. Connective Tissue Research 44, 5–9. https://doi.org/10.1080/03008200390152007

Boulakia, J.D.C., 1972. Lead in the Roman World. American Journal of Archaeology 76, 139–144. https://doi.org/10.2307/503857

Boutron, C.F., Patterson, C.C., 1987. Relative levels of natural and anthropogenic lead in recent Antarctic snow. Journal of Geophysical Research: Atmospheres 92, 8454–8464. https://doi.org/10.1029/JD092iD07p08454

Boyle, E.A., Chapnick, S.D., Shen, G.T., Bacon, M.P., 1986. Temporal variability of lead in the western North Atlantic. Journal of Geophysical Research: Oceans 91, 8573–8593. https://doi.org/10.1029/JC091iC07p08573

Boyle, E.A., Lee, J.-M., Echegoyen, Y., Noble, A., Moos, S., Carrasco, G., Zhao, N., Kayser, R., Zhang, J., Gamo, T., Obata, H., Norisuye, K., 2014. Anthropogenic Lead Emissions in the Ocean: The Evolving Global Experiment. Oceanography 27, 69–75.

Bradl, H.B., 2004. Adsorption of heavy metal ions on soils and soils constituents. Journal of Colloid and Interface Science 277, 1–18. https://doi.org/10.1016/j.jcis.2004.04.005

Brännvall, M.-L., Bindler, R., Emteryd, O., Renberg, I., 2001. Vertical Distribution of Atmospheric Pollution Lead in Swedish Boreal Forest Soils. Water, Air, & Soil Pollution: Focus 1, 357–370. https://doi.org/10.1023/A:1017513802959

Bressler, J.P., Goldstein, G.W., 1991. Mechanisms of lead neurotoxicity. Biochemical Pharmacology 41, 479–484. https://doi.org/10.1016/0006-2952(91)90617-E

Brito, J.A.A., McNeill, F.E., Webber, C.E., Wells, S., Richard, N., Carvalho, M.L., Chettle, D.R., 2002. Evaluation of a novel structural model to describe the endogenous release of lead from bone. J. Environ. Monit. 4, 194–201. https://doi.org/10.1039/B108817C

Brookins, D.G., 1988. Lead, in: Brookins, D.G. (Ed.), Eh-pH Diagrams for Geochemistry. Springer, Berlin, Heidelberg, pp. 42–43. https://doi.org/10.1007/978-3-642-73093-1_16

Buckberry, J., 2000. Missing, Presumed Buried? Bone Diagenesis and the Under-Representation of Anglo-Saxon Children.

Buckwalter, J.A., Glimcher, M.J., Cooper, R.R., Recker, R., 1995. Bone Biology. Journal of Bone and Joint Surgery 77, 1256.

Buesseler, K.O., Lamborg, C., Cai, P., Escoube, R., Johnson, R., Pike, S., Masque, P., McGillicuddy, D., Verdeny, E., 2008. Particle fluxes associated with mesoscale eddies in the Sargasso Sea. Deep Sea Research Part II: Topical Studies in Oceanography, Mesoscale Physical-Biological-Biogeochemical Linkages in the Open Ocean: Results from the E-FLUX and EDDIES Programs 55, 1426–1444. https://doi.org/10.1016/j.dsr2.2008.02.007

Buffle, J., Chalmers, R.A., Masson, M.R., Midgley, D., 1988. Complexation Reactions in Aquatic Systems: An Analytical Approach. E. Horwood.

Buikstra, J.E., 2010. Paleopathology: A Contemporary Perspective, in: A Companion to Biological Anthropology. pp. 395–411. https://doi.org/10.1002/9781444320039.ch22

Buikstra, J.E., DeWitte, S., 2019. A Brief History and 21st Century Challenges, in: Buikstra, J.E. (Ed.), Ortner's Identification of Pathological Conditions in Human Skeletal Remains (Third Edition). Academic Press, San Diego, pp. 11–19. https://doi.org/10.1016/B978-0-12-809738-0.00002-8

Burstein, S.M., Finch, C.E., 2022. Lead Poisoning in Ancient Rome: The State of the Question. Journal of Ancient Civilizations 37, 225–246. https://doi.org/10.16758/j.cnki.1004-9371.2022.04.015

Bushnell, P.J., Bowman, R.E., 1979. Effects of chronic lead ingestion on social development in infant rhesus monkeys. Neurobehav Toxicol 1, 207–219.

Canfield, R.L., Henderson, C.R., Cory-Slechta, D.A., Cox, C., Jusko, T.A., Lanphear, B.P., 2003. Intellectual Impairment in Children with Blood Lead Concentrations below 10 μg per Deciliter. New England Journal of Medicine 348, 1517–1526. https://doi.org/10.1056/NEJMoa022848

Caruso, V., Marinoni, N., Diella, V., Berna, F., Cantaluppi, M., Mancini, L., Trombino, L., Cattaneo, C., Pastero, L., Pavese, A., 2020. Bone diagenesis in archaeological and contemporary human remains: an investigation of bone 3D microstructure and minero-chemical assessment. Archaeol Anthropol Sci 12, 162. https://doi.org/10.1007/s12520-020-01090-6

Centers for Disease Control and Prevention (CDC), 2005. Blood lead levels--United States, 1999-2002. MMWR Morb Mortal Wkly Rep 54, 513–516.

Chamel, G., Gourlan, A.T., Télouk, P., Sayag, D., Milliard, V., Loiseau, C., Simon, M., Buff, S., Ponce, F., 2017. Retrospective evaluation of blood copper stable isotopes ratio 65Cu/63Cu as a biomarker of cancer in dogs. Veterinary and Comparative Oncology 15, 1323–1332. https://doi.org/10.1111/vco.12273

Cheema, A.I., Liu, G., Yousaf, B., Abbas, Q., Zhou, H., 2020. A comprehensive review of biogeochemical distribution and fractionation of lead isotopes for source tracing in distinct interactive environmental compartments. Science of The Total Environment 719, 135658. https://doi.org/10.1016/j.scitotenv.2019.135658

Chelly, J., Tümer, Z., Tønnesen, T., Petterson, A., Ishikawa-Brush, Y., Tommerup, N., Horn, N., Monaco, A.P., 1993. Isolation of a candidate gene for Menkes disease that encodes a potential heavy metal binding protein. Nat Genet 3, 14–19. https://doi.org/10.1038/ng0193-14

Chernykh, E.N., 1992. Ancient metallurgy in the USSR: the early metal age / E.N. Chernykh ; translated by Sarah Wright., New studies in archaeology. Cambridge University Press, New York.

Christensen, A.M., Passalacqua, N.V., Bartelink, E.J., 2014. Chapter 5 - Forensic Taphonomy, in: Christensen, A.M., Passalacqua, N.V., Bartelink, E.J. (Eds.), Forensic Anthropology. Academic Press, San Diego, pp. 119–147. https://doi.org/10.1016/B978-0-12-418671-2.00005-7

Clark, I.D., Fritz, P., 1997. Environmental Isotopes in Hydrogeology. CRC Press, Boca Raton. https://doi.org/10.1201/9781482242911

Cochet, A., 2000. Le Plomb en Gaule romaine. Techniques de fabrication et produits, Editions Mergoil. ed.

Confavreux, C.B., 2011. Bone: from a reservoir of minerals to a regulator of energy metabolism. Kidney International, 50 Years of Research and Discovery in Chronic Kidney Disease and Mineral & Bone Disorder: The Central Role of Phosphate 79, S14–S19. https://doi.org/10.1038/ki.2011.25

Copp, D.H., Shim, S.S., 1963. The homeostatic function of bone as a mineral reservoir. Oral Surgery, Oral Medicine, Oral Pathology 16, 738–744. https://doi.org/10.1016/0030-4220(63)90081-1

Costas-Rodríguez, M., Delanghe, J., Vanhaecke, F., 2016. High-precision isotopic analysis of essential mineral elements in biomedicine: natural isotope ratio variations as potential diagnostic and/or prognostic markers. TrAC Trends in Analytical Chemistry 76, 182–193. https://doi.org/10.1016/j.trac.2015.10.008

Craddock, P., 1991. 4. Mining and Smelting in Antiquity, in: Science and the Past. University of Toronto Press, pp. 57–73. https://doi.org/10.3138/9781442679634-007

Cullen, J.T., McAlister, J., 2017. 2. Biogeochemistry of Lead. Its Release to the Environment and Chemical Speciation, in: Lead: Its Effects on Environment and Health. De Gruyter, pp. 21–48. https://doi.org/10.1515/9783110434330-002

Dal Sasso, G., Maritan, L., Usai, D., Angelini, I., Artioli, G., 2014. Bone diagenesis at the micro-scale: Bone alteration patterns during multiple burial phases at Al Khiday (Khartoum, Sudan) between the Early Holocene and the II century AD. Palaeogeography, Palaeoclimatology, Palaeoecology, Bone and enamel diagenesis: From the crystal to the environment - A tribute to Jean-François Saliège 416, 30–42. https://doi.org/10.1016/j.palaeo.2014.06.034

Dallas, S.L., Prideaux, M., Bonewald, L.F., 2013. The Osteocyte: An Endocrine Cell … and More. Endocrine Reviews 34, 658–690. https://doi.org/10.1210/er.2012-1026

Darrah, T., 2009. Inorganic trace element composition of modern human bones : relation to bone pathology and geographical provenance.

Darrah, T.H., Prutsman-Pfeiffer, J.J., Poreda, R.J., Ellen Campbell, M., Hauschka, P.V., Hannigan, R.E., 2009. Incorporation of excess gadolinium into human bone from medical contrast agents. Metallomics 1, 479–488. https://doi.org/10.1039/b905145g

Degryse, F., Smolders, E., Parker, D.R., 2009. Partitioning of metals (Cd, Co, Cu, Ni, Pb, Zn) in soils: concepts, methodologies, prediction and applications – a review. European Journal of Soil Science 60, 590–612. https://doi.org/10.1111/j.1365-2389.2009.01142.x

Delile, H., Blichert-Toft, J., Goiran, J.-P., Keay, S., Albarède, F., 2014. Lead in ancient Rome's city waters. Proceedings of the National Academy of Sciences 111, 6594–6599. https://doi.org/10.1073/pnas.1400097111

Delile, H., Keenan-Jones, D., Blichert-Toft, J., Goiran, J.-P., Arnaud-Godet, F., Albarède, F., 2017. Rome's urban history inferred from Pb-contaminated waters trapped in its ancient harbor basins. Proceedings of the National Academy of Sciences 114, 10059–10064. https://doi.org/10.1073/pnas.1706334114

Deming, D., 2020. The Aqueducts and Water Supply of Ancient Rome. Groundwater 58, 152–161. https://doi.org/10.1111/gwat.12958

Driessens, F.C.M., 1988. Physiology of Hard Tissues in Comparison with the Solubility of Synthetic Calcium Phosphates. Annals of the New York Academy of Sciences 523, 131–136. https://doi.org/10.1111/j.1749-6632.1988.tb38507.x

Driessens, F.C.M., Verbeeck, R.M.H., 1990. Biominerals. CRC Press, Boca Raton.

Duce, R.A., Liss, P.S., Merrill, J.T., Atlas, E.L., Buat-Menard, P., Hicks, B.B., Miller, J.M., Prospero, J.M., Arimoto, R., Church, T.M., Ellis, W., Galloway, J.N., Hansen, L., Jickells, T.D., Knap, A.H., Reinhardt, K.H., Schneider, B., Soudine, A., Tokos, J.J., Tsunogai, S., Wollast, R., Zhou, M., 1991. The atmospheric input of trace species to the world ocean. Global Biogeochemical Cycles 5, 193–259. https://doi.org/10.1029/91GB01778

Eisinger, J., 1982. Lead and wine. Eberhard Gockel and the colica Pictonum. Medical History 26, 279–302. https://doi.org/10.1017/S0025727300041508

Elliott, J.C., 2002. Calcium Phosphate Biominerals. Reviews in Mineralogy and Geochemistry 48, 427–453. https://doi.org/10.2138/rmg.2002.48.11

Erel, Y., Morgan, J.J., Patterson, C.C., 1991. Natural levels of lead and cadmium in a remote mountain stream. Geochimica et Cosmochimica Acta 55, 707–719. https://doi.org/10.1016/0016-7037(91)90335-3

Ericson, B., Hu, H., Nash, E., Ferraro, G., Sinitsky, J., Taylor, M.P., 2021. Blood lead levels in low-income and middle-income countries: a systematic review. The Lancet Planetary Health 5, e145–e153. https://doi.org/10.1016/S2542-5196(20)30278-3

Ericson, J.E., Smith, D.R., Flegal, A.R., 1991. Skeletal concentrations of lead, cadmium, zinc, and silver in ancient North American Pecos Indians. Environmental Health Perspectives 93, 217–223. https://doi.org/10.1289/ehp.9193217

Fabig, A., Herrmann, B., 2002. Trace elements in buried human bones: intra-population variability of Sr/Ca and Ba/Ca ratios – diet or diagenesis? Naturwissenschaften 89, 115–119. https://doi.org/10.1007/s00114-001-0294-7

Fahy, G.E., Deter, C., Pitfield, R., Miszkiewicz, J.J., Mahoney, P., 2017. Bone deep: Variation in stable isotope ratios and histomorphometric measurements of bone remodelling within adult humans. Journal of Archaeological Science 87, 10–16. https://doi.org/10.1016/j.jas.2017.09.009

Faure, G., 1986. Principles of isotope geology. New York : Wiley.

Fergusson, D.M., Horwood, L.J., Lynskey, M.T., 1997. Early Dentine Lead Levels and Educational Outcomes at 18 Years. Journal of Child Psychology and Psychiatry 38, 471–478. https://doi.org/10.1111/j.1469-7610.1997.tb01532.x

Fewtrell, L.J., Prüss-Üstün, A., Landrigan, P., Ayuso-Mateos, J.L., 2004. Estimating the global burden of disease of mild mental retardation and cardiovascular diseases from environmental lead exposure. Environmental Research 94, 120–133. https://doi.org/10.1016/S0013-9351(03)00132-4

Filella, M., Town, R.M., Buffle, J., 2001. Chemical Speciation in the Environment, 2nd Edition | Wiley, in: Ure, A.M., Davidson, C.M. (Eds.), Chemical Speciation in the Environment. p. 480.

Fisher, N.S., Cochran, J.K., Krishnaswami, S., Livingston, H.D., 1988. Predicting the oceanic flux of radionuclides on sinking biogenic debris. Nature 335, 622–625. https://doi.org/10.1038/335622a0

Flaux, C., Save, S., Scrinzi, M., Larousse, N.M., Vaschalde, C., Renaud, A., Tillier, M., Guihou, A., Deschamps, P., Véron, A., 2023. Roman-era alluvial waste in the Vistre de la Fontaine (Nîmes, southeast France): from a sacred spring to a contaminated river. Journal of Roman Archaeology 36, 50–72. https://doi.org/10.1017/S1047759423000132

Flegal, A.R., Gallon, C., Ganguli, P.M., Conaway, C.H., 2013. All the Lead in China. Critical Reviews in Environmental Science and Technology 43, 1869–1944. https://doi.org/10.1080/10643389.2012.671738

Florencio-Silva, R., Sasso, G.R. da S., Sasso-Cerri, E., Simões, M.J., Cerri, P.S., 2015. Biology of Bone Tissue: Structure, Function, and Factors That Influence Bone Cells. BioMed Research International 2015, e421746. https://doi.org/10.1155/2015/421746

Foldes, J., Parfitt, A.M., Shih, M.S., Rao, D.S., Kleerekoper, M., 1991. Structural and geometric changes in iliac bone: Relationship to normal aging and osteoporosis. Journal of Bone and Mineral Research 6, 759–766. https://doi.org/10.1002/jbmr.5650060714

Forbes, R.J., 1950. Metallurgy in Antiquity: A Notebook for Archaeologists and Technologists. Brill Archive.

Fox, D.A., Campbell, M.L., Blocker, Y.S., 1997. Functional alterations and apoptotic cell death in the retina following developmental or adult lead exposure. Neurotoxicology 18, 645–664.

Frame, L.D., 2012. Reconstructing Ancient Technologies: Chalcolithic Crucible Smelting at Tal-i Iblis, Iran, in: Jett, P., McCarthy, B., Douglas, J.G. (Eds.), Scientific Research on Ancient Asian Metallurgy. London, pp. 181–202.

Franz-Odendaal, T.A., Hall, B.K., Witten, P.E., 2006. Buried alive: How osteoblasts become osteocytes. Developmental Dynamics 235, 176–190. https://doi.org/10.1002/dvdy.20603

Fu, J., Tang, X.-L., Zhang, J., Balzer, W., 2013. Estuarine modification of dissolved and particulate trace metals in major rivers of East-Hainan, China. Continental Shelf Research, Land – Sea Interactions in Tropical Ecosystems of Hainan, China 57, 59–72. https://doi.org/10.1016/j.csr.2012.06.015

Fuchs, R.K., Warden, S.J., Turner, C.H., 2009. 2 - Bone anatomy, physiology and adaptation to mechanical loading, in: Planell, J.A., Best, S.M., Lacroix, D., Merolli, A. (Eds.), Bone Repair Biomaterials, Woodhead Publishing Series in Biomaterials. Woodhead Publishing, pp. 25–68. https://doi.org/10.1533/9781845696610.1.25

Gajić-Kvaščev, M., Stojanović, M.M., Šmit, Ž., Kantarelou, V., Karydas, A.G., Šljivar, D., Milovanović, D., Andrić, V., 2012. New evidence for the use of cinnabar as a colouring pigment in the Vinča culture. Journal of Archaeological Science 39, 1025–1033. https://doi.org/10.1016/j.jas.2011.11.023

Galloway, A., Snyder, L., Willey, P., 1997. Human Bone Mineral Densities and Survival of Bone Elements: A Contemporary Sample, in: Haglund, W., Sorg, M. (Eds.), Forensic Taphonomy: The Post Mortem Fate of Human Remains. CRC Press. https://doi.org/10.1201/9781439821923.ch19

Gordon, J.A.R., Tye, C.E., Sampaio, A.V., Underhill, T.M., Hunter, G.K., Goldberg, H.A., 2007. Bone sialoprotein expression enhances osteoblast differentiation and matrix mineralization *in vitro*. Bone 41, 462–473. https://doi.org/10.1016/j.bone.2007.04.191

Goren, Y., Goring-Morris, A.N., Segal, I., 2001. The Technology of Skull Modelling in the Pre-Pottery Neolithic B (PPNB): Regional Variability, the Relation of Technology and Iconography and their Archaeological Implications. Journal of Archaeological Science 28, 671–690. https://doi.org/10.1006/jasc.1999.0573

Green, R.E., Krause, J., Briggs, A.W., Maricic, T., Stenzel, U., Kircher, M., Patterson, N., Li, H., Zhai, W., Fritz, M.H.-Y., Hansen, N.F., Durand, E.Y., Malaspinas, A.-S., Jensen, J.D., Marques-Bonet, T., Alkan, C., Prüfer, K., Meyer, M., Burbano,

H.A., Good, J.M., Schultz, R., Aximu-Petri, A., Butthof, A., Höber, B., Höffner, B., Siegemund, M., Weihmann, A., Nusbaum, C., Lander, E.S., Russ, C., Novod, N., Affourtit, J., Egholm, M., Verna, C., Rudan, P., Brajkovic, D., Kucan, Ž., Gušic, I., Doronichev, V.B., Golovanova, L.V., Lalueza-Fox, C., de la Rasilla, M., Fortea, J., Rosas, A., Schmitz, R.W., Johnson, P.L.F., Eichler, E.E., Falush, D., Birney, E., Mullikin, J.C., Slatkin, M., Nielsen, R., Kelso, J., Lachmann, M., Reich, D., Pääbo, S., 2010. A Draft Sequence of the Neandertal Genome. Science 328, 710–722. https://doi.org/10.1126/science.1188021

Gross, K.A., Berndt, C.C., 2002. Biomedical Application of Apatites. Reviews in Mineralogy and Geochemistry 48, 631–672. https://doi.org/10.2138/rmg.2002.48.17

Gulson, B.L., Mahaffey, K.R., Mizon, K.J., Korsch, M.J., Cameron, M.A., Vimpani, G., 1995. Contribution of tissue lead to blood lead in adult female subjects based on stable lead isotope methods. J Lab Clin Med 125, 703–712.

Halstead, M.J.R., Cunninghame, R.G., Hunter, K.A., 2000. Wet deposition of trace metals to a remote site in Fiordland, New Zealand. Atmospheric Environment 34, 665–676. https://doi.org/10.1016/S1352-2310(99)00185-5

Han, F.X., Banin, A., Su, Y., Monts, D.L., Plodinec, J.M., Kingery, W.L., Triplett, G.E., 2002. Industrial age anthropogenic inputs of heavy metals into the pedosphere. Naturwissenschaften 89, 497–504. https://doi.org/10.1007/s00114-002-0373-4

Harkness, J.S., Darrah, T.H., 2019. From the crust to the cortical: The geochemistry of trace elements in human bone. Geochimica et Cosmochimica Acta 249, 76–94. https://doi.org/10.1016/j.gca.2019.01.019

Harris, E.D., 1991. Copper Transport: An Overview. Proceedings of the Society for Experimental Biology and Medicine 196, 130–140. https://doi.org/10.3181/00379727-196-43171B

Hasan, N.M., Lutsenko, S., 2012. Chapter Six - Regulation of Copper Transporters in Human Cells, in: Argüello, J.M., Lutsenko, S. (Eds.), Current Topics in Membranes, Metal Transporters. Academic Press, pp. 137–161. https://doi.org/10.1016/B978-0-12-394390-3.00006-9

Hastuti, A.A.M.B., Costas-Rodríguez, M., Matsunaga, A., Ichinose, T., Hagiwara, S., Shimura, M., Vanhaecke, F., 2020. Cu and Zn isotope ratio variations in plasma for survival prediction in hematological malignancy cases. Sci Rep 10, 16389. https://doi.org/10.1038/s41598-020-71764-7

Hauge, E.M., Qvesel, D., Eriksen, E.F., Mosekilde, L., Melsen, F., 2001. Cancellous Bone Remodeling Occurs in Specialized Compartments Lined by Cells Expressing Osteoblastic Markers. Journal of Bone and Mineral Research 16, 1575–1582. https://doi.org/10.1359/jbmr.2001.16.9.1575

Haynes, W.M. (Ed.), 2014. CRC Handbook of Chemistry and Physics, 95th ed. CRC Press, Boca Raton. https://doi.org/10.1201/b17118

He, L., Poblenz, A.T., Medrano, C.J., Fox, D.A., 2000. Lead and Calcium Produce Rod Photoreceptor Cell Apoptosis by Opening the Mitochondrial Permeability Transition Pore*. Journal of Biological Chemistry 275, 12175–12184. https://doi.org/10.1074/jbc.275.16.12175

Hedges, R.E.M., 2002. Bone diagenesis: an overview of processes. Archaeometry 44, 319–328. https://doi.org/10.1111/1475-4754.00064

Hedges, R.E.M., Millard, A.R., Pike, A.W.G., 1995. Measurements and Relationships of Diagenetic Alteration of Bone from Three Archaeological Sites. Journal of Archaeological Science 22, 201–209. https://doi.org/10.1006/jasc.1995.0022

Heinrichs, H., Schulz-Dobrick, B., Wedepohl, K.H., 1980. Terrestrial geochemistry of Cd, Bi, Tl, Pb, Zn and Rb. Geochimica et Cosmochimica Acta 44, 1519–1533. https://doi.org/10.1016/0016-7037(80)90116-7

Heintzenberg, J., Covert, D.C., Dingenen, R. van, 2000. Size distribution and chemical composition of marine aerosols: a compilation and review 52, 1104–1122. https://doi.org/10.3402/tellusb.v52i4.17090

Hettiarachchi, G.M., Pierzynski, G.M., 2004. Soil lead bioavailability and in situ remediation of lead-contaminated soils: A review. Environmental Progress 23, 78–93. https://doi.org/10.1002/ep.10004

Hodge, A.T., 1981. Vitruvius, Lead Pipes and Lead Poisoning. American Journal of Archaeology 85, 486–491. https://doi.org/10.2307/504874

Holland, H.D., Turekian, K.K., 2013. Treatise on Geochemistry - 2nd Edition | Elsevier Shop. Elsevier.

Hollinger, J.O., Srinivasan, A., Alvarez, P., Hsu, E., McBride, S., Eppell, S., Baskin, J., Waters, H., Gruber, R., 2011. 5.522 - Bone Tissue Engineering: Growth Factors and Cytokines, in: Ducheyne, P. (Ed.), Comprehensive Biomaterials. Elsevier, Oxford, pp. 281–301. https://doi.org/10.1016/B978-0-08-055294-1.00160-4

Holm, R.H., Kennepohl, P., Solomon, E.I., 1996. Structural and Functional Aspects of Metal Sites in Biology. Chem. Rev. 96, 2239–2314. https://doi.org/10.1021/cr9500390

Holtzman, D., DeVries, C., Nguyen, H., Olson, J., Bensch, K., 1984. Maturation of resistance to lead encephalopathy: cellular and subcellular mechanisms. Neurotoxicology 5, 97–124.

Hong, S., Candelone, J.-P., Patterson, C.C., Boutron, C.F., 1996. History of Ancient Copper Smelting Pollution During Roman and Medieval Times Recorded in Greenland Ice. Science 272, 246–249. https://doi.org/10.1126/science.272.5259.246

Hong, S., Candelone, J.-P., Patterson, C.C., Boutron, C.F., 1994. Greenland Ice Evidence of Hemispheric Lead Pollution Two Millennia Ago by Greek and Roman Civilizations. Science 265, 1841–1843. https://doi.org/10.1126/science.265.5180.1841

Hunter, G.K., Goldberg, H.A., 1993. Nucleation of hydroxyapatite by bone sialoprotein. Proceedings of the National Academy of Sciences 90, 8562–8565. https://doi.org/10.1073/pnas.90.18.8562

Iavicoli, I., Carelli, G., Sgambato, A., Masci, O., Ardito, R., Cittadini, A., Castellino, N., 2001. Lead inhibits growth and induces apoptosis in normal rat fibroblasts. Altern Lab Anim 29, 461–469.

Iolascon, A., De Falco, L., 2009. Mutations in the Gene Encoding DMT1: Clinical Presentation and Treatment. Seminars in Hematology, Iron Deficiency and Metabolism 46, 358–370. https://doi.org/10.1053/j.seminhematol.2009.06.005

Jacques, J.-M., 1955. Les « Alexipharmaques » de Nicandre. Revue des Études Anciennes 57, 5–35. https://doi.org/10.3406/rea.1955.3519

Jilka, R.L., Weinstein, R.S., Bellido, T., Parfitt, A.M., Manolagas, S.C., 1998. Osteoblast Programmed Cell Death (Apoptosis): Modulation by Growth Factors and Cytokines. Journal of Bone and Mineral Research 13, 793–802. https://doi.org/10.1359/jbmr.1998.13.5.793

Jouttijärvi, A., 2017. Roman alloying practice. Materials and Manufacturing Processes 32, 813–826. https://doi.org/10.1080/10426914.2017.1279325

Kabata-Pendias, A., 2010. Trace Elements in Soils and Plants, 4th ed. CRC Press, Boca Raton. https://doi.org/10.1201/b10158

Kaler, S.G., 2011. ATP7A-related copper transport diseases—emerging concepts and future trends. Nat Rev Neurol 7, 15–29. https://doi.org/10.1038/nrneurol.2010.180

Kazi Tani, L.S., Gourlan, A.T., Dennouni-Medjati, N., Telouk, P., Dali-Sahi, M., Harek, Y., Sun, Q., Hackler, J., Belhadj, M., Schomburg, L., Charlet, L., 2021. Copper Isotopes and Copper to Zinc Ratio as Possible Biomarkers for Thyroid Cancer. Front Med (Lausanne) 8, 698167. https://doi.org/10.3389/fmed.2021.698167

Keenan, S.W., 2016. From bone to fossil: A review of the diagenesis of bioapatite. American Mineralogist 101, 1943–1951. https://doi.org/10.2138/am-2016-5737

Keenan, S.W., Engel, A.S., Roy, A., Lisa Bovenkamp-Langlois, G., 2015. Evaluating the consequences of diagenesis and fossilization on bioapatite lattice structure and composition. Chemical Geology 413, 18–27. https://doi.org/10.1016/j.chemgeo.2015.08.005

Kelly, A.E., Reuer, M.K., Goodkin, N.F., Boyle, E.A., 2009. Lead concentrations and isotopes in corals and water near Bermuda, 1780–2000. Earth and Planetary Science Letters 283, 93–100. https://doi.org/10.1016/j.epsl.2009.03.045

Kendall, C., Eriksen, A.M.H., Kontopoulos, I., Collins, M.J., Turner-Walker, G., 2018. Diagenesis of archaeological bone and tooth. Palaeogeography, Palaeoclimatology, Palaeoecology 491, 21–37. https://doi.org/10.1016/j.palaeo.2017.11.041

Kidane, T.Z., Farhad, R., Lee, K.J., Santos, A., Russo, E., Linder, M.C., 2012. Uptake of copper from plasma proteins in cells where expression of CTR1 has been modulated. Biometals 25, 697–709. https://doi.org/10.1007/s10534-012-9528-8

Killick, D., Fenn, T., 2012. Archaeometallurgy: The Study of Preindustrial Mining and Metallurgy. https://doi.org/10.1146/annurev-anthro-092611-145719

King, C.L., Tayles, N., Gordon, K.C., 2011. Re-examining the chemical evaluation of diagenesis in human bone apatite. Journal of Archaeological Science, Satellite remote sensing in archaeology: past, present and future perspectives 38, 2222–2230. https://doi.org/10.1016/j.jas.2011.03.023

Knudson, K.J., Price, T.D., 2007. Utility of multiple chemical techniques in archaeological residential mobility studies: Case studies from Tiwanaku- and Chiribaya-affiliated sites in the Andes. American Journal of Physical Anthropology 132, 25–39. https://doi.org/10.1002/ajpa.20480

Komárek, M., Ettler, V., Chrastný, V., Mihaljevič, M., 2008. Lead isotopes in environmental sciences: A review. Environment International 34, 562–577. https://doi.org/10.1016/j.envint.2007.10.005

Kosman, D.J., 2002. FET3P, ceruloplasmin, and the role of copper in iron metabolism, in: Advances in Protein Chemistry, Copper-Containing Proteins. Academic Press, pp. 221–269. https://doi.org/10.1016/S0065-3233(02)60055-5

Kozelka, P.B., Sañudo-Wilhelmy, S., Flegal, A.R., Bruland, K.W., 1997. Physico-chemical Speciation of Lead in South San Francisco Bay. Estuarine, Coastal and Shelf Science 44, 649–658. https://doi.org/10.1006/ecss.1996.0129

Krigman, M.R., 1978. Neuropathology of heavy metal intoxication. Environmental Health Perspectives 26, 117–120. https://doi.org/10.1289/ehp.7826117

Kristiansen, K., Larsson, T.B., 2005. The Rise of Bronze Age Society: Travels, Transmissions and Transformations. Cambridge University Press.

Lancranjan, I., Popescu, H.I., Găvănescu, O., Klepsch, I., Serbănescu, M., 1975. Reproductive Ability of Workmen Occupationally Exposed to Lead. Archives of Environmental Health: An International Journal 30, 396–401. https://doi.org/10.1080/00039896.1975.10666733

Landrigan, P., Baloh, R., Barthel, W., Whitworth, R., Staehling, N., Rosenblum, B., 1975. Neuropsychological dysfunction in children with chronic low-level lead absorption. The Lancet, Originally published as Volume 1, Issue 7909 305, 708–712. https://doi.org/10.1016/S0140-6736(75)91627-X

Lang, J., 2017. Roman iron and steel: A review. Materials and Manufacturing Processes 32, 857–866. https://doi.org/10.1080/10426914.2017.1279326

Larsen, C.S., Walker, P.L., 2012. Chapter 8 The Ethics of Bioarchaeology, in: Biological Anthropology and Ethics. SUNY Press, pp. 111–119.

Laxen, D.P.H., 1985. Trace metal adsorption/coprecipitation on hydrous ferric oxide under realistic conditions: The role of humic substances. Water Research 19, 1229–1236. https://doi.org/10.1016/0043-1354(85)90175-7

Lee, J., Petris, M.J., Thiele, D.J., 2002. Characterization of Mouse Embryonic Cells Deficient in the Ctr1 High Affinity Copper Transporter: IDENTIFICATION OF A Ctr1-INDEPENDENT COPPER TRANSPORT SYSTEM*. Journal of Biological Chemistry 277, 40253–40259. https://doi.org/10.1074/jbc.M208002200

Lee, K., Hur, S.D., Hou, S., Hong, S., Qin, X., Ren, J., Liu, Y., Rosman, K.J.R., Barbante, C., Boutron, C.F., 2008. Atmospheric pollution for trace elements in the remote high-altitude atmosphere in central Asia as recorded in snow from Mt. Qomolangma (Everest) of the Himalayas. Science of The Total Environment 404, 171–181. https://doi.org/10.1016/j.scitotenv.2008.06.022

Lee-Thorp, J., Sealy, J., 2008. Beyond documenting diagenesis: The fifth international bone diagenesis workshop. Palaeogeography, Palaeoclimatology, Palaeoecology, Beyond documenting diagenesis: The fifth international bone diagenesis workshop 266, 129–133. https://doi.org/10.1016/j.palaeo.2008.03.025

Leinen, M., Sarnthein, M., 1989. Paleoclimatology and Paleometeorology: Modern and Past Patterns of Global Atmospheric Transport. Kluwer Academic Publishers.

Lewis Jr, C.M., Tung, T.F., 2013. Methodological and Ethical Considerations When Sampling Human Osteological Remains, in: The Dead Tell Tales: Essays in Honor of Jane E. Buikstra, Monographs. Cotsen Institute of Archaeology Press at UCLA, p. 208. https://doi.org/10.2307/j.ctvdjrq6v

Li, Y.-H., 1991. Distribution patterns of the elements in the ocean: A synthesis. Geochimica et Cosmochimica Acta, The Macalpine Hills Lunar Meteorite Consortium 55, 3223–3240. https://doi.org/10.1016/0016-7037(91)90485-N

Linder, M.C., 2001. Copper and genomic stability in mammals. Mutation Research/Fundamental and Molecular Mechanisms of Mutagenesis, Micronutrients and Genomic Stability 475, 141–152. https://doi.org/10.1016/S0027-5107(01)00076-8

Linder, M.C., 1991. Biochemistry of Copper. Springer US, Boston, MA. https://doi.org/10.1007/978-1-4757-9432-8

Lindsay, W.L., 1979. Chemical equilibria in soils. Wiley, New York.

Liu, Y., Hou, S., Hong, S., Hur, S.-D., Lee, K., Wang, Y., 2011. Atmospheric pollution indicated by trace elements in snow from the northern slope of Cho Oyu range, Himalayas. Environ Earth Sci 63, 311–320. https://doi.org/10.1007/s12665-010-0714-0

Longman, J., Veres, D., Ersek, V., Tamas, C.G., Haliuc, A., Magyari, E., Gogaltan, F., Panajiotidis, S., Papadopoulou, M., 2024. Central-Eastern Europe as a centre of Middle Ages extractive metallurgy. Journal of Archaeological Science 172, 106093. https://doi.org/10.1016/j.jas.2024.106093

López-Costas, O., Kylander, M., Mattielli, N., Álvarez-Fernández, N., Pérez-Rodríguez, M., Mighall, T., Bindler, R., Martínez Cortizas, A., 2020. Human bones tell the story of atmospheric mercury and lead exposure at the edge of Roman World. Science of The Total Environment 710, 136319. https://doi.org/10.1016/j.scitotenv.2019.136319

Lustberg, M., Silbergeld, E., 2002. Blood Lead Levels and Mortality. Archives of Internal Medicine 162, 2443–2449. https://doi.org/10.1001/archinte.162.21.2443

Lutsenko, S., 2016. Copper trafficking to the secretory pathway. Metallomics 8, 840–852. https://doi.org/10.1039/c6mt00176a

Lutsenko, S., 2010. Human copper homeostasis: a network of interconnected pathways. Current Opinion in Chemical Biology, Biocatalysis and Biotransformation/Bioinorganic Chemistry 14, 211–217. https://doi.org/10.1016/j.cbpa.2010.01.003

Madupalli, H., Pavan, B., Tecklenburg, M.M.J., 2017. Carbonate substitution in the mineral component of bone: Discriminating the structural changes, simultaneously imposed by carbonate in A and B sites of apatite. Journal of Solid State Chemistry 255, 27–35. https://doi.org/10.1016/j.jssc.2017.07.025

Makarewicz, C.A., Sealy, J., 2015. Dietary reconstruction, mobility, and the analysis of ancient skeletal tissues: Expanding the prospects of stable isotope research in archaeology. Journal of Archaeological Science, Scoping the Future of Archaeological Science: Papers in Honour of Richard Klein 56, 146–158. https://doi.org/10.1016/j.jas.2015.02.035

Manolagas, S.C., 2000. Birth and Death of Bone Cells: Basic Regulatory Mechanisms and Implications for the Pathogenesis and Treatment of Osteoporosis*. Endocrine Reviews 21, 115–137. https://doi.org/10.1210/edrv.21.2.0395

Markovac, J., Goldstein, G.W., 1988. Picomolar concentrations of lead stimulate brain protein kinase C. Nature 334, 71–73. https://doi.org/10.1038/334071a0

Marshall, C.P., Fairbridge, R.W., 1998. Lead: Element and geochemistry, in: Geochemistry. Encyclopedia of Earth Science. Springer Dordrecht, pp. 645–648.

Martin, J.M., Guan, D.M., Elbaz-Poulichet, F., Thomas, A.J., Gordeev, V.V., 1993. Preliminary assessment of the distributions of some trace elements (As, Cd, Cu, Fe, Ni, Pb and Zn) in a pristine aquatic environment: The Lena River estuary (Russia). Marine Chemistry, Second International Symposium on the Biogeochemistry of Model Estuaries: Estuarine Processes in Global Change 43, 185–199. https://doi.org/10.1016/0304-4203(93)90224-C

Martin, J.-M., Whitfield, M., 1983. The Significance of the River Input of Chemical Elements to the Ocean, in: Wong, C.S., Boyle, E., Bruland, K.W., Burton, J.D., Goldberg, E.D. (Eds.), Trace Metals in Sea Water, NATO Conference Series. Springer US, Boston, MA, pp. 265–296. https://doi.org/10.1007/978-1-4757-6864-0_16

McConnell, D., 1962. The Crystal Structure of Bone. Clinical Orthopaedics and Related Research® 23, 253.

McConnell, J.R., Wilson, A.I., Stohl, A., Arienzo, M.M., Chellman, N.J., Eckhardt, S., Thompson, E.M., Pollard, A.M., Steffensen, J.P., 2018. Lead pollution recorded in Greenland ice indicates European emissions tracked plagues, wars, and imperial expansion during antiquity. Proceedings of the National Academy of Sciences 115, 5726–5731. https://doi.org/10.1073/pnas.1721818115

McDonough, W.F., Sun, S. -s., 1995. The composition of the Earth. Chemical Geology, Chemical Evolution of the Mantle 120, 223–253. https://doi.org/10.1016/0009-2541(94)00140-4

McLennan, S.M., 1995. Sediments and Soils: Chemistry and Abundances, in: Rock Physics & Phase Relations. American Geophysical Union (AGU), pp. 8–19. https://doi.org/10.1029/RF003p0008

Milne, D., 1998. Copper intake and assessment of copper status. The American Journal of Clinical Nutrition 67, 1041S-1045S. https://doi.org/10.1093/ajcn/67.5.1041S

Mims, M.P., Prchal, J.T., 2005. Divalent metal transporter 1. Hematology 10, 339–345. https://doi.org/10.1080/10245330500093419

Molenda, M., Kolmas, J., 2023. The Role of Zinc in Bone Tissue Health and Regeneration—a Review. Biol Trace Elem Res 201, 5640–5651. https://doi.org/10.1007/s12011-023-03631-1

Monier-Faugere, M.-C., Chris Langub, M., Malluche, H.H., 1998. Chapter 8 - Bone Biopsies: A Modern Approach, in: Avioli, L.V., Krane, S.M. (Eds.), Metabolic Bone Disease and Clinically Related Disorders (Third Edition). Academic Press, San Diego, pp. 237–280e. https://doi.org/10.1016/B978-012068700-8/50009-8

Montgomery, J., Evans, J.A., Chenery, S.R., Pashley, V., Killgrove, K., 2010. Gleaming, white and deadly": using lead to track human exposure and geographic origins in the Roman period in Britain. Journal of Roman Archaeology.

Morel, F.M.M., Hering, J.G., 1993. Principles and Applications of Aquatic Chemistry | Wiley. Wiley.

Morgan, E.F., Barnes, G.L., Einhorn, T.A., 2013. Chapter 1 - The Bone Organ System: Form and Function, in: Marcus, R., Feldman, D., Dempster, D.W., Luckey, M., Cauley, J.A. (Eds.), Osteoporosis (Fourth Edition). Academic Press, San Diego, pp. 3–20. https://doi.org/10.1016/B978-0-12-415853-5.00001-7

Muldoon, S.B., Cauley, J.A., Kuller, L.H., Morrow, L., Needleman, H.L., Scott, J., Hooper, F.J., 1996. Effects of Blood Lead Levels on Cognitive Function of Older Women. Neuroepidemiology 15, 62–72. https://doi.org/10.1159/000109891

Muller, F.L.L., 1996. Interactions of copper, lead and cadmium with the dissolved, colloidal and particulate components of estuarine and coastal waters. Marine Chemistry 52, 245–268. https://doi.org/10.1016/0304-4203(95)00097-6

Murozumi, M., Chow, T.J., Patterson, C., 1969. Chemical concentrations of pollutant lead aerosols, terrestrial dusts and sea salts in Greenland and Antarctic snow strata. Geochimica et Cosmochimica Acta 33, 1247–1294. https://doi.org/10.1016/0016-7037(69)90045-3

Mylon, S.E., Twining, B.S., Fisher, N.S., Benoit, G., 2003. Relating the Speciation of Cd, Cu, and Pb in Two Connecticut Rivers with Their Uptake in Algae. Environ. Sci. Technol. 37, 1261–1267. https://doi.org/10.1021/es0259281

Needleman, H.L., 2004. Lead Poisoning. Annual Review of Medicine 55, 209–222. https://doi.org/doi.org/10.1146/annurev.med.55.091902.103653

Needleman, H.L., Gatsonis, C.A., 1990. Low-Level Lead Exposure and the IQ of Children: A Meta-analysis of Modern Studies. JAMA 263, 673–678. https://doi.org/10.1001/jama.1990.03440050067035

Needleman, H.L., Gunroe, C., Leviton, A., Reed, R., Peresie, H., Maher, C., Barett, P., 1979. Deficits in psychologic and classroom performance of children with elevated dentine lead levels. The New England journal of medicine 300. https://doi.org/10.1056/NEJM197903293001301

Needleman, H.L., McFarland, C., Ness, R.B., Fienberg, S.E., Tobin, M.J., 2002. Bone lead levels in adjudicated delinquents. A case control study. Neurotoxicol Teratol 24, 711–717. https://doi.org/10.1016/s0892-0362(02)00269-6

Needleman, H.L., Riess, J.A., Tobin, M.J., Biesecker, G.E., Greenhouse, J.B., 1996. Bone Lead Levels and Delinquent Behavior. JAMA 275, 363–369. https://doi.org/10.1001/jama.1996.03530290033034

Needleman, H.L., Schell, A., Bellinger, D., Leviton, A., Allred, E.N., 1990. The Long-Term Effects of Exposure to Low Doses of Lead in Childhood. New England Journal of Medicine 322, 83–88. https://doi.org/10.1056/NEJM199001113220203

Needleman, L., Needleman, D., 1985. Lead Poisoning and the Decline of the Roman Aristocracy. Echos du monde classique: Classical views 29, 63–94.

Nelson, W.O., Campbell, P.G.C., 1991. The effects of acidification on the geochemistry of Al, Cd, Pb and Hg in freshwater environments: A literature review. Environmental Pollution, Environmental Acidification and Metals 71, 91–130. https://doi.org/10.1016/0269-7491(91)90030-Z

Nielsen-Marsh, C.M., Hedges, R.E.M., 2000. Patterns of Diagenesis in Bone I: The Effects of Site Environments. Journal of Archaeological Science 27, 1139–1150. https://doi.org/10.1006/jasc.1999.0537

Nielsen-Marsh, C.M., Smith, C.I., Jans, M.M.E., Nord, A., Kars, H., Collins, M.J., 2007. Bone diagenesis in the European Holocene II: taphonomic and environmental considerations. Journal of Archaeological Science 34, 1523–1531. https://doi.org/10.1016/j.jas.2006.11.012

Nikita, E., 2017a. Chapter 1 - The Human Skeleton, in: Nikita, E. (Ed.), Osteoarchaeology. Academic Press, pp. 1–75. https://doi.org/10.1016/B978-0-12-804021-8.00001-2

Nikita, E., 2017b. Chapter 8 - Pathological Conditions, in: Nikita, E. (Ed.), Osteoarchaeology. Academic Press, pp. 301–354. https://doi.org/10.1016/B978-0-12-804021-8.00008-5

Noble, A.E., Echegoyen-Sanz, Y., Boyle, E.A., Ohnemus, D.C., Lam, P.J., Kayser, R., Reuer, M., Wu, J., Smethie, W., 2015. Dynamic variability of dissolved Pb and Pb isotope composition from the U.S. North Atlantic GEOTRACES transect. Deep Sea Research Part II: Topical Studies in Oceanography, GEOTRACES GA-03 - The U.S. GEOTRACES North Atlantic Transect 116, 208–225. https://doi.org/10.1016/j.dsr2.2014.11.011

Nriagu, J.O., 1996. A History of Global Metal Pollution. Science 272, 223–223. https://doi.org/10.1126/science.272.5259.223

Nriagu, J.O., 1990. Global Metal Pollution: Poisoning the Biosphere? Environment: Science and Policy for Sustainable Development.

Nriagu, J.O., 1989. A global assessment of natural sources of atmospheric trace metals. Nature 338, 47–49. https://doi.org/10.1038/338047a0

Nriagu, J.O., 1983. Lead and lead poisoning in antiquity, Antiquities. Wiley, New York.

Nriagu, J.O., 1978. The Biogeochemistry of Lead in the Environment. Elsevier/North-Holland Biomedical Press.

Nriagu, J.O., Davidson, C.I., 1985. Toxic metals in the atmosphere.

Nriagu, J.O., Pacyna, J.M., 1988. Quantitative assessment of worldwide contamination of air, water and soils by trace metals. Nature 333, 134–139. https://doi.org/10.1038/333134a0

O'Connor, D., Hou, D., Ye, J., Zhang, Y., Ok, Y.S., Song, Y., Coulon, F., Peng, T., Tian, L., 2018. Lead-based paint remains a major public health concern: A critical review of global production, trade, use, exposure, health risk, and implications. Environment International 121, 85–101. https://doi.org/10.1016/j.envint.2018.08.052

Oflaherty, E.J., 1995. Physiologically Based Models for Bone-Seeking Elements: V. Lead Absorption and Disposition in Childhood. Toxicology and Applied Pharmacology 131, 297–308. https://doi.org/10.1006/taap.1995.1072

Ohgami, R.S., Campagna, D.R., McDonald, A., Fleming, M.D., 2006. The Steap proteins are metalloreductases. Blood 108, 1388–1394. https://doi.org/10.1182/blood-2006-02-003681

Oliver, T., 1911. A Lecture ON LEAD POISONING AND THE RACE: Delivered to the Eugenics Education Society, London, May 4th, 1911. Br Med J 1, 1096–1098. https://doi.org/10.1136/bmj.1.2628.1096

Ortner, D.J., 2003. CHAPTER 7 - Theoretical Issues in Paleopathology, in: Ortner, D.J. (Ed.), Identification of Pathological Conditions in Human Skeletal Remains (Second Edition). Academic Press, San Diego, pp. 109–118. https://doi.org/10.1016/B978-012528628-2/50044-2

Ortner, D.J., Turner-walker, G., 2003. CHAPTER 2 - The Biology of Skeletal Tissues, in: Ortner, D.J. (Ed.), Identification of Pathological Conditions in Human Skeletal Remains (Second Edition). Academic Press, San Diego, pp. 11–35. https://doi.org/10.1016/B978-012528628-2/50039-9

Ou-Yang, H., Paschalis, E.P., Mayo, W.E., Boskey, A.L., Mendelsohn, R., 2001. Infrared Microscopic Imaging of Bone: Spatial Distribution of CO_3^{2-}. Journal of Bone and Mineral Research 16, 893–900. https://doi.org/10.1359/jbmr.2001.16.5.893

Pääbo, S., Poinar, H., Serre, D., Jaenicke-Després, V., Hebler, J., Rohland, N., Kuch, M., Krause, J., Vigilant, L., Hofreiter, M., 2004. Genetic Analyses from Ancient DNA. Annual Review of Genetics 38, 645–679. https://doi.org/10.1146/annurev.genet.37.110801.143214

Pacyna, J.M., Pacyna, E.G., 2001. An assessment of global and regional emissions of trace metals to the atmosphere from anthropogenic sources worldwide. Environmental Reviews 9, 269–298.

Page, G.William., 1981. Comparison of groundwater and surface water for patterns and levels of contamination by toxic substances. Environ. Sci. Technol. 15, 1475–1481. https://doi.org/10.1021/es00094a008

Parfitt, A.M., 2013. Chapter 36 - Skeletal Heterogeneity and the Purposes of Bone Remodeling: Implications for the Understanding of Osteoporosis, in: Marcus, R., Feldman, D., Dempster, D.W., Luckey, M., Cauley, J.A. (Eds.), Osteoporosis (Fourth Edition). Academic Press, San Diego, pp. 855–872. https://doi.org/10.1016/B978-0-12-415853-5.00036-4

Pasteris, J.D., 2016. A mineralogical view of apatitic biomaterials. American Mineralogist 101, 2594–2610. https://doi.org/10.2138/am-2016-5732

Patterson, C.C., Settle, D.M., 1987. Review of data on eolian fluxes of industrial and natural lead to the lands and seas in remote regions on a global scale. Marine Chemistry, IX International Symposium on the Chemistry of the Mediterranean 22, 137–162. https://doi.org/10.1016/0304-4203(87)90005-3

Pederzani, S., Britton, K., 2019. Oxygen isotopes in bioarchaeology: Principles and applications, challenges and opportunities. Earth-Science Reviews 188, 77–107. https://doi.org/10.1016/j.earscirev.2018.11.005

Pentschew, A., 1965. Morphology and morphogenesis of lead encephalopathy. Acta Neuropathol 5, 133–160. https://doi.org/10.1007/BF00686515

Pernicka, E., 2020. Development of metallurgy in Eurasia. Quaternary International 560–561, 38–44.

Pinheiro, J.P., Mota, A.M., Benedetti, M.F., 1999. Lead and Calcium Binding to Fulvic Acids: Salt Effect and Competition. Environ. Sci. Technol. 33, 3398–3404. https://doi.org/10.1021/es990210f

Piotrowska, N., Goslar, T., 2002. Preparation of Bone Samples in the Gliwice Radiocarbon Laboratory for AMS Radiocarbon Dating. Isotopes in Environmental and Health Studies 38, 267–275. https://doi.org/10.1080/10256010208033272

Planchon, F.A.M., Boutron, C.F., Barbante, C., Cozzi, G., Gaspari, V., Wolff, E.W., Ferrari, C.P., Cescon, P., 2002. Changes in heavy metals in Antarctic snow from Coats Land since the mid-19th to the late-20th century. Earth and Planetary Science Letters 200, 207–222. https://doi.org/10.1016/S0012-821X(02)00612-X

Plank, T., Langmuir, C.H., 1998. The chemical composition of subducting sediment and its consequences for the crust and mantle. Chemical Geology 145, 325–394. https://doi.org/10.1016/S0009-2541(97)00150-2

Pocock, S.J., Smith, M., Baghurst, P., 1994. Environmental lead and children's intelligence: a systematic review of the epidemiological evidence. BMJ 309, 1189–1197. https://doi.org/10.1136/bmj.309.6963.1189

Powell, K.J., Brown, P.L., Byrne, R.H., Gajda, T., Hefter, G., Leuz, A.-K., Sjöberg, S., Wanner, H., 2009. Chemical speciation of environmentally significant metals with inorganic ligands. Part 3: The Pb2+ + OH–, Cl–, CO32–, SO42–, and PO43– systems (IUPAC Technical Report). Pure and Applied Chemistry 81, 2425–2476. https://doi.org/10.1351/PAC-REP-09-03-05

Price, T.D., 2014. An Introduction to the Isotopic Studies of Ancient Human Remains. Journal of the North Atlantic 7, 71–87. https://www.jstor.org/stable/26671846

Price, T.D., Blitz, J., Burton, J., Ezzo, J.A., 1992. Diagenesis in prehistoric bone: Problems and solutions. Journal of Archaeological Science 19, 513–529. https://doi.org/10.1016/0305-4403(92)90026-Y

Quinn, R.L., 2024. How much time is recorded with a rib bone isotope? Journal of Archaeological Science: Reports 57, 104593. https://doi.org/10.1016/j.jasrep.2024.104593

Rabinowitz, M.B., 1991. Toxicokinetics of bone lead. Environmental Health Perspectives 91, 33–37. https://doi.org/10.1289/ehp.919133

Radivojević, M., Rehren, T., Pernicka, E., Šljivar, D., Brauns, M., Borić, D., 2010. On the origins of extractive metallurgy: new evidence from Europe. Journal of Archaeological Science 37, 2775–2787. https://doi.org/10.1016/j.jas.2010.06.012

Rahn, K.A., 1976. The Chemical Composition of the Atmospheric Aerosol. Graduate School of Oceanography, University of Rhode Island.

Rainbow, P.S., Poirier, L., Smith, B.D., Brix, K.V., Luoma, S.N., 2006. Trophic transfer of trace metals from the polychaete worm Nereis diversicolor to the polychaete N. virens and the decapod crustacean Palaemonetes varians. Marine Ecology Progress Series 321, 167–181.

Rasmussen, K.L., Skytte, L., Jensen, A.J., Boldsen, J.L., 2015. Comparison of mercury and lead levels in the bones of rural and urban populations in Southern Denmark and Northern Germany during the Middle Ages. Journal of Archaeological Science: Reports 3, 358–370. https://doi.org/10.1016/j.jasrep.2015.06.021

Rauch, J.N., Pacyna, J.M., 2009. Earth's global Ag, Al, Cr, Cu, Fe, Ni, Pb, and Zn cycles. Global Biogeochemical Cycles 23. https://doi.org/10.1029/2008GB003376

Reddy, A., Braun, C.L., 2010. Lead and the Romans. J. Chem. Educ. 87, 1052–1055. https://doi.org/10.1021/ed100631y

Reiche, I., Favre-Quattropani, L., Vignaud, C., Bocherens, H., Charlet, L., Menu, M., 2003. A multi-analytical study of bone diagenesis: the Neolithic site of Bercy (Paris, France). Meas. Sci. Technol. 14, 1608. https://doi.org/10.1088/0957-0233/14/9/312

Reinfelder, J.R., Fisher, N.S., Luoma, S.N., Nichols, J.W., Wang, W.-X., 1998. Trace element trophic transfer in aquatic organisms: A critique of the kinetic model approach. Science of The Total Environment 219, 117–135. https://doi.org/10.1016/S0048-9697(98)00225-3

Retief, F.P., Cilliers, L., 2006. Lead poisoning in ancient Rome. Acta Theologica 26, 147–164. https://doi.org/10.4314/actat.v26i2.52570

Reuer, M.K., Weiss, D.J., 2002. Anthropogenic lead dynamics in the terrestrial and marine environment. Philosophical Transactions of the Royal Society of London. Series A: Mathematical, Physical and Engineering Sciences 360, 2889–2904. https://doi.org/10.1098/rsta.2002.1095

Rey, C., Combes, C., 2016. 3 - Physical chemistry of biological apatites, in: Aparicio, C., Ginebra, M.-P. (Eds.), Biomineralization and Biomaterials. Woodhead Publishing, Boston, pp. 95–127. https://doi.org/10.1016/B978-1-78242-338-6.00004-1

Reynard, B., Balter, V., 2014. Trace elements and their isotopes in bones and teeth: Diet, environments, diagenesis, and dating of archeological and paleontological samples. Palaeogeography, Palaeoclimatology, Palaeoecology, Bone and enamel diagenesis: From the crystal to the environment - A tribute to Jean-François Saliège 416, 4–16. https://doi.org/10.1016/j.palaeo.2014.07.038

Richards, M.P., 2015. Stable Isotope Analysis of Bone and Teeth as a Means for Reconstructing Past Human Diets in Greece. Hesperia Supplements 49, 15–23.

Roach, H.I., 1994. Why Does Bone Matrix Contain Non-Collagenous Proteins? The Possible Roles of Osteocalcin, Osteonectin, Osteopontin and Bone Sialoprotein in Bone Mineralisation and Resorption. Cell Biology International 18, 617–628. https://doi.org/10.1006/cbir.1994.1088

Roberts, B.W., Thornton, C.P., Pigott, V.C., 2009. Development of metallurgy in Eurasia. Antiquity 83, 1012–1022. https://doi.org/10.1017/S0003598X00099312

Rosman, K.J.R., Chisholm, W., Boutron, C.F., Candelone, J.P., Görlach, U., 1993. Isotopic evidence for the source of lead in Greenland snows since the late 1960s. Nature 362, 333–335. https://doi.org/10.1038/362333a0

Rosman, K.J.R., Chisholm, W., Hong, S., Candelone, J.-P., Boutron, C.F., 1997. Lead from Carthaginian and Roman Spanish Mines Isotopically Identified in Greenland Ice Dated from 600 B.C. to 300 A.D. Environ. Sci. Technol. 31, 3413–3416. https://doi.org/10.1021/es970038k

Rosner, D., Markowitz, G., 1985. A "gift of God"?: The public health controversy over leaded gasoline during the 1920s. Am J Public Health 75, 344–352. https://doi.org/10.2105/AJPH.75.4.344

Rossmann, R., Barres, J., 1988. Trace Element Concentrations in Near-Surface Waters of the Great Lakes and Methods of Collection, Storage, and Analysis. Journal of Great Lakes Research 14, 188–204. https://doi.org/10.1016/S0380-1330(88)71548-8

Rudnick, R.L., Gao, S., 2003. Composition of the Continental Crust, in: Holland, H.D., Turekian, K.K. (Eds.), Treatise on Geochemistry. Pergamon, Oxford, pp. 1–64. https://doi.org/10.1016/B0-08-043751-6/03016-4

Salesse, K., Dufour, E., Lebon, M., Wurster, C., Castex, D., Bruzek, J., Zazzo, A., 2014. Variability of bone preservation in a confined environment: The case of the

catacomb of Sts Peter and Marcellinus (Rome, Italy). Palaeogeography, Palaeoclimatology, Palaeoecology, Bone and enamel diagenesis: From the crystal to the environment - A tribute to Jean-François Saliège 416, 43–54. https://doi.org/10.1016/j.palaeo.2014.07.021

Salters, V.J.M., Stracke, A., 2004. Composition of the depleted mantle. Geochemistry, Geophysics, Geosystems 5. https://doi.org/10.1029/2003GC000597

Sandstead, H., 1982. Copper bioavailability and requirements. The American Journal of Clinical Nutrition 35, 809–814. https://doi.org/10.1093/ajcn/35.4.809

Sañudo-Wilhelmy, S.A., Rossi, F.K., Bokuniewicz, H., Paulsen, R.J., 2002. Trace Metal Levels in Uncontaminated Groundwater of a Coastal Watershed: Importance of Colloidal Forms. Environ. Sci. Technol. 36, 1435–1441. https://doi.org/10.1021/es0109545

Sasaki, N., Sudoh, Y., 1997. X-ray Pole Figure Analysis of Apatite Crystals and Collagen Molecules in Bone. Calcif Tissue Int 60, 361–367. https://doi.org/10.1007/s002239900244

Sauvé, S., Hendershot, W., Allen, H.E., 2000. Solid-Solution Partitioning of Metals in Contaminated Soils: Dependence on pH, Total Metal Burden, and Organic Matter. Environ. Sci. Technol. 34, 1125–1131. https://doi.org/10.1021/es9907764

Schauble, E.A., 2004. Applying Stable Isotope Fractionation Theory to New Systems. Reviews in Mineralogy and Geochemistry 55, 65–111. https://doi.org/10.2138/gsrmg.55.1.65

Schaule, B.K., Patterson, C.C., 1981. Lead concentrations in the northeast Pacific: evidence for global anthropogenic perturbations. Earth and Planetary Science Letters 54, 97–116. https://doi.org/10.1016/0012-821X(81)90072-8

Schoeninger, M.J., 2010. Diet Reconstruction and Ecology Using Stable Isotope Ratios, in: A Companion to Biological Anthropology. John Wiley & Sons, Ltd, pp. 445–464. https://doi.org/10.1002/9781444320039.ch25

Schoeninger, M.J., Moore, K., 1992. Bone Stable Isotope Studies in Archaeology. Journal of World Prehistory 6, 247–296. https://www.jstor.org/stable/25800615

Schwartz, B.S., Stewart, W.F., Bolla, K.I., Simon, D., Bandeen-Roche, K., Gordon, B., Links, J.M., Todd, A.C., 2000. Past adult lead exposure is associated with longitudinal decline in cognitive function. Neurology 55, 1144–1150. https://doi.org/10.1212/WNL.55.8.1144

Schweissing, M.M., Grupe, G., 2003. Stable strontium isotopes in human teeth and bone: a key to migration events of the late Roman period in Bavaria. Journal of Archaeological Science 30, 1373–1383. https://doi.org/10.1016/S0305-4403(03)00025-6

Seeman, E., 2008. Chapter 1 - Modeling and Remodeling: The Cellular Machinery Responsible for the Gain and Loss of Bone's Material and Structural Strength, in: Bilezikian, J.P., Raisz, L.G., Martin, T.J. (Eds.), Principles of Bone Biology (Third Edition). Academic Press, San Diego, pp. 1–28. https://doi.org/10.1016/B978-0-12-373884-4.00023-9

Settle, D.M., Patterson, C.C., 1982. Magnitudes and sources of precipitation and dry deposition fluxes of indestrial and natural leads to the North Pacific at Enewetak. Journal of Geophysical Research: Oceans 87, 8857–8869. https://doi.org/10.1029/JC087iC11p08857

Shabani, A., Rabbani, A., 2000. Lead nitrate induced apoptosis in alveolar macrophages from rat lung. Toxicology 149, 109–114. https://doi.org/10.1016/S0300-483X(00)00232-8

Shen, G.T., Boyle, E.A., 1987. Lead in corals: reconstruction of historical industrial fluxes to the surface ocean. Earth and Planetary Science Letters 82, 289–304. https://doi.org/10.1016/0012-821X(87)90203-2

Sherrell, R.M., Boyle, E.A., Falkner, K.K., Harris, N.R., 2000. Temporal variability of Cd, Pb, and Pb isotope deposition in central Greenland snow. Geochemistry, Geophysics, Geosystems 1. https://doi.org/10.1029/1999GC000007

Shotyk, W., Le Roux, G., 2005. Biogeochemistry and cycling of lead. Met Ions Biol Syst 43, 239–275. https://doi.org/10.1201/9780824751999.ch10

Shotyk, W., Weiss, D., Kramers, J.D., Frei, R., Cheburkin, A.K., Gloor, M., Reese, S., 2001. Geochemistry of the peat bog at Etang de la Gruère, Jura Mountains, Switzerland, and its record of atmospheric Pb and lithogenic trace metals (Sc, Ti, Y, Zr, and REE) since 12,370 14C yr BP. Geochimica et Cosmochimica Acta 65, 2337–2360. https://doi.org/10.1016/S0016-7037(01)00586-5

Sigel, H. (Ed.), 2014. Metal Ions in Biological Systems: Volume 40: The Lanthanides and Their Interrelations with Biosystems. CRC Press, Boca Raton. https://doi.org/10.1201/9781482293074

Silva-Sánchez, N., Armada, X.-L., 2023. Environmental Impact of Roman Mining and Metallurgy and Its Correlation with the Archaeological Evidence: A European Perspective. Environmental Archaeology 0, 1–25. https://doi.org/10.1080/14614103.2023.2181295

Simons, T.J., 1993. Lead-calcium interactions in cellular lead toxicity. Neurotoxicology 14, 77–85.

Simpson, R., Cooper, D.M.L., Swanston, T., Coulthard, I., Varney, T.L., 2021. Historical overview and new directions in bioarchaeological trace element analysis: a review. Archaeol Anthropol Sci 13, 24. https://doi.org/10.1007/s12520-020-01262-4

Skinner, H.C.W., 2013. Mineralogy of Bones, in: Selinus, O. (Ed.), Essentials of Medical Geology: Revised Edition. Springer Netherlands, Dordrecht, pp. 665–687. https://doi.org/10.1007/978-94-007-4375-5_30

Smith, C.I., Nielsen-Marsh, C.M., Jans, M.M.E., Collins, M.J., 2007. Bone diagenesis in the European Holocene I: patterns and mechanisms. Journal of Archaeological Science 34, 1485–1493. https://doi.org/10.1016/j.jas.2006.11.006

Solecki, R.S., 1969. A Copper Mineral Pendant from Northern Iran. Antiquity 43, 311–314. https://doi.org/10.1017/S0003598X00107525

Squires, K., Booth, T., Roberts, C.A., 2019. The Ethics of Sampling Human Skeletal Remains for Destructive Analyses, in: Squires, K., Errickson, D., Márquez-Grant, N. (Eds.), Ethical Approaches to Human Remains: A Global Challenge in Bioarchaeology and Forensic Anthropology. Springer International Publishing, Cham, pp. 265–297. https://doi.org/10.1007/978-3-030-32926-6_12

Stech, T., 1999. Aspects of early metallurgy in Mesopotamia and Anatolia, in: The Archaeometallurgy of the Asian Old World. University Museum, University of Pennsylvania, Philadelphia, pp. 59–71.

Steinmann, M., Stille, P., 1997. Rare earth element behavior and Pb, Sr, Nd isotope systematics in a heavy metal contaminated soil. Applied Geochemistry 12, 607–623. https://doi.org/10.1016/S0883-2927(97)00017-6

Sterner, R.W., Smutka, T.M., McKay, R.M.L., Xiaoming, Q., Brown, E.T., Sherrell, R.M., 2004. Phosphorus and trace metal limitation of algae and bacteria in Lake Superior. Limnology and Oceanography 49, 495–507. https://doi.org/10.4319/lo.2004.49.2.0495

Strawn, D.G., Sparks, D.L., 2000. Effects of Soil Organic Matter on the Kinetics and Mechanisms of Pb(II) Sorption and Desorption in Soil. Soil Science Society of America Journal 64, 144–156. https://doi.org/10.2136/sssaj2000.641144x

Stretesky, P.B., Lynch, M.J., 2001. The Relationship Between Lead Exposure and Homicide. Archives of Pediatrics & Adolescent Medicine 155, 579–582. https://doi.org/10.1001/archpedi.155.5.579

Suedel, B.C., Boraczek, J.A., Peddicord, R.K., Clifford, P.A., Dillon, T.M., 1994. Trophic Transfer and Biomagnification Potential of Contaminants in Aquatic Ecosystems, in: Ware, G.W. (Ed.), Reviews of Environmental Contamination and Toxicology. Springer, New York, NY, pp. 21–89. https://doi.org/10.1007/978-1-4612-2656-7_2

Sulzman, E.W., 2007. Stable Isotope Chemistry and Measurement: A Primer, in: Stable Isotopes in Ecology and Environmental Science. John Wiley & Sons, Ltd, pp. 1–21. https://doi.org/10.1002/9780470691854.ch1

Sunda, W.G., 1994. Trace Metal/Phytoplankton Interactions in the Sea, in: Bidoglio, G., Stumm, W. (Eds.), Chemistry of Aquatic Systems: Local and Global Perspectives, EUROCOURSES. Springer Netherlands, Dordrecht, pp. 213–247. https://doi.org/10.1007/978-94-017-1024-4_9

Sykes, J.P., Wright, J.P., Trench, A., 2016. Discovery, supply and demand: From Metals of Antiquity to critical metals. Applied Earth Science 125, 3–20. https://doi.org/10.1080/03717453.2015.1122274

Taillefert, M., Lienemann, C.-P., Gaillard, J.-F., Perret, D., 2000. Speciation, reactivity, and cycling of Fe and Pb in a meromictic lake. Geochimica et Cosmochimica Acta 64, 169–183. https://doi.org/10.1016/S0016-7037(99)00285-9

Tanzi, R.E., Petrukhin, K., Chernov, I., Pellequer, J.L., Wasco, W., Ross, B., Romano, D.M., Parano, E., Pavone, L., Brzustowicz, L.M., Devoto, M., Peppercorn, J., Bush, A.I., Sternlieb, I., Pirastu, M., Gusella, J.F., Evgrafov, O., Penchaszadeh, G.K., Honig, B., Edelman, I.S., Soares, M.B., Scheinberg, I.H., Gilliam, T.C., 1993. The Wilson disease gene is a copper transporting ATPase with homology to the Menkes disease gene. Nat Genet 5, 344–350. https://doi.org/10.1038/ng1293-344

Tapiero, H., Townsend, D.M., Tew, K.D., 2003. Trace elements in human physiology and pathology. Copper. Biomedicine & Pharmacotherapy 57, 386–398. https://doi.org/10.1016/S0753-3322(03)00012-X

Tavakoli-Nezhad, M., Barron, A.J., Pitts, D.K., 2001. Postnatal Inorganic Lead Exposure Decreases the Number of Spontaneously Active Midbrain Dopamine Neurons in the Rat. NeuroToxicology 22, 259–269. https://doi.org/10.1016/S0161-813X(01)00010-9

Télouk, P., Puisieux, A., Fujii, T., Balter, V., Bondanese, V.P., Morel, A.-P., Clapisson, G., Lamboux, A., Albarede, F., 2015. Copper isotope effect in serum of cancer patients. A pilot study. Metallomics 7, 299–308. https://doi.org/10.1039/c4mt00269e

Terada, K., Aiba, N., Yang, X.-L., Iida, M., Nakai, M., Miura, N., Sugiyama, T., 1999. Biliary excretion of copper in LEC rat after introduction of copper transporting P-type ATPase, ATP7B. FEBS Letters 448, 53–56. https://doi.org/10.1016/S0014-5793(99)00319-1

Thiemens, M.H., 2013. Introduction to Chemistry and Applications in Nature of Mass Independent Isotope Effects Special Feature. Proceedings of the National Academy of Sciences 110, 17631–17637. https://doi.org/10.1073/pnas.1312926110

Thiemens, M.H., 2006. HISTORY AND APPLICATIONS OF MASS-INDEPENDENT ISOTOPE EFFECTS. Annual Review of Earth and Planetary Sciences 34, 217–262. https://doi.org/10.1146/annurev.earth.34.031405.125026

Thiemens, M.H., Chakraborty, S., Dominguez, G., 2012. The Physical Chemistry of Mass-Independent Isotope Effects and Their Observation in Nature. Annual Review of Physical Chemistry 63, 155–177. https://doi.org/10.1146/annurev-physchem-032511-143657

Thomas, V.M., 1995. The Elimination of Lead in Gasoline. Annual Review of Environment and Resources 20, 301–324. https://doi.org/10.1146/annurev.eg.20.110195.001505

Toubhans, B., Gourlan, A.T., Telouk, P., Lutchman-Singh, K., Francis, L.W., Conlan, R.S., Margarit, L., Gonzalez, D., Charlet, L., 2020. Cu isotope ratios are meaningful in ovarian cancer diagnosis. Journal of Trace Elements in Medicine and Biology 62, 126611. https://doi.org/10.1016/j.jtemb.2020.126611

Trueman, C.N., 2013. Chemical taphonomy of biomineralized tissues. Palaeontology 56, 475–486. https://doi.org/10.1111/pala.12041

Trueman, C.N., Martill, D.M., 2002. The long–term survival of bone: the role of bioerosion. Archaeometry 44, 371–382. https://doi.org/10.1111/1475-4754.t01-1-00070

Trueman, C.N., Tuross, N., 2002. Trace Elements in Recent and Fossil Bone Apatite. Reviews in Mineralogy and Geochemistry 48, 489–521. https://doi.org/10.2138/rmg.2002.48.13

Turner, D.R., 1987. Speciation and Cycling of Arsenic, Cadmium, Lead and Mercury in Natural Waters, in: Hutchinson, T.C., Meema, K.M. (Eds.), Lead, Mercury, Cadmium and Arsenic in the Environment.

Turnlund, J., 1998. Human whole-body copper metabolism. The American Journal of Clinical Nutrition 67, 960S-964S. https://doi.org/10.1093/ajcn/67.5.960S

Tuross, N., 2003. CHAPTER 5 - Recent Advances in Bone, Dentin, and Enamel Biochemistry, in: Ortner, D.J. (Ed.), Identification of Pathological Conditions in Human Skeletal Remains (Second Edition). Academic Press, San Diego, pp. 65–72. https://doi.org/10.1016/B978-012528628-2/50042-9

Tütken, T., Vennemann, T.W., 2011. Fossil bones and teeth: Preservation or alteration of biogenic compositions? Palaeogeography, Palaeoclimatology, Palaeoecology, Special Issue: Fossil bones and teeth: preservation or alteration of biogenic compositions? 310, 1–8. https://doi.org/10.1016/j.palaeo.2011.06.020

Tylecote, R.F., 1992. HISTORY OF METALLURGY 2nd Edition.

van Der Merwe, N.J., 1982. Carbon Isotopes, Photosynthesis, and Archaeology: Different pathways of photosynthesis cause characteristic changes in carbon isotope ratios that make possible the study of prehistoric human diets. American Scientist 70, 596–606. https://www.jstor.org/stable/27851731

Verhoeven, J.D., Pendray, A.H., Dauksch, W.E., Wagstaff, S.R., 2018. Damascus Steel Revisited. JOM 70, 1331–1336. https://doi.org/10.1007/s11837-018-2915-z

Véron, A.J., Flaux, C., Marriner, N., Poirier, A., Rigaud, S., Morhange, C., Empereur, J.-Y., 2013. A 6000-year geochemical record of human activities from Alexandria (Egypt). Quaternary Science Reviews 81, 138–147. https://doi.org/10.1016/j.quascirev.2013.09.029

Veysseyre, A., Moutard, K., Ferrari, C., Velde, K.V. de, Barbante, C., Cozzi, G., Capodaglio, G., Boutron, C., 2001. Heavy metals in fresh snow collected at different altitudes in the Chamonix and Maurienne valleys, French Alps: initial

results. Atmospheric Environment 35, 415–425. https://doi.org/10.1016/S1352-2310(00)00125-4

Vidaud, C., Bourgeois, D., Meyer, D., 2012. Bone as Target Organ for Metals: The Case of f-Elements. Chem. Res. Toxicol. 25, 1161–1175. https://doi.org/10.1021/tx300064m

Viers, J., Dupré, B., Gaillardet, J., 2009. Chemical composition of suspended sediments in World Rivers: New insights from a new database. Sci Total Environ 407, 853–868. https://doi.org/10.1016/j.scitotenv.2008.09.053

Von Endt, D.W., Ortner, D.J., 1984. Experimental effects of bone size and temperature on bone diagenesis. Journal of Archaeological Science 11, 247–253. https://doi.org/10.1016/0305-4403(84)90005-0

Vuceta, J., Morgan, J.J., 1978. Chemical modeling of trace metals in fresh waters: role of complexation and adsorption. ACS Publications 12, 1302–1309. https://doi.org/10.1021/es60147a007

Vulpe, C., Levinson, B., Whitney, S., Packman, S., Gitschier, J., 1993. Isolation of a candidate gene for Menkes disease and evidence that it encodes a copper–transporting ATPase. Nat Genet 3, 7–13. https://doi.org/10.1038/ng0193-7

Vuorio, E., Crombrugghe, B. de, 1990. THE FAMILY OF COLLAGEN GENES. Annual Review of Biochemistry 59, 837–872. https://doi.org/10.1146/annurev.bi.59.070190.004201

Wadsworth, J., Sherby, O.D., 1982. Damascus Steel-Making. Science 218, 328–330. https://doi.org/10.1126/science.218.4570.328.c

Waeles, M., Riso, R.D., Maguer, J.-F., Guillaud, J.-F., Le Corre, P., 2008. On the distribution of dissolved lead in the Loire estuary and the North Biscay continental shelf, France. Journal of Marine Systems, Oceanography of the Bay of Biscay 72, 358–365. https://doi.org/10.1016/j.jmarsys.2007.01.012

Waldron, H.A., 1973. Lead Poisoning in the Ancient World. Med. Hist. 17, 391–399. https://doi.org/10.1017/S0025727300019013

Weiss, D., Boyle, E.A., Wu, J., Chavagnac, V., Michel, A., Reuer, M.K., 2003. Spatial and temporal evolution of lead isotope ratios in the North Atlantic Ocean between 1981 and 1989. Journal of Geophysical Research: Oceans 108. https://doi.org/10.1029/2000JC000762

Wertime, T.A., Muhly, J.D., 1980. The Coming of the age of iron. Yale University Press, New Haven.

Weston, D.A., 2020. Human Osteology, in: Britton, K., Richards, M.P. (Eds.), Archaeological Science: An Introduction. Cambridge University Press, Cambridge, pp. 147–169. https://doi.org/10.1017/9781139013826.007

Whitehead, K., Ramsey, M.H., Maskall, J., Thornton, I., Bacon, J.R., 1997. Determination of the extent of anthropogenic Pb migration through fractured sandstone using Pb isotope tracing. Applied Geochemistry 12, 75–81. https://doi.org/10.1016/S0883-2927(96)00055-8

Whitfield, M., Turner, D.R., 1980. The Theoretical Studies of the Chemical Speciation of Lead in Seawater, in: Branica, M., Konrad, Z. (Eds.), Lead in the Marine Environment. Pergamon, pp. 109–148. https://doi.org/10.1016/B978-0-08-022960-7.50015-4

Wiederhold, J.G., 2015. Metal Stable Isotope Signatures as Tracers in Environmental Geochemistry. Environ. Sci. Technol. 49, 2606–2624. https://doi.org/10.1021/es504683e

Wilson, M.A., Johnston, M.V., Goldstein, G.W., Blue, M.E., 2000. Neonatal lead exposure impairs development of rodent barrel field cortex. Proceedings of the

National Academy of Sciences 97, 5540–5545. https://doi.org/10.1073/pnas.97.10.5540

Woosley, R.J., Millero, F.J., 2013. Pitzer model for the speciation of lead chloride and carbonate complexes in natural waters. Marine Chemistry 149, 1–7. https://doi.org/10.1016/j.marchem.2012.11.004

Wopenka, B., Pasteris, J.D., 2005. A mineralogical perspective on the apatite in bone. Materials Science and Engineering: C, NATO Advanced Study Institute (ASI on Learning from Nature How to design New Implantable Biomaterials: From Biomineralization Fundamentals to Biomimetic Materials and Processing Routes) 25, 131–143. https://doi.org/10.1016/j.msec.2005.01.008

Workman, R.K., Hart, S.R., 2005. Major and trace element composition of the depleted MORB mantle (DMM). Earth and Planetary Science Letters 231, 53–72. https://doi.org/10.1016/j.epsl.2004.12.005

Wu, J., Boyle, E.A., 1997. Lead in the western North Atlantic Ocean: Completed response to leaded gasoline phaseout. Geochimica et Cosmochimica Acta 61, 3279–3283. https://doi.org/10.1016/S0016-7037(97)89711-6

Yamaguchi, M., 2007. Role of Zinc in Bone Metabolism and Preventive Effect on Bone Disorder. Biomedical Research on Trace Elements 18, 346–366. https://doi.org/10.11299/brte.18.346

Chapter 2: Provenance of lead ores used for water pipes production in the ancient Roman Gaul (Vienne, France)

This article has been submitted to the journal Quaternary Science Reviews.

Résumé

Le tissu urbain des villes romaines s'est développé grâce à l'installation de réseaux d'adduction d'eau, principalement en plomb (Pb). En Gaule, la ville de Vienne (France) était au centre de la fabrication d'artefacts en Pb, y compris de grandes quantités de conduites d'eau. Bien que les artefacts en Pb soient souvent marqués d'estampilles romaines indiquant le lieu de fabrication, notre connaissance de la provenance des minerais de Pb extraits et de la manière dont ils étaient importés reste limitée. Dans cette étude, des artefacts romains ont été analysés pour les signatures isotopiques du Pb afin de documenter la source du minerai de Pb utilisé dans les manufactures de Vienne. Les signatures isotopiques ont ensuite été comparées à de nouvelles données sur les minerais de Pb locaux et à une base de données isotopiques du Pb mise à jour à l'aide d'un nouvel algorithme afin d'en identifier la provenance d'identifier la provenance du Pb. Les résultats indiquent que celui utilisé pour la fabrication d'artefacts à Vienne provient principalement d'une source unique. Le traitement des données à l'aide du nouvel algorithme identifie la région minière du massif rhénan comme la source principale et la plus probable, mais certains artefacts présentent une composition isotopique similaire à celle des minerais de Pb locaux. La similitude des signatures isotopiques du Pb des artefacts produits à Vienne avec celles des tuyaux de Mayence et des lingots de plomb du massif rhénan, ainsi que le synchronisme des périodes d'exploitation minière dans cette région, confirment que cette région est la source la plus probable de Pb pour Vienne. Enfin, nous proposons que le Rhin et la Saône soient les voies d'acheminement les plus probables des minerais de Pb vers Vienne pendant la période romaine.

Provenance of lead ores used for water pipes production in the ancient Roman Gaul (Vienne, France)

C. Heredia[1*], S. Guédron[1], A. T. Gourlan[1], F. Albarede[2], H. Delile[3], L. Calzolari[4], S. Campillo[1], S. Santenac[1], L. Audin[1], P. Telouk[2] and B. Helly[5].

[1] Université Grenoble Alpes, Université Savoie Mont Blanc, CNRS, IRD, IFSTAR, ISTerre, 38000, Grenoble, France.

[2] Ecole Normale Supérieure de Lyon, CNRS, and Université de Lyon, 46 Allée d'Italie, 69007, Lyon, France

[3] CNRS, Archéorient, UMR 5133, Maison de l'Orient et de la Méditerranée, University of Lyon 2, Lyon, France.

[4] Department of Earth Sciences, Sapienza University of Rome, Piazzale A. Moro, 5, 00185 Rome, Italy.

[5] Laboratoire ArAr Archéologie et Archéometrie, Maison de l'Orient et de la Méditerranée, University of Lyon 2, Lyon, France.

*Corresponding author:

Carlos Heredia A.; carlos.heredia-aguilar@univ-grenoble-alpes.fr

Keywords: Lead, Pollution, Roman, pipe, lead isotopes

Highlights:

- Intense manufacturing of lead (Pb) artifacts in Vienne during the Roman period
- Artifacts exhibit narrow range of Pb isotope compositions
- Only few artifacts exhibit Pb isotope signature consistent with local Pb ores
- Algorithmic isotope modeling attributes mainly Pb ores to Rhenish Massif mines
- Pb ores were probably shipped by Romans down the Rhine River to Vienne

Abstract

The urban fabric of Roman cities developed through the installation of water supply networks, mainly made of lead (Pb). In Gaul, the city of Vienne (France) was central to the manufacturing of Pb artifacts, *including large volumes of Pb* water pipes. Although Pb artifacts were often labeled with Roman stamps indicating the location of manufacturing, our knowledge of the provenance of extracted Pb ore and the way they were imported remains limited. In this study, Roman artifacts were analyzed for Pb isotope signatures to document the source of Pb ore used in Vienne's manufactories. Pb isotope signatures were then compared with new local Pb ores data and an updated Pb isotope database using a new algorithm to identify the provenance of Pb. Results indicate that Pb used for artifacts manufacturing at Vienne originates mainly from a single source. Data treatment with the new algorithm identifies the Rhenish Massif mining region as the primary and most probable source, but some artifacts exhibit similar isotope composition as local Pb ores. The similarity of the Pb isotopic signatures of the artefacts produced in Vienne with those of Mainz pipes and lead ingots from the Rhenish massif, as well as the synchronicity of the mining periods in this region, support this region as the most likely source of Pb for Vienna. Finally, we propose the Rhine and Saone Rivers as the most probable Pb ores conveyance routes to Vienne during the Roman Period.

2.1. Introduction

Lead (Pb) had considerable industrial importance in the Roman world and was used for the development of urban centers, as well as in the manufacture of ordinary objects (Boulakia, 1972; Delile et al., 2014; Delile et al., 2017). Specifically, the production of lead pipes (i.e., *fistulae*) for urban freshwater supply from the head of the aqueducts (castellum) to private and public buildings played a key role in the development of the Empire (Deming, 2020). Lead was also extensively used in an array of public and domestic applications, such as household and cooking utensils (crafted from pure lead or other alloys like pewter), as an ingredient in cosmetics, medicine, food (i.e., as sweetener and food preserver), and paints (Needleman and Needleman, 1985; Nriagu, 1983).

Lead was mined and smelted in various places within the Empire (e.g., Spain, England, Sardinia…), and its massive extraction has resulted in regional and global Pb contamination recorded in many environmental records around the world (Corella et al., 2021; McConnell et al., 2018; Rosman et al., 1997; Thevenon et al., 2011). As a function of the local market price, Pb could be either extracted locally or imported from distant areas. Hence, to supply urban centers in this strategic metal, numerous terrestrial and navigable (i.e., both maritime and fluvial) transportation routes were developed and mapped (i.e., *Tabula Peutingeriana*) within the Empire (Miller, 1916). In Gaul, Pb extraction by the Gauls predated the Roman invasion. The Greek historian and geographer Strabo of Amasia mentions (3.2.8; 4.1.12; 4.2.2) silver mining in the lands of the *Ruteni* (southern Massif Central) and the *Gabales* (northern Cévennes) (Hirt, 2020). The Romans shaped the Pb mining landscape by expanding existing operations and introducing mining districts like the Cevennes, the Auvergne, and the Alpes (Arnaud et al., 2006; Domergue, 2008; Domergue et al., 2006). In parallel, several metallurgical centers, such as the city of Vienne (*Vienna*, France), were central in manufacturing Pb

artifacts (Adjajd and Lauxerois, 2014). In particular, *large volumes of Pb* water pipes labeled with the mention VF (*Vienna Fecit*) were produced in Vienne to develop the aqueduct network of regional cities (e.g., Vienne, Lyon) during the High Roman Empire, i.e., between 31 BCE and 235 CE (Brissaud, 2015; Cochet, 2000; Cochet and Hansen, 1986). Although numerous Pb artifacts (i.e., pipes) were labeled by the Romans with stamps indicating the manufacturing location, limited information is available on the origin of extracted lead ore and the way they were imported.

To assign the provenance of the lead used for the production of Pb artifacts, Pb isotope signatures are commonly used (Albarède et al., 2020; Albarède et al., 2012; Durali-Mueller et al., 2007; Guédron et al., 2021; Macfarlane and Lechtman, 2014). The geolocation of the Pb source ore has been improved by the development of a new algorithm (Albarede et al., 2024a) that statistically measures the distances between the 3-dimensional space of Pb isotope compositions of artifacts and compares them with those of the isotope compositions of the end-members (ores) derived from a new database taking mass-dependent fractionation into account (Albarede et al., 2024b).

In this study, 22 Roman artifacts, including 16 water pipes, recovered in the ancient city of Vienne (France) and surroundings, together with soil samples from two boreholes collected in the Forum place of the city were analyzed for elemental and Pb isotope signatures, to document the source of Pb and the extent of Pb contamination related to Vienne's metallurgy and manufacturing. In addition, Pb isotope compositions were measured in 29 galena ores collected in 9 local mining areas to complement the existing Pb isotope database. Finally, Pb transport routes to Vienne during the Roman Period are proposed.

2.2. Material and methods

2.2.1. Environmental and archaeological context.

The city of Vienne is located in southeast France at the confluence of the Rhône with a small tributary, the Gère River, 35 km south of Lyon (Fig. 2.1). The city was built on ancient meanders of the Rhône and stretched along both banks of the Rhône River, covering an area of around 200 hectares, including the modern cities of Vienne, Saint-Roman-en-Gal, and Sainte-Colombe (Pelletier, 2001). Vienne's geological context belongs to the Peri-Alpine domain, between two major geological regions: the Hercynian Massif Central (granitic, metamorphic, and basaltic rocks), west of the Rhône River, and the Alpine foothills of Bas-Dauphiné (Miocene and Pliocene Tertiary soils), east of the Rhône River. The bedrock (mostly schists, micaschists, and gneisses) is cut by the glacial valley, with shreds of Tertiary and Quaternary sedimentary formations, predominantly of glacial origin (Donsimoni, 2008; Helly et al., 2017).

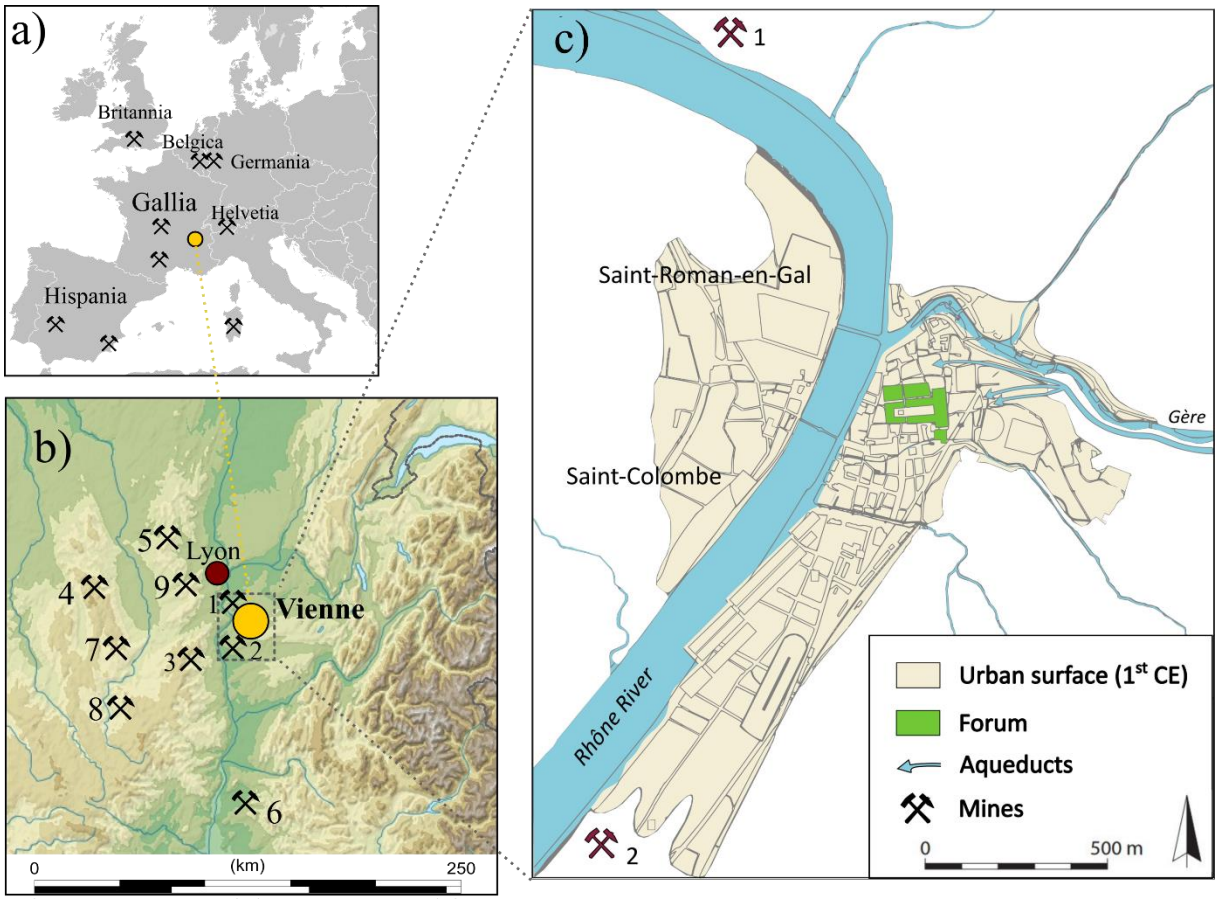

Figure 2.1. *a) Map of the western Roman Empire, including the location of Vienne (yellow dot) and known lead extraction areas (mining symbols), including Gallia (Gaul, now France), Britannia (United Kingdoms), Belgica (Belgium), Germania (Germany), Hispania (Spain) and Sardinia. b) Location of Vienne and the local mines where galena ores were collected and analyzed in this study (1: Estressin, 2: La Poype, 3: Saint-Julien-Molin-Molette, 4: Saint-Martin-La-Sauvauté, 5: Beaujolais, 6: Serves, 7: Monistrol-sur-Loire, 8: Versilhac, and 9: Vaugneray). c) Map of the ancient city of Vienne during the 1st century CE (adapted from (Adjajd and Lauxerois, 2014) with the location of aqueducts and of the Forum in the upper part of the city.*

Vienna is one of the oldest cities in eastern France, with abundant water resources, elevated terrains suitable for agriculture, and endowed natural defenses (i.e., surrounded by 5 hills), which make the city a strategic position. As early as the 5th century BCE, human settlements were identified through archaeological excavations, and in the 3rd century BCE, the city became the capital of the Gallic Allobroges (Adjajd and Lauxerois, 2014). Then, Vienna came under Roman rule in 121 BCE and became a wealthy, well-known port during the High Empire (27 BCE – 235 CE), allowing the connection between the strategic Agrippa and Antoninian Roman road networks (Adjajd and Lauxerois, 2014;

Helly et al., 2017). At that time, lead pipe manufacturing was Vienna's hallmark of metallurgical production (Cochet, 2000; Cochet and Hansen, 1986), and numerous Pb pipes have been excavated throughout the whole Allobroge region, i.e., the French Alpes (Adjajd and Lauxerois, 2014). Archaeological surveys revealed at least 70 workshops [identifiable by their stamped artifacts (Brissaud, 2016)]. Although Pb mines were locally exploited during the Industrial Revolution (Chermette, 1989), no information is available on its exploitation during the Roman times.

2.2.2. Sample collection and preparation for analysis

Twenty-two Gallo-roman lead artifacts were recovered from the archives of the Saint-Roman-en-Gal Museum collection (Tab. S1, Annex 1). The artifacts stem from Vienne (VI, n = 8), Sainte-Colombe (SC, n = 8), Saint-Roman-en-Gal (SRG, n = 3), and Lyon (LY, n = 3), and comprise mostly pipes (n = 16), and a diversity of Roman objects like vessels, sarcophagus, and valves (n = 6, Tab. S1, Annex 1). Within the set of artifacts, 19 were dated to the Early Roman Empire (i.e., -27 BCE – 235 CE), and one to Late Antiquity (i.e., 4th century CE, Tab. S1, Annex 1).

Two 17-meter-long boreholes (SC1 and SC4, Tab. S2, Annex 1) were drilled at the Vienne Forum site during a geotechnical study (2015). The boreholes were re-sampled for the present study every one or two meters. Samples were freeze-dried, sieved at 2mm, and the remaining fraction was crushed with an agate mortar to obtain a fraction below 63µm. The sequence of each borehole covers the last three thousand years, from Quaternary alluvium at the bottom [ca. 6000 year BP, (Bravard and Gaydou, 2015)] to contemporary backfill material on top. Their relative chronologies have been established by archaeologists.

To document Pb isotope signatures of local mines, twenty-one galena ores (PbS, Tab. S3, Annex 1) were sampled from Saint-Julien-Molin-Molette (SJMM, n = 10), Saint-Martin-La-Sauvauté (SMLS, n = 3), and from the mine of Estressin (ES, n = 2) and La Poype (LP, n = 6) located north and south of Vienne, respectively (Fig. 2.1c). However, there is a lack of available information about the history of these mines, except for the 18th and 19th centuries, when some of them were exploited under the Blumenstein mining concession (Chermette, 1989). Four additional mining sites from the Massif Central were also collected to get a regional map of ores, including the Beaujolais (BJ, n = 3), Serves (SR, n = 2), Versilhac (VH, n = 1), Vaugneray (VG, n = 1), and Monistrol-sur-Loire (MSL, n = 1) (Fig. 2.1c and Tab.S1, Annex 1). These data provided a high-resolution focus on the available Pb isotopic data compiled from regional lead ores in the literature (Blichert-Toft et al., 2016; Delile et al., 2014).

2.2.3. Elemental and isotope analysis

Lead artifact samples used for chemical analyses were pried out using metallic pliers. These samples were then leached with 2 ml of double-distilled HCl 7N at room temperature for one hour and sonicated for 10 minutes.

Galena ores and borehole samples were ground in ceramic mortars until a fine powder was obtained (< 63 µm). Then, about 50 mg of powder was digested following a microwave-assisted digestion with concentrated bi-distilled HNO_3 and HCl in a ratio of 3:1 (US EPA Method 3052; (US EPA, 2015). Trace element analysis was performed by inductively coupled plasma mass spectrometry (ICP-MS, Agilent, model 7900) within the analytical chemistry platform of ISTerre (OSUG-France) using a modified version of the method published by (Chauvel et al., 2011). Be, In, and Bi were used as internal standards to correct for instrumental mass bias. The QA/QC for the digestion procedure

was assessed using the certified reference material NIST 2709a, together with sample replicates, providing recoveries of 95 ± 5% for all analyzed elements.

Lead isotopic analyses (^{204}Pb, ^{206}Pb, ^{207}Pb, ^{208}Pb) were obtained with a multi-collector inductively coupled plasma mass spectrometer (MC-ICP-MS, Nu Instruments, NuPlasma HR) at Ecole Normale Supérieure de Lyon using thallium doping, sample standard bracketing (White et al., 2000) and the values for NIST 981 standard of Eisle et al. (2003). Samples were precisely weighted (around 50 mg) and dissolved using 5 ml of concentrated HNO_3 (double-distilled) and 1 ml of concentrated HF (Merck Suprapur quality) either in Savillex® vessels (galena ores and artifacts) at 120 °C for 72 hours or with microwave-assisted digestion (soil) following the US EPA method 3051a (US EPA, 2015). Lead yield (~ 95 %) was checked on an Agilent 7900 quadrupole ICP-MS within the analytical chemistry platform of ISTerre (OSUG-France). Lead was separated and purified from each sample in an HBr medium using anion-exchange columns loaded with AG1-X8 resin (200–400 mesh, Acros Organics) according to a conventional method (Monna et al., 1997; Weeks et al., 2009). The total procedural Pb blank was < 10 pg. The external reproducibility of the reported Pb isotope ratios, assessed through repeated runs of NIST 981 (performed every two samples), is within the range of 100–200 ppm (or 0.01–0.02 %) for ratios based on 204 ($^{206}Pb/^{204}Pb$, $^{207}Pb/^{204}Pb$, $^{208}Pb/^{204}Pb$) and ≈ 50 ppm (or 0.005%) for $^{207}Pb/^{206}Pb$, $^{208}Pb/^{206}Pb$, and $^{207}Pb/^{208}Pb$.

2.2.4. Data treatment and calculations

The three geochemically informed parameters (model age T_{mod}, $\mu = {}^{238}U/^{204}Pb$, and $k = {}^{232}Th/^{238}U$) were obtained with the equations given by Albarède et al. (2012) and using the Matlab code found in Delile et al. (2015). Statistical analyses were performed using SigmaPlot version 12.5. Probability values (p) and correlation coefficients (R) are

reported for linear regression analyses. In all cases, a p-value of 0.05 was chosen to indicate significance at the 95 percent confidence level. All Pb isotope data and calculations are provided in supplementary tables S1, S2 and S3 (Annex 1).

2.3. Results and discussions

2.3.1. Singular lead isotope signature of artifacts manufactured in Vienna

Almost all the Pb artifacts analyzed in this study (Tab. S1, Annex 1) exhibit a tightly clustered isotopic distribution (i.e., $^{208}Pb/^{206}Pb$ = 2.088 ± 0.003, $^{207}Pb/^{206}Pb$ = 0.849 ± 0.001, $^{204}Pb/^{206}Pb$ = 0.054 ± 0.0001, Fig. 2.2a), independently of the nature of Pb artifact and the period in which they were cast (i.e., first to fourth century CE, i.e., Roman period, Fig. 2.2).

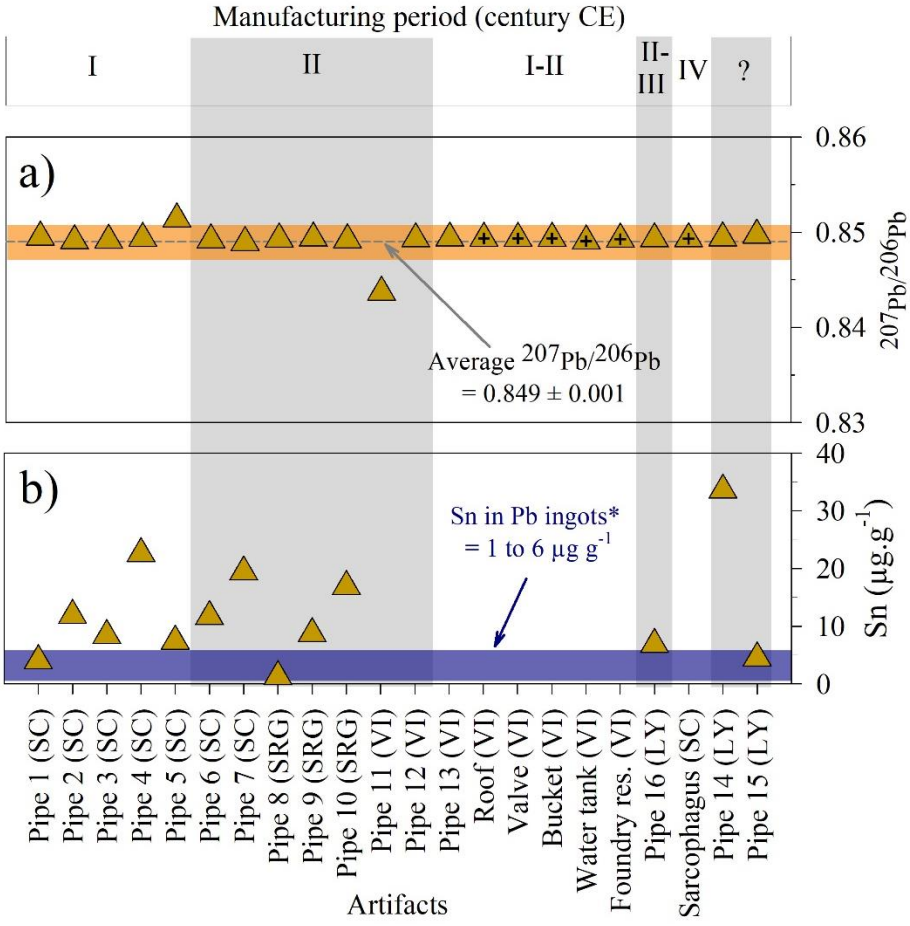

Figure 2.2. *$^{207}Pb/^{206}Pb$ isotopic ratios of water pipes (up triangles, open), and other artifacts (up triangles, cross-hair) retrieved from Vienne (VI), Lyon (LY), Saint-Colombe*

(SC), and Saint-Roman-en-Gal (SRG) in relation to the period of manufacturing. Dark yellow vertical band in panel a) indicates the average $^{207}Pb/^{206}Pb$ isotopic ratios obtained from all studied artifact. Bleu band in panel b) indicates the Sn concentration in a Pb ingots (Baron and Cochet, 2003; Cochet, 2000).*

Pipe 5 ($^{208}Pb/^{206}Pb$ = 2.099, $^{207}Pb/^{206}Pb$ = 0.851, $^{204}Pb/^{206}Pb$ = 0.0544, 1st century CE) and Pipe 11 ($^{208}Pb/^{206}Pb$ = 2.081, $^{207}Pb/^{206}Pb$ = 0.844, $^{204}Pb/^{206}Pb$ = 0.0539, 2nd century CE) deviate from the cluster group. A narrow isotopic distribution was previously found for pipes and ingots retrieved at Trier and Mainz (Durali-Mueller et al., 2007). Such narrow distribution can be attributed to two potential causes: i) the sources of Pb remained relatively unchanged over the four centuries of artifact manufacturing, or ii) lead was recycled and fully homogenized, which is not consistent with the long period of production. Consistently, low Tin (Sn) concentrations measured in our artifacts (12 ± 9 µg.g^{-1}, Fig. 2.2b) do not support repeated re-melting, as re-melted Pb objects should be enriched (by 0.3 to 1%) in solder alloy compounds (Sn) over time (Baron and Cochet, 2003). Hence, the clustered Pb isotopic signature of 20 of the 22 artifacts from Vienne supports a single source of Pb ores for their manufacturing.

2.3.2. Inherited lead pollution at Vienna

Total lead concentration and isotope profiles obtained in the forum boreholes (SC1 and SC4, Fig. 2.3 and Tab. S2, Annex 1) allow the reconstruction of historical Pb pollution in the city of Vienne. The lowest Pb concentrations are found in the deepest layer dated to the Iron Age (av. ± SD = 28 ± 11 µg.g^{-1}, n = 3, red symbols Fig. 2.3a), which are indistinguishable from the local geochemical background of the Rhône [i.e., 17.7 to 22.3 µg.g^{-1}, (Cossa et al., 2018; Dendievel et al., 2020)], and the Upper Continental Crust [i.e., 17 ± 0.5 µg.g^{-1} (Rudnick and Gao, 2010)]. The associated isotopic signatures exhibit the lowest $^{207}Pb/^{206}Pb$ ratios of the record (av. ± SD = 18.778 ± 0.040, n = 3, Fig. 2.3b) and are in the range of reported values for the Upper Continental Crust [i.e., 18.93 ± 0.02

(Millot et al., 2004)]. A major increase in total Pb concentration up to 114 and 893 µg.g^{-1} is observed in both SC1 and SC4 boreholes, respectively, at a depth corresponding to the Roman occupation (i.e., ca 50 BCE – 400 CE, dark yellow symbols, Fig. 2.3a). Accordingly, $^{206}Pb/^{204}Pb$ ratios shift to lower values (18.564 ± 0.097, n = 6, dark yellow, Fig. 2.3b), which are in the range found for our set of Pb artifacts manufactured at Vienne (18.422 ± 0.033, Fig. 2.2a), testifying to the change in Pb source compared to the previous period, likely related to urban runoff and increased local atmospheric emission of Pb during smelting operation in the city. Pb concentrations remained high with similar isotope ratios during the following post-Roman period (green symbols; [Pb] = 200 ± 111 µg.g^{-1}, $^{206}Pb/^{204}Pb$ = 18.505 ± 0.075, n = 4, Fig. 2.3).

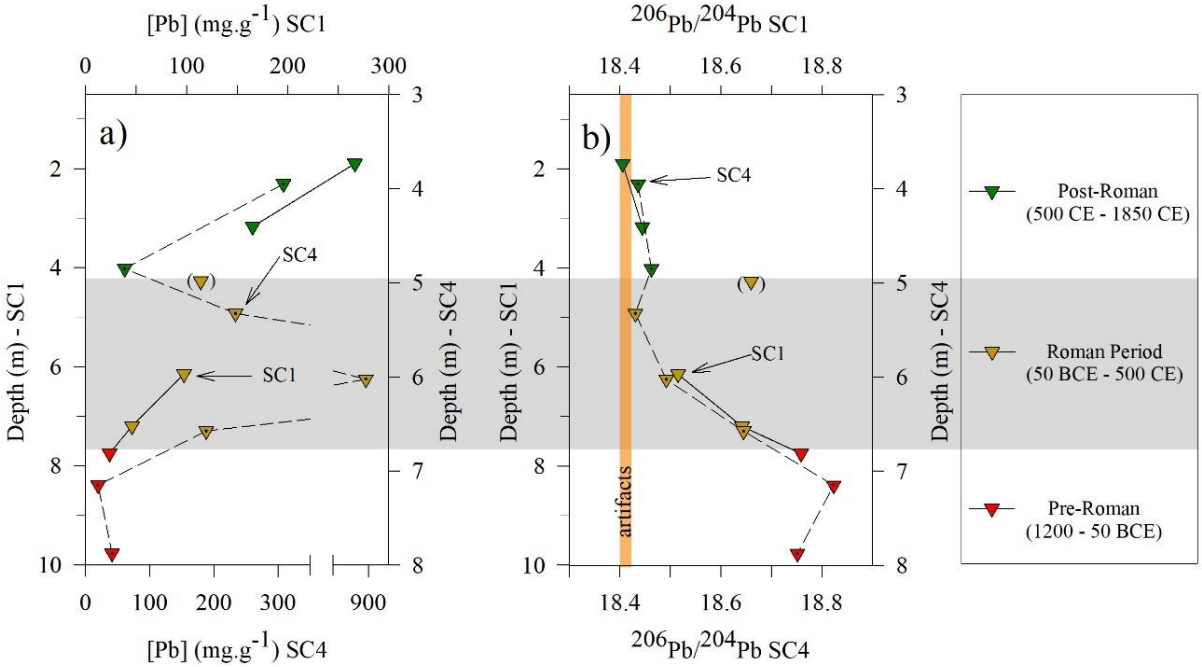

Figure 2.3. *Stratigraphic profile (down triangles) of a) total lead concentrations, and b) $^{207}Pb/^{206}Pb$ isotopic ratios of boreholes SC1(straight line) and SC4 (dotted line) retrieved from Vienne's Forum. Scales between plots were adapted to match ages and periods. Symbol colors indicate their relative age obtained from ceramological dating of borehole layers by archeologists. Red colors refer to the pre-Roman period, dark yellow to the Roman Empire, and dark green to post-roman (i.e., middle age to modern) periods. The average $^{206}Pb/^{204}Pb$ isotopic ratios obtained from studied artifacts from the Roman period are also indicated as a yellowish vertical band. The sample in brackets for core SC1 (at 4.2m deep) is considered to be an outlier due to a singular elemental composition characteristic of a backfill sample [see Fig. S3, Annex 1 and table S2(extended, Annex 1)].*

In the city of Vienne, around 30 km of Pb pipes were needed to connect the aqueducts to the houses (Fig. S1, Annex 1) during the Roman period (Helly, 2018). With an average weight of 10.8 kg for each linear meter of pipe, at least 323 tons of Pb was required to craft and set up this web of pipes. Hence, the increase in Pb concentrations, together with the shift to lower $^{206}Pb/^{204}Pb$ values from the onset of the Roman period onward, indicates a major non-geogenic Pb contamination consistent with the reported peak of Pb manufacturing activities in Vienne (Arnaud et al., 2010, 2006; Cochet and Hansen, 1986). The high Pb levels with similar isotopic signatures after the decline of the Roman Empire suggests the persistence in the soil of historical pollution similar to what has been observed in Rome with Pb isotopic fingerprint of the Rome's fistulae found in the bedload of the Tiber River delta sediments (Delile et al., 2014).

2.3.3. Sources of Pb ores used for water pipe production during the Roman period

2.3.3.1. Limited local mining source during the roman period

In order to determine the main source of Pb used for water pipe production during the Roman period, we compared the isotope ratios ($^{207}Pb/^{206}Pb$ vs $^{208}Pb/^{206}Pb$ and $^{204}Pb/^{206}Pb$ vs $^{208}Pb/^{206}Pb$, ^{206}Pb was taken at both denominators to keep mixing relationships linear) of the Pb artifacts with local galena ores (Fig. 2.4).

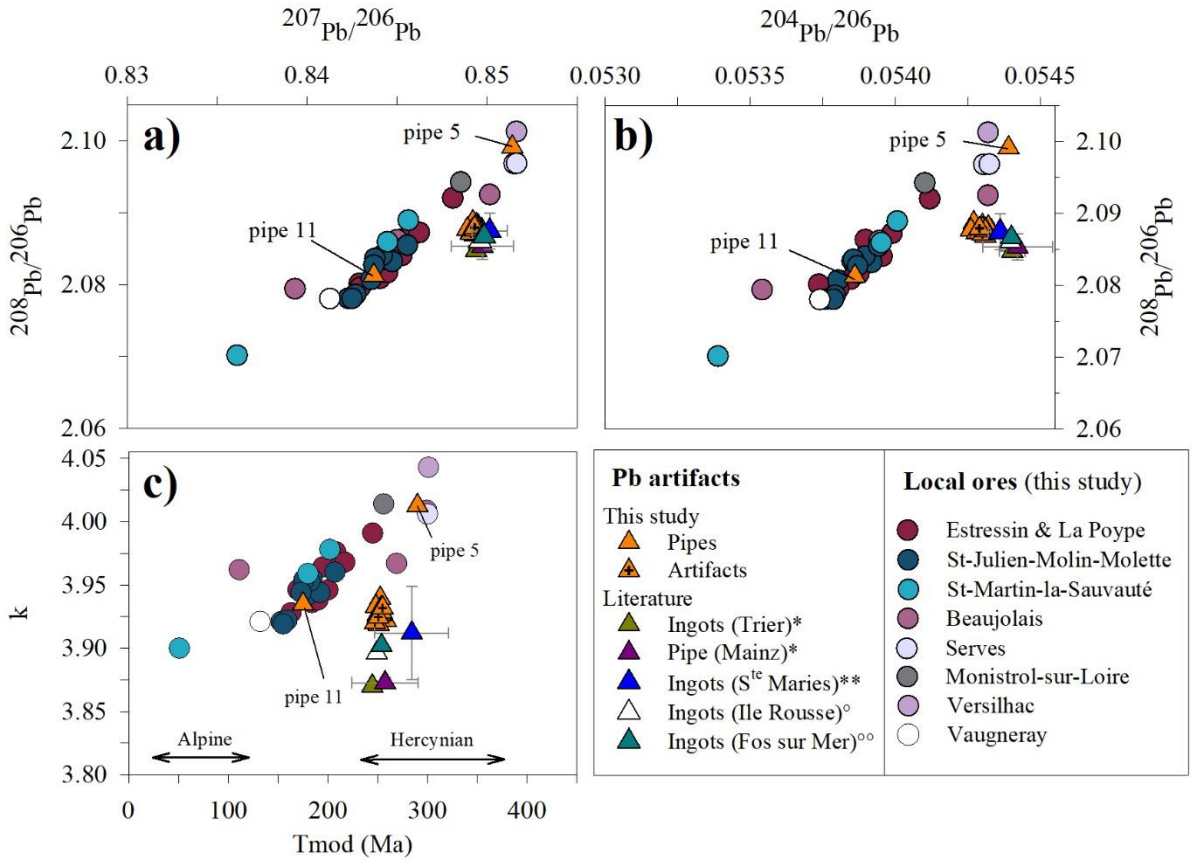

Figure 2.4. *Lead isotope ratios of Roman lead artifacts (up triangles in orange for Vienne, pink for Mainz*), ingots* (Trier = light yellow up triangles, S^{te}. Maries = light green up triangles), and local ores (colored circles) plotted in a) $^{207}Pb/^{206}Pb$ vs $^{208}Pb/^{206}Pb$, b) $^{204}Pb/^{206}Pb$ vs $^{208}Pb/^{206}Pb$, and c) geological parameters (k vs T_{mod}). Error bars represent the standard deviation of the average values for lead pipes from Mainz*, and ingots from Trier* (Durali-Mueller et al., 2007), Saintes-Maries-de-la-Mer** (Baron et al., 2011), Ile Rousse° (Raepsaet et al., 2015), and Fos sur Mer°° (Raepsaet-Charlier, 2011; Raepsaet et al., 2015).*

Isotope ratios of the artifacts exhibit distinct signatures from that of the 29 local galena analyzed. Only pipes 5 and 11 overlap, respectively, with the ores from Serves and Monistrol-sur-Loire and Saint-Julien-Molin-Molette, Estressin, and La Poype (Fig. 2.4a and b). All this suggests that local Pb sources were probably known and exploited occasionally during the Roman times but that local mining only became significant during the 18th and 19th centuries, i.e., a period of intense local mining during the Industrial Revolution (Chermette, 1989).

2.3.3.2. Identification of the most probable mining source of Pb ores used in Vienna

Mining in Gaul experienced a significant boost after the Roman conquests and was mainly focused on iron extraction, whereas Gaul's resources for lead, silver, and copper were of lesser importance when compared with those of other provinces (Domergue et al., 2006). Indeed, within the western Roman Empire, major Pb extraction areas were Spain (Cartagena-Mazarron and Sierra Morena), Belgium/Germany (Rhenish Massif), England (Pennines), and Sardinia (Bode et al., 2009; Domergue and Rico, 2014a). The Iberian region, whose Pb signal is recorded in numerous sediment archives in Europe (Corella et al., 2021; Elbaz-Poulichet et al., 2011; Elbaz-Poulichet et al., 2020; Martínez Cortizas et al., 2013; Thevenon et al., 2011) and polar ice (McConnell et al., 2018; Rosman et al., 1997), was mined as early as the sixth century BC, then by the Romans in the first century CE, after which activity declined considerably probably due to high costs and the incorporation of new mining territories such as the British and German mines (Boulakia, 1972).

To test these potential sources and to assign the provenance of Pb ores used at Vienne, Pb isotope signatures of each Pb artifact were individually implemented in a new algorithm (Albarede et al., 2024a) to compare the distances between the 3-dimensional space of their Pb isotope compositions with those of a new reference database of ores Pb isotope (Albarede et al., 2024b). Except for pipes 5 and 11, which match with regional ores (Fig. S3, Annex 1), the algorithm's outputs for the independent analyses of the remaining 20 artifacts converge on 6 possible locations (Figs. 2.5 and S3, Annex 1) as the main source of Pb ores, i.e., i) the Rhenish Massif (i.e., Gallia Belgica /Germania), ii) the Pennine (i.e., Britannia), iii) the Wallis (i.e., Vallesia), iv) the Cevennes (i.e., Cevenna), v) Sardinia, and vi) the Brittany peninsula (i.e., Armorica).

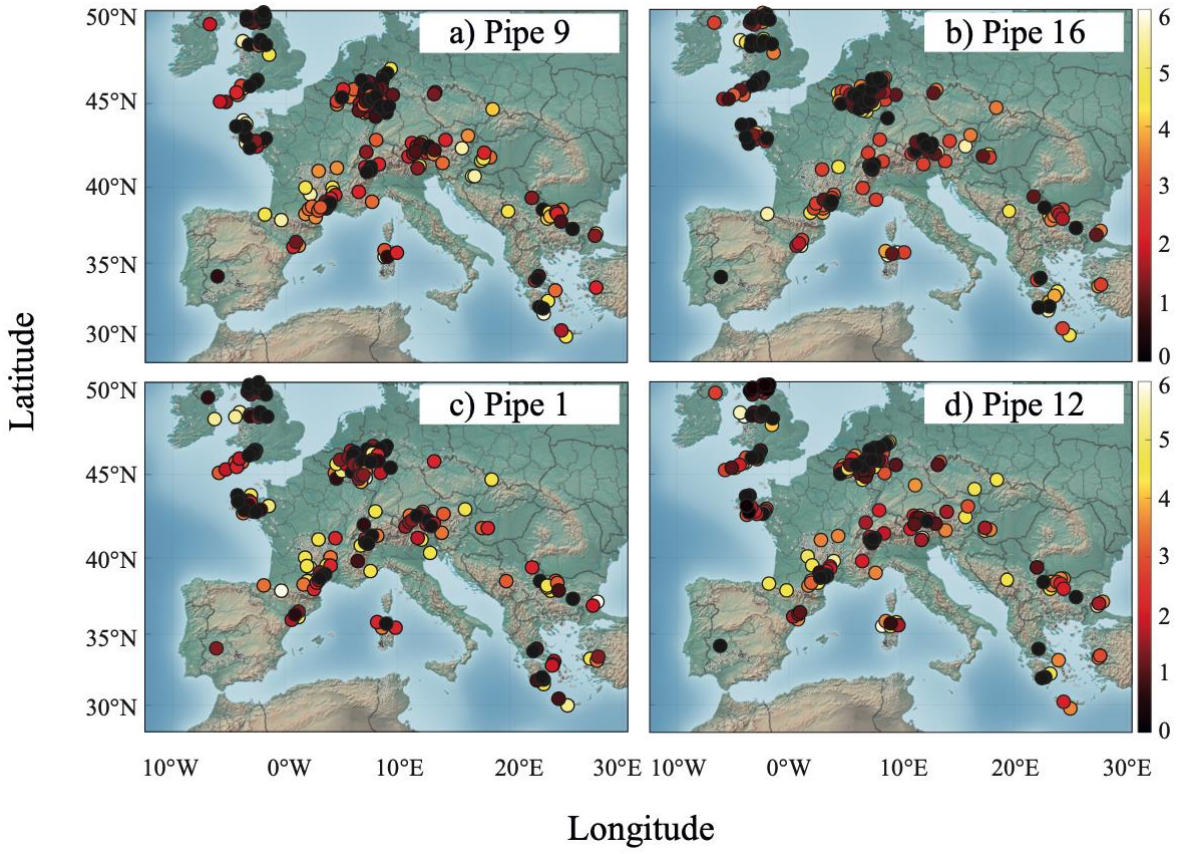

Figure 2.5. *Four outputs of the data treatment obtained with the newly published algorithm (Albarede et al., 2024a) showing the statistical probability of correspondence of Pb isotope compositions of artifacts from Vienne; a) pipe 9 from St-Roman-en-Gal, b) pipe 16 from Lyon, c) sarcophagus from Sainte Colombe, and d) bucket from Vienne, compared with the isotope compositions of end-members (ores) derived from a new database (Albarede et al., 2024b). The statistical probability of correspondence increases from white (value of 6) to black (value of 0) dots. The size of dots with a high probability of correspondence (dark colors) was increased to ease the reading. The treatment for all the other artifacts is presented in Fig. S3, Annex 1.*

Such matches in isotopic signatures between Pb mineralization from distant regions are common because ores belong to the Hercynian domain. However, several sources can easily be dismissed as their period of exploitation is inconsistent with the Viennese manufacturing period. This is the case for the Armorican Brittany and the Cevennes, which all present lower statistical probabilities (Figs. 2.4 and S3, Annex 1), and were respectively exploited during the first and second centuries BCE, the fourth century CE and the medieval period [(Baron et al., 2006; Domergue et al., 2006), Fig. S4, Annex 1]. In the case of Sardinia, the statistical probabilities are similar, and although the period of Pb mining is consistent with the period of Viennese artifacts manufacturing, most of

studies focusing on Pb exportation routes report fluxes centralized towards Italy [i.e., Roma (Boni et al., 2000; Domergue et al., 2006; Ingo et al., 1996)].

Of the three remaining sites with the best statistical matches for the 20 artifacts (Figs. 2.4 and S3, Annex 1), the Rhenish Massif is the most likely source, given the period of exploitation of the mines and evidence of regional export network for lead ingots in the Roman Empire. This mining region corresponds to both the Eifel district in current Germany (Durali-Mueller et al., 2007) and the Belgian zinc-lead deposits of the Hautes Fagnes Plateau (Cauet et al., 1982; Dejonghe, 1998; Renson et al., 2008). Archaeologists report Roman occupation in this mining district from ca. 50 BCE to 400 CE (Fig. S4, Annex 1) with extensive mining (Domergue and Rico, 2014a; Rothenhöfer et al., 2013), consistently with the period of Pb artifacts manufacturing at Vienne (Allan et al., 2018; Renson et al., 2008). The Rhenish district has been mined since the first century BCE (Domergue, 2008), and isotopically identified as the source of Pb artifacts (Fig. 2.4) found at numerous archaeological sites of the Rhine basin (Germany), including waterpipes from Mainz, and Pb ingots recovered in Trier (Bode et al., 2009; Durali-Mueller et al., 2007). In addition, Roman wrecks discovered in the Mediterranean sea (first century CE), at Les Saintes-Maries-de-la-Mer (Baron and Cochet, 2003; Baron et al., 2011), Fos-Sur-Mer, and in Corsica (Ile Rousse) or Sardina (Riccardi, Genovesi 2002) have revealed Pb ingots stamped "*plumbum Germanicum"*, isotopically matching with the Rhenish massif ores (Bode et al., 2009; Raepsaet-Charlier, 2011; Raepsaet et al., 2015), highlighting a major export network of German Pb within the Roman Empire. In addition, the presence of the Emperor's name in the main seal molded of these ingots indicates that Pb production and export was a direct state management operation, relying, in certain circumstances, on the technical resources of the army and local populations (Raepsaet et al., 2015).

In contrast, the Swiss Alpine region (Wallis area) silver-lead mines (galena) remained relatively small-scale and local Pb resources only appeared in a late phase of the Roman era, indicating that this source was certainly secondary, if not minor during the Roman period (Guénette-Beck et al., 2009; Guénette-Beck and Serneels, 2011; Köppel et al., 1993). In Roman Britain, ore deposits of Derbyshire and Cumberland (Central and Northwestern England, respectively) have produced and exported large amounts of Pb after the Roman conquest in the second half of the first century CE (Boulakia, 1972; Domergue, 2008; Tylecote, 1964). However, this period of Roman Britain mining appears in the second half of the production period of Viennese artifacts [i.e., between 31 BCE and 235 CE (Brissaud, 2015; Cochet, 2000; Cochet and Hansen, 1986)].

Hence, this supports the Rhenish Massif as the most probable mining area that provided large amounts of Pb for the manufacturing of Pb artifacts in Vienne during at least the two first centuries CE.

2.3.4. Potential routes of Pb export to the Gallo-Roman city of Vienna

Within the Roman empire, Pb ingots were transported through a vast and well-established network of land, fluvial, and maritime trade routes (Domergue and Rico, 2014b). Among the network of Roman roads in Gaul, the *Viae Agrippae*, built in the 1st century BCE, radiated from the strategic Roman settlement of Lyon (*Lugdunum*) to the Atlantic Ocean, the Mediterranean, and the Rhine region (Purcell, 1990). Because imperial roads (e.g., *Viae Agrippae*) were mainly designed for military and administrative purposes, fluvial transport was often preferred to support heavy transport (Duval, 1989). As the upstream river travel was constraining, it is likely that overland routes, located mainly on towpaths, were often preferred, whereas river traffic was probably favored for the downstream

navigation. Moreover, the transport of Pb ingots does not entail volume constraints but does require sufficient animal towing power.

Based on the main mapped strategic routes (i.e., *Tabula Peutingeriana*) of the Roman Empire (Miller, 1916), using the ORBIS Geospatial Network Model of the Roman World (Scheidel and Meeks, 2012), we identified the most relevant and reliable routes for connecting a chosen mining district to Vienne. Three routes are tested from a) the Rhenish Massif, b) the Alpes, and c) England, identified as the main probable sources of Pb for Vienne (Fig. 2.6).

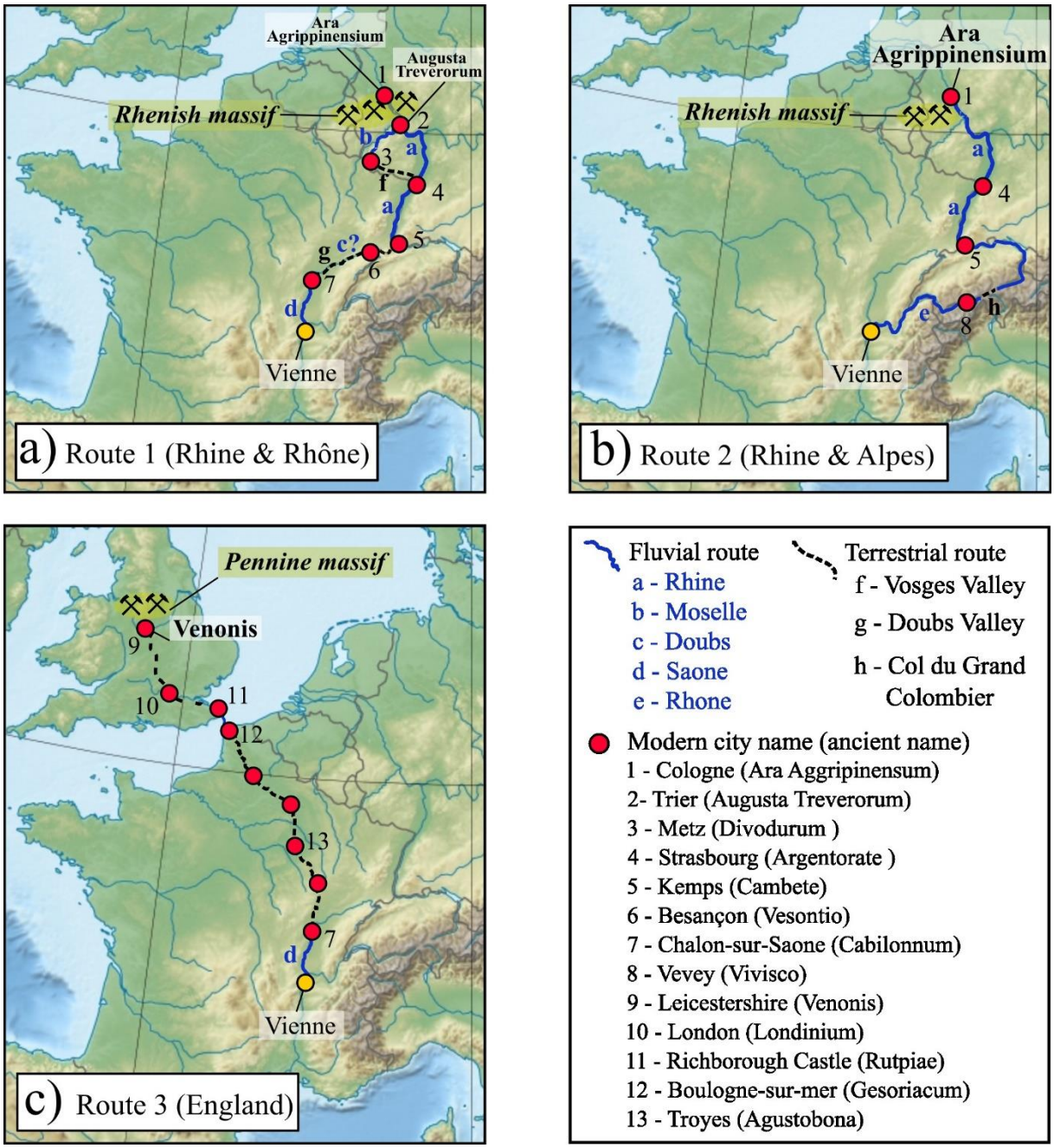

Figure 2.6. *Three most probable routes of conveyance of Pb ingots to Vienne from the Rhenish Massif via the Rhine (a) or the Alpes (b), and from England (c), using the ORBIS Geospatial Network Model of the Roman World (Scheidel and Meeks, 2012). Terrestrial routes following the riverbank (towpath) are indicated with a prime after the letter.*

From the Rhenish massif mining district to Lyon a roman network of forts and cities (i.e., Neuss, Bonn, Mainz, Strasbourg, Basel) was established along the Rhine, linked by direct routes that served mainly for military and administrative purposes but also as supply routes in Gaul (Dalgaard et al., 2022; Franconi, 2014). The first possible route (Fig. 2.6a) passes through or along the Rhine River from Cologne to Kemps, or alternatively along

the Moselle River, followed by an overland route to the Rhine in the Vosges valley between Metz and Strasbourg, and continued by the Doubs River to Chalon-sur-Saone, and by the Saone and Rhône River to Vienne. An alternative route through the Alpes (Fig. 2.6b) follows the same path as route 1 until Kemps, but then continues overland to Vevey through the Alpes and rejoins Vienne through or along the Rhone River. This later route segment corresponds to the route between Wallis and Vienne (i.e., route 4 in Table 2.1). The comparison of routes 1 and 2 (Table 2.1) shows that when upstream river travel by towpath is chosen, the cost is almost similar for the two routes, but Route 1 is the fastest route to Vienne.

Table 2.1. *Estimation of the distance, time, and cost per kg. of Pb of the three probable routes connecting the Rhenish Massif to Vienne using the ORBIS Geospatial Network Model of the Roman World (Scheidel and Meeks, 2012). The mean daily travel speeds established by the model are 20 km/day by donkey or wagon, 65 km/day for downriver travel, and 15 km/day for upriver travel. Freight charges for road and river transport are set according to the Tetrarchic price Edict of 301 CE (Roueché et al., 1989). For route 1, an alternative (*) via the Moselle River is proposed, and information is presented as numbers in parenthesis.*

	Route 1: Rhine (via Moselle)*		**Route 2: Alpes**		**Route 3: Britannia**	**Route 4: Wallis**
	Fluvial/ terrestrial	Terrestrial only	Fluvial/ terrestrial	Terrestrial only	Maritime/ terrestrial	Terrestrial only
Distance (Km)	1025 (983)	911 (873)	968	923	1412	320
Time (days)	46 (41)	44 (42)	55	46	49	16
Cost per Kg. of goods by donkey (denarii)	10 (13)	26 (25)	16	26	26	9
Cost per Kg. of goods by wagon (denarii)	11 (15)	32 (29)	19	32	30	11

When the combination of fluvial and terrestrial routes is considered, transport duration is almost similar for the two routes, but routes 1 is the cheapest itinerary, all modes of transport considered. Marked volumes of traffic on the Rhine River have been reported

since the first century CE (Ellmers, 1980; Ollive et al., 2006; Ollive et al., 2008), and flat-bottomed Roman Barges with load capacities estimated between 65 and 110 tons have been excavated throughout the Rhine basin (Bockius, 2004; Vos et al., 2011). In the continuity of the Rhine, the Saone/Rhône Rivers were also major routes for Roman inland water shipping (Christol and Fiches, 1999; Lonchambon et al., 2009). Consistently, the large number of Pb ingots retrieved in the Mediterranean Sea support the fluvial transport at least for the Saone/Rhône part of the routes. Hence, roads and rivers were surely used to complement each other.

From the Pennines mining district to Vienne, the route (Fig. 2.6c) passes through England from Venonis to the port of Richborough, followed by a maritime navigation to Boulogne-sur-Mer, and a terrestrial route to Vienne via Troyes. In comparison to the route 1 from the Rhenish massif, the transport of Pb from the Pennines (route 3) shows similar travel duration but higher cost of transport (Table 2.1) when the combination of fluvial and terrestrial routes is considered.

2.4. Conclusion

The study of the Pb isotopic signatures of Roman pipes and artifacts from Vienna suggests that most of the lead used by the manufacturers at Vienna was of distant origin. The most probable source is attributed to the mines in the Rhenish massif, but one cannot exclude a contribution from mines in Roman Britain. Surprisingly, local and regional mines appear to be secondary in the composition of Viennese Pb products.

This certainly reflects the economic market for Pb during Imperial Rome, where, as today, Pb manufacturers in Vienna bought raw materials at the best price, according to the existing market, and made stocks according to metal prices and dependence on supply and demand. One also have to consider that Pb production and export from the Rhenish

massif was managed by the state. Hence, supply costs were probably not a major obstacle in the centralized economy of the Roman era, and transport from Gallia Belgica seems realistic. The presence of local signatures on a small number of objects also reveals that, in some cases, local mines were probably used when Pb prices rose or for smaller production runs.

Future archaeological discoveries and the study of other artifacts will certainly complete this picture, refine the chronology, and identify importation routes for this metal, which was central to the development of Roman Gaul.

Acknowledgments

This study received financial support from the French National program EC2CO (Ecosphère Continentale et Côtière) of CNRS, and the ISTerre (Institute of earth Science, Grenoble) internal grants. This work was also conducted with the support of the LABEX IMU (ANR-10-LABX-0088) of the University of Lyon, within the framework of the "Investissements d'Avenir" program managed by the Agence Nationale de la Recherche (ANR).

This study was performed using the INSU/CNRS MC-ICP-MS national facility at ENS-LYON. The authors would like to thank the SRA (Service Regional de l'Archéologie), the DRAC (Direction Régionale des affaires culturelles), and the Museum Gallo-Romain St-Romain-en-Gal of Vienna for the access to the artefacts. They also thank the mayor of Vienne City for authorizing us to study the boreholes drilled for a preliminary study for the creation of a future parking. The authors wish to express their gratitude to Patrick Joly for providing us the ore samples analyzed in this study from his private collection, to Benjamin Clément (Senior Lecturer, Université de Franche-Comté, Laboratoire Chrono-environnement - UMR 6249 CNRS-UFC), the Archeodunum preventive archaeology

office, and Hugues Savay Guerraz (director of the Lugdunum Museum & Roman Theatres) for giving us access to the artifacts.

Authors contributions:

Carlos Heredia, Alexandra T. Gourlan, Stéphane Guédron, Sylvain Campillo, Sabine Santenac, and Philippe Telouk made the data analysis. Alexandra T. Gourlan, Stéphane Guédron, Benoit Helly, and Laurence Audin contributed to the study's conception and design. Carlos Heredia, Stéphane Guédron, and Alexandra T. Gourlan contributed to the drafting of the manuscript, and in addition, Hugo Delile, Benoit Helly, Francis Albarede and Laura Calzolari helped with the critical interpretation of data. The authors read, amended, and approved the final manuscript.

References

Adjajd, F., Lauxerois, R., 2014. Carte archéologique de la Gaule 38-3 : Vienne. Académie des inscriptions et belles-lettres.

Adkins, L., Adkins, R.A., Adkins, L., Adkins, R.A., 1999. Handbook to Life in Ancient Rome. Oxford University Press, Oxford, New York.

Albarede, F., Blichert-Toft, J., Gentelli, L., Milot, J., Vaxevanopoulos, M., Klein, S., Westner, K., Birch, T., Davis, G., de Callataÿ, F., 2020. A miner's perspective on Pb isotope provenances in the Western and Central Mediterranean. Journal of Archaeological Science 121, 105194. https://doi.org/10.1016/j.jas.2020.105194

Albarede, F., Davis, G., Blichert-Toft, J., Gentelli, L., Gitler, H., Pinto, M., Telouk, P., 2024a. A new algorithm for using Pb isotopes to determine the provenance of bullion in ancient Greek coinage. Journal of Archaeological Science 163, 105919. https://doi.org/10.1016/j.jas.2023.105919

Albarede, F., Davis, G., Gentelli, L., Blichert-Toft, J., Gitler, H., Pinto, M., Telouk, P., 2024b. Bullion mixtures in silver coinage from ancient Greece and Egypt. Journal of Archaeological Science 162, 105918. https://doi.org/10.1016/j.jas.2023.105918

Albarède, F., Desaulty, A.-M., Blichert-Toft, J., 2012. A GEOLOGICAL PERSPECTIVE ON THE USE OF Pb ISOTOPES IN ARCHAEOMETRY. Archaeometry 54, 853–867. https://doi.org/10.1111/j.1475-4754.2011.00653.x

Allan, M., Pinti, D.L., Ghaleb, B., Verheyden, S., Mattielli, N., Fagel, N., 2018. Reconstruction of Atmospheric Lead Pollution During the Roman Period Recorded in Belgian Ombrotrophic Peatlands Cores. Atmosphere 9, 253. https://doi.org/10.3390/atmos9070253

Arnaud, F., Serralongue, J., Winiarski, T., Desmet, M., 2010. Une pollution métallique antique en haute vallée de l'Arve. ArcheoSciences. Revue d'archéométrie 197–201. https://doi.org/10.4000/archeosciences.2759

Arnaud, F., Serralongue, J., Winiarski, T., Desmet, M., Paterne, M., 2006. Pollution au plomb dans la Savoie antique (II–IIIe s. apr. J.-C.) en relation avec une installation métallurgique de la cité de Vienne. Comptes Rendus Geoscience 338, 244–252. https://doi.org/10.1016/j.crte.2005.11.008

Arthur, P., Marsh, G., 1978. Early Fine Wares in Roman Britain. BAR Publishing. https://doi.org/10.30861/9780860540410

Baron, S., Carignan, J., Laurent, S., Ploquin, A., 2006. Medieval lead making on Mont-Lozère Massif (Cévennes-France): Tracing ore sources using Pb isotopes. Applied Geochemistry 21, 241–252. https://doi.org/10.1016/j.apgeochem.2005.09.005

Baron, S., Cochet, A., 2003. Étude d'un lot de lingots de plomb antiques des Saintes-Maries-de-la-Mer. Ségrégations et analyses chimiques élémentaires. ArchéoSciences, revue d'Archéométrie 27, 147–163. https://doi.org/10.3406/arsci.2003.1051

Baron, S., Coustures, M.-P., Béziat, D., Guérin, M., Huez, J., Robbiola, L., 2011. Lingots de plomb et barres de fer des épaves romaines des Saintes-Maries-de-la-Mer (Bouches-du-Rhône, France) : Questions de traçabilité comparée. Revue archéologique de Narbonnaise 44, 71–97. https://doi.org/10.3406/ran.2011.1820

Blichert-Toft, J., Delile, H., Lee, C.-T., Stos-Gale, Z., Billström, K., Andersen, T., Hannu, H., Albarède, F., 2016. Large-scale tectonic cycles in Europe revealed by distinct Pb isotope provinces. Geochemistry, Geophysics, Geosystems 17, 3854–3864. https://doi.org/10.1002/2016GC006524

Bockius, R., 2003. Ancient riverborne transport of heavy loads, in: Pasquinucci, M., Weski, T. (Eds.), Close Encounters: Sea- and Riverborne Trade, Ports and Hinterlands, Ship Construction and Navigation in Antiquity, the Middle Ages and in Modern Time. Oxford : Archaeopress, Oxford, pp. 105–116.

Bode, M., Hauptmann, A., Mezger, K., 2009. Tracing Roman lead sources using lead isotope analyses in conjunction with archaeological and epigraphic evidence—a case study from Augustan/Tiberian Germania. Archaeol Anthropol Sci 1, 177–194. https://doi.org/10.1007/s12520-009-0017-0

Boni, M., Maio, G.D., Frei, R., Villa, I.M., 2000. Lead Isotopic Evidence for a Mixed Provenance for Roman Water Pipes from Pompeii*. Archaeometry 42, 201–208. https://doi.org/10.1111/j.1475-4754.2000.tb00876.x

Boulakia, J.D.C., 1972. Lead in the Roman World. American Journal of Archaeology 76, 139–144. https://doi.org/10.2307/503857

Bravard, J.-P., Gaydou, P., 2015. Historical Development and Integrated Management of the Rhône River Floodplain, from the Alps to the Camargue Delta, France, in: Hudson, P.F., Middelkoop, H. (Eds.), Geomorphic Approaches to Integrated Floodplain Management of Lowland Fluvial Systems in North America and Europe. Springer, New York, NY, pp. 289–320. https://doi.org/10.1007/978-1-4939-2380-9_12

Brissaud, L., 2016. Les fistulae estampillées VASSEDO. VF : réflexion critique sur la valeur et la fonction d'un nom, in: Brancier, J., Vallette, T., Rémeaud, C. (Eds.), Des vestiges aux sociétés : Regards croisés sur le passage des données archéologiques à la société sous-jacente, Archéo.doct. Éditions de la Sorbonne, Paris, pp. 57–83. https://doi.org/10.4000/books.psorbonne.4822

Cauet, S., Weis, D., Herbosch, A., 1982. Genetic study of Belgian lead zinc mineralizations in carbonate environments through lead isotopic geochemistry. Bulletin du BRGM.

Chauvel, C., Bureau, S., Poggi, C., 2011. Comprehensive Chemical and Isotopic Analyses of Basalt and Sediment Reference Materials. Geostandards and Geoanalytical Research 35, 125–143. https://doi.org/10.1111/j.1751-908X.2010.00086.x

Chermette, A., 1989. La famille de Blumenstein et l'exploitation des mines du Forez aux XVIIIe et XIXe siècles. Publications de la Société Linnéenne de Lyon 58, 1–12. https://doi.org/10.3406/linly.1989.10872

Christol, M., Fiches, J.-L., 1999. Le Rhône : batellerie et commerce dans l'Antiquité. Gallia 56, 141–155. https://doi.org/10.3406/galia.1999.3251

Cilliers, L., Retief, F., 2019. Lead Poisoning and the Downfall of Rome: Reality or Myth?, in: Wexler, P. (Ed.), Toxicology in Antiquity (Second Edition), History of Toxicology and Environmental Health. Academic Press, pp. 221–229. https://doi.org/10.1016/B978-0-12-815339-0.00014-7

Cochet, A., 2000. Le Plomb en Gaule romaine. Techniques de fabrication et produits, Editions Mergoil. ed.

Cochet, A., Hansen, J., 1986. Conduites et objets de plomb gallo-romains de Vienne (Isère). CNRS.

Corella, J.P., Sierra, M.J., Garralón, A., Millán, R., Rodríguez-Alonso, J., Mata, M.P., de Vera, A.V., Moreno, A., González-Sampériz, P., Duval, B., Amouroux, D., Vivez, P., Cuevas, C.A., Adame, J.A., Wilhelm, B., Saiz-Lopez, A., Valero-Garcés, B.L., 2021. Recent and historical pollution legacy in high altitude Lake Marboré (Central Pyrenees): A record of mining and smelting since pre-Roman times in

the Iberian Peninsula. Science of The Total Environment 751, 141557. https://doi.org/10.1016/j.scitotenv.2020.141557

Cossa, D., Fanget, A.-S., Chiffoleau, J.-F., Bassetti, M.-A., Buscail, R., Dennielou, B., Briggs, K., Arnaud, M., Guédron, S., Berné, S., 2018. Chronology and sources of trace elements accumulation in the Rhône pro-delta sediments (Northwestern Mediterranean) during the last 400 years. Progress in Oceanography, Special issue of MERMEX project: Recent advances in the oceanography of the Mediterranean Sea 163, 161–171. https://doi.org/10.1016/j.pocean.2017.01.008

Dalgaard, C.-J., Kaarsen, N., Olsson, O., Selaya, P., 2022. Roman roads to prosperity: Persistence and non-persistence of public infrastructure. Journal of Comparative Economics 50, 896–916. https://doi.org/10.1016/j.jce.2022.05.003

De Keersmaecker, M., Dowsett, M., Adriaens, M., 2018. A short historical overview on the use of lead, in: Chemical Interactions between Cultural Artefacts and Indoor Environment. ACCO, pp. 193–214.

Dejonghe, L., 1998. Zinc–lead deposits of Belgium. Ore Geology Reviews 12, 329–354. https://doi.org/10.1016/S0169-1368(98)00007-9

Delile, H., Blichert-Toft, J., Goiran, J.-P., Keay, S., Albarède, F., 2014. Lead in ancient Rome's city waters. Proceedings of the National Academy of Sciences 111, 6594–6599. https://doi.org/10.1073/pnas.1400097111

Delile, H., Blichert-Toft, J., Goiran, J.-P., Stock, F., Arnaud-Godet, F., Bravard, J.-P., Brückner, H., Albarède, F., 2015. Demise of a harbor: a geochemical chronicle from Ephesus. Journal of Archaeological Science 53, 202–213. https://doi.org/10.1016/j.jas.2014.10.002

Deming, D., 2020. The Aqueducts and Water Supply of Ancient Rome. Groundwater 58, 152–161. https://doi.org/10.1111/gwat.12958

Dendievel, A.-M., Mourier, B., Dabrin, A., Delile, H., Coynel, A., Gosset, A., Liber, Y., Berger, J.-F., Bedell, J.-P., 2020. Metal pollution trajectories and mixture risk assessed by combining dated cores and subsurface sediments along a major European river (Rhône River, France). Environment International 144, 106032. https://doi.org/10.1016/j.envint.2020.106032

Domergue, C., 2010. Les mines antiques. La production des métaux aux époques grecque et romaine. Picard.

Domergue, C., Cauuet, B., Orzechowski, S., Vincent, S., 2006. Mines et métallurgies en Gaule à la fin de lâge du Fer et à lépoque romaine. Gallia.

Domergue, C., Rico, C., 2014a. L'approvisionnement en métaux de l'Occident méditerranéen à la fin de la République et sous le Haut-Empire. Flux, routes, organisation, in: Infrastructure and Distribution in Ancient Economies, Proceedings of a Conference Held at the Austrian Academy of Sciences. pp. 193–252.

Domergue, C., Rico, C., 2014b. Les itinéraires du commerce du cuivre et du plomb hispanique à l'époque romaine dans le monde méditerranéen. Bulletin de la Société des Sciences historiques et naturelles de la Corse 135.

Donsimoni, M., 2008. Carte géologique harmonisée du département de l'Isère. (Rapport Technique No. BRGM/RP-56424-FR). BRGM.

Durali-Mueller, S., Brey, G.P., Wigg-Wolf, D., Lahaye, Y., 2007. Roman lead mining in Germany: its origin and development through time deduced from lead isotope provenance studies. Journal of Archaeological Science 34, 1555–1567. https://doi.org/10.1016/j.jas.2006.11.009

Duval, P.-M., 1989. Les voies gallo-romaines. Publications de l'École Française de Rome 116, 739–756.

Eisele, J., Abouchami, W., Galer, S.J.G., Hofmann, A.W., 2003. The 320 kyr Pb isotope evolution of Mauna Kea lavas recorded in the HSDP-2 drill core. Geochemistry, Geophysics, Geosystems 4. https://doi.org/10.1029/2002GC000339

Elbaz-Poulichet, F., Dezileau, L., Freydier, R., Cossa, D., Sabatier, P., 2011. A 3500-Year Record of Hg and Pb Contamination in a Mediterranean Sedimentary Archive (The Pierre Blanche Lagoon, France). Environ. Sci. Technol. 45, 8642–8647. https://doi.org/10.1021/es2004599

Elbaz-Poulichet, F., Guédron, S., Anne-Lise, D., Freydier, R., Perrot, V., Rossi, M., Piot, C., Delpoux, S., Sabatier, P., 2020. A 10,000-year record of trace metal and metalloid (Cu, Hg, Sb, Pb) deposition in a western Alpine lake (Lake Robert, France): Deciphering local and regional mining contamination. Quaternary Science Reviews 228, 106076. https://doi.org/10.1016/j.quascirev.2019.106076

Ellmers, D., 1978. Shipping on the Rhine during the Roman period: the pictorial evidence, in: Taylor, J. du P., Cleere, H. (Eds.), Roman Shipping and Trade: Britain and Rhine Provinces. London, pp. 1–14.

Franconi, T., 2014. The economic development of the Rhine river basin in the Roman period (30 BC - AD 406) (http://purl.org/dc/dcmitype/Text). Oxford University, UK.

Guénette-Beck, B., Meisser, N., Curdy, P., 2009. New insights into the ancient silver production of the Wallis area, Switzerland. Archaeol Anthropol Sci 1, 215–229. https://doi.org/10.1007/s12520-009-0014-3

Guénette-Beck, B., Serneels, V., 2010. L'interprétation archéologique des données isotopiques de plomb. ArcheoSciences. Revue d'archéométrie 289–297. https://doi.org/10.4000/archeosciences.2850

Helly, B., Delile, H., 2018. Les gisements de plomb argentifères de Vienne aux XVIII et XIXe siècles étaient-ils déjà exploités à la période romaine ? Méthodologie sur l'approche archéométrique du traçage des sources de plomb argentifère, in: Regards sur l'archéologie de la Loire. Thoba's, St. Chamond, France.

Helly, B., Granier, G., Lucas, G., 2017. Vienne antique - Sainte-Colombe, Saint-Romain-en-Gal, Vienne, Guides archéologicques de la France.

Hirt, A.M., 2020. Gold and Silver Mining in the Roman Empire, in: Butcher, K. (Ed.), Debasement: Manipulation of Coin Standards in Pre-Modern Monetary Systems. Oxbow Books, pp. 111–124. https://doi.org/10.2307/j.ctv138wssp

Ingo, G.M., Agus, T., Ruggeri, R., Amore Bonapasta, A., Bultrini, G., Chiozzini, G., 1996. Lead and Silver Production in the Montevecchio Basin (Western Sardinia, Italy). MRS Online Proceedings Library 462, 411–416. https://doi.org/10.1557/PROC-462-411

Köppel, V., Neubauer, F., Schroll, E., 1993. Pre-Alpidic Ore Deposits in the Central, Eastern and Southern Alps, in: von Raumer, J.F., Neubauer, Franz (Eds.), Pre-Mesozoic Geology in the Alps. Springer, Berlin, Heidelberg, pp. 145–162. https://doi.org/10.1007/978-3-642-84640-3_9

Lonchambon, C., Bonnamour, L., Connan, J., Thômé, P., Michel, C., 2009. Les bateaux du pont romain de Chalon-sur-Saône (Saône-et-Loire) : des témoins de l'évolution des techniques de construction navale au Ier s. apr. J.-C. Gallia 66, 59–112. https://doi.org/10.3406/galia.2009.3367

Macfarlane, A.W., Lechtman, H.N., 2016. Andean Ores, Bronze Artifacts, and Lead Isotopes: Constraints on Metal Sources in Their Geological Context. J Archaeol Method Theory 23, 1–72. https://doi.org/10.1007/s10816-014-9225-8

Martinez-Cortizas, A., Lopez-Merino, L., Bindler, R., Mighall, T., Kylander, M., 2013. Atmospheric Pb pollution in N Iberia during the late Iron Age/Roman times

reconstructed using the high-resolution record of La Molina mire (Asturias, Spain). Journal of Paleolimnology 50, 71–86.

Mays, L.W., Koutsoyiannis, D., Angelakis, A.N., 2007. A brief history of urban water supply in antiquity. Water Supply 7, 1–12. https://doi.org/10.2166/ws.2007.001

McConnell, J.R., Wilson, A.I., Stohl, A., Arienzo, M.M., Chellman, N.J., Eckhardt, S., Thompson, E.M., Pollard, A.M., Steffensen, J.P., 2018. Lead pollution recorded in Greenland ice indicates European emissions tracked plagues, wars, and imperial expansion during antiquity. Proceedings of the National Academy of Sciences 115, 5726–5731. https://doi.org/10.1073/pnas.1721818115

Miller, K., 1916. Itineraria romana: Römische reisewege an der hand der Tabula peutingeriana. Strecker und Schröder.

Millot, R., Allègre, C.-J., Gaillardet, J., Roy, S., 2004. Lead isotopic systematics of major river sediments: a new estimate of the Pb isotopic composition of the Upper Continental Crust. Chemical Geology 203, 75–90. https://doi.org/10.1016/j.chemgeo.2003.09.002

Monna, F., Lancelot, J., Croudace, I.W., Cundy, A.B., Lewis, J.T., 1997. Pb Isotopic Composition of Airborne Particulate Material from France and the Southern United Kingdom: Implications for Pb Pollution Sources in Urban Areas. Environ. Sci. Technol. 31, 2277–2286. https://doi.org/10.1021/es960870+

Needleman, L., Needleman, D., 1985. Lead Poisoning and the Decline of the Roman Aristocracy. Echos du monde classique: Classical views 29, 63–94.

Nriagu, J.O., 1983. Lead and lead poisoning in antiquity, Antiquities. Wiley, New York.

Ollive, V., Petit, C., Garcia, J.-P., Reddé, M., 2006. Rhine flood deposits recorded in the Gallo-Roman site of Oedenburg (Haut-Rhin, France). Quaternary International, Impact of rapid environmental changes on humans and ecosystems 150, 28–40. https://doi.org/10.1016/j.quaint.2006.01.006

Ollive, V., Petit, C., Garcia, J.-P., Reddé, M., Biellmann, P., Popovitch, L., Chateau-Smith, C., 2008. Roman Rhine settlement dynamics evidenced by coin distribution in a fluvial environment (Oedenburg, Upper Rhine, France). Journal of Archaeological Science 35, 643–654. https://doi.org/10.1016/j.jas.2007.05.015

Pelletier, A., 2001. Vienna, Vienne. Presses Universitaires de Lyon.

Purcell, N., 1990. The creation of provincial landscape: the Roman impact on Cisalpine Gaul, in: Blagg, T., Milett, M. (Eds.), The Early Roman Empire in the West. Oxbow Books, Oxford, pp. 7–29.

Rackham, H. (Tran.), 1938. Pliny. Natural History, Volume I: Books 1-2, Loeb Classical Library 330. ed. Harvard University Press, Cambridge, MA.

Raepsaet, G., Demaiffe, D., Charlier, M.-T., 2015. La production, la diffusion et la consommation du “plomb germanique” en Gaule du Nord.: Apports des isotopes du plomb. Vie Archéologique 74, 65–89.

Raepsaet-Charlier, M.-T., 2011. Plumbum Germanicum. Nouvelles données. L’Antiquité Classique 80, 185–197.

Renson, V., Fagel, N., Mattielli, N., Nekrassoff, S., Streel, M., De Vleeschouwer, F., 2008. Roman road pollution assessed by elemental and lead isotope geochemistry in East Belgium. Applied Geochemistry 23, 3253–3266. https://doi.org/10.1016/j.apgeochem.2008.06.010

Retief, F.P., Cilliers, L., 2006. Lead poisoning in ancient Rome. Acta Theologica 26, 147–164. https://doi.org/10.4314/actat.v26i2.52570

Rosman, K.J.R., Chisholm, W., Hong, S., Candelone, J.-P., Boutron, C.F., 1997. Lead from Carthaginian and Roman Spanish Mines Isotopically Identified in Greenland

Ice Dated from 600 B.C. to 300 A.D. Environ. Sci. Technol. 31, 3413–3416. https://doi.org/10.1021/es970038k

Rothenhoefer, P., Hanel, N., 2013. The Romans and Their Lead - Tracing Innovations in the Production, Distribution, and Secondary Processing of an Ancient Metal, in: Burmeister, S., Hansen, S., Kunst, M., Müller-Scheeßel, N. (Eds.), Metal Matters ; Innovative Technologies and Social Change in Prehistory and Antiquity. Rahden/Westf.: Leidorf.

Roueché, C., 1989. Aphrodisias in Late Antiquity. The Society for the Promotion of Roman Studies 41, 201–203.

Rudnick, R.L., Gao, S., 2003. Composition of the Continental Crust, in: Holland, H.D., Turekian, K.K. (Eds.), Treatise on Geochemistry. Pergamon, Oxford, pp. 1–64. https://doi.org/10.1016/B0-08-043751-6/03016-4

Scheidel, W., Meeks, E., 2012. ORBIS: The Stanford Geospatial Network Model of the Roman World. Stanford University, Stanford.

Thevenon, F., Guédron, S., Chiaradia, M., Loizeau, J.-L., Poté, J., 2011. (Pre-) historic changes in natural and anthropogenic heavy metals deposition inferred from two contrasting Swiss Alpine lakes. Quaternary Science Reviews 30, 224–233. https://doi.org/10.1016/j.quascirev.2010.10.013

Tylecote, R.F., 1964. Roman Lead Working in Britain. The British Journal for the History of Science 2, 25–43.

US EPA, O., 2015. SW-846 Test Method 3052: Microwave Assisted Acid Digestion of Siliceous and Organically Based Matrices [WWW Document]. URL https://www.epa.gov/hw-sw846/sw-846-test-method-3052-microwave-assisted-acid-digestion-siliceous-and-organically-based (accessed 5.30.23).

Vos, W.K., Morel, J., Hazenberg, T., 2011. The “Woerden 7”: an oar-powered Roman barge built in the Netherlands: details on the excavation at the Nieuwe Markt in Woerden (Hoochwoert). Archäologisches Korrespondenzblatt 41, 101–118.

Weeks, L., Keall, E., Pashley, V., Evans, J., Stock, S., 2009. Lead Isotope Analyses of Bronze Age Copper-Base Artefacts from Al-Midamman, Yemen: Towards the Identification of an Indigenous Metal Production and Exchange System in the Southern Red Sea Region*. Archaeometry 51, 576–597. https://doi.org/10.1111/j.1475-4754.2008.00429.x

Welcomme, E., Walter, P., van Elslande, E., Tsoucaris, G., 2006. Investigation of white pigments used as make-up during the Greco-Roman period. Appl. Phys. A 83, 551–556. https://doi.org/10.1007/s00339-006-3559-3

White, W.M., Albarède, F., Télouk, P., 2000. High-precision analysis of Pb isotope ratios by multi-collector ICP-MS. Chemical Geology 167, 257–270. https://doi.org/10.1016/S0009-2541(99)00182-5

Chapter 3: Copper and lead isotopes composition of ancient Roman human bones reveal health degradation attributed to lead poisoning (Vienne, France)

This article has been submitted to the journal Medical Research Archives

Résumé

La pollution par les métaux est un problème de santé majeur dont les origines sont antérieures à l'industrialisation. Les Romains ont largement utilisé le plomb (Pb) dans toute une série d'applications urbaines et domestiques, notamment dans les conduites d'eau et les ustensiles du quotidiens. Cette étude présente un ensemble complet de données sur les concentrations de Pb, de mercure (Hg) et de cuivre (Cu), ainsi que sur la composition isotopique du Pb plomb et du Cu cuivre dans d'anciens squelettes humains, afin d'étudier l'exposition environnementale historique et d'évaluer la dégradation de la santé de la population romaine de la ville de Vienne (Vienne, France). La ville de Vienne était un important site de fabrication de tuyaux en plomb pendant le Haut-Empire romain. Les concentrations de Pb varient de 10 à 624 $\mu g.g^{-1}$, ce qui est significativement plus élevé que celles trouvées dans d'autres populations romaines rurales. Les résultats montrent des valeurs de Pb et de Hg plus élevées dans les os pour la période romaine que pour la période post-romaine, ce qui est cohérent avec la chronologie historique. L'absence de relation entre les niveaux de Pb et de Hg et le sexe et l'âge suggère une contamination généralisée par le Pb (par l'ingestion d'eau et d'aliments) et des niveaux atmosphériques élevés de Hg. Les valeurs $\delta^{65}Cu$ étaient inférieurs à ceux observés dans les populations non exposées à la pollution métallurgique, ce qui suggère une détérioration de la santé liée aux effets néfastes négatifs de l'exposition au Pb. Cette étude soutient l'utilisation des os archéologiques comme archives pour reconstituer l'exposition métallique des populations humaines anciennes aux métaux.

Copper and lead isotopes composition of ancient Roman human bones reveal health degradation attributed to lead poisoning (Vienne, France)

C. Heredia[1*], A. T. Gourlan[1], S. Guédron[1], F. Albarede[2], H. Delile[3], G. Granier[4], S. Campillo[1], S. Santenac[1], L. Audin[1], P. Telouk[2] and B. Helly[5].

[1] Université Grenoble Alpes, Université Savoie Mont Blanc, CNRS, IRD, IFSTAR, ISTerre, 38000, Grenoble, France.

[2] Ecole Normale Supérieure de Lyon, CNRS, and Université de Lyon, 46 Allée d'Italie, 69007, Lyon, France

[3] CNRS, Archéorient, UMR 5133, Maison de l'Orient et de la Méditerranée, University of Lyon 2, Lyon, France.

[4] Aix-Marseille Université, CNRS, 13007, Marseille, France.

[5] Laboratoire ArAr Archéologie et Archéometrie, Maison de l'Orient et de la Méditerranée, University of Lyon 2, Lyon, France.

*Corresponding author:

Carlos Heredia A.; carlos.heredia-aguilar@univ-grenoble-alpes.fr

Keywords: Lead, Pollution, Degradation of health status, Roman, France, lead and Copper isotopes

Highlights:

- Roman human bones have the same lead (Pb) isotope signature as Vienna pipes
- High Pb concentrations of bones highlight Pb contamination of Roman population in Vienna
- Cu isotopic composition of bones shows negative shift compared to control population
- This shift suggests degradation of health status attributed to ingestion of Pb

Abstract

Metal pollution is a major health problem whose origins predate industrialization. Romans extensively used lead (Pb) in an array of urban and domestic applications, including water pipes and daily utensils. This study reports a complete dataset of Pb, mercury (Hg), and copper (Cu) concentrations, together with lead and copper isotope composition of ancient human skeletons to investigate historical environmental exposure and assess the health degradation in the Roman population of the city of Vienna (Vienne, France). The city of Vienna was a significant manufacturing site for lead pipes during the High Roman Empire. Pb concentrations ranged from 10 to 624 $\mu g.g^{-1}$, significantly higher than those found in other rural Roman populations. Results show higher Pb and Hg values in bone for the Roman period compared to post-roman ones, consistent with historical chronology. Absence of relation between Pb and Hg levels with sex and age suggest widespread Pb contamination (through water and food ingestion) and high background atmospheric Hg levels. δ65Cu ratios were lower than those observed in populations non-exposed to metallurgical pollution, suggesting a deterioration of health related to the negative effects of exposure to Pb. This study supports the use of archaeological bones as archives to reconstruct the metallic exposure of ancient human populations.

3.1. Introduction

Environmental and physiological levels of lead (Pb) exposure in the population are a global public health concern (W.H.O, 2022). Pb has been used in the manufacturing of balconies, paintwork, ancient pipes, and roofs. The alteration of these materials (e.g., paint peeling, dissolution of Pb pipes), and the ingestion or inhalation of water or dust can have serious health consequences. Recently, the structural fire of Notre Dame de Paris (April 2019) has put the spotlight back on this contamination issue, as 450 tons of Pb contained in the roof and framework of the spire have been released into the atmosphere in the form of particles, endangering the population, especially children (van Geen et al., 2020). Exposure, even at low levels, can have complex and serious effects on health, including developmental delays, cancers, brain and kidney disorders, cardiovascular problems, and even death (Järup, 2003; W.H.O, 2022). Once in the body, lead accumulates in the skeleton (Schroeder and Tipton, 1968) but can be released during periods of physiological stress and bone turnover (Silbergeld et al., 1988).

Recently, copper (Cu), zinc (Zn), or iron (Fe) stable isotopes have been identified as potential new medical diagnostic tools due to their specificity in biological functions as well as their relatively short turnover time in the body (Albarède, 2015). For example, Fe isotopes have been used as tracers of inherited diseases such as Hemochromatosis (Krayenbuehl et al., 2005), Zn isotopes to track inflammation and diseases affecting the immune system (Bonaventura et al., 2015), and Cu isotopes as a tool for cancer diagnosis (Gourlan et al., 2019; Télouk et al., 2015). For this latter, medical research has shown a systematic enrichment in light Cu isotopes (^{63}Cu) in the blood of patients with different types of cancer (prostate, ovary, thyroid, breast...) compared to controls (healthy individuals), resulting in a decrease in the ^{65}Cu/^{63}Cu isotopic ratio (Kazi Tani et al., 2021; Télouk et al., 2015; Toubhans et al., 2020). Similar drops in the ^{65}Cu/^{63}Cu have been

found in the blood of felines and dogs that had developed cancer (e.g., breast cancer, lymphoma, or fibrosarcoma, (Chamel et al., 2017; Gourlan et al., 2019; Leroi et al., 2003; Pesavento et al., 2018; Vittecoq et al., 2015), but also for dogs diagnosed with chronic non-oncologic diseases like chronic kidney disease, pancreatitis and bronchitis (Chamel et al., 2017). Hence, the study of Cu isotopes appears as a relevant tool for the assessment of health deterioration status in both animals and humans. The mechanism involved in the isotopic fractionation remains, however, poorly understood, but the most likely hypothesis is preferential chelation of ^{65}Cu by lactate, which is produced in large quantities by the tumor (Télouk et al., 2015).

Lead has been mined since ancient times and was fundamental in the development of modern industrialized societies (Killick and Fenn, 2012). Traces of ore processing to produce metals used for a wide spectrum of applications have been discovered as early as 5000 BCE in various locations in the Balkans (Pernicka et al., 1997; Radivojević et al., 2013) and the Middle East (Roberts et al., 2009). In Europe, the most significant metal pollution is attributed to large-scale mining during the Roman Period (Hong et al., 1994; McConnell et al., 2018; Nriagu, 1983; Silva-Sánchez and Armada, 2023). Romans extensively used Pb in an array of public and domestic applications, such as household and cooking utensils (crafted from pure lead or other alloys like pewter), as an ingredient in cosmetics, medicine, food (i.e., as sweetener and food preserver), paints (Needleman and Needleman, 1985; Nriagu, 1983), and in water distribution systems (i.e., pipes, pipe seals, and aqueduct lining), which played a key role in the evolution and development of the Empire (Deming, 2020). The use of these water supply systems has resulted in Pb-contaminated waters of ancient urban centers (Delile et al., 2017, 2014; Flaux et al., 2023; Véron et al., 2013).

While Greco-Roman writers observed and were aware of lead's toxicity, the classic chronic symptoms of lead poisoning (saturnism) were not comprehensively documented until the 7th century CE (Burstein and Finch, 2022; Hodge, 1981; Retief and Cilliers, 2006). To understand and identify the source and exposure of ancient populations to mining pollution, a recent study has shown that human bones are relevant historical archives (López-Costas et al., 2020). These authors showed that populations in rural Roman areas incorporated four times as much lead (Pb) and mercury (Hg) in their bones compared to post-Roman populations on the same site. It has thus been suggested that Roman air pollution sources contributed an average of 57% of the total lead incorporated into bone at that time (dropping to 24% after the decline of Rome).

In this study, we analyzed both the Pb and Cu isotope signatures and multi-elemental composition (i.e., Hg, Mn, Fe, Co, Ni, Zn, Sr, Al, Ba, Ca, K, Na, Mg, and P) of ancient human bones recovered from the Roman capital of Vienna (modern-day Vienne, France), which was a major Pb pipe manufacturing site during the High Roman Empire (-27 BCE – 245 CE). Lead isotope signatures of ancient human skeletons were used to identify the historical exposure pathway (by inhalation and/or ingestion), and Cu isotope signatures to detect a degraded state of health associated with metal exposure. The results will constitute a proof of concept to better constrain the exposure of historical populations through the use of these new isotopic tools as tracers of processes in archaeological environments contaminated by mining and metallurgical activities.

3.2. Material and methods

3.2.1. Study site and archaeological context

The contemporary city of Vienne is located in the southeastern part of France, where the Rhône and Gère rivers meet, 35 kilometers to the south of Lyon (Fig. 3.1). Vienna was an important city during the Roman Empire, ideally situated along the Rhône on a major

communication axis, extending across both shores of the river, which now includes the present-day towns of Vienne, Saint-Roman-en-Gal, and Sainte-Colombe (Pelletier, 2001).

Lead pipe manufacturing was Vienna's hallmark of metallurgical production during the High Roman Empire (31 BCE – 235 CE, (Cochet, 2000; Cochet and Hansen, 1986), with at least 70 craftsmen working in the city (Brissaud, 2016). It has been estimated around 30 km of lead-piped water installations at Saint Romain en Gal (Heredia et al., 2024; (Gosselin et al., 2011; Helly et al., 2017). A recent article has shown that Pb used in Vienna's manufactures was mainly imported from the Rhine Massif and was transported to Vienna via the Rhine and Saône rivers (Heredia et al., 2024). Moreover, high Pb concentrations (up to 893 $\mu g.g^{-1}$) measured in two boreholes have shown major contamination during the Roman period in the city of Vienna.

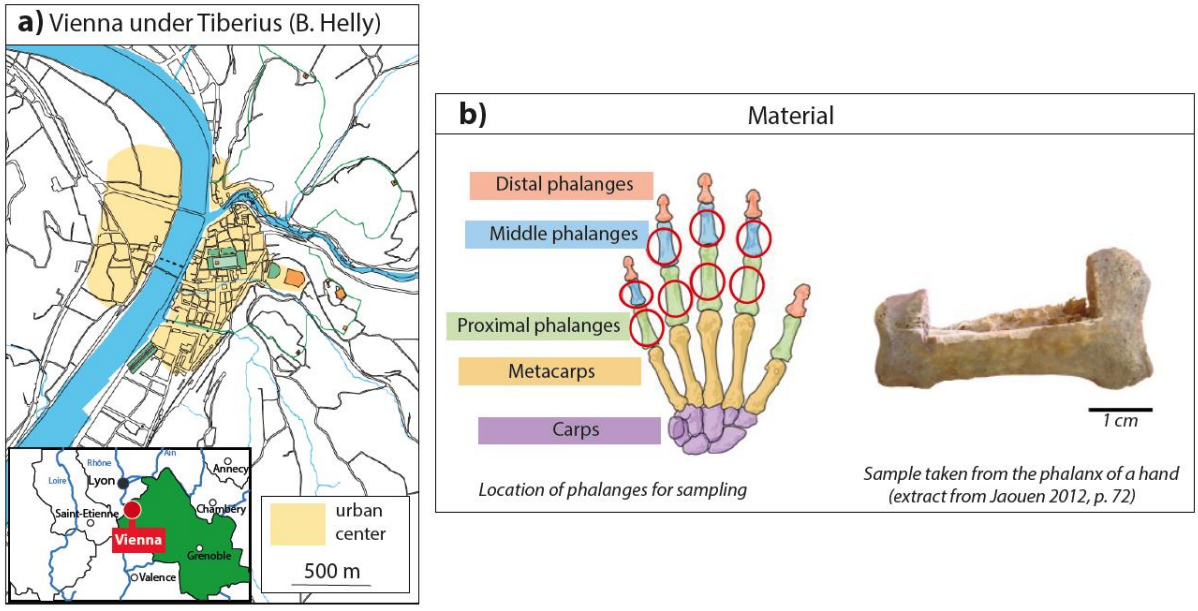

Figure 3.1. a) *Map of the ancient city of Vienna during the 1st century CE within the Roman Empire [adapted from* (Adjajd and Lauxerois, 2014)*] and b) diagram location and example of phalanx collected in the Roman sepultures of Vienne.*

3.2.2. Human remains

To assess the potential exposure to lead in the ancient city of Vienna, thirty-five human remains excavated from Vienne (VI), Sainte-Colombe (SC), and Saint-Roman-en-Gal (SRG) were collected from the archives of the SRG museum (Table S1, Annex 2). Bones included phalanges (Fig.3.1.b) of both male and female individuals (men = 13, women = 9, unknown = 13), and range from infancy to old age. Individuals were divided into five main age groups: infant/juvenile (IJ, 0 – 20 years old), young adult (YA, 20 – 29 years old), mature adult (MA, 30 – 59 years old), old adult (OA, > 60 years old) and unknown (n.a.). This morphometric data is important, as it enables us to assess the duration of exposure (age of the individual) and the type of exposure (men vs. women) linked to the individual's activities. Additionally, five animal remains excavated from Vienne were analyzed for comparison, which include individuals of four families: Bovidae (cattle, sheep), Suidae (pig), Phasianidae (chicken), and Leporidae (hare) (Vicard, 2021).

Human bones were recovered by archaeologists from various burial contexts: wooden or nailed wood trunk (n = 16), trunk (n = 1), stone trunk with wood roofing (n = 5), stone trunk (n = 1), masonry trunk (n = 1), pit with wooden covering (n = 2), pit (n = 3), lead sarcophagus (n = 1), nd (n = 5). The skeletal sample set covers the period from the Roman Empire (-27 BCE – 450 CE) to the Early Middle Ages (450 to 800 CE). When possible, museum curators provided information concerning sex and probable age at death, which was obtained from biometric skeletal analysis (i.e., sexual morphological characteristics of coxal bones, age, lifetime, Table S1, Annex 2).

3.2.3. Sample preparation

The method requires bone sampling and is, therefore, destructive. In order to minimize the impact of this sampling on human bones and potential future analyses, the protocol

adopted by K. Jaouen was applied (Jaouen et al., 2017, 2016, 2012). Bone samples were obtained from the phalanges and/or metacarpals in the case of human individuals and from the upper or lower extremities in the case of animals (e.g., tibiae, calcaneus, navicular). Bone surfaces were abraded with a diamond drill to avoid contamination from soil particles or post-excavation handling. Cortical bone was cut and recovered using a diamond disk following an established protocol (Jaouen et al., 2012). Briefly, all drill bits were washed and sonicated in ultra-pure water for 10 minutes and heated with a propane flame between each drilling procedure. Both the cleaning and the cutting were performed using a Dremel 8220. Cortical (compact) bone was chosen for two reasons: i) it is less biologically active and has a slower turnover rate (2 to 5 % per year) compared to trabecular bone [15 to 35 % per year, (Nanci, 2013; Parfitt, 2013)], ii) it is more resistant to diagenetic alteration than trabecular bone (Price et al., 1992). Hence, cortical bone is the final repository of Pb and can serve as an indicator of cumulative, integrated exposure over many years (Barbosa et al., 2005).

Around 50 mg of the sample was reduced to powder using a mortar, leached with 2 ml acetic acid 0.2 N for 1h at room temperature, and sonicated for 15 minutes. Samples were rinsed three times with MQ water and evaporated to dryness. They were then dissolved using 5 ml of concentrated HNO_3 (double-distilled) and 1 ml of concentrated H_2O_2 (Merck Suprapur quality) in Savillex® vessels at 60 °C for 24 hours.

3.2.4. Trace elements

Major elements (Al, Ba, Ca, K, Na, Mg, and P) were analyzed with an inductively coupled plasma optical spectrometer (ICP-OES, Varian 720-ES) within the analytical chemistry platform of ISTerre (Grenoble-France). Pb, Cu and complementary trace elements (Mn, Fe, Co, Ni, Zn, Sr) were measured by inductively coupled plasma mass spectrometry

(ICP-MS, Agilent, 7500 CX quadrupole ICP-MS) using Be, In, and Bi as internal standards to correct for instrumental mass bias. The digestion procedure was assessed using certified materials for bone (bone meal, NIST 1486). Samples were diluted in 2% (v/v) HNO_3 to obtain a dilution factor of 100 (to minimize matrix effects) before measurements. All elements were within the satisfactory target recovery of 93 ± 10 %, and the analytical detection limits were well below the measurements of the samples analyzed.

Total mercury concentrations (THg) were determined by combustion and atomic absorption spectrophotometry using an AMA 254 analyzer (Altec), following the procedure described in Guédron et al. (2009). Concentrations obtained for repeated analyses of certified reference materials [i.e., bone meal (NIST 1486) and loam soil (ERM CC141)] never exceeded the published range of concentrations (NIST 1486: 0.03 ± 0.01 $\mu g.g^{-1}$and ERM CC141: 83 ± 17 $\mu g.g^{-1}$).

3.2.5. Lead purification and isotope measurements

Samples were initially redissolved in 1ml of 14N HNO_3 and evaporated with 1 drop of concentrated HBr. Then, redissolved with 2 ml HBr 0.7N at 80 °C for 24 hours, evaporated to dryness, and redissolved again with 0.5 ml HBr 0.7N at 80 °C for 24h. Lead was separated and purified from each sample in an HBr medium using anion-exchange columns loaded with AG1-X8 resin (200–400 mesh, Acros Organics) according to a conventional method (Monna et al., 1997; Weeks et al., 2009). The total procedural Pb blank was < 15 pg.

The isotopic analyses of lead (^{204}Pb, ^{206}Pb, ^{207}Pb, ^{208}Pb) were carried out using a multi-collector inductively coupled plasma mass spectrometer (MC-ICP-MS, Nu Instruments, NuPlasma HR) at the Ecole Normale Supérieure de Lyon. Full analytical details are

available in White et al. (2000). Pb yield (100 ± 5 %) was verified on an Agilent 7500 CX quadrupole ICP-MS at the ISTerre analytical chemistry platform (Grenoble, France). Lead was separated and purified from each sample in an HBr medium using AG1-X8 resin-loaded anion exchange columns (200-400 mesh, Acros Organics) following a conventional method (Monna et al., 1997; Weeks et al., 2009). A thallium standard (Tl; NIST 997) was added to all samples to correct for instrument drift. Isotopic fractionation effects were corrected by standard calibration using lead reference material (SRM 981). The external reproducibility of reported Pb isotope ratios, assessed through repeated NIST 981 analyses (performed every two samples), is in the range of 100 to 200 ppm (or 0.01 to 0.02%) for ^{204}-based ratios ($^{206}Pb/^{204}Pb$, $^{207}Pb/^{204}Pb$, $^{208}Pb/^{204}Pb$) and around 50 ppm (or 0.005%) for $^{207}Pb/^{206}Pb$, $^{208}Pb/^{206}Pb$ and $^{207}Pb/^{208}Pb$.

3.2.6. Cu purification and isotope measurements

Samples were initially redissolved in 1ml of 14N HNO_3, and a 50-µL aliquot was taken for elemental concentration measurements before and after purification. The dissolved samples were completely evaporated and redissolved in 1 mL of 7 N HCl + 0.001% H_2O_2 twice to eliminate any traces of residual nitric acid. Then, samples were dissolved in 1 mL 7 N HCl + 0.001% H_2O_2 in Savillex® vessels at 80 °C for 24h. Purification was performed twice using the AG MP-1 anion-exchange resin (100–200 mesh, BioRad), and Cu was eluted with 20 mL of 7 N HCl + 0.001% H_2O_2 following the technique of Maréchal and Albarède (Maréchal and Albarède, 2002). The total procedural Pb blank was < 10 pg. Cu yield (100 ± 5 %) was verified on an Agilent 7500 CX quadrupole ICP-MS at the ISTerre analytical chemistry platform (Grenoble, France).

Copper stable isotope compositions were determined by multi-collector inductively coupled plasma mass spectrometry (MC-ICPMS) using a Nu plasma 500 HR double-

focusing mass spectrometer of ENS-Lyon. Gas flow instrumental mass fractionation was controlled both by dual standard-sample bracketing and the addition of an external standard [i.e., Zn for Cu samples, (Maréchal et al., 1999)]. The isotope reference solution used was NIST 976 (Cu). The precision (external reproducibility, two-sigma) on the isotopic ratios is 0.05%.

3.2.7. Data treatment and statistical analyses

Statistical analyses and non-parametric tests (Mann-Whitney U and Kruskal-Wallis) were performed using the package R studio version R 4.4.0 and SigmaPlot 12.5. Probability values (*p*) and correlation coefficients (R^2) are reported for linear regression analyses. In all cases, a p-value of 0.05 was chosen to indicate significance at the 95 percent confidence level. All data and calculations are provided in supplementary tables S3 to S8 (Annex 2).

3.3. Results and discussion

3.3.1. Assessment of bone diagenesis

Characterizing the archaeological context is essential when working with human burials, as it provides a better understanding of the circumstances surrounding the internment, including soil properties, composition, and water-table oscillations. Contextual analysis of the burial sites also helps elucidate the taphonomic processes and preservation conditions that affect the chemical stability and physical integrity of skeletal remains over time, offering insights into post-mortem alterations [i.e., diagenesis (Gregory and Matthiesen, 2023)]. However, working with human bones from archived archaeological collections presents limitations, especially when these collections lack fully documented soil studies, as it is the case in this study.

During diagenesis, secondary minerals transported by groundwater such as calcite, pyrite, and Fe-Mn (hydr)oxides can penetrate within the bone pore structure (i.e., the macroporosity of blood vessels and Haversian canals and the microporosity associated with collagen loss due to degradation) and modify the pre-mortem elemental and isotopic composition of archaeological bones (Rasmussen et al., 2019; Trueman and Tuross, 2002; Tütken and Vennemann, 2011). Evaluating the content of bio-essential [i.e., Fe, Cu, Zn, (Jaouen et al., 2012)] and non-essential, lithogenic elements [i.e., Al, Mn, Sr, Ba, (Giffin et al., 2017; Kamenov et al., 2018; Rasmussen et al., 2017)] as well as their ratios [i.e., Sr/Ca, Ba/Ca, Ca/P (Fabig and Herrmann, 2002)] are a common way to infer a potential effect of diagenetic alteration on skeletal remains (Simpson et al., 2021). Because these diagenetic indicators generally do not correlate with each other, several of these were evaluated here.

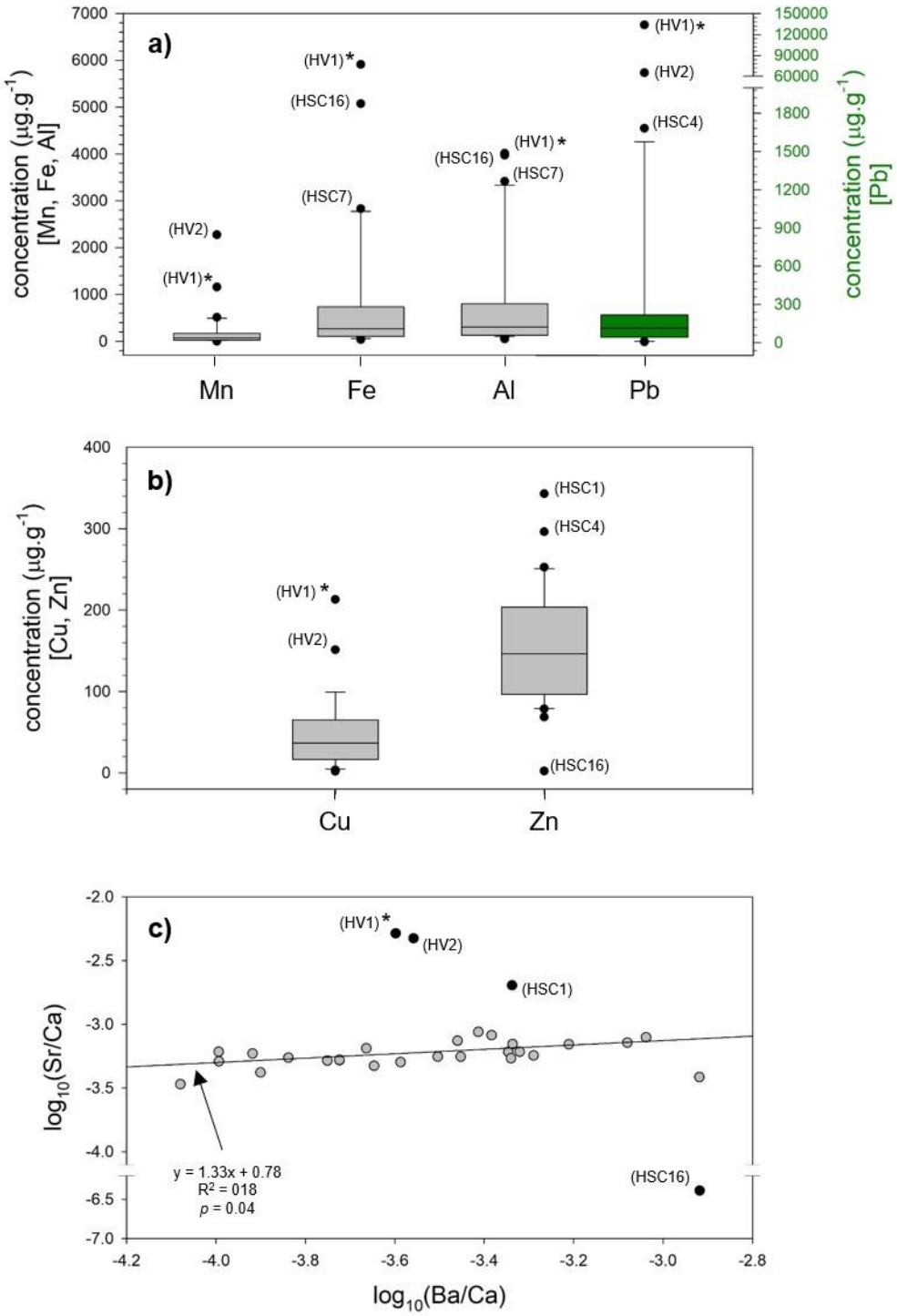

Figure 3.2. *Hair-and-whisker box plots of the measured concentrations for total (a)* redox sensitive *(Mn, Fe, Al) and Pb, b) essential elements (Cu, Zn), and c) bivariate plot of log Sr/Ca and log Ba/Ca ratios in cortical human bone samples of thirty-five individuals from the ancient city of Vienna (regression and equation for the Ca biopurification line is marked with an arrow). Each box represents the 25th–75th percentiles (with the median as a bold horizontal line) and the whiskers show the 10th–90th percentiles. Statistical outliers outside of the two standard deviation range with respect to the median are marked as black dots (sample ID in parenthesis). Excluded samples were: HV1, HV2, HSC1, HSC4, HSC7 AND HSC16. Asterisk (*) denotes burial in lead sarcophagus.*

The total distribution of concentration for the redox sensitive (Mn, Fe, Al), bio-essential elements (Cu, Zn) and elemental ratios (Sr/Ca and Ba/Ca) provides a comparative overview of elemental distribution within the buried population at Vienna, and allows the identification of some outliers (black dots, Fig. 3.2). Diagenetic alteration of bone, reflected in the degree of histomorphological bone preservation, is expected to increase the concentration of trace elements within the bone (Fabig and Herrmann, 2002). Hence, samples that fell outside the two standard deviation range with respect to the median (Fig. 3.2a and b) or that scattered unexpectedly from the Ca bio-purification line (Fig. 3.2c) were considered altered by diagenesis. In total, the bones of five adults (HV1, HV2, HSC1, HSC7, HSC16) and one infant (HSC4) were considered affected by diagenesis and excluded from further analysis. In particular, sample HV1, exhibited extremely high levels of Pb (133,914 $\mu g.g^{-1}$), Al (4017 $\mu g.g^{-1}$), Fe (5912 $\mu g.g^{-1}$), Co (11 $\mu g.g^{-1}$), Cu (213 $\mu g.g^{-1}$), Sr (1200 $\mu g.g^{-1}$), and Mn (1158 $\mu g.g^{-1}$), together with high Ca substitutions (Fig. 3.2c) that can be attributed to the burial of the body within a Pb sarcophagus, which completely altered the pre-mortem Pb signal (Waldron, 1981). Sample HV2, found in the same necropolis as HV1 but buried in a wooden box, also exhibited high levels of Pb (65,200 $\mu g.g^{-1}$), Co (15 $\mu g.g^{-1}$), Ni (13 $\mu g.g^{-1}$), Cu (151 $\mu g.g^{-1}$), Sr (1,550 $\mu g.g^{-1}$), and Mn (1,158 $\mu g.g^{-1}$). This likely indicates that the Pb sarcophagus had a local impact on the entire necropolis.

Once these outliers removed, the remaining samples were in the range of values of essential and major elements expected for fresh bone ([Fe] = 100 – 2000, [Cu] = 1 – 50 $\mu g.g^{-1}$, [Zn] = 50 – 400 $\mu g.g^{-1}$, [Sr] = 180 – 280 $\mu g.g^{-1}$, [Ca] = 66 – 411 $mg.g^{-1}$, [Na] = 2 – 15 $mg.g^{-1}$, [Mg] = 0.6 – 9 $mg.g^{-1}$, [P] = 3 – 18 $mg.g^{-1}$, table S7, Annex 2) (Harkness and Darrah, 2019; Lyengar and Tandom, 1999; Martínez-García et al., 2005; Reiche et al., 2003; Zioła-Frankowska et al., 2017, 2015)].

3.3.2. Evidence of major human exposure to Pb

The ancient city of Vienna achieved its peak of prosperity at the beginning of the 3rd century CE, and declined from the second half of the 3rd century onwards (Helly, 2013). During this latter period, residential districts of Saint-Colombe and Saint-Roman-en-Gal and the Southern District were progressively abandoned, followed by the repurposing of buildings in these areas as quarries (Helly, 2013). This city-wide recession had an estimated decrease in the population from 25,000 to 5,000 habitants between 250 and 350 CE (Helly, 2013). Abandoned sites where often used as burial spaces. Archaeological evidence show that the last necropolises of the High Empire date to the early 3rd century CE and the new ones from the Late Antiquity date from the late 3rd century (Granier, 2013). A second transition from settlement structures to new burial sites occurred in the 5th century CE, reflecting changes in land use likely associated with the emergence of early Christian buildings (Granier, 2013). Hence, based on the organization, location, and topographical evolution of funerary sites within the urban space of Vienna, two chronologically defined transitions can be established: 250 CE as the transition from the High Empire to Late Antiquity, and 450 CE as the transition to the Early Medieval Period (Fig. 3.3).

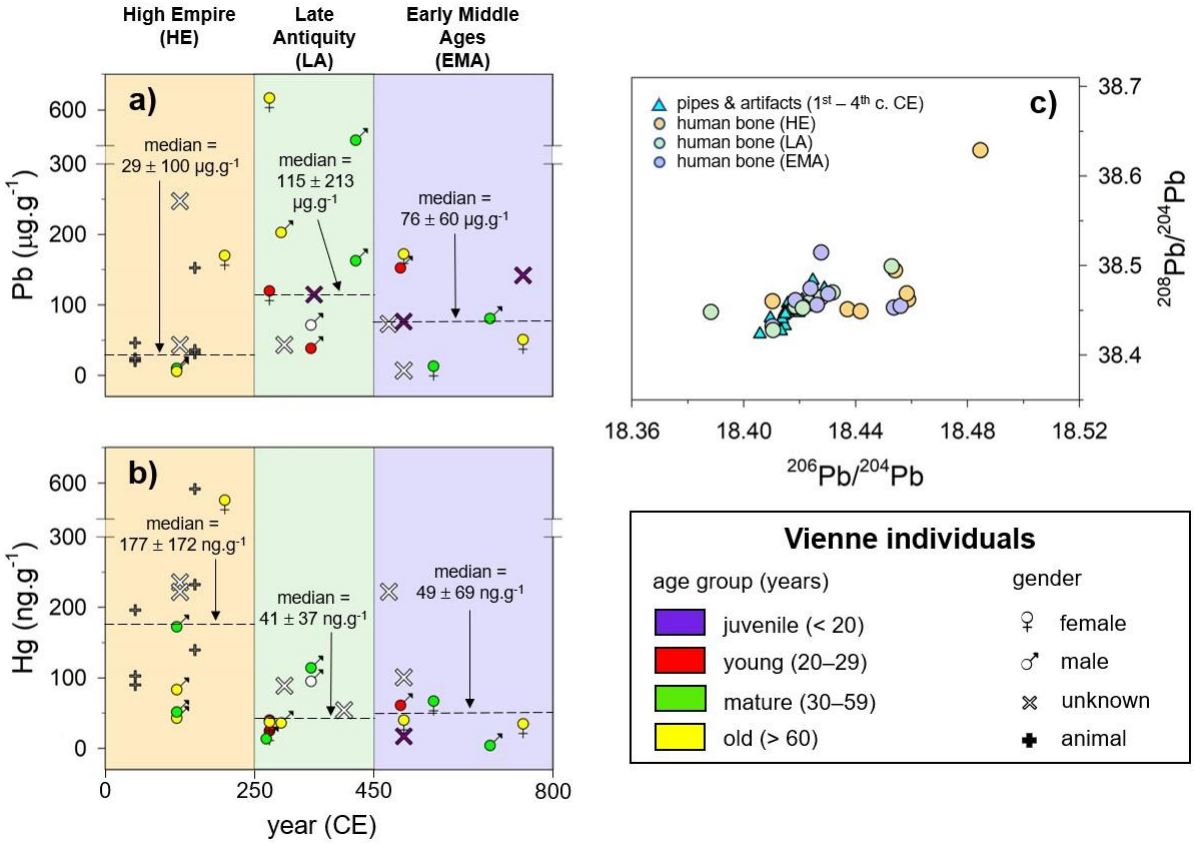

Figure 3.3. Evolution of a) *lead (Pb) and b) mercury (Hg) concentrations over time and c)* $^{208}Pb/^{204}$ *vs* $^{206}Pb/^{204}Pb$ *biplot with pipes and artifacts (up triangle, cyan) and human bones (circles) from the High Empire (0 – 250 CE, light yellow), Late Antiquity (250 – 450 CE, light green), and Early Middle Ages (450 – 800 CE, light blue). The sex of human individuals is represented by masculine (♂), feminine (♀), and unknown (x) symbols. The age group includes four categories: IJ = Infant/Juvenile (purple), YA = young adult (red), MA= mature adult (green), and OA = old adult (yellow). Animals are represented by a cross symbol.*

The Pb levels of human bones collected in Vienna range from 10 to 624 µg.g^{-1}, with an average of 132 ± 153 µg.g^{-1} (Table S7, Annex 2). No significant difference was found in Pb content between the sex or age of studied individuals (Fig. 3.3 and Table S8, Annex 2). Higher Pb levels in bones were found during the LA (median ± SD = 115 ± 213 µg.g^{-1}) as compared to the EMA (76 ± 60 µg.g^{-1}) and the HE (29 ± 100 µg.g^{-1}, fig. 3.3a). This latter is closer to Pb values observed for animal bones (34 ± 50 µg.g^{-1}, Table 3.1). When the HE and LA are considered together (i.e., the entire Roman Period), Pb values in bones are 1.5 times higher (median ± SD = 115 ± 184 µg.g^{-1}, Table 3.1) than for the post-Roman period (76 ± 60 µg.g^{-1}, Table 3.1).

Overall, Pb levels measured in bones from Vienna are thirty times higher than those reported in rural Roman individuals from A Lanzada (Iberia, Spain) dated to the same period (i.e., 1st to 7th century CE), which range from 0.1 to 20.9 $\mu g.g^{-1}$, and an average of 4.4 $\mu g.g^{-1}$ (López-Costas et al., 2020). These Iberian individuals belonging to the Roman period were reported to have incorporated four times as much Pb into their bones as post-Romans living on the same site, mainly from atmospheric pollution sources from nearby mining sites (López-Costas et al., 2020). A similar drop in Pb levels between the Roman and Post-Roman periods was observed in Vienna (Fig. 3.3a). However, the significant difference between Pb values in bones from these two sites ($p < 0.001$, table S8, Annex 2) suggests that the source of human exposure in Vienna differs from that identified at A Lazada.

Table 3.1. *Statistical summary of the Pb ($\mu g.g^{-1}$) and Hg ($ng.g^{-1}$) concentration of cortical human bones (phalanges) from Vienna.*

	Roman (HE + LA)	Post-Roman (EMA)	animals
	(n = 21)	(n = 9)	(n = 6)
Pb ($\mu g.g^{-1}$)			
Average	160.6	84.7	51.8
Median	114.8	76.3	33.6
SD	184.3	60.1	50.2
Hg ($ng.g^{-1}$)			
Average	117.3	67.8	224.1
Median	72.0	48.9	167.8
SD	132.6	69.1	184.4

Additionally, the Pb concentrations reported for the Roman period in Vienna are similar to those observed in human bones from the ancient city of Cartago Nova in the Iberian Peninsula for the same period (Martínez-García et al., 2005). Cartago Nova was notable for its significant Ag mines and extensive use of Pb in water pipes, cooking utensils, and as a wine additive (Boeckx, 1986). Hence, the high Pb values in bones reported here indicate a significant Pb contamination of the population in Vienna during the Roman

period, linked to metallurgical activities and the use of Pb objects. Both were major contributors to the total Pb burden in ancient human remains (changes in Pb exposure routes are discussed in section 3.3). The absence of difference in concentration between sex or age groups supports that human exposure to Pb was widespread throughout the entire city of Vienna, meaning that occupation or location within the city did not influence the inhabitant's exposure to Pb.

3.3.3. Route of Pb exposure for Vienna's inhabitants

To identify the routes of exposure of Vienna's Roman population, we compared the Pb isotope composition recorded in bones to those from local geochemical background, local Pb mines (i.e., galena mines), and Pb pipes and artifacts documented in a recent publication (Heredia et al., 2024). The Pb isotopic composition of the human bones (average: $^{208}Pb/^{206}Pb = 2.087 \pm 0.002$, $^{207}Pb/^{206}Pb = 0.848 \pm 0.001$, $^{204}Pb/^{206}Pb = 0.0543 \pm 0.0001$, n = 29) closely resembles that of the Pb artifacts ($^{208}Pb/^{206}Pb = 2.088 \pm 0.003$, $^{207}Pb/^{206}Pb = 0.849 \pm 0.001$, $^{204}Pb/^{206}Pb = 0.0543 \pm 0.0001$, n = 22, table S2, Annex 2 and Fig. 3.3b). In addition, the absence of change in Pb isotope composition between individuals from all three periods indicate that the Pb exposure of ancient Roman population of Vienne was tightly related to this single main source. Exposure can be related to multiple routes such as i) inhalation of particles enriched in Pb from local Pb manufacturers, and/or ii) consumption of Pb-contaminated water flowing through Pb pipes, as well as ingestion of contaminated foods [i.e., vegetables and locally produced meat, (Retief and Cilliers, 2006)].

During Vienna's apogee at the beginning of the 3rd century CE, a vast network of Pb pipes was constructed to connect the aqueducts to houses, and at least 323 tons of Pb was used to craft and set up this network at Vienna (Helly, 2018). Hence, it is conceivable that the

elevated Pb levels detected in Roman bones could result from the exposure of Roman inhabitants to metallurgical activities carried out in Vienna. Consistently, a recent study in Vienna's central district found high levels of Pb (up to 250 $\mu g.g^{-1}$) in soils and vegetable leaves near the Pipet mine, exceeding the limits of European legislation (Azzopardi et al., 2023). The study suggests potential exposure of residents through soil dust inhalation and consumption of metal-polluted vegetables. This pollution has been attributed to mining activities dating back to the 18th century (BRGM, 2017; DREAL, 2016).

Another probable route of exposure for Romans is through drinking water that flows through lead pipes (Wani et al., 2015), as already documented at the epoch of Vitruvius (Hodge, 1981). Lead pipes are more likely to dissolve in slightly acidic water than in more alkaline and harder water, where carbonate deposits in the pipes act as a protective barrier against corrosion (Kim et al., 2011), as seen in Rome and Nîmes where calcium carbonate buildup reduced lead leaching (Bennett, 1925). Continuous water flow in ancient systems like Vienna minimizes metal contact, but the absence of calcareous concretions suggests soft water flowed through lead pipes, potentially carrying lead contamination due to continuous contact with the pipe surface. In addition, Romans also used Pb in different contexts, such as medicines, cosmetics, wine storage, and cooking utensils (Retief and Cilliers, 2006). Hence, both food and wine consumption were other probable routes for Pb intoxication in Roman times. For example, the production of condiments based on unfermented grape juice (i.e., defrutum or sapa) boiled to concentrate its sugar was used to sweeten and preserve the win. The sweet taste of these syrups resulted from both the grape juice and the lead acetate released by the lead cooking vessels (In Cato's *De Agri Cultura*, the earliest example of Latin prose, circa 160 BC). Pb concentrations in defrutum and wine were estimated at 1000 $\mu g.g^{-1}$ and 20 $\mu g.g^{-1}$, respectively (Needleman and Needleman, 1985; Nriagu, 1983; Patterson et al., 1987),

suggesting that the Roman aristocracy was clearly intoxicated, even if this intoxication was not attributed to the fall of the Empire. In addition, Moore et al. (2021) also found that childhood lead poisoning may have been a contributing factor to the high infant mortality rates which was observed in Roman skeleton populations.

All this suggests that manufactured items such as pipes and containers are the primary source of lead exposure. Local mining appears to be of secondary importance, as evidenced by only one individual showing a deviation from the clustered values (Fig. 3.3c). Pb water pipes and daily household artifacts manufactured at Vienne are known to originate from a single, predominant source of lead (Heredia et al. 2024), making it difficult to distinguish between exposure from water (i.e., canalizations) or food (deposition from metallurgical activities). Regardless, such elevated lead exposure during Roman times undoubtedly had physiological consequences.

3.3.4. Higher mercury levels in human bones during the Roman times

Mercury (Hg) concentrations in human bones collected at Vienna range from 9 to 543 $ng.g^{-1}$ with an average of 100 ± 116 $ng.g^{-1}$ (Table S7, Annex 2). As for Pb, no significant difference was observed between the sex or age of the studied individuals (Fig. 3.3b and Table S8, Annex 2). Higher Hg concentrations and variability were found in human and animal bones during the HE (median ± SD = 177 ± 171 $ng.g^{-1}$ and 168 ± 184 $ng.g^{-1}$, respectively, Fig. 3.3b and Table 3.1) as compared to the LA and the EMA, whereas Hg levels for these last two periods were indistinguishable (Fig. 3.3b). As for Pb, Hg values in bone of individuals of the Roman Period (i.e., HE + LA) were 1.5 times higher (median ± SD = 72 ± 133 $ng.g^{-1}$) compared to Post-Romans (49 ± 69 $ng.g^{-1}$, Table 3.1).

For the Roman Period, Hg concentrations in bones from Vienna are not statistically different (Table S8, Annex 2) from those reported for rural individuals of A Lanzada

(average = 96 ± 103 $ng.g^{-1}$, range: 12 to 516 $ng.g^{-1}$) showing a similar decline between Romans and Post-Romans (López-Costas et al., 2020). This is consistent with previous studies focusing on the same period (Álvarez-Fernández et al., 2020; López-Costas et al., 2020). Elevated Hg levels in human bones are often related to post-mortem burial customs and occupational exposure (Emslie et al., 2019) or, especially during the Middle Ages, to urban contexts (Bocca et al., 2018) and medication habits, as Hg was used to treat diseases like syphilis and leprosy (Rasmussen et al., 2017, 2015, 2008). Additionally, it has been observed that the diagenetic incorporation of Hg into bone is negligible; rather, skeletal remains tend to contribute Hg to the soil (Álvarez-Fernández et al., 2022, 2021; Rasmussen et al., 2008; Walser III et al., 2019).

Unlike Pb, Hg is primarily absorbed through the lungs (i.e., by inhalation) with lower absorption rates through the skin or the gut (Park and Zheng, 2012). Fish and seafood are the main dietary source of Hg in humans (Bjørklund et al., 2017; Liu et al., 2011; Mahaffey et al., 2009) although there is no available data on dietary proxies (i.e., collagen or $\delta^{15}N$) or specific archaeological information regarding the common types of food in Vienna during Roman times. It unlikely that fish had a dominant place in the diet given Vienna's geographical position. In contrast, considerable amounts of wood were cut and burned (B. Helly, personal communication) at that time to supply both the metallurgy and manufacturing of Pb artifacts, and the Roman bath complex of *Thermes de Lutteurs* at Saint Roman in Gal during the 1st and 2nd centuries CE (Goulpeau and Savay-Guerraz, 1998). Such biomass burning is known to release Hg (De Simone et al., 2017). Numerous environmental records indicate that background mercury levels were likely higher during the Roman period than in preceding and subsequent periods (Cooke et al., 2020), even in remote locations like the Mediterranean Abyssal Plain (Cossa et al., 2024, 2021). Hence, the elevated Hg content found in human bones from the Roman period indicates increased

atmospheric background levels and continuous human exposure, regardless of location, especially in regions like Europe where mining activities were prevalent. The absence of concentration differences between sex or age groups suggests that inhabitants of Vienna were equally exposed to Hg during their lifetimes.

3.3.5. Deterioration in health status: Cu isotope composition

The δ^{65}Cu values in ancient bones from Vienna range from -0.86 to 0.14 ‰, (average = -0.5 ± 0.2 ‰, Fig. 3.4a). As for Pb and Hg, no significant difference in the δ^{65}Cu was observed between sex or age for the of studied individuals (Table S8, Annex 2).

In order to assess the reliability of the δ^{65}Cu as a marker of health deterioration, we first combined measurements of total Cu concentrations and stable isotope compositions in bones (Fig. 3.4b). This approach can provide information on the diagenetic alteration of Cu (Reynard and Balter, 2014) because external addition from soil into the bone should produce a correlation (or mixing line) between concentrations and isotopic compositions (Albarède, 1996). Cu concentrations (i.e., Cu and 1/Cu) and isotope ratios were not correlated (Fig. 3.4b and Table S6, Annex 2), which corroborates previous observations (i.e., section 3.3.1) indicating that diagenetic incorporation of Cu into the bone is negligible.

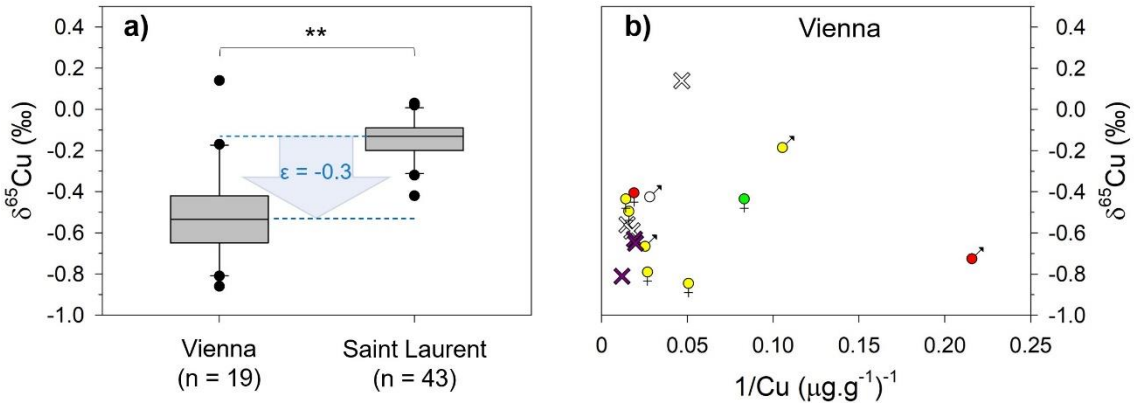

Figure 3.4. a) *Copper isotope composition (δ^{65}Cu) of bone samples of Vienna (this study) and Saint Laurent (Grenoble), and b) relationship between the Cu concentration and δ^{65}Cu of bones of Vienna. Each boxplot represents the 25th–75th percentiles (with the median as a bold horizontal line) and the whiskers show the 10th–90th percentiles. Data of Saint-Laurent comes from Jaouen et al. (2012). A significant difference between the two data sets is indicated by **(p < 0.001). The symbol and color codes are the same as in Figure 3.3.*

The δ^{65}Cu values reported here are significantly lower than those from bones collected in the nearby cemetery of Saint Laurent in Grenoble (i.e., 0.3 ‰ difference, $p < 0.001$, Fig. 3.4a and Table S8, Annex 2). At Saint Laurent, the bone samples belonged to individuals who lived during the 17th –18th century CE in an urban economy context, distant from any mining and metallurgical centers. Saint Laurent's inhabitants had access to diverse food resources and exhibited a variety of dietary behaviors (Herrscher et al., 2001). Hence, these δ^{65}Cu values can reasonably be considered a reference for individuals not exposed to metallurgical pollution. Considering the individuals from Saint Laurent as a control group, the depletion in the δ^{65}Cu observed for Vienna suggests health deterioration, likely due to the negative physiological consequences of the human exposure to Pb (Moore et al., 2021). Recent studies have indeed observed a systematic decrease in Cu isotopic composition for various types of cancer (leukemia, lymphoma, gastrointestinal, gynecological, breast, and lung cancer) compared with healthy individuals (Costas-Rodríguez et al., 2016) (Télouk et al., 2015).

3.4. Conclusions

The multi-elemental and isotopic (Pb) analyses of ancient human skeletons allowed tracing Vienna's human exposure to potentially toxic metals (i.e., Pb and Hg) and relating it to the production and use of lead artifacts, especially pipes. We report for the first time the use of Cu isotope ratios to explore the potential physiological consequences of Pb exposure in ancient skeletal remains. Combining the use of elemental concentration measurements, isotopic composition, and the correlation between the two proves that the diagenetic perturbation of bones studied from Vienna is negligible. No significant differences were found for sex and age for both Pb and Hg, indicating that individuals were equally and consistently exposed to both Pb and Hg pollution, and that population dynamics and structure were not a factor.

Differences in Pb concentrations between individuals of the Roman and post-Roman periods are in agreement with the chronology of other environmental archives. Data provided in this study does not allow the distinction between the two possible routes of chronic exposure, i.e., inhalation vs ingestion. Further studies on human bones of the same periods should provide information on individuals from control sites (rural areas), including Pb content and copper isotope composition. Both at the study and control sites, additional information is needed regarding dietary habits including the use of Pb in everyday life (utensils for storage and cooking).

Acknowledgments

This study benefited from the financial support from ISTerre and the Ec2CO (ref dycovi…) of CNRS. This study was performed using the INSU/CNRS MC-ICP-MS national facility at ENS-LYON. The authors would like to thank the SRA. This work was conducted with the support of the LABEX IMU (ANR-10-LABX-0088) of the University

of Lyon, within the framework of the “Investissements d’Avenir” program managed by the Agence Nationale de la Recherche (ANR).

Authors contributions:

Carlos Heredia, Alexandra T. Gourlan, and Sylvain Campillo made the data analysis. Alexandra T. Gourlan and Stéphane Guédron contributed to the study’s conception and design. Data collection was made thanks to Benoit Helly and G. Granier. Carlos Heredia, Alexandra T. Gourlan, and Stéphane Guédron contributed to the drafting of the manuscript, and in addition, Hugo Delile, Benoit Helly, and Francis Albarede helped with the critical interpretation of data. The authors read, amended, and approved the final manuscript.

References

Adjajd, F., Lauxerois, R., 2014. Carte archéologique de la Gaule 38-3 : Vienne. Académie des inscriptions et belles-lettres.

Albarède, F., 2015. Metal Stable Isotopes in the Human Body: A Tribute of Geochemistry to Medicine. Elements 11, 265–269. https://doi.org/10.2113/gselements.11.4.265

Álvarez-Fernández, N., Martínez Cortizas, A., García-López, Z., López-Costas, O., 2021. Approaching mercury distribution in burial environment using PLS-R modelling. Sci Rep 11, 21231. https://doi.org/10.1038/s41598-021-00768-8

Álvarez-Fernández, N., Martínez Cortizas, A., López-Costas, O., 2022. Structural equation modelling of mercury intra-skeletal variability on archaeological human remains. Science of The Total Environment 851, 158015. https://doi.org/10.1016/j.scitotenv.2022.158015

Álvarez-Fernández, N., Martínez Cortizas, A., López-Costas, O., 2020. Atmospheric mercury pollution deciphered through archaeological bones. Journal of Archaeological Science 119, 105159. https://doi.org/10.1016/j.jas.2020.105159

Azzopardi, J.I., Cuschieri, A., Blundell, R., 2023. General Heavy Metal Regulations: Focus on the USA and the EU, in: Heavy Metals in the Environment: Management Strategies for Global Pollution, ACS Symposium Series. American Chemical Society, pp. 71–76. https://doi.org/10.1021/bk-2023-1456.ch005

Barbosa, F., Tanus-Santos, J.E., Gerlach, R.F., Parsons, P.J., 2005. A critical review of biomarkers used for monitoring human exposure to lead: advantages, limitations, and future needs. Environ Health Perspect 113, 1669–1674. https://doi.org/10.1289/ehp.7917

Bennett, C., 1925. FRONTINUS, Stratagems. Aqueducts of Rome, Loeb Classical Series.

Bjørklund, G., Dadar, M., Mutter, J., Aaseth, J., 2017. The toxicology of mercury: Current research and emerging trends. Environmental Research 159, 545–554. https://doi.org/10.1016/j.envres.2017.08.051

Bocca, B., Forte, G., Giuffra, V., Serra, R.M., Asara, Y., Farace, C., Milanese, M., Tognotti, E., Montella, A., Bandiera, P., Madeddu, R., 2018. Metals in bones of the middle-aged inhabitants of Sardinia island (Italy) to assess nutrition and environmental exposure. Environ Sci Pollut Res 25, 8404–8414. https://doi.org/10.1007/s11356-017-1140-6

Boeckx, R.L., 1986. Lead poisoning in children. Anal Chem 58, 274A-288A.

Bonaventura, P., Benedetti, G., Albarède, F., Miossec, P., 2015. Zinc and its role in immunity and inflammation. Autoimmunity Reviews 14, 277–285. https://doi.org/10.1016/j.autrev.2014.11.008

BRGM, 2017. Concessions de La Poype et de Vienne - Evaluation et cartographie des aléas mouvements de terrain (No. 2017/038DE-17RHA22020). GEOREDIS, Ales.

Brissaud, L., 2016. Les fistulae estampillées VASSEDO. VF : réflexion critique sur la valeur et la fonction d'un nom, in: Brancier, J., Vallette, T., Rémeaud, C. (Eds.), Des vestiges aux sociétés : Regards croisés sur le passage des données archéologiques à la société sous-jacente, Archéo.doct. Éditions de la Sorbonne, Paris, pp. 57–83. https://doi.org/10.4000/books.psorbonne.4822

Burstein, S.M., Finch, C.E., 2022. Lead Poisoning in Ancient Rome: The State of the Question. Journal of Ancient Civilizations 37, 225–246. https://doi.org/10.16758/j.cnki.1004-9371.2022.04.015

Chamel, G., Gourlan, A.T., Télouk, P., Sayag, D., Milliard, V., Loiseau, C., Simon, M., Buff, S., Ponce, F., 2017. Retrospective evaluation of blood copper stable isotopes ratio 65Cu/63Cu as a biomarker of cancer in dogs. Veterinary and Comparative Oncology 15, 1323–1332. https://doi.org/10.1111/vco.12273

Cochet, A., 2000. Le Plomb en Gaule romaine. Techniques de fabrication et produits, Editions Mergoil. ed.

Cochet, A., Hansen, J., 1986. Conduites et objets de plomb gallo-romains de Vienne (Isère). CNRS.

Cooke, C.A., Martínez-Cortizas, A., Bindler, R., Sexauer Gustin, M., 2020. Environmental archives of atmospheric Hg deposition – A review. Science of The Total Environment 709, 134800. https://doi.org/10.1016/j.scitotenv.2019.134800

Cossa, D., Buscail, R., Dennielou, B., Radakovitch, O., Puig, P., Khripounoff, A., Boutier, B., Berné, S., 2024. Sources, Transport, and accumulation of Mercury in the northwestern Mediterranean margin sediments during the Industrial Era and influence of turbiditic events. Progress in Oceanography 220, 103186. https://doi.org/10.1016/j.pocean.2023.103186

Cossa, D., Mucci, A., Guédron, S., Coquery, M., Radakovitch, O., Escoube, R., Campillo, S., Heussner, S., 2021. Mercury accumulation in the sediment of the Western Mediterranean abyssal plain: A reliable archive of the late Holocene. Geochimica et Cosmochimica Acta 309, 1–15. https://doi.org/10.1016/j.gca.2021.06.014

Costas-Rodríguez, M., Delanghe, J., Vanhaecke, F., 2016. High-precision isotopic analysis of essential mineral elements in biomedicine: natural isotope ratio variations as potential diagnostic and/or prognostic markers. TrAC Trends in Analytical Chemistry 76, 182–193. https://doi.org/10.1016/j.trac.2015.10.008

De Simone, F., Artaxo, P., Bencardino, M., Cinnirella, S., Carbone, F., D'Amore, F., Dommergue, A., Feng, X.B., Gencarelli, C.N., Hedgecock, I.M., Landis, M.S., Sprovieri, F., Suzuki, N., Wängberg, I., Pirrone, N., 2017. Particulate-phase mercury emissions from biomass burning and impact on resulting deposition: a modelling assessment. Atmospheric Chemistry and Physics 17, 1881–1899. https://doi.org/10.5194/acp-17-1881-2017

Delile, H., Blichert-Toft, J., Goiran, J.-P., Keay, S., Albarède, F., 2014. Lead in ancient Rome's city waters. Proceedings of the National Academy of Sciences 111, 6594–6599. https://doi.org/10.1073/pnas.1400097111

Delile, H., Keenan-Jones, D., Blichert-Toft, J., Goiran, J.-P., Arnaud-Godet, F., Albarède, F., 2017. Rome's urban history inferred from Pb-contaminated waters trapped in its ancient harbor basins. Proceedings of the National Academy of Sciences 114, 10059–10064. https://doi.org/10.1073/pnas.1706334114

Deming, D., 2020. The Aqueducts and Water Supply of Ancient Rome. Groundwater 58, 152–161. https://doi.org/10.1111/gwat.12958

DREAL, 2016. Étude approfondie concernant la présence du plomb dans le sol - Secteur de la Butte Sainte-Blandine à Vienne (38) (No. AIX 11 001 IS). ICF Environnement.

Emslie, S.D., Alderman, A., McKenzie, A., Brasso, R., Taylor, A.R., Molina Moreno, M., Cambra-Moo, O., González Martín, A., Silva, A.M., Valera, A., García Sanjuán, L., Vijande Vila, E., 2019. Mercury in archaeological human bone: biogenic or diagenetic? Journal of Archaeological Science 108, 104969. https://doi.org/10.1016/j.jas.2019.05.005

Fabig, A., Herrmann, B., 2002. Trace elements in buried human bones: intra-population variability of Sr/Ca and Ba/Ca ratios – diet or diagenesis? Naturwissenschaften 89, 115–119. https://doi.org/10.1007/s00114-001-0294-7

Flaux, C., Save, S., Scrinzi, M., Larousse, N.M., Vaschalde, C., Renaud, A., Tillier, M., Guihou, A., Deschamps, P., Véron, A., 2023. Roman-era alluvial waste in the Vistre de la Fontaine (Nîmes, southeast France): from a sacred spring to a contaminated river. Journal of Roman Archaeology 36, 50–72. https://doi.org/10.1017/S1047759423000132

Giffin, K.L., Swanston, T., Coulthard, I., Murphy, A.R., Cooper, D.M.L., Varney, T.L., 2017. Skeletal Lead Burden of the British Royal Navy in Colonial Antigua. International Journal of Osteoarchaeology 27, 672–682. https://doi.org/10.1002/oa.2589

Gosselin, S., Durand, V., Lauxerrois, R., Boissin-Pierrot, M.F., Helly, B., Savay, - Guerraz, 2011. Des objets qui racontent l'histoire, Vienne, d'une rive à l'autre, volume II : des origines à la période romaine.

Goulpeau, L., Savay-Guerraz, H., 1998. Datation archéomagnétique des grandes étapes du fonctionnement des « Thermes des Lutteurs » à Saint-Romain-en-Gal (Rhône). Revue archéologique de Narbonnaise 31, 159–184. https://doi.org/10.3406/ran.1998.1502

Gourlan, A.T., Douay, G., Telouk, P., 2019. Copper isotopes as possible neoplasia biomarkers in captive wild felids. Zoo Biology 38, 371–383. https://doi.org/10.1002/zoo.21504

Granier, G., 2013. Espaces, pratiques funéraires et populations à Vienne du Ier au VIe siècle, in: Adjajd, F., Lauxerois, R. (Eds.), Guide Archeologique de la Gaule - Vienne 38/8. Académie des Inscriptions et Belles-Lettres, Paris, pp. 171–180.

Gregory, D., Matthiesen, H., 2023. Defining the Burial Environment, in: Handbook of Archaeological Sciences. John Wiley & Sons, Ltd, pp. 1075–1088. https://doi.org/10.1002/9781119592112.ch53

Guedron, S., Grangeon, S., Lanson, B., Grimaldi, M., 2009. Mercury speciation in a tropical soil association; Consequence of gold mining on Hg distribution in French Guiana. Geoderma 153, 331–346. https://doi.org/10.1016/j.geoderma.2009.08.017

Harkness, J.S., Darrah, T.H., 2019. From the crust to the cortical: The geochemistry of trace elements in human bone. Geochimica et Cosmochimica Acta 249, 76–94. https://doi.org/10.1016/j.gca.2019.01.019

Helly, B., 2013. Évolution de la topographie de Vienne, du Ier siècle av. J.-C au Ve siècle apr. J.-C., in: Adjajd, F., Lauxerois, R. (Eds.), Carte Archeologique de la Gaule - Vienne 38/3. Académie des Inscriptions et Belles-Lettres, Paris, pp. 116–148.

Helly, B., Granier, G., Lucas, G., 2017. Vienne antique - Sainte-Colombe, Saint-Romain-en-Gal, Vienne, Guides archéologicques de la France.

Herrscher, E., Bocherens, H., Valentin, F., Colardelle, R., 2001. Comportements alimentaires au Moyen Âge à Grenoble : application de la biogéochimie isotopique à la nécropole Saint-Laurent (XIIIe–XVe siècles, Isère, France). Comptes Rendus de l'Académie des Sciences - Series III - Sciences de la Vie 324, 479–487. https://doi.org/10.1016/S0764-4469(01)01316-6

Hodge, A.T., 1981. Vitruvius, Lead Pipes and Lead Poisoning. American Journal of Archaeology 85, 486–491. https://doi.org/10.2307/504874

Hong, S., Candelone, J.-P., Patterson, C.C., Boutron, C.F., 1994. Greenland Ice Evidence of Hemispheric Lead Pollution Two Millennia Ago by Greek and Roman Civilizations. Science 265, 1841–1843. https://doi.org/10.1126/science.265.5180.1841

Jaouen, K., Balter, V., Herrscher, E., Lamboux, A., Telouk, P., Albarède, F., 2012. Fe and Cu stable isotopes in archeological human bones and their relationship to sex.

American Journal of Physical Anthropology 148, 334–340. https://doi.org/10.1002/ajpa.22053

Jaouen, K., Herrscher, E., Balter, V., 2017. Copper and zinc isotope ratios in human bone and enamel. American Journal of Physical Anthropology 162, 491–500. https://doi.org/10.1002/ajpa.23132

Jaouen, K., Szpak, P., Richards, M.P., 2016. Zinc Isotope Ratios as Indicators of Diet and Trophic Level in Arctic Marine Mammals. PLOS ONE 11, e0152299. https://doi.org/10.1371/journal.pone.0152299

Järup, L., 2003. Hazards of heavy metal contamination. Br Med Bull 68, 167–182. https://doi.org/10.1093/bmb/ldg032

Kamenov, G.D., Lofaro, E.M., Goad, G., Krigbaum, J., 2018. Trace elements in modern and archaeological human teeth: Implications for human metal exposure and enamel diagenetic changes. Journal of Archaeological Science 99, 27–34. https://doi.org/10.1016/j.jas.2018.09.002

Kazi Tani, L.S., Gourlan, A.T., Dennouni-Medjati, N., Telouk, P., Dali-Sahi, M., Harek, Y., Sun, Q., Hackler, J., Belhadj, M., Schomburg, L., Charlet, L., 2021. Copper Isotopes and Copper to Zinc Ratio as Possible Biomarkers for Thyroid Cancer. Front Med (Lausanne) 8, 698167. https://doi.org/10.3389/fmed.2021.698167

Killick, D., Fenn, T., 2012. Archaeometallurgy: The Study of Preindustrial Mining and Metallurgy. https://doi.org/10.1146/annurev-anthro-092611-145719

Kim, E.J., Herrera, J.E., Huggins, D., Braam, J., Koshowski, S., 2011. Effect of pH on the concentrations of lead and trace contaminants in drinking water: a combined batch, pipe loop and sentinel home study. Water Res 45, 2763–2774. https://doi.org/10.1016/j.watres.2011.02.023

Krayenbuehl, P.-A., Walczyk, T., Schoenberg, R., von Blanckenburg, F., Schulthess, G., 2005. Hereditary hemochromatosis is reflected in the iron isotope composition of blood. Blood 105, 3812–3816. https://doi.org/10.1182/blood-2004-07-2807

Leroi, A.M., Koufopanou, V., Burt, A., 2003. Cancer selection. Nat Rev Cancer 3, 226–231. https://doi.org/10.1038/nrc1016

Liu, G., Cai, Y., O'Driscoll, N., Feng, X., Jiang, G., 2011. Overview of Mercury in the Environment, in: Environmental Chemistry and Toxicology of Mercury. John Wiley & Sons, Ltd, pp. 1–12. https://doi.org/10.1002/9781118146644.ch1

López-Costas, O., Kylander, M., Mattielli, N., Álvarez-Fernández, N., Pérez-Rodríguez, M., Mighall, T., Bindler, R., Martínez Cortizas, A., 2020. Human bones tell the story of atmospheric mercury and lead exposure at the edge of Roman World. Science of The Total Environment 710, 136319. https://doi.org/10.1016/j.scitotenv.2019.136319

Lyengar, G.V., Tandom, L., 1999. Minor and Trace Elements in Human Bones and Teeth (No. NAHRES-39). International Atomic Energy Agency, Viena.

Mahaffey, K.R., Clickner, R.P., Jeffries, R.A., 2009. Adult Women's Blood Mercury Concentrations Vary Regionally in the United States: Association with Patterns of Fish Consumption (NHANES 1999–2004). Environmental Health Perspectives 117, 47–53. https://doi.org/10.1289/ehp.11674

Maréchal, C., Albarède, F., 2002. Ion-exchange fractionation of copper and zinc isotopes. Geochimica et Cosmochimica Acta 66, 1499–1509. https://doi.org/10.1016/S0016-7037(01)00815-8

Maréchal, C.N., Télouk, P., Albarède, F., 1999. Precise analysis of copper and zinc isotopic compositions by plasma-source mass spectrometry. Chemical Geology 156, 251–273. https://doi.org/10.1016/S0009-2541(98)00191-0

Martínez-García, M.J., Moreno, J.M., Moreno-Clavel, J., Vergara, N., García-Sánchez, A., Guillamón, A., Portí, M., Moreno-Grau, S., 2005. Heavy metals in human bones in different historical epochs. Science of The Total Environment 348, 51–72. https://doi.org/10.1016/j.scitotenv.2004.12.075

McConnell, J.R., Wilson, A.I., Stohl, A., Arienzo, M.M., Chellman, N.J., Eckhardt, S., Thompson, E.M., Pollard, A.M., Steffensen, J.P., 2018. Lead pollution recorded in Greenland ice indicates European emissions tracked plagues, wars, and imperial expansion during antiquity. Proceedings of the National Academy of Sciences 115, 5726–5731. https://doi.org/10.1073/pnas.1721818115

Monna, F., Lancelot, J., Croudace, I.W., Cundy, A.B., Lewis, J.T., 1997. Pb Isotopic Composition of Airborne Particulate Material from France and the Southern United Kingdom: Implications for Pb Pollution Sources in Urban Areas. Environ. Sci. Technol. 31, 2277–2286. https://doi.org/10.1021/es960870+

Moore, J., Filipek, K., Kalenderian, V., Gowland, R., Hamilton, E., Evans, J., Montgomery, J., 2021. Death metal: Evidence for the impact of lead poisoning on childhood health within the Roman Empire. International Journal of Osteoarchaeology 31, 846–856. https://doi.org/10.1002/oa.3001

Nanci, A. (Ed.), 2013. Chapter 6 - Bone, in: Ten Cate's Oral Histology (Eighth Edition). Mosby, St. Louis (MO), pp. 95–121. https://doi.org/10.1016/B978-0-323-07846-7.00006-9

Needleman, L., Needleman, D., 1985. Lead Poisoning and the Decline of the Roman Aristocracy. Echos du monde classique: Classical views 29, 63–94.

Nriagu, J.O., 1983. Lead and lead poisoning in antiquity, Antiquities. Wiley, New York.

Parfitt, A.M., 2013. Chapter 36 - Skeletal Heterogeneity and the Purposes of Bone Remodeling: Implications for the Understanding of Osteoporosis, in: Marcus, R., Feldman, D., Dempster, D.W., Luckey, M., Cauley, J.A. (Eds.), Osteoporosis (Fourth Edition). Academic Press, San Diego, pp. 855–872. https://doi.org/10.1016/B978-0-12-415853-5.00036-4

Park, J.-D., Zheng, W., 2012. Human Exposure and Health Effects of Inorganic and Elemental Mercury. JPMPH 45, 344–352. https://doi.org/10.3961/jpmph.2012.45.6.344

Patterson, C.C., Shirahata, H., Ericson, J.E., 1987. Lead in ancient human bones and its relevance to historical developments of social problems with lead. Science of The Total Environment 61, 167–200. https://doi.org/10.1016/0048-9697(87)90366-4

Pelletier, A., 2001. Vienna, Vienne. Presses Universitaires de Lyon.

Pernicka, E., Begemann, F., Schmitt-Strecker, S., Todorova, K., Kuleff, I., 1997. Prehistoric copper in Bulgaria: its composition and provenance. Eurasia antiqua : Zeitschrift fur Archaologie Eurasiens / Deutsches Archaologisches Institut, Eurasien-Abteilung 3, 41–180.

Pesavento, P.A., Agnew, D., Keel, M.K., Woolard, K.D., 2018. Cancer in wildlife: patterns of emergence. Nat Rev Cancer 18, 646–661. https://doi.org/10.1038/s41568-018-0045-0

Price, T.D., Blitz, J., Burton, J., Ezzo, J.A., 1992. Diagenesis in prehistoric bone: Problems and solutions. Journal of Archaeological Science 19, 513–529. https://doi.org/10.1016/0305-4403(92)90026-Y

Radivojević, M., Rehren, T., Kuzmanović-Cvetković, J., Jovanović, M., Northover, J.P., 2013. Tainted ores and the rise of tin bronzes in Eurasia, c. 6500 years ago. Antiquity 87, 1030–1045. https://doi.org/10.1017/S0003598X0004984X

Rasmussen, K., Skytte, L., D'imporzano, P., Orla Thomsen, P., Søvsø, M., Lier Boldsen, J., 2017. On the distribution of trace element concentrations in multiple bone

elements in 10 Danish medieval and post-medieval individuals. Am J Phys Anthropol 162, 90–102. https://doi.org/10.1002/ajpa.23099

Rasmussen, K.L., Boldsen, J.L., Kristensen, H.K., Skytte, L., Hansen, K.L., Mølholm, L., Grootes, P.M., Nadeau, M.-J., Flöche Eriksen, K.M., 2008. Mercury levels in Danish Medieval human bones. Journal of Archaeological Science 35, 2295–2306. https://doi.org/10.1016/j.jas.2008.03.003

Rasmussen, K.L., Milner, G., Skytte, L., Lynnerup, N., Thomsen, J.L., Boldsen, J.L., 2019. Mapping diagenesis in archaeological human bones. Heritage Science 7, 41. https://doi.org/10.1186/s40494-019-0285-7

Rasmussen, K.L., Skytte, L., Jensen, A.J., Boldsen, J.L., 2015. Comparison of mercury and lead levels in the bones of rural and urban populations in Southern Denmark and Northern Germany during the Middle Ages. Journal of Archaeological Science: Reports 3, 358–370. https://doi.org/10.1016/j.jasrep.2015.06.021

Reiche, I., Favre-Quattropani, L., Vignaud, C., Bocherens, H., Charlet, L., Menu, M., 2003. A multi-analytical study of bone diagenesis: the Neolithic site of Bercy (Paris, France). Meas. Sci. Technol. 14, 1608. https://doi.org/10.1088/0957-0233/14/9/312

Retief, F.P., Cilliers, L., 2006. Lead poisoning in ancient Rome. Acta Theologica 26, 147–164. https://doi.org/10.4314/actat.v26i2.52570

Reynard, B., Balter, V., 2014. Trace elements and their isotopes in bones and teeth: Diet, environments, diagenesis, and dating of archeological and paleontological samples. Palaeogeography, Palaeoclimatology, Palaeoecology, Bone and enamel diagenesis: From the crystal to the environment - A tribute to Jean-François Saliège 416, 4–16. https://doi.org/10.1016/j.palaeo.2014.07.038

Roberts, B.W., Thornton, C.P., Pigott, V.C., 2009. Development of metallurgy in Eurasia. Antiquity 83, 1012–1022. https://doi.org/10.1017/S0003598X00099312

Schroeder, H.A., Tipton, I.H., 1968. The Human Body Burden of Lead. Archives of Environmental Health: An International Journal 17, 965–978. https://doi.org/10.1080/00039896.1968.10665354

Silbergeld, E.K., Schwartz, J., Mahaffey, K., 1988. Lead and osteoporosis: Mobilization of lead from bone in postmenopausal women. Environmental Research 47, 79–94. https://doi.org/10.1016/S0013-9351(88)80023-9

Silva-Sánchez, N., Armada, X.-L., 2023. Environmental Impact of Roman Mining and Metallurgy and Its Correlation with the Archaeological Evidence: A European Perspective. Environmental Archaeology 0, 1–25. https://doi.org/10.1080/14614103.2023.2181295

Simpson, R., Cooper, D.M.L., Swanston, T., Coulthard, I., Varney, T.L., 2021. Historical overview and new directions in bioarchaeological trace element analysis: a review. Archaeol Anthropol Sci 13, 24. https://doi.org/10.1007/s12520-020-01262-4

Télouk, P., Puisieux, A., Fujii, T., Balter, V., Bondanese, V.P., Morel, A.-P., Clapisson, G., Lamboux, A., Albarede, F., 2015. Copper isotope effect in serum of cancer patients. A pilot study. Metallomics 7, 299–308. https://doi.org/10.1039/c4mt00269e

Toubhans, B., Gourlan, A.T., Telouk, P., Lutchman-Singh, K., Francis, L.W., Conlan, R.S., Margarit, L., Gonzalez, D., Charlet, L., 2020. Cu isotope ratios are meaningful in ovarian cancer diagnosis. Journal of Trace Elements in Medicine and Biology 62, 126611. https://doi.org/10.1016/j.jtemb.2020.126611

Trueman, C.N., Tuross, N., 2002. Trace Elements in Recent and Fossil Bone Apatite. Reviews in Mineralogy and Geochemistry 48, 489–521. https://doi.org/10.2138/rmg.2002.48.13

Tütken, T., Vennemann, T.W., 2011. Fossil bones and teeth: Preservation or alteration of biogenic compositions? Palaeogeography, Palaeoclimatology, Palaeoecology, Special Issue: Fossil bones and teeth: preservation or alteration of biogenic compositions? 310, 1–8. https://doi.org/10.1016/j.palaeo.2011.06.020

van Geen, A., Yao, Y., Ellis, T., Gelman, A., 2020. Fallout of Lead Over Paris From the 2019 Notre-Dame Cathedral Fire. GeoHealth 4, e2020GH000279. https://doi.org/10.1029/2020GH000279

Véron, A.J., Flaux, C., Marriner, N., Poirier, A., Rigaud, S., Morhange, C., Empereur, J.-Y., 2013. A 6000-year geochemical record of human activities from Alexandria (Egypt). Quaternary Science Reviews 81, 138–147. https://doi.org/10.1016/j.quascirev.2013.09.029

Vicard, T., 2021. Vienne – Place François-Mitterrand, implantation d'un parking enterré. ADLFI. Archéologie de la France.

Vittecoq, M., Ducasse, H., Arnal, A., Møller, A.P., Ujvari, B., Jacqueline, C.B., Tissot, T., Missé, D., Bernex, F., Pirot, N., Lemberger, K., Abadie, J., Labrut, S., Bonhomme, F., Renaud, F., Roche, B., Thomas, F., 2015. Animal behaviour and cancer. Animal Behaviour 101, 19–26. https://doi.org/10.1016/j.anbehav.2014.12.001

Waldron, H.A., 1981. Postmortem absorption of lead by the skeleton. American Journal of Physical Anthropology 55, 395–398. https://doi.org/10.1002/ajpa.1330550313

Walser III, J.W., Kristjánsdóttir, S., Gowland, R., Desnica, N., 2019. Volcanoes, medicine, and monasticism: Investigating mercury exposure in medieval Iceland. International Journal of Osteoarchaeology 29, 48–61. https://doi.org/10.1002/oa.2712

Wani, A.L., Ara, A., Usmani, J.A., 2015. Lead toxicity: a review. Interdiscip Toxicol 8, 55–64. https://doi.org/10.1515/intox-2015-0009

Weeks, L., Keall, E., Pashley, V., Evans, J., Stock, S., 2009. Lead Isotope Analyses of Bronze Age Copper-Base Artefacts from Al-Midamman, Yemen: Towards the Identification of an Indigenous Metal Production and Exchange System in the Southern Red Sea Region*. Archaeometry 51, 576–597. https://doi.org/10.1111/j.1475-4754.2008.00429.x

W.H.O, 2022. Lead poisoning [WWW Document].

Zioła-Frankowska, A., Dąbrowski, M., Kubaszewski, Ł., Rogala, P., Kowalski, A., Frankowski, M., 2017. An analysis of factors affecting the mercury content in the human femoral bone. Environ Sci Pollut Res 24, 547–557. https://doi.org/10.1007/s11356-016-7784-9

Zioła-Frankowska, A., Kubaszewski, Ł., Dąbrowski, M., Kowalski, A., Rogala, P., Strzyżewski, W., Łabędź, W., Uklejewski, R., Novotny, K., Kanicky, V., Frankowski, M., 2015. The Content of the 14 Metals in Cancellous and Cortical Bone of the Hip Joint Affected by Osteoarthritis. BioMed Research International 2015, e815648. https://doi.org/10.1155/2015/815648

Chapter 4: Human bones from a medieval alpine miners' cemetery reveal post-mortem polymetallic contamination (Brandes, France)

This article will be submitted to the Journal: Applied Geochemistry

Résumé

Les os récupérés lors de fouilles archéologiques peuvent constituer des archives précieuses, car ils peuvent conserver des informations sur l'histoire de la vie des animaux et des êtres humains. L'analyse biogéochimique de ces tissus minéralisés peut aider à évaluer l'exposition des individus au cours de leur vie, influencée par des facteurs culturels et la pollution environnementale. Dans cette étude, la contamination polymétallique d'ossements humains provenant de la communauté minière alpine médiévale de Brandes en Oisans, en France, a été étudiée et comparée à deux sites témoins (Huez et La Garde, en France). L'analyse a révélé des concentrations élevées de plomb (Pb), d'arsenic (As), d'antimoine (Sb) et de cuivre (Cu) dans les ossements de Brandes, suggérant à la fois une exposition environnementale importante et une possible altération diagénétique. La combinaison de proxies diagénétiques conventionnels (c.-à-d. Sr/Ca et Ba/Ca) et non conventionnels (c.-à-d. rapports isotopiques du cuivre ; $\delta^{65}Cu$) a révélé des altérations diagénétiques complexes qui sont spécifiques à l'élément et indépendantes du type d'os (fémur vs phalanges). Cette étude démontre la complexité de l'évaluation de l'altération diagénétique post-mortem et confirme que les approches conventionnelles utilisant des proxies simples peuvent être biaisées par des conditions géochimiques singulières dans l'environnement d'enfouissement. Il n'existe donc pas de méthode générique pour évaluer une telle perturbation diagénétique, et celle-ci doit être évaluée à l'aide d'approches multi-proxy ainsi que par la caractérisation du contexte d'inhumation.

Human bones from a medieval alpine miners' cemetery reveal post-mortem polymetallic contamination (Brandes, France)

C. Heredia[1*], A. T. Gourlan[1], S. Guédron[1] , L. Hammann[1], S. Campillo[1], S. Santenac[1], P. Telouk[2] and M.C. Bailly-Maître[3] .

[1] Université Grenoble Alpes, Université Savoie Mont Blanc, CNRS, IRD, IFSTAR, ISTerre, 38000, Grenoble, France.

[2] Ecole Normale Supérieure de Lyon, CNRS, and Université de Lyon, 46 Allée d'Italie, 69007, Lyon, France

[3] Laboratoire d'Archéologie Médiévale et Moderne en Méditerranée, Aix-Marseille Université, CNRS, 13007, Marseille, France, France.

*Corresponding author:

Carlos Heredia A.; carlos.heredia-aguilar@univ-grenoble-alpes.fr

Keywords: Metals, bone, diagenesis, mining pollution, Middle Age

Highlights:

- Human bones from an medieval miner's cementery and two control sites were studied
- Multielemental analysis reveal polymetallic contamination for miners bones
- Diagenetic proxies and copper isotope composition revealed post-mortem contamination
- Diagenetic alteration was found in both phalanges and femurs

Abstract

Bones retrieved from archaeological excavations can be valuable archives, as they may preserve information regarding animal and human life histories. The biogeochemical analysis of these mineralized tissues can help assessing the individual exposure during its lifetime, influenced by cultural factors and environmental pollution. In this study, the polymetallic contamination of human bones from the alpine medieval mining community of Brandes en Oisans, France was investigated and compared to two control sites (Huez and La Garde, France). Analysis revealed elevated concentrations of lead (Pb), arsenic (As), antimony (Sb), and copper (Cu) in bones from Brandes, suggesting both significant environmental exposure and possible diagenetic alteration. The combination of conventional (i.e., Sr/Ca and Ba/Ca) and unconventional (i.e., copper isotope ratios; $\delta^{65}Cu$) diagenetic proxies revealed complex diagenetic alterations that are element-specific and independent of the bone type (femur vs phalanges). This study demonstrates the complexity of assessing post-mortem diagenetic alteration and confirms that conventional approaches using simple proxies can be biased by singular geochemical conditions in the burial environment. There is, therefore, no generic method for assessing such diagenetic disturbance, and it must be evaluated using multiproxy approaches together with the characterization of the burial context.

4.1. Introduction

Bones retrieved from archaeological excavations can be valuable archives, as they may preserve information regarding animal and human life histories (Ericson et al., 1979; Kuitems et al., 2015; Rasmussen et al., 2017; Wooller et al., 2021), habitats (Knudson and Price, 2007), diet (Jaouen et al., 2019; Maurer et al., 2019), and past climatic and environmental conditions (Hedges et al., 2004; López-Costas et al., 2020). These biogeochemical data, incorporated into living mineralized tissues during their formation, are crucial for archaeological, anthropological, and forensic investigations (Balter and Zazzo, 2014).

The analysis of heavy metal content in bones has been used to study human occupational exposure to mining and metallurgical industries (Baranowska et al., 1995; Keinonen, 1992; Lindh et al., 1981, 1980; Morgan et al., 1990). For example, elevated levels of elements like lead (Pb) and mercury (Hg) have been attributed to high metal exposure during an individual's lifetime, influenced by cultural factors and environmental pollution (Ericson et al., 1991; López-Costas et al., 2020; Martínez-García et al., 2005; Rasmussen et al., 2008). Yet, only a few studies have investigated the exposure of ancient populations to mining activities using osteoarcheological records (Grattan et al., 2005, 2002; Oakberg et al., 2000; Pyatt et al., 2005) and the possibility of detecting health deterioration (Heredia et al., 2024). Recently, stable isotopes of specific elements such as copper (Cu), zinc (Zn), and iron (Fe) have emerged as potential diagnostic tools in medical research due to their specificity in biological functions and relatively short turnover time in the body (Albarède, 2015). Specifically, Cu isotopes have been used as a tool for cancer diagnosis in animals and humans, demonstrating a systematic enrichment in light Cu isotopes (e.g., ^{63}Cu) in the blood of cancer patients compared to healthy controls, leading to a decrease in the $^{65}Cu/^{63}Cu$ isotopic ratio (Télouk et al., 2015b; Toubhans et al., 2020).

This tool thus offers new insights into disease pathology and progression (Leroi et al., 2003; Vittecoq et al., 2015; Pesavento et al., 2018; Gourlan et al., 2017). In recent archaeological studies the Cu isotope composition of bones has been used to evaluate the health deterioration status in ancient human populations exposed to Pb (Heredia et al. 2024).

Several studies have, however, questioned the use of bones as archives because of high metal contents reported for some individuals, suggesting that diagenetic alteration could mask the lifetime exposure signal (Millard, 2006; Pike and Richards, 2002). Post-mortem processes resulting from exposure to necrosol and groundwater, known as diagenesis, can significantly alter skeletal remains after death and during fossilization (Maurer and Salesse, 2023). Although the alteration of buried skeletal material is inherent to their preservation in the soil, assessing the degree of preservation of the biogenic substrate is, therefore, essential. Only well-preserved bio-proxies enable accurate and reliable reconstructions of life history and environmental conditions (Tütken and Vennemann, 2011). During diagenesis, secondary minerals like calcite, pyrite, and Fe-Mn (hydr)oxides infiltrate the bone's pore structure, affecting both macroporosity (blood vessels and Haversian canals) and microporosity (related to collagen degradation), which alters the elemental and isotopic composition of archaeological bones (Rasmussen et al., 2019; Trueman and Tuross, 2002; Tütken and Vennemann, 2011). The study of the elemental composition of bones, including major and trace elements in bone (e.g., Al, Mn, Ca, Sr, Ba, Fe, Cu, Zn), and their ratios (e.g., Sr/Ca, Ba/Ca, Ca/P) is common practice for identifying post-mortem contamination in skeletal remains (Fabig and Herrmann, 2002; Giffin et al., 2017; Jaouen et al., 2012; Kamenov et al., 2018; Rasmussen et al., 2017; Simpson et al., 2021). The correlation between the total elemental concentration with the stable isotope composition of certain elements such as Sr (Budd et al., 2000) or Cu

(Jaouen et al., 2012) has also been proposed to elucidate diagenesis (Reynard and Balter, 2014) because any diagenetic addition to the bone should create a correlation (or mixing line) between the concentrations and isotopic compositions (Albarède, 1995).

In this work, we studied the potential human exposure to mining contaminants and the related health degradation of ancient human bones from an alpine medieval mining community. For this purpose, we analyzed the composition of major and trace elements, including metals (Pb, Cu, Fe, Zn, …), and copper isotopes composition of ancient human bones recovered from the medieval mining town of Brandes (Oisans, France) and from two control towns exempt from mining activity (Huez and La Garde). Conventional diagenetic tracers, together with unconventional ones (i.e., copper isotopes), were used to evaluate the potential effect of diagenesis and the reliability of interpretation on the lifetime exposure from these human remains.

4.2. Material and Methods

4.2.1. Study site and archaeological context

4.2.1.1. Brandes

The Oisans Massif (1800 m.a.s.l.) is located in the French Western Alps (Fig. 4.1). During the Middle Ages, it was an important place of passage for merchants and armies because it was one of the two major routes to Italy (Bailly-Maître, 2006). The Brandes plateau is located in a contact zone between Würmian glacial deposits (clays) and the crystalline rocks (gneisses and leptynites) that make up the Rousses Massif, which is Hercynian in origin (Bailly-Maître, 1996). The town of Brandes (1800 m.a.s.l) was established during the second half of the 12th century and the first half of the 14th century on the site of an Ag-Pb mine, which was exploited between 1236 and 1339 AD, partially for the benefit of the Dauphiné (Bailly-Maître, 2006). Other activities, such as wool, leather working,

and domestic animal breeding, were of minor interest and only served to ensure the long-term survival of the mining community (Bailly-Maître, 2006).

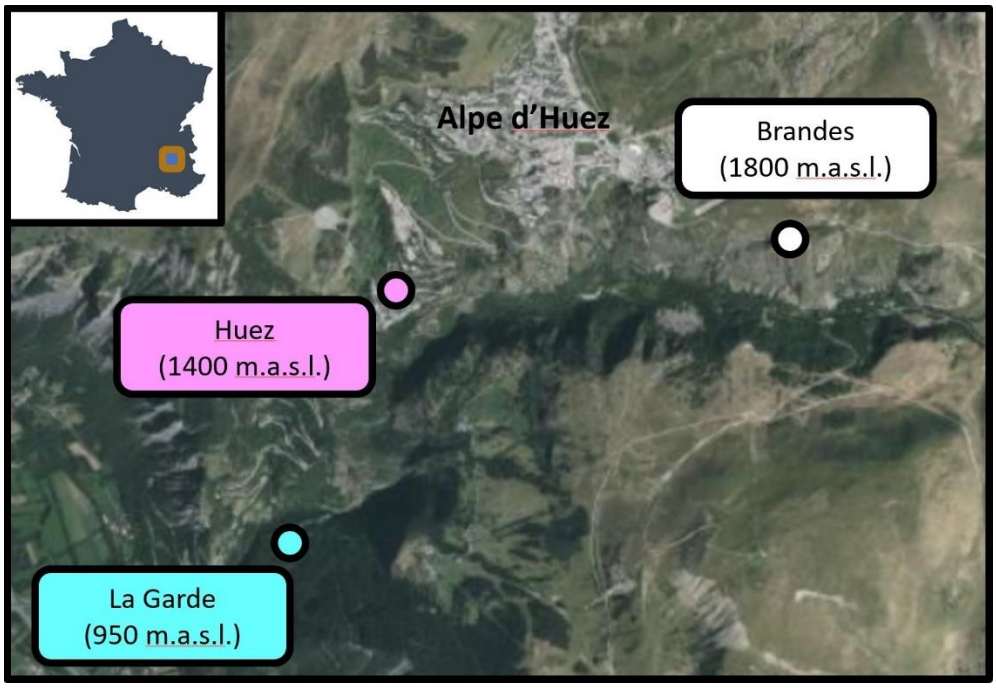

Figure 4.1. *Map of the study site, including the mining town of Brandes (Saint-Nicolas church) and the towns of Huez (Saint Ferreol church) and La Garde (Saint Pierre church) downhill Oisans.*

The village included dwellings, open-air and underground mining sites, mineral processing workshops, hydraulic installations necessary for the extraction of minerals, and a church surrounded in its three sites by the necropolis, which exhibits a high rate of re-interment (Bailly-Maître, 2008). The funerary rituals were consistent with the time period, with all individuals being buried dressed, lying on their backs, and with their heads towards the west (Peloux et al., 2015).

4.2.1.2. Huez and La Garde

During the Middle Ages, the primary access to the Brandes plateau was through the Romanche and the Grésivaudan valleys, uphill passing by the towns of La Garde (950 m.a.s.l.) and Huez (1400 m.a.s.l.) (Colardelle et al., 1979). The Saint Pierre church of La Garde was a priory church that became a parish in 1339 AD (Bailly-Maître, 1992). It

contained a large number of burials dating from the 15th to 16th centuries against its choir wall (Bailly-Maitre, 1991). Saint Ferreol is an ancient church of Huez, mentioned as early as the 11th century, like that of Brandes and La Garde (Dupraz and Bailly-Maître, 1981).

4.2.2. Sample collection

Twenty-seven human remains were recovered by archaeologists from the Saint Nicolas church at Brandes (BR, n = 20), Saint Pierre church at La Garde (LG, n = 2), and Saint Ferreol church at Huez (HU, n = 5). Samples include both male and female (men = 17, women = 4, unknown = 6) belonging to four age groups: infant/juvenile (IJ, 0 – 20 years old), young adult (YA, 20 – 29 years old), mature adult (MA, 30 – 59 years old), old adult (OA, > 60 years old) and unknown (n.a.). Phalange and femur samples from the same skeleton were recovered for the seventeenth of the twenty-seven individuals in order to evaluate the effect of diagenesis on these two types of bones. Additionally, five animal remains (i.e., cattle) were also recovered from the dumping grounds at Brandes and analyzed for comparison. Information concerning sex and probable age at death was provided by museum curators when possible and obtained from biometric skeletal analysis (i.e., bone and tooth maturation, senescence indicators, sexual morphological characteristics of coxal bones, identification of pathological conditions; Table S1, Annex 3).

4.2.3. Sample preparation

Cortical (compact) bone was selected for elemental and isotope analysis because it is less biologically active and has a slow turnover rate (2 – 5 % per year) compared to trabecular bone [15 – 35 % per year, (Nanci, 2013; Parfitt, 2013)]. Additionally, cortical bone is more resistant to diagenesis than trabecular bone (Price et al., 1992). Thus, it acts as the final repository of metals and can serve as an indicator of cumulative, integrated exposure

to mining activities over time (Barbosa et al., 2005). Cortical (compact) bone samples were obtained from the femur and the phalanges or metacarpals in the case of human individuals and from the upper or lower extremities in the case of animals (e.g., tibiae, calcaneus, navicular). Both the cleaning and the cutting were performed with a Dremel 8220 using a diamond disk following an established protocol (Jaouen et al., 2012). Briefly, all drill bits were washed and sonicated in ultra-pure water for 10 minutes and heated with a propane flame between each drilling procedure. Bone surfaces were abraded with a diamond drill to avoid contamination from soil particles or post-excavation handling (Lambert et al., 1991).

Around 50 mg of the sample was reduced to powder using a mortar, leached with 2 ml acetic acid 0.2 N for 1h at room temperature, and sonicated for 15 minutes. Samples were rinsed three times with MQ water and evaporated to dryness. They were then dissolved using 5 ml of concentrated HNO_3 (double-distilled) and 1 ml of concentrated H_2O_2 (Merck Suprapur quality) in Savillex® vessels at 90 °C for 24 hours.

4.2.4. Trace elements

Major elements (Ca, Na, Fe, Mg, K, and P) were analyzed with an inductively coupled plasma optical spectrometer (ICP-OES, Varian 720-ES) within the analytical chemistry platform of ISTerre (Grenoble-France). Pb, Cu, and complementary trace elements (Al, Cr, Mn, Co, Ni, Zn, As, Sr, Cd, Sn, Sb, Ba, Th, U) were measured by inductively coupled plasma mass spectrometry (ICP-MS, Agilent, 7500 CX quadrupole ICP-MS) using Be, In, and Bi as internal standards to correct for instrumental mass bias. The digestion procedure was assessed using certified materials for bone (bone meal, NIST 1486), together with sample replicates, providing recoveries of 95 ± 5% for all analyzed elements.

4.2.5. Cu purification and isotope measurements

Samples were initially redissolved in 1ml of 14N HNO_3, and a 50-µL aliquot was taken for elemental concentration measurements before and after purification. The dissolved samples were completely evaporated and redissolved in 1 mL of 7 N HCl + 0.001% H_2O_2 twice to eliminate any traces of residual nitric acid. Then, samples were dissolved in 1 mL 7 N HCl + 0.001% H_2O_2 in Savillex® vessels at 80 °C for 24h. Purification was performed twice using the AG MP-1 anion-exchange resin (100–200 mesh, BioRad), and Cu was eluted with 20 mL of 7 N HCl + 0.001% H_2O_2 following the technique of Maréchal and Albarède (Maréchal and Albarède, 2002). The total procedural Pb blank was < 10 pg. Cu yield (100 ± 5 %) was verified on an Agilent 7500 CX quadrupole ICP-MS at the ISTerre analytical chemistry platform (Grenoble, France).

Copper stable isotope compositions were determined by multi-collector inductively coupled plasma mass spectrometry (MC-ICPMS) using a Nu plasma 500 HR double-focusing mass spectrometer of ENS-Lyon. Gas flow instrumental mass fractionation was controlled both by dual standard-sample bracketing and the addition of an external standard [i.e., Zn for Cu samples (Maréchal et al., 1999)]. The isotope reference solution used was NIST 976 (Cu). The precision (external reproducibility, two-sigma) on the isotopic ratios is 0.05%.

4.2.6. Data treatment and statistical analyses

Statistical analyses were performed using SigmaPlot 12.5. Probability values (*p*) and correlation coefficients (R^2) are reported for linear regression analyses. In all cases, a *p*-value of 0.05 was chosen to indicate significance at the 95 percent confidence level. All data and calculations are provided in supplementary tables S1 to S8 (Annex 3).

4.3. Results and Discussion

When working with human burials, it is essential to characterize the archaeological context. Understanding soil properties and underground water provides insight into the preservation conditions affecting the chemical and physical stability of bones over time. This, in turn, enhances our understanding of the intensity of the diagenetic alteration of skeletal remains (Gregory and Matthiesen, 2023). However, limitations arise when working with human bones from archived collections due to the absence of this type of information, as is the case in this study.

4.3.1. Polymetallic contamination at Brandes

High elemental concentrations were observed in the bones from the miners' community of Brandes (Fig. 4.2, Table S6 to S8, Annex 3). Lead (Pb) concentrations ranged from 11 to 1991 $\mu g.g^{-1}$, with a median of 211 ± 525 $\mu g.g^{-1}$, and were higher than those in bones from Huez (HU, median ± SD, Pb = 28 ± 27 $\mu g.g^{-1}$) and La Garde (LG, median ± SD, Pb = 39 ± 14 $\mu g.g^{-1}$) (Fig. 4.2). Elevated levels of other mining-related elements such as arsenic (As) and antimony (Sb) were also found in Brandes bones (median ± SD, As = 12 ± 13 $\mu g.g^{-1}$, Sb = 109 ± 64 $\mu g.g^{-1}$), compared to HU (median ± SD, As = 2.2 ± 0.5 $\mu g.g^{-1}$, Sb = 0.9 ± 0.4 $\mu g.g^{-1}$) and LG (median ± SD, As = 1.7 ± 0.6 $\mu g.g^{-1}$, Sb = 1.9 ± 2.2 $\mu g.g^{-1}$) (Fig. 4.2, top panel). Similarly, essential elements such as copper (Cu), iron (Fe), and zinc (Zn) were found in higher concentrations at Brandes (median ± SD, Cu = 82 ± 112 $\mu g.g^{-1}$, Fe = 51 ± 138 $\mu g.g^{-1}$, Zn = 170 ± 531 $\mu g.g^{-1}$) compared to HU (median ± SD, Cu = 3 ± 14 $\mu g.g^{-1}$, Fe = 37 ± 67 $\mu g.g^{-1}$, Zn = 122 ± 54 $\mu g.g^{-1}$) and LG (median ± SD, Cu = 5 ± 3 $\mu g.g^{-1}$, Fe = 12 ± 54 $\mu g.g^{-1}$, Zn = 127 ± 65 $\mu g.g^{-1}$) (Fig. 4.2, bottom panel).

In comparison, animal bones collected at Brandes showed the highest overall values (Fig. 4.2, Table S6 to S8, Annex 3). Pb concentrations in animal bones ranged from 76 up to

158,108 µg.g^{-1}, with a median of 1220 ± 68,225 µg.g^{-1} (Fig. 4.2, top). This pattern was consistent across most of the elements analyzed here, with median ± SD values for As = 15 ± 746 µg.g^{-1}, Sb = 386 ± 718 µg.g^{-1}, Cu = 1273 ± 19,042 µg.g^{-1}, Fe = 41 ± 8255 µg.g^{-1}, and Zn = 4308 ± 2385 µg.g^{-1}.

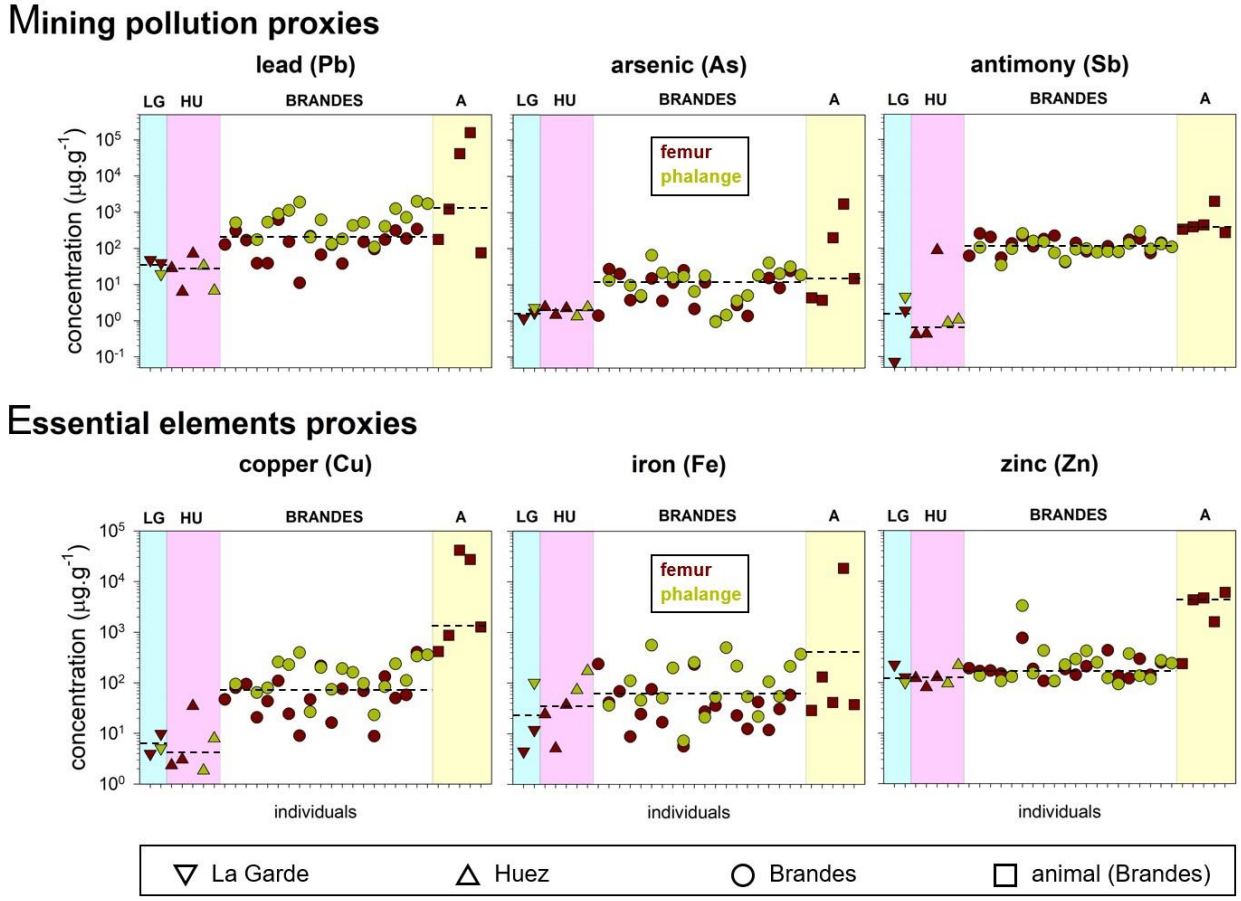

Figure 4.2. *(Top) Trace element concentration of mining pollution (top) and essential element (bottom) proxies retrieved from the cortical bone of femur (red) and phalanges (green) samples, coming from La Garde (LG, down triangles), Huez (HU, top triangles), Brandes (circles), and animals (A, squares). The dotted lines represent the median value for each site (both types of bones comprised).*

Mining activities at Brandes were mainly centered on the extraction of silver from argentiferous galena ores, which also contain high levels of other metals (Bailly-Maître, 1996) . Hence, elevated concentrations measured in bones from Brandes miners reflect high polymetallic levels reported for local ores (average, Pb = 41,046 µg.g^{-1}, Sb = 691 µg.g^{-1}, Cu = 232 µg.g^{-1}), soils (average, Pb = 17,224 µg.g^{-1}, Sb = 1986 µg.g^{-1}, Cu = 5311

µg.g^{-1}), and mine tailing (average, Pb = 26,351 µg.g^{-1}, Sb = 1022 µg.g^{-1}, Cu = 1545 µg.g^{-1}) (Elbaz-Poulichet et al., 2020).

Although significantly lower (p < 0.001) than values reported for Brandes, Pb concentrations in individuals from HU and LG were higher than those observed for urban medieval towns in Denmark (Rasmussen et al., 2015), Sardinia (Bocca et al., 2018), and Tuscany (Bianchi et al., 2017). Pb levels in HU and LG individual, however, were comparable to levels observed in the medieval urban harbor of Svendborg in Denmark (Rasmussen et al., 2017), where high Pb levels were associated with Pb exposure through the widespread use of Pb-glazed ceramics by the urban population. In the region of Oisans, individuals from Huez and La Garde were possibly exposed to Pb to some extent, considering that Pb was ubiquitous in medieval times, as Rasmussen et al. (2015) proposed a medieval Pb background level for cortical bone of 5 µg.g^{-1}.

Unlike human remains, animal bones from Brandes were recovered from dumping grounds that included not only domestic waste but also slag and other wastes from the mining activity. The exceptionally high values observed here can thus be explained by post-mortem incorporation due to contact with metal-rich mine wastes. While diagenesis typically does not cause visible macroscopic alterations on the bone (Booth et al., 2022), the diagenetic perturbation in this case was so intense that some of the animal bones turned green (Figure S1 Annex 3), likely due to the presence of copper phosphates within the bone matrix (Franchet, 1933; Reiche et al., 2000), as previously observed in animal bones excavated from a medieval Cu workshop (Müller et al., 2011).

Elevated metal concentrations of metals in osteoarcheological records are often related to i) mining exposure (Grattan et al., 2005; Pyatt et al., 2005), ii) growing up and living in medieval urban contexts (Boldsen et al., 2024; Rasmussen et al., 2017, 2020, 2015), iii) use of cosmetics and medicines (Alexandrovskaya and Alexandrovskiy, 2005;

Rasmussen et al., 2008), and iv) diagenesis (Güner et al., 2011). Since Brandes was a community exclusively dedicated to the extraction and refinement of argentiferous galena, the high background pollution levels documented by Elbaz-Poulichet et al. (2020) and those observed in the bones of Brandes' inhabitants can be attributed to either mining pollution or diagenetic alteration.

4.3.2. Assessment of bone diagenesis

4.3.2.1. Femur vs phalange

The comparaison of elemental concentration between femur and phalange shows that femur from Brandes had lower polymetallic levels compared to those of the phalanges for Pb (median ± SD, Pb_{fem} = 152 ± 148 µg.g^{-1}, Pb_{pha} = 526 ± 612 µg.g^{-1}), As (median ± SD, As_{fem} = 10 ± 9 µg.g^{-1}, As_{pha} = 16 ± 16 µg.g^{-1}), and Cd (median ± SD, Cd_{fem} = 0.4 ± 0.9 µg.g^{-1}, Cd_{pha} = 2 ± 4 µg.g^{-1}, Fig 4.3, top panel). This was also the case for the bio-essential proxies Fe (median ± SD, Fe_{fem} = 30 ± 70 µg.g^{-1}, Fe_{pha} = 80 ± 168 µg.g^{-1}), Cu (median ± SD, Cu_{fem} = 54 ± 95 µg.g^{-1}, Cu_{pha} = 136 ± 115 µg.g^{-1}), and Zn (median ± SD, Zn_{fem} = 170 ± 157 µg.g^{-1}, Zn_{pha} = 188 ± 375 µg.g^{-1}, Fig 4.3, bottom panel). This difference was significant for Pb ($p < 0.001$), Cd ($p < 0.001$), Fe ($p = 0.002$), and Cu ($p = 0.008$), but also for Al ($p = 0.002$) and Sr ($p = 0.02$) (Table S2, Annex 3). The same pattern (i.e., low femur vs. high phalange concentrations) was also observed for the control sites (i.e., HU and LG, dashed lines, Fig. 4.3), except for Pb (median ± SD, Pb_{fem} = 39 ± 24 µg.g^{-1}, Pb_{pha} = 19 ± 13 µg.g^{-1}). This is consistent with previous studies, which reported that diagenesis affects bones differently depending on their type, with long bones being less susceptible to diagenetic alteration than flat or small ones (Lambert et al., 1982; López-Costas et al., 2016). Such difference is related to the thickness and the proportion of the

cortical bone in relation to the total bone mass, which is higher in long bones (Fuchs et al., 2009).

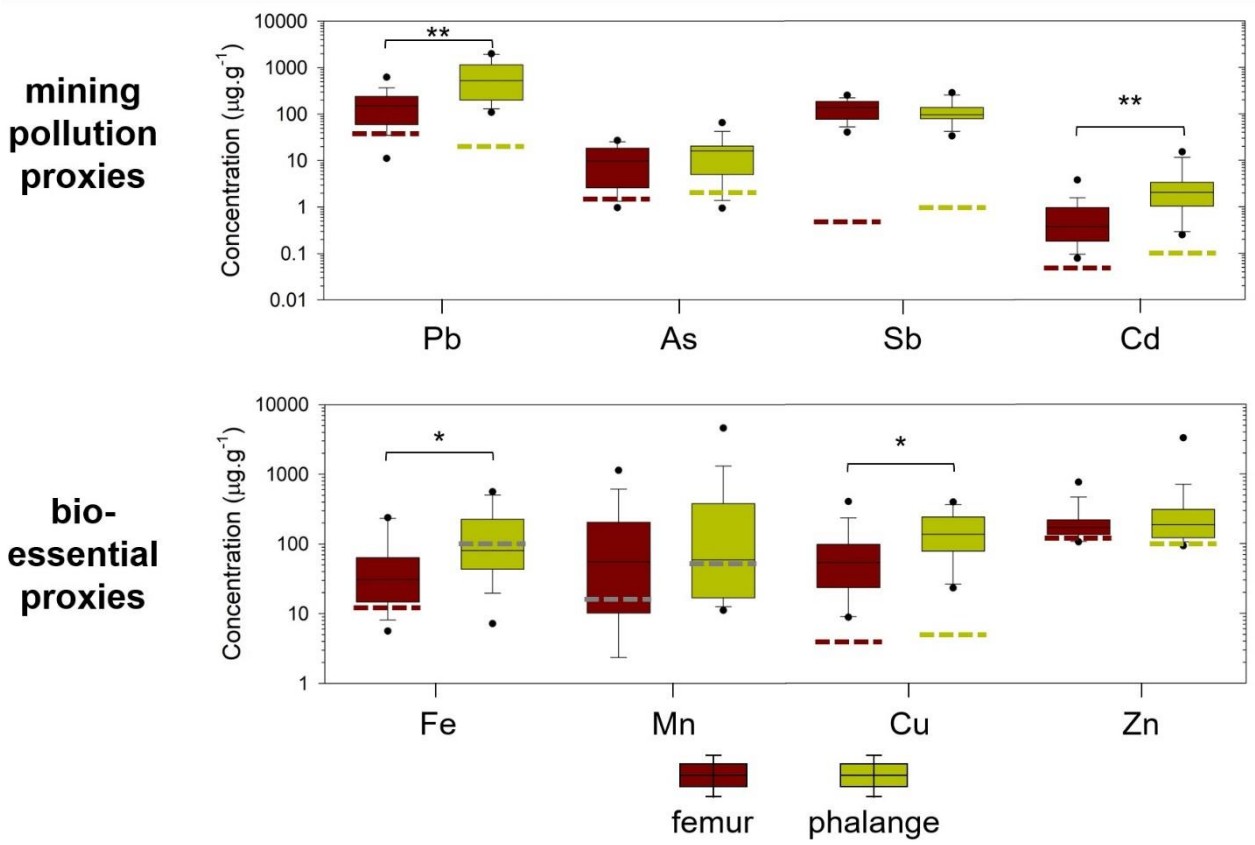

Figure 4.3. *Hair-and-whisker box plots of the measured concentrations of mining (top panel) and bio-essential proxies (bottom panel) in bones of Brandes. Boxplot color corresponds to the femur (red) and green (phalange). Each box represents the 25th–75th percentiles (with the median as a bold horizontal line), and the whiskers show the 10th–90th percentiles. Dashed lines correspond to the median values of the femur (red) and phalange (green) for the control sites (Huez and La Garde). A significant difference between the two data sets is indicated by * ($p < 0.05$) and ** ($p < 0.001$).*

This is due to the greater thickness and higher proportion of cortical bone in long bones Hence, the differences in concentrations observed at Brandes and the control sites between femur and phalanges suggest that the latter were more susceptible to diagenetic incorporation. The opposite trend observed for Pb at the control sites (HU and LG) suggests that other factors, such as the use and consumption of Pb containing cosmetics or medicines , may have played a role (Alexandrovskaya and Alexandrovskiy, 2005; Rasmussen et al., 2008), but also to an elevated Pb background at that time.

4.3.2.2. Sr/Ca and Ba/Ca

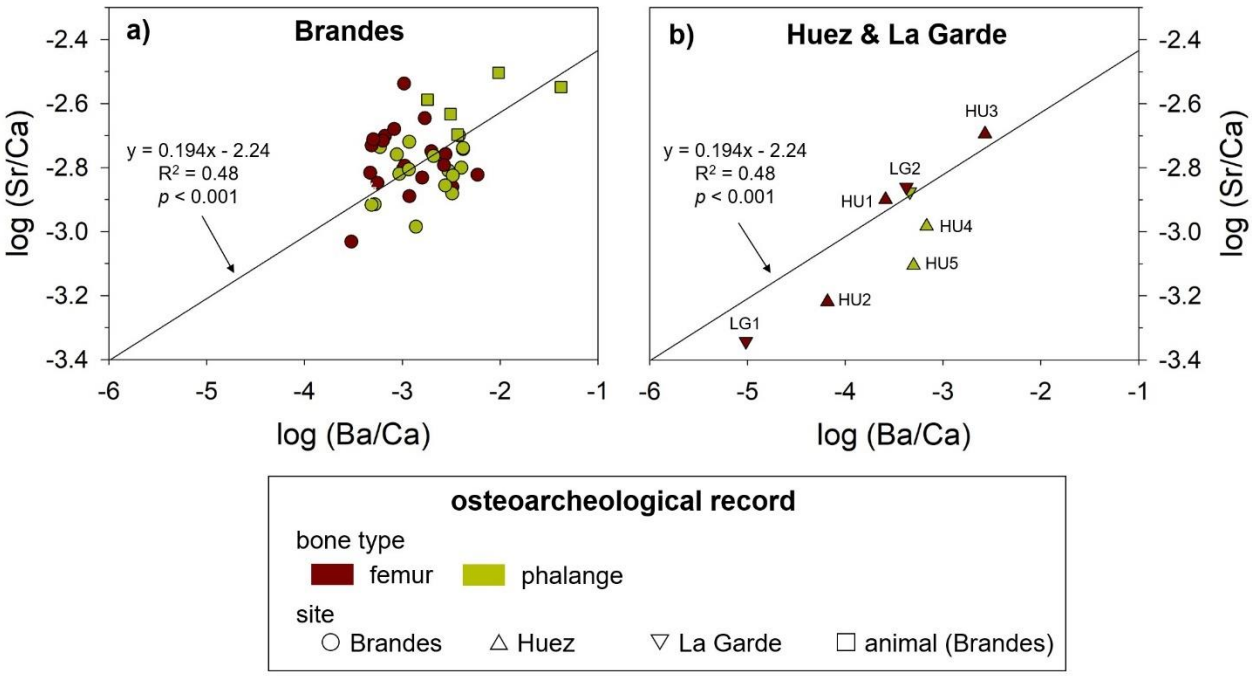

Figure 4.4. *Bivariate plot of log (Sr/Ca) and log (Ba/Ca) ratios from a) Brandes (human = circles, animal = squares) and b) control sites i.e., La Garde (down triangles) and Huez (top triangles) retrieved from the cortical bone of femur (red) and phalanges (green). The regression and equation for the Ca bio purification line (marked with an arrow) were calculated for the entire dataset.*

The Sr/Ca and Ba/Ca ratios were significantly correlated ($p < 0.001$, $R^2 = 0.5$, Fig. 4.4) when considering the entire datasets, i.e., Brandes, control sites and animals. The Sr/Ca and Ba/Ca ratios for bones of Brandes were lower than those of animals (Fig. 4.4a) but higher than those of the control sites (Fig. 4.4b and Table S5, Annex 3), and also exhibited a higher dispersion with respect to the Ca bio-purification line, independently of the type of bone.

Previous studies reported that a significant correlation between Sr/Ca and Ba/Ca indicates the absence of diagenetic alteration, reflecting intact pre-mortem values (Bocca et al., 2018; Burton et al., 1999; Heredia et al., 2024)] because it is assumed that if diagenesis should alter the bone concentrations towards equilibrium with the soil, thus preventing both ratios from remaining correlated (Burton et al., 1999). In the case of Brande,

although polymetallic contamination is evident, this type of proxy is probably not relevant for assessing diagenesis because the carbonate-free geological context limits potential Sr and Ba substitutions in bones. On the other hand, the Sr/Ca and Ba/Ca ratios tend to increase with a decreasing degree of histomorphological preservation (Fabig and Herrmann, 2002), which, in turn, is correlatedto higher diagenetic perturbation (Trueman and Tuross, 2002). In this sense, the Sr/Ca and Ba/Ca ratios suggest that the animal bones of Brandes were the most affected by diagenesis, while those from LG1 and HU2 were not. The rest of the bones from Huez and La Garde (i.e., HU1, HU3, HU4, HU5, and LG2) exhibit different degrees of diagenetic incorporation comparable to that observed in Brandes (Fig. 4.4). However, caution should be taken when interpreting mammalian bone ratios because Sr/Ca and Ba/Ca are also related to diet, i.e., they increase with decreasing trophic position due to Ca bio purification along the food chain (Burton et al., 1999; Elias et al., 1982). The miners of Brandes had a good social status and a diet rich in animal protein (i.e., carnivores) due to well-managed breeding practices (Bailly-Maître et al., 2008). Since the animal bone samples analyzed in this study come from cattle (i.e., herbivores), higher Sr/Ca and Ba/Ca ratios are expected in animals compared to humans, regardless of any diagenetic alteration.

Unexpected scattering of Sr/Ca and Ba/Ca from the Ca bio-purification line was also proposed as an indicator of the influence of diagenetic perturbation in bones (Reynard and Balter, 2014). In this sense, the bones of Brandes exhibit a variable degree of diagenetic incorporation, which is not related to the type of bone (Fig. 4.4a). For the control sites, Sr/Ca and Ba/Ca ratios suggest that HU1, HU3, and LG2 were unaffected by diagenesis, whereas LG1, HU2, and the rest of the phalanges (HU4 and HU5) were affected (Fig. 4.4b), contradicting the previous approach.

Finally, the use of Sr/Ca and Ba/Ca ratios provided contradictory interpretations for Brandes and the control sites of Huez and La Garde, showing their limitations in identifying post-mortem contamination in skeletal remains in such mining context.

4.3.2.3.Cu isotopes

The average $\delta^{65}Cu$ values in bones of Brandes, Huez, and La Garde are 0.01 ± 0.12 ‰, -0.09 ± 0.12, and -0.23 ± 0.04 ‰, respectively (Table S4). In the bones of Brandes, femur showed higher $\delta^{65}Cu$ values compared to phalange ($\delta^{65}Cu_{femur}$ = 0.07 ± 0.09 ‰, and $\delta^{65}Cu_{phalange}$ = -0.03 ± 0.12 ‰, respectively, Fig. 4.5 and Table S4). The $\delta^{65}Cu$ and Cu concentration in femur of Brandes were significantly correlated (R^2 = 0.7, p = 0.02, red dashed line, Fig. 4.5).

Overall, the $\delta^{65}Cu$ of Brandes are comparatively higher than values reported for human bones of Saint Laurent in Grenoble [i.e., -0.15 ± 0.1 ‰, grey band, Fig. 4.5, (Jaouen et al., 2012)], which can be considered as a control group because these individuals lived in an urban context, with access to diverse food sources and away from any mining or metallurgical activites (Herrscher et al., 2001). A deterioration in the state of health was associated with a decrease in the $\delta^{65}Cu$ (Kazi Tani et al., 2021; Télouk et al., 2015b; Toubhans et al., 2020).

This was observed for Roman individuals exposed to Pb in the ancient city of Vienne (Heredia et al., 2024). However, positive $\delta^{65}Cu$ values in human bones or tooth enamel (i.e., higher than 1 ‰) have not been reported to date (Jaouen et al., 2017).

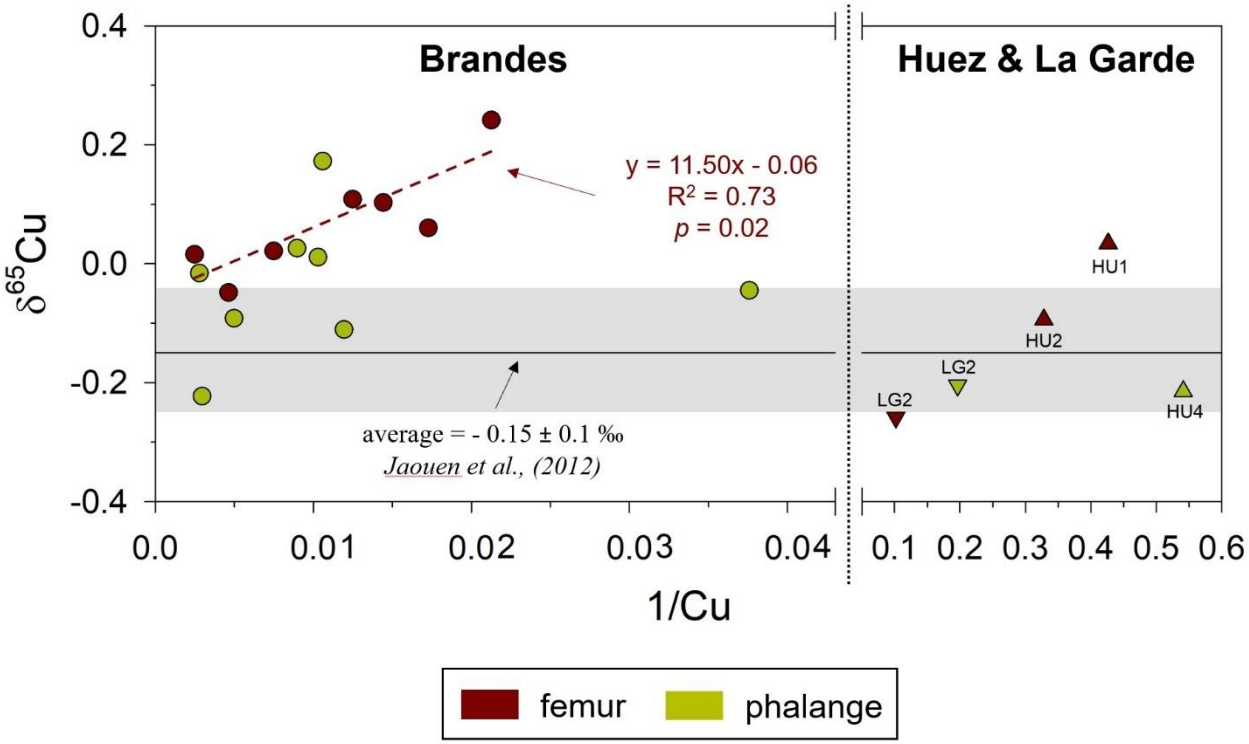

Figure 4.5. *Relationship between the Cu concentration and the isotopic composition ($\delta^{65}Cu$) of human cortical bone of phalanges (green) and femur (red) from Brandes (circles) and control sites i.e., La Garde (down triangles) and Huez (top triangles). The average $\delta^{65}Cu$ and SD of reference for a healthy population are indicated by a grey horizontal band and were taken from Jaouen et al.* (2012) .

The correlation between 1/Cu and Cu isotopic composition observed in femurs highlights diagenetic alteration of Cu (Reynard and Balter, 2014), which results from external Cu addition from soil into the bone that produce a correlation (or mixing line) between concentrations and isotopic compositions (Albarède, 1996). Accordingly, positive $\delta^{65}Cu$ values (0.27 to 5 ‰) are characteristic of Cu- rich ores like chalcopyrite and azurite (Maréchal et al., 1999). Hence, both the concentrations and Cu isotope composition found in femur of Brandes demonstrate post-mortem incorporation of Cu from soil. Altogether, these Cu data shows limitation in using $\delta^{65}Cu$ to infer a degradation in the health status of the individuals in such mining context, as bones from Brandes were altered by diagenesis, independently of bone type (femur or phalange). Although the data is limited for the control sites, results indicate that bones from Huez and La Garde were, to a lesser extent, affected by diagenetic alteration. Although Lander et al. (2023) showed that intra-

cortical bone is the best candidate for paleoenvironmental studies despite high histological degradation, our results suggest that this is not always the case, especially at sites like Brandes, where the geochemical background is very high as a result of historical pollution due to mining activities.

4.4. Conclusion and perspectives

The analysis of human bones from the medieval miners' community of Brandes has revealed significant polymetallic contamination, with markedly higher concentrations of lead (Pb), arsenic (As), antimony (Sb), and copper (Cu) compared to the non-related mining control sites of Huez and La Garde. These elevated concentrations in the bones are linked to both environmental exposure during the inhabitants' lifetimes and post-mortem diagenetic processes that have further altered the bones' elemental composition. While both femur and phalanges from Brandes exhibited significant diagenetic alteration, femurs were less affected compared to phalanges. However, it is not possible to elucidate the extent of diagenetic contribution to the biogenic composition in bones. The assessment of diagenetic alterations using multi-elemental and isotopic ratios (i.e., Sr/Ca, Ba/Ca, δ^{65}Cu) revealed complex, element-specific diagenetic interactions. In particular, the use of Sr/Ca and Ba/Ca ratios showed limitations when interpreting bioarchaeological data affected by diagenesis, particularly at highly contaminated sites like Brandes, with elevated geochemical background. The analysis of the δ^{65}Cu indicated diagenetic incorporation of Cu into the bone, and isotope mixing between the biogenic δ^{65}Cu with the one of the surrounding necrosoil. Further studies focusing on necrosol properties, burial contexts, and dietary habits, including the use of Pb and Cu in everyday utensils, are essential to better constrain the diagenetic influences and improve archaeological interpretations.

Acknowledgments

This study benefited from the financial support from ISTerre and the EC2CO of CNRS. It was performed using the INSU/CNRS MC-ICP-MS national facility at ENS-LYON. The authors would like to thank the Museum of Huez and Oisans and Marie Christine Bailly-Maître, curator of the museum's archaeological collection. This work was conducted with the support of the LABEX IMU (ANR-10-LABX-0088) of the University of Lyon, within the framework of the "Investissements d'Avenir" program managed by the Agence Nationale de la Recherche (ANR).

Authors contributions:

Carlos Heredia, Alexandra T. Gourlan, Sylvain Campillo, Sabine Sentenac, and Liliam Hammann made the data analysis. Alexandra T. Gourlan and Stéphane Guédron contributed to the study's conception and design. Data collection was made thanks to Marie Christine Bailly-Maître. Carlos Heredia, Alexandra T. Gourlan, and Stéphane Guédron contributed to the drafting of the manuscript, and in addition, Marie Christine Bailly-Maître helped with the critical interpretation of data. The authors read, amended, and approved the final manuscript.

References

Albarède, F., 2015. Metal Stable Isotopes in the Human Body: A Tribute of Geochemistry to Medicine. Elements 11, 265–269. https://doi.org/10.2113/gselements.11.4.265

Albarède, F., 1995. Introduction to Geochemical Modeling. Cambridge University Press, Cambridge. https://doi.org/10.1017/CBO9780511622960

Alexandrovskaya, E., Alexandrovskiy, A., 2005. Radiocarbon data and anthropochemistry of ancient Moscow. Geochronometria - Journal on Methods and Applications of Absolute Chronology 24, 87–95.

Bailly-Maître, M.-C., 2008. Une Aventure minière : Huez et l'argent au moyen âge, L'argenteria de brandis. Musée d'Huez.

Bailly-Maître, M.-C., 2006. Fortifications ou structures de contrôle ? Les reliefs aménagés du massif de l'Oisans. Presented at the Château Gaillard : études de castellologie médiévale. 22, Château et peuplement : actes du colloque international de Voiron, Isère, France, 28 août-4 septembre 2004, CRAHAM, France, p. 13.

Bailly-Maître, M.-C., 1996. Brandes-en-Oisans : incidences d'un milieu alpin sur une exploitation minière médiévale. Actes des congrès de la Société d'Archéologie Médiévale 5, 235–245.

Bailly-Maître, M.-C., 1992. Garde (La) (Isère). Église du prieuré. Archéologie médiévale 22, 449–449.

Bailly-Maitre, M.C., 1991. La Garde – Église Saint-Pierre. ADLFI. Archéologie de la France - Informations.

Bailly-Maître, M.-C., Martin, L.E., Herrscher, E., Hervieu, P., 2008. Se nourrir en haute montagne aux XIIIe et XIVe Siècles. Le village de Brandes (Huez-Isère) : apports comparés de l'archéologie, des textes, de l'archéobotanique et de l'anthropologie. Histoire des Alpes 13, 83.

Balter, V., Zazzo, A., 2014. Bone and enamel diagenesis: From the crystal to the environment — A tribute to Jean-François Saliège. Palaeogeography, Palaeoclimatology, Palaeoecology, Bone and enamel diagenesis: From the crystal to the environment - A tribute to Jean-François Saliège 416, 1–3. https://doi.org/10.1016/j.palaeo.2014.09.017

Baranowska, I., Czernicki, K., Aleksandrowicz, R., 1995. The analysis of lead, cadmium, zinc, copper and nickel content in human bones from the Upper Silesian industrial district. Science of The Total Environment 159, 155–162. https://doi.org/10.1016/0048-9697(95)04218-P

Barbosa, F., Tanus-Santos, J.E., Gerlach, R.F., Parsons, P.J., 2005. A critical review of biomarkers used for monitoring human exposure to lead: advantages, limitations, and future needs. Environ Health Perspect 113, 1669–1674. https://doi.org/10.1289/ehp.7917

Bianchi, N., Moroni, A., Bonucci, S., Capecchi, J., Ancora, S., Ricci, S., Loenzio, C., 2017. Trace Elements in Eneolithic and Late Medieval Human Bones from Two Archaeological Sites in Tuscany: Evaluation of Diagenetic Processes, Diet and Exposure to Heavy Metals. Journal of Anthropology and Archaeology 5, 31–43. https://doi.org/10.15640/jaa.v5n2a3

Bocca, B., Forte, G., Giuffra, V., Serra, R.M., Asara, Y., Farace, C., Milanese, M., Tognotti, E., Montella, A., Bandiera, P., Madeddu, R., 2018. Metals in bones of the middle-aged inhabitants of Sardinia island (Italy) to assess nutrition and

environmental exposure. Environ Sci Pollut Res 25, 8404–8414. https://doi.org/10.1007/s11356-017-1140-6

Boldsen, J.L., Pedersen, D.D., Milner, G.R., Kristensen, V.R.L., Skytte, L., Møller, S.B., Sarauw, T.B., Andersen, C.B.H., Larsen, L.A., Hyldgaard, I.M., Klingenberg, M., Larsen, L.K., Mollerup, L., Seeberg, L., Bentsen, L.C., Søvsø, M., Kristensen, T., Christensen, J.T., Heide, P.B., Nørgaard, L.C., Uldum, O., Engberg, N., Simonsen, R., Dahlstrøm, H., Langkilde, J., Wickman, N., Hansen, P.B., Wille-Jørgensen, D., Stjernqvist, K.W., Rasmussen, A., Rasmussen, K.L., 2024. Variation in bioavailable lead, copper, and strontium concentrations in human skeletons from medieval to early modern Denmark. Journal of Anthropological Archaeology 74, 101587. https://doi.org/10.1016/j.jaa.2024.101587

Booth, T.J., Brönnimann, D., Madgwick, R., Portmann, C., 2022. The Taphonomic and Archaeothanatological Potentials of Diagenetic Alterations of Archaeological Bone, in: The Routledge Handbook of Archaeothanatology. Routledge.

Budd, P., Montgomery, J., Barreiro, B., Thomas, R.G., 2000. Differential diagenesis of strontium in archaeological human dental tissues. Applied Geochemistry 15, 687–694. https://doi.org/10.1016/S0883-2927(99)00069-4

Burton, J.H., Price, T.D., Middleton, W.D., 1999. Correlation of Bone Ba/Ca and Sr/Ca due to Biological Purification of Calcium. Journal of Archaeological Science 26, 609–616. https://doi.org/10.1006/jasc.1998.0378

Colardelle, M., Mazard, C., Bailly-Maître, M.-C., Bois, M., Dupraz, J., Carbonnières, P. de, Sirot, É., 1979. Premiers résultats des recherches sur les « mottes » médiévales en Dauphiné et en Savoie. Archéologie médiévale 9, 65–95. https://doi.org/10.3406/arcme.1979.1352

Dupraz, J., Bailly-Maître, M.-C., 1981. Huez (Isère). Chapelle Saint-Ferréol. Archéologie médiévale 11, 281–281.

Elbaz-Poulichet, F., Guédron, S., Anne-Lise, D., Freydier, R., Perrot, V., Rossi, M., Piot, C., Delpoux, S., Sabatier, P., 2020. A 10,000-year record of trace metal and metalloid (Cu, Hg, Sb, Pb) deposition in a western Alpine lake (Lake Robert, France): Deciphering local and regional mining contamination. Quaternary Science Reviews 228, 106076. https://doi.org/10.1016/j.quascirev.2019.106076

Elias, R.W., Hirao, Y., Patterson, C.C., 1982. The circumvention of the natural biopurification of calcium along nutrient pathways by atmospheric inputs of industrial lead. Geochimica et Cosmochimica Acta 46, 2561–2580. https://doi.org/10.1016/0016-7037(82)90378-7

Ericson, J.E., Shirahata, H., Patterson, C.C., 1979. Skeletal Concentrations of Lead in Ancient Peruvians. New England Journal of Medicine 300, 946–951. https://doi.org/10.1056/NEJM197904263001703

Ericson, J.E., Smith, D.R., Flegal, A.R., 1991. Skeletal concentrations of lead, cadmium, zinc, and silver in ancient North American Pecos Indians. Environmental Health Perspectives 93, 217–223. https://doi.org/10.1289/ehp.9193217

Fabig, A., Herrmann, B., 2002. Trace elements in buried human bones: intra-population variability of Sr/Ca and Ba/Ca ratios – diet or diagenesis? Naturwissenschaften 89, 115–119. https://doi.org/10.1007/s00114-001-0294-7

Franchet, L., 1933. La coloration des os dans le sol : le bouillage des cadavres au Moyen-âge, l'incinération et ses phénomènes. Editions de la Revue politique et littéraire (Revue bleue) et de la Revue scientifique, Paris.

Fuchs, R.K., Warden, S.J., Turner, C.H., 2009. 2 - Bone anatomy, physiology and adaptation to mechanical loading, in: Planell, J.A., Best, S.M., Lacroix, D., Merolli, A. (Eds.), Bone Repair Biomaterials, Woodhead Publishing Series in

Biomaterials. Woodhead Publishing, pp. 25–68. https://doi.org/10.1533/9781845696610.1.25

Giffin, K.L., Swanston, T., Coulthard, I., Murphy, A.R., Cooper, D.M.L., Varney, T.L., 2017. Skeletal Lead Burden of the British Royal Navy in Colonial Antigua. International Journal of Osteoarchaeology 27, 672–682. https://doi.org/10.1002/oa.2589

Grattan, J., Huxley, S., Karaki, L.A., Toland, H., Gilbertson, D., Pyatt, B., al Saad, Z., 2002. 'Death... more desirable than life'? The human skeletal record and toxicological implications of ancient copper mining and smelting in Wadi Faynan, southwestern Jordan. Toxicol Ind Health 18, 297–307. https://doi.org/10.1191/0748233702th153oa

Grattan, J., Karaki, L.A., Hine, D., Toland, H., Gilbertson, D., Al-Saad, Z., Pyatt, B., 2005. Analyses of patterns of copper and lead mineralization in human skeletons excavated from an ancient mining and smelting centre in the Jordanian desert: a reconnaissance study. Mineralogical Magazine 69, 653–666. https://doi.org/10.1180/0026461056950277

Güner, C., Aliyev, V., Atamtürk, D., Duyar, İ., Söylemezoğlu, T., 2011. Retention of Zn, Cu, Cd, Pb, and As on human bones unearthed at a Central Anatolian Early Bronze Age excavation site (Resuloğlu, Turkey). Euras J Anthropol 2, 27–39.

Hedges, R.E.M., Stevens, R.E., Richards, Michael.P., 2004. Bone as a stable isotope archive for local climatic information. Quaternary Science Reviews, Isotopes in Quaternary Paleoenvironmental reconstruction 23, 959–965. https://doi.org/10.1016/j.quascirev.2003.06.022

Herrscher, E., Bocherens, H., Valentin, F., Colardelle, R., 2001. Comportements alimentaires au Moyen Âge à Grenoble : application de la biogéochimie isotopique à la nécropole Saint-Laurent (XIIIe–XVe siècles, Isère, France). Comptes Rendus de l'Académie des Sciences - Series III - Sciences de la Vie 324, 479–487. https://doi.org/10.1016/S0764-4469(01)01316-6

Jaouen, K., Balter, V., Herrscher, E., Lamboux, A., Telouk, P., Albarède, F., 2012. Fe and Cu stable isotopes in archeological human bones and their relationship to sex. American Journal of Physical Anthropology 148, 334–340. https://doi.org/10.1002/ajpa.22053

Jaouen, K., Herrscher, E., Balter, V., 2017. Copper and zinc isotope ratios in human bone and enamel. American Journal of Physical Anthropology 162, 491–500. https://doi.org/10.1002/ajpa.23132

Jaouen, K., Richards, M.P., Le Cabec, A., Welker, F., Rendu, W., Hublin, J.-J., Soressi, M., Talamo, S., 2019. Exceptionally high δ15N values in collagen single amino acids confirm Neandertals as high-trophic level carnivores. Proceedings of the National Academy of Sciences 116, 4928–4933. https://doi.org/10.1073/pnas.1814087116

Kamenov, G.D., Lofaro, E.M., Goad, G., Krigbaum, J., 2018. Trace elements in modern and archaeological human teeth: Implications for human metal exposure and enamel diagenetic changes. Journal of Archaeological Science 99, 27–34. https://doi.org/10.1016/j.jas.2018.09.002

Kazi Tani, L.S., Gourlan, A.T., Dennouni-Medjati, N., Telouk, P., Dali-Sahi, M., Harek, Y., Sun, Q., Hackler, J., Belhadj, M., Schomburg, L., Charlet, L., 2021. Copper Isotopes and Copper to Zinc Ratio as Possible Biomarkers for Thyroid Cancer. Front Med (Lausanne) 8, 698167. https://doi.org/10.3389/fmed.2021.698167

Keinonen, M., 1992. The isotopic composition of lead in man and the environment in Finland 1966–1987: isotope ratios of lead as indicators of pollutant source.

Science of The Total Environment 113, 251–268. https://doi.org/10.1016/0048-9697(92)90004-C

Knudson, K.J., Price, T.D., 2007. Utility of multiple chemical techniques in archaeological residential mobility studies: Case studies from Tiwanaku- and Chiribaya-affiliated sites in the Andes. American Journal of Physical Anthropology 132, 25–39. https://doi.org/10.1002/ajpa.20480

Kuitems, M., van der Plicht, J., Drucker, D.G., Van Kolfschoten, T., Palstra, S.W.L., Bocherens, H., 2015. Carbon and nitrogen stable isotopes of well-preserved Middle Pleistocene bone collagen from Schöningen (Germany) and their paleoecological implications. Journal of Human Evolution, Special Issue: Excavations at Schöningen: New Insights into Middle Pleistocene Lifeways in Northern Europe 89, 105–113. https://doi.org/10.1016/j.jhevol.2015.01.008

Lambert, J.B., Vlasak, S.M., Thometz, A.C., Buikstra, J.E., 1982. A comparative study of the chemical analysis of ribs and femurs in woodland populations. American Journal of Physical Anthropology 59, 289–294. https://doi.org/10.1002/ajpa.1330590308

Lambert, J.B., Xue, L., Buikstra, J.E., 1991. Inorganic analysis of excavated human bone after surface removal. Journal of Archaeological Science 18, 363–383. https://doi.org/10.1016/0305-4403(91)90072-W

Lander, S.L., Hosie, M., Brits, D., 2023. The Diagenetic Alterations of Historic Skeletons from the Crown Mines Cemetery, South Africa. Biology 12, 378. https://doi.org/10.3390/biology12030378

Lindh, U., Brune, D., Nordberg, G., Wester, P.O., 1981. Levels of cadmium in bone tissue (femur) of industrially exposed workers - A reply. Science of The Total Environment 20, 3–11. https://doi.org/10.1016/0048-9697(81)90031-0

Lindh, U., Brune, D., Nordberg, G., Wester, P.-O., 1980. Levels of antimony, arsenic, cadmium, copper, lead, mercury, selenium, silver, tin and zinc in bone tissue of industrially exposed workers. Science of The Total Environment 16, 109–116. https://doi.org/10.1016/0048-9697(80)90018-2

López-Costas, O., Kylander, M., Mattielli, N., Álvarez-Fernández, N., Pérez-Rodríguez, M., Mighall, T., Bindler, R., Martínez Cortizas, A., 2020. Human bones tell the story of atmospheric mercury and lead exposure at the edge of Roman World. Science of The Total Environment 710, 136319. https://doi.org/10.1016/j.scitotenv.2019.136319

López-Costas, O., Lantes-Suárez, Ó., Martínez Cortizas, A., 2016. Chemical compositional changes in archaeological human bones due to diagenesis: Type of bone vs soil environment. Journal of Archaeological Science 67, 43–51. https://doi.org/10.1016/j.jas.2016.02.001

Maréchal, C., Albarède, F., 2002. Ion-exchange fractionation of copper and zinc isotopes. Geochimica et Cosmochimica Acta 66, 1499–1509. https://doi.org/10.1016/S0016-7037(01)00815-8

Maréchal, C.N., Télouk, P., Albarède, F., 1999. Precise analysis of copper and zinc isotopic compositions by plasma-source mass spectrometry. Chemical Geology 156, 251–273. https://doi.org/10.1016/S0009-2541(98)00191-0

Martínez-García, M.J., Moreno, J.M., Moreno-Clavel, J., Vergara, N., García-Sánchez, A., Guillamón, A., Portí, M., Moreno-Grau, S., 2005. Heavy metals in human bones in different historical epochs. Science of The Total Environment 348, 51–72. https://doi.org/10.1016/j.scitotenv.2004.12.075

Maurer, A.-F., Barrulas, P., Person, A., Mirão, J., Barrocas Dias, C., Boudouma, O., Segalen, L., 2019. Testing LA-ICP-MS analysis of archaeological bones with

different diagenetic histories for paleodiet prospect. Palaeogeography, Palaeoclimatology, Palaeoecology 534, 109287. https://doi.org/10.1016/j.palaeo.2019.109287

Maurer, A.-F., Salesse, K., 2023. Diagenesis in Progress, Progress in Diagenesis – The Skeletal Archives. Quaternary International, Diagenesis in Progress, Progress in Diagenesis – The Skeletal Archives 660, 1–3. https://doi.org/10.1016/j.quaint.2023.05.004

Millard, A., 2006. Comment on Martínez-García et al. "Heavy metals in human bones in different historical epochs." Science of The Total Environment 354, 295–297. https://doi.org/10.1016/j.scitotenv.2005.11.010

Morgan, W.D., Ryde, S.J.S., Jones, S.J., Wyatt, R.M., Hainsworth, I.R., Cobbold, S.S., Evans, C.J., Braithwaite, R.A., 1990. In vivo measurements of cadmium and lead in occupationally-exposed workers and an urban population. Biol Trace Elem Res 26, 407–414. https://doi.org/10.1007/BF02992695

Müller, K., Chadefaux, C., Thomas, N., Reiche, I., 2011. Microbial attack of archaeological bones versus high concentrations of heavy metals in the burial environment. A case study of animal bones from a mediaeval copper workshop in Paris. Palaeogeography, Palaeoclimatology, Palaeoecology, Special Issue: Fossil bones and teeth: preservation or alteration of biogenic compositions? 310, 39–51. https://doi.org/10.1016/j.palaeo.2011.03.023

Nanci, A. (Ed.), 2013. Chapter 6 - Bone, in: Ten Cate's Oral Histology (Eighth Edition). Mosby, St. Louis (MO), pp. 95–121. https://doi.org/10.1016/B978-0-323-07846-7.00006-9

Oakberg, K., Levy, T., Smith, P., 2000. A Method for Skeletal Arsenic Analysis, Applied to the Chalcolithic Copper Smelting Site of Shiqmim, Israel. Journal of Archaeological Science 27, 895–901. https://doi.org/10.1006/jasc.1999.0505

Parfitt, A.M., 2013. Chapter 36 - Skeletal Heterogeneity and the Purposes of Bone Remodeling: Implications for the Understanding of Osteoporosis, in: Marcus, R., Feldman, D., Dempster, D.W., Luckey, M., Cauley, J.A. (Eds.), Osteoporosis (Fourth Edition). Academic Press, San Diego, pp. 855–872. https://doi.org/10.1016/B978-0-12-415853-5.00036-4

Peloux, F., Bailly-Maître, M.-C., Viallet, H., 2015. L'histoire si curieuse des mines de Brandes. Presses Universitaires de Grenoble, Grenoble.

Pike, A.W.G., Richards, M.P., 2002. Diagenetic Arsenic Uptake in Archaeological Bone. Can we Really Identify Copper Smelters? Journal of Archaeological Science 29, 607–611. https://doi.org/10.1006/jasc.2001.0754

Price, T.D., Blitz, J., Burton, J., Ezzo, J.A., 1992. Diagenesis in prehistoric bone: Problems and solutions. Journal of Archaeological Science 19, 513–529. https://doi.org/10.1016/0305-4403(92)90026-Y

Pyatt, F.B., Pyatt, A.J., Walker, C., Sheen, T., Grattan, J.P., 2005. The heavy metal content of skeletons from an ancient metalliferous polluted area in southern Jordan with particular reference to bioaccumulation and human health. Ecotoxicology and Environmental Safety 60, 295–300. https://doi.org/10.1016/j.ecoenv.2004.05.002

Rasmussen, K., Skytte, L., D'imporzano, P., Orla Thomsen, P., Søvsø, M., Lier Boldsen, J., 2017. On the distribution of trace element concentrations in multiple bone elements in 10 Danish medieval and post-medieval individuals. Am J Phys Anthropol 162, 90–102. https://doi.org/10.1002/ajpa.23099

Rasmussen, K.L., Boldsen, J.L., Kristensen, H.K., Skytte, L., Hansen, K.L., Mølholm, L., Grootes, P.M., Nadeau, M.-J., Flöche Eriksen, K.M., 2008. Mercury levels in

Danish Medieval human bones. Journal of Archaeological Science 35, 2295–2306. https://doi.org/10.1016/j.jas.2008.03.003

Rasmussen, K.L., Milner, G., Skytte, L., Lynnerup, N., Thomsen, J.L., Boldsen, J.L., 2019. Mapping diagenesis in archaeological human bones. Heritage Science 7, 41. https://doi.org/10.1186/s40494-019-0285-7

Rasmussen, K.L., Milner, G.R., Delbey, T., Skytte, L., Søvsø, M., Callesen, F., Boldsen, J.L., 2020. Copper exposure in medieval and post-medieval Denmark and northern Germany: its relationship to residence location and social position. Heritage Science 8, 18. https://doi.org/10.1186/s40494-020-00365-4

Rasmussen, K.L., Skytte, L., Jensen, A.J., Boldsen, J.L., 2015. Comparison of mercury and lead levels in the bones of rural and urban populations in Southern Denmark and Northern Germany during the Middle Ages. Journal of Archaeological Science: Reports 3, 358–370. https://doi.org/10.1016/j.jasrep.2015.06.021

Reiche, I., Vignaud, C., Menu, M., 2000. Heat induced transformation of fossil mastodon ivory into turquoise 'odontolite'. Structural and elemental characterisation. Solid State Sciences 2, 625–636. https://doi.org/10.1016/S1293-2558(00)01067-0

Reynard, B., Balter, V., 2014. Trace elements and their isotopes in bones and teeth: Diet, environments, diagenesis, and dating of archeological and paleontological samples. Palaeogeography, Palaeoclimatology, Palaeoecology, Bone and enamel diagenesis: From the crystal to the environment - A tribute to Jean-François Saliège 416, 4–16. https://doi.org/10.1016/j.palaeo.2014.07.038

Simpson, R., Cooper, D.M.L., Swanston, T., Coulthard, I., Varney, T.L., 2021. Historical overview and new directions in bioarchaeological trace element analysis: a review. Archaeol Anthropol Sci 13, 24. https://doi.org/10.1007/s12520-020-01262-4

Télouk, P., Puisieux, A., Fujii, T., Balter, V., Bondanese, V.P., Morel, A.-P., Clapisson, G., Lamboux, A., Albarede, F., 2015. Copper isotope effect in serum of cancer patients. A pilot study. Metallomics 7, 299–308. https://doi.org/10.1039/c4mt00269e

Toubhans, B., Gourlan, A.T., Telouk, P., Lutchman-Singh, K., Francis, L.W., Conlan, R.S., Margarit, L., Gonzalez, D., Charlet, L., 2020. Cu isotope ratios are meaningful in ovarian cancer diagnosis. Journal of Trace Elements in Medicine and Biology 62, 126611. https://doi.org/10.1016/j.jtemb.2020.126611

Trueman, C.N., Tuross, N., 2002. Trace Elements in Recent and Fossil Bone Apatite. Reviews in Mineralogy and Geochemistry 48, 489–521. https://doi.org/10.2138/rmg.2002.48.13

Tütken, T., Vennemann, T.W., 2011. Fossil bones and teeth: Preservation or alteration of biogenic compositions? Palaeogeography, Palaeoclimatology, Palaeoecology, Special Issue: Fossil bones and teeth: preservation or alteration of biogenic compositions? 310, 1–8. https://doi.org/10.1016/j.palaeo.2011.06.020

Wooller, M.J., Bataille, C., Druckenmiller, P., Erickson, G.M., Groves, P., Haubenstock, N., Howe, T., Irrgeher, J., Mann, D., Moon, K., Potter, B.A., Prohaska, T., Rasic, J., Reuther, J., Shapiro, B., Spaleta, K.J., Willis, A.D., 2021. Lifetime mobility of an Arctic woolly mammoth. Science 373, 806–808. https://doi.org/10.1126/science.abg1134

Chapter 5: Conclusions and Perspectives

5.1. PhD contribution

This work was set up to increase the understanding of the sources and pathways of human exposure related to mining and metallurgical pollution in historical times through the study of archaeological human remains. For this purpose, a combination of multi-elemental and multi-isotopic approaches was used to address the following questions:

- What is the source of Pb used for the manufacturing of Gallo-Roman artifacts in Vienna?
- What was the extent of Pb contamination and the route of exposure related to metallurgical activity at Vienna?
- Is it possible to detect a degraded state of health associated with mining/metallurgical pollution?
- What is the effect of diagenesis in highly contaminated archaeological settings? Are bones still reliable archives for investigating health status?

To answer these questions, we studied archaeological human remains from a Roman capital (Vienna) and a medieval alpine town (Brandes). We used a multi-element and multi-isotopic approach, including lead (Pb) and copper (Cu) stable isotope compositions, trace elements content, and elemental ratios (e.g., Sr/Ca, Ba/Ca). In addition to this, we also used, in the case of Vienna, a new algorithm (Albarede et al. 2024a) and the latest database of ores Pb isotopes to assign the provenance of Pb. This chapter concludes this research by summarizing the main findings and briefly discussing the implications and limitations of this study.

5.2. Answering scientific questions

The source of Pb for the manufacturing of artifacts and pipes at Vienna was of distant origin. The Pb isotopic composition of artifacts suggests that the most probable origin is the Rhenish massif (Hercynian). The contribution of local and regional mines is secondary in supplying Pb to Vienna. However, contributions coming from Roman Britain cannot be excluded entirely.

Human exposure in Vienna is related to the production and use of Pb artifacts. The Pb isotopic composition of bones is similar to those of artifacts, especially pipes. The lack of correlation between age or sex with the heavy metal content indicates that pollution was widespread throughout the city, meaning an equal and consistent exposition of the population to both Pb and Hg. However, the distinction between the routes of exposure (i.e., inhalation vs ingestion) cannot be conclusively determined.

We report for the first time the use of Cu isotope ratios in ancient human remains to explore potential physiological consequences. The Cu isotopic composition of bones exhibited a negative shift compared to a control population, suggesting the deterioration of health linked to Pb exposure from fabrication and use of this metal.

The assessment of diagenesis in highly contaminated sites revealed complex, site-specific, and element-specific interactions. Diagenetic incorporation of Cu from the necrosol into the bone masks the biogenic δ^{65}Cu signal, preventing any interpretation of an individual's state of health. The conventional approach of using single diagenetic proxies can be biased. Therefore, it is essential to evaluate diagenesis using multiple proxies in conjunction with the characterization of the burial context.

5.3. Perspectives

5.3.1. Amount of samples and characterization of the burial context

This study was performed entirely on human bones retrieved from archived archaeological collections. While cooperation with museum curators of archaeological collections allows access to a variety of documented and available bones and skeletons, the number of samples, their characterization (i.e., origin, sex, age, burial conditions), the representativity of individuals within the population, and the bone type can quickly become a limiting factor. Therefore, it is recommended, when possible, to address, from the beginning, a multidisciplinary approach with archaeologists and/or anthropologists to determine the sampling and bone collection campaign properly, including access to archaeological reports, historical archives, and any information about the historical context (i.e., diet, social status) of the studied individuals. This approach can provide the most relevant elements to evaluate factors such as diagenesis and characteristics during the life of individuals that may affect the reconstruction of past environments.

5.3.2. The need of a control group (reference values)

This work focused on studying archaeological sites framed in mining environments. In this context, it is essential to have a control group that can provide reference values to which we can compare our studied individuals. However, this is not always easy due to the complexity of finding historically relevant analogs of the studied populations (i.e., similar time period, location, context, healthy individuals). Future research should focus on this issue by studying rural populations preferentially from the same period (so that background levels can be determined and compared). For the case of Vienna and Brandes, research should focus on small towns that were not involved in mining or metallurgy and were not exposed to regular use of Pb pipes or metallic utensils. This will also require a

combined approach between archaeologists and geochemists to investigate archeological sites with these specific characteristics. In the present state, there is no reference population for ancient periods such as Medieval or Roman times. Nor is there a consensus on the "normal" values obtained from modern individuals who have highly variable elemental concentrations.

5.3.3. Combining isotopic tracers

In the case of Vienna, we identified the source of Pb supply for artifact production, and observed a generalized exposure of Pb by the population. However, we were not able to discriminate between the pathways of Pb incorporation in humans (inhalation vs. ingestion). Future research should study the combination of other isotopic tracers (Ag, Sn, Sb) with the ones used here that could bring new dimensions to better discriminate and refine the identification of sources and pathways of exposure.

Additionally, while a health status degradation has been shown here with the use of Cu isotopes, the causes and consequences of such degradation have not yet been elucidated. Future research should focus on this issue by integrating the historical context (i.e., diet, social status) and the osteo-pathological characterization of the studied population.

5.3.4. Evaluating diagenesis

Here, we observed that diagenetic alterations in human bones are site-specific, even bone-specific, and there is no universally accepted methodology to access diagenesis. Therefore, it is first recommended that future studies on buried bones systematically evaluate diagenesis by developing a case-specific methodology for each site (i.e., combining physical anthropology and chemical proxies) before attempting any paleoenvironmental reconstructions. Second, we recommend sampling the soil surrounding the exhumated bones (i.e., the necrosoil) to better constrain the diagenetic

incorporation. Future research should also focus on studying the interactions between soil pore water and bones, especially the reactivity and isotope fractionation of elements such as Cu and Zn.

5.3.5. Final conclusion

This work has contributed, with its multi-isotopic approach, to show that the isotopic tracers applied on archaeological remains are powerful tools to identify i) sources of metal supply, ii) sources and pathways of human exposure to Pb, and iii) degraded state of health of ancient populations exposed to metallurgy. However, this approach is limited by diagenesis.

ANNEXES

Annex 1: Provenance of lead ores used for water pipes production in the ancient Roman Gaul (Vienne, France)

Annex 2: Copper and lead isotopes composition of ancient Roman human bones reveal health degradation due to lead poisoning (Vienne, France)

Annex 3: Human bones from a medieval alpine miners' cemetery reveal post-mortem polymetallic contamination (Brandes, France)

Annex 4: Lead and mercury mining pollution over the last 2500 years in Europe: deciphering the contribution of Central and Eastern regions from western ones

Annex 5: Anthropogenic eutrophication of Lake Titicaca (Bolivia) revealed by carbon and nitrogen stable isotopes fingerprinting

Annex 1:

Supplementary information for the research article entitled:

Provenance of lead ores used for water pipes production in the ancient Roman Gaul (Vienne, France)

Table S1. Summary of the analytical data of this study for the Roman artifacts.

Material	Location	Sample ID	Datation (CE)	$^{206}Pb/^{204}Pb$	$^{207}Pb/^{204}Pb$	$^{208}Pb/^{204}Pb$	$^{207}Pb/^{206}Pb$	$^{208}Pb/^{206}Pb$	$^{204}Pb/^{206}Pb$	T_{mod} (MA)	μ	κ	Sn ($\mu g.g^{-1}$)
pipe	SC	Pipe 1	1st - 2nd	18.415	15.641	38.446	0.849	2.088	0.05430	273.56	9.77	3.92	33.6
pipe	SC	Pipe 2	1st - 2nd	18.406	15.640	38.423	0.850	2.088	0.05433	277.84	9.77	3.92	4.5
pipe	SC	Pipe 3	1st - 2nd	18.413	15.638	38.427	0.849	2.087	0.05431	268.97	9.76	3.91	6.8
pipe	SC	Pipe 4	2nd	18.410	15.639	38.441	0.850	2.088	0.05432	273.39	9.76	3.92	4.0
pipe	SC	Pipe 5	2nd	18.425	15.646	38.484	0.849	2.089	0.05427	275.78	9.79	3.94	11.7
pipe	SC	Pipe 6	2nd	18.429	15.645	38.475	0.849	2.088	0.05426	270.47	9.78	3.93	19.4
pipe	SC	Pipe 7	2nd	18.416	15.641	38.450	0.849	2.088	0.05430	272.10	9.77	3.93	1.26
pipe	SRG	Pipe 8	2nd	18.416	15.642	38.450	0.849	2.088	0.05430	274.91	9.77	3.93	8.71
pipe	SRG	Pipe 9	2nd	18.418	15.641	38.450	0.849	2.088	0.05429	270.35	9.77	3.92	16.9
pipe	SRG	Pipe 10	1st	18.423	15.643	38.454	0.849	2.087	0.05428	271.07	9.78	3.92	11.9
pipe	VI	Pipe 11	1st	18.420	15.641	38.447	0.849	2.087	0.05429	269.88	9.77	3.92	8.40
pipe	VI	Pipe 12	1st	18.416	15.642	38.458	0.849	2.088	0.05430	274.22	9.77	3.93	22.6
pipe	VI	Pipe 13	1st	18.387	15.655	38.597	0.851	2.099	0.05439	320.98	9.83	4.03	7.42
pierced roof	VI	Roof	2nd	18.567	15.665	38.642	0.844	2.081	0.05386	206.95	9.83	3.94	*n.a.*
valve	VI	Valve	2nd	18.418	15.643	38.454	0.849	2.088	0.05430	274.64	9.78	3.93	*n.a.*
situla	VI	Bucket	1st - 2nd	18.415	15.641	38.448	0.849	2.088	0.05430	274.47	9.77	3.93	*n.a.*
water tank	VI	Water tank	1st - 2nd	18.414	15.641	38.444	0.849	2.088	0.05431	273.05	9.77	3.92	*n.a.*
foundry	VI	Foundry res.	1st - 2nd	18.415	15.640	38.446	0.849	2.088	0.05431	272.33	9.77	3.92	*n.a.*
pipe	LY	Pipe 14	--	18.416	15.642	38.450	0.849	2.088	0.05430	274.42	9.77	3.93	*n.a.*
pipe	LY	Pipe 15	--	18.415	15.636	38.433	0.849	2.087	0.05430	263.73	9.75	3.92	*n.a.*
pipe	LY	Pipe 16	2nd - 3rd	18.414	15.638	38.440	0.849	2.088	0.05431	268.67	9.76	3.92	*n.a.*
sarco-phagus	SC	Sarcophagus	4th	18.421	15.646	38.462	0.849	2.088	0.05429	278.22	9.79	3.93	*n.a.*

SC = Saint-Colombe; SRG = Saint-Roman-en-Gal ; VI = Vienne ; LY = Lyon. n.a. : not analyzed

Table S2. Summary of the analytical data of this study for the borehole samples drilled at Vienne (Forum).

Location	Sample ID	Datation	Depth (m)	$^{206}Pb/^{204}Pb$	$^{207}Pb/^{204}Pb$	$^{208}Pb/^{204}Pb$	$^{207}Pb/^{206}Pb$	$^{208}Pb/^{206}Pb$	$^{204}Pb/^{206}Pb$	T_{mod} (MA)	μ	κ	Pb ($\mu g.g^{-1}$)
SC1	SC1-E	Post-Roman $^{+++}$	1.9	18.406	15.647	38.494	0.850	2.091	0.05433	291.46	9.7960	3.9582	266
SC1	SC1-F	Post-Roman $^{++}$	3.2	18.445	15.644	38.509	0.848	2.088	0.05421	257.15	9.7758	3.9387	165
SC1	SC1-G	Roman**	4.3	18.660	15.670	38.720	0.840	2.075	0.05359	147.80	9.8320	3.9164	114
SC1	SC1-I	Roman**	6.2	18.516	15.661	38.615	0.846	2.086	0.05401	237.35	9.8272	3.9534	97
SC1	SC1-J	Roman**	7.2	18.642	15.661	38.625	0.840	2.072	0.05364	143.60	9.8006	3.8768	46.0
SC1	SC1-K	Pre-Roman*	7.8	18.759	15.662	38.744	0.835	2.065	0.05331	57.73	9.7808	3.8630	23.9
SC4	SC4-M	Post-Roman $^{++}$	4.0	18.437	15.629	38.439	0.848	2.085	0.05424	233.91	9.7168	3.9021	308
SC4	SC4-H	Post-Roman $^{++}$	4.9	18.463	15.655	38.548	0.848	2.088	0.05416	264.23	9.8136	3.9517	60.8
SC4	SC4-N	Post-Roman^{+}	5.3	18.431	15.642	38.476	0.849	2.088	0.05426	264.02	9.7715	3.9299	233
SC4	SC4-O	Roman**	6.0	18.492	15.652	38.561	0.846	2.085	0.05408	236.71	9.7953	3.9375	893
SC4	SC4-P	Roman**	6.6	18.645	15.677	38.905	0.841	2.087	0.05363	171.55	9.8607	4.0234	188
SC4	SC4-Q	Pre-Roman*	7.2	18.824	15.678	38.903	0.833	2.067	0.05312	41.52	9.8307	3.9068	19.3
SC4	SC4-R	Pre-Roman*	7.9	18.752	15.675	38.824	0.836	2.070	0.05333	89.77	9.8340	3.9123	41.0

**: Iron Age; **: High Empire; $^{+}$: Late Antiquity; $^{++}$: Early Middle Ages; $^{+++}$: Early Modern*

Table S2 (Extended). Summary of the elemental composition of the borehole samples drilled at Vienne (Forum).

Sample ID	SC1-E +++	SC1-F ++	SC1-G **	SC1-I **	SC1-J **	SC1-K *	SC4-M ++	SC4-H ++	SC4-N +	SC4-O **	SC4-P **	SC4-Q *	SC4-R *
Li ($\mu g.g^{-1}$)	17.5	19.1	43.7	33.7	25.3	41.0	18.9	14.4	18.6	21.7	30.7	24.8	26.6
Mg ($mg.g^{-1}$)	4.5	3.6	6.1	6.0	4.9	4.8	4.4	2.5	4.8	4.8	5.3	4.8	4.4
Al ($mg.g^{-1}$)	37.4	39.1	56.5	52.4	48.9	53.2	37.2	21.8	41.1	43.7	49.3	40.7	38.9
K ($mg.g^{-1}$)	15.1	20.1	23.1	16.1	19.3	17.5	15.1	11.9	17.4	19.3	19.5	13.2	13.9
Ca ($mg.g^{-1}$)	8.9	8.0	10.5	8.0	6.7	5.1	10.3	7.4	9.7	7.3	6.1	5.1	6.3
Mg ($mg.g^{-1}$)	15.6	14.1	18.3	14.1	11.6	8.8	17.8	13.4	17.4	13.1	10.7	8.9	10.6
Sc ($\mu g.g^{-1}$)	5.6	5.0	8.6	9.1	6.5	8.7	5.7	2.7	6.1	6.0	8.0	7.0	6.5
Ti ($mg.g^{-1}$)	1.4	1.3	2.1	2.1	1.7	1.5	1.9	1.1	1.6	1.7	2.2	2.3	2.1
V ($\mu g.g^{-1}$)	36.3	28.1	38.7	59.1	39.2	58.0	36.4	26.2	37.4	36.7	50.5	49.7	43.1
Cr ($\mu g.g^{-1}$)	40.2	33.3	49.0	55.4	43.6	59.2	34.7	28.9	37.2	39.1	45.0	44.7	53.5
Mn ($mg.g^{-1}$)	1.4	1.2	0.6	0.9	0.8	0.6	2.0	0.6	1.4	1.1	0.9	1.3	0.9
Fe ($mg.g^{-1}$)	42.5	17.8	23.1	25.6	20.8	19.6	17.0	19.0	18.3	25.8	22.9	20.5	20.0

Table S2 (Extended, continued). Summary of the elemental composition of the borehole samples drilled at Vienne (Forum).

Sample ID	SC1-E +++	SC1-F ++	SC1-G **	SC1-I **	SC1-J **	SC1-K *	SC4-M ++	SC4-H ++	SC4-N +	SC4-O **	SC4-P **	SC4-Q *	SC4-R *
Co ($\mu g.g^{-1}$)	11.4	8.5	8.9	9.4	22.7	9.0	8.0	40.2	147.4	20.4	12.1	9.9	7.4
Ni ($\mu g.g^{-1}$)	44.7	24.2	23.7	31.9	30.1	32.3	29.7	34.2	27.2	58.6	29.7	28.9	25.6
Cu ($mg.g^{-1}$)	2.92	0.19	0.08	0.06	0.10	0.02	0.10	0.13	0.18	0.42	0.21	0.06	0.09
Zn ($mg.g^{-1}$)	0.2	0.2	2.5	0.2	0.3	0.1	0.2	0.2	0.2	0.3	0.1	0.1	0.3
Ge ($\mu g.g^{-1}$)	2.2	2.1	2.8	2.6	2.5	2.3	2.4	1.6	2.1	2.4	3.3	2.5	2.6
As ($\mu g.g^{-1}$)	24.3	13.4	17.0	19.4	14.1	14.2	12.8	6.1	9.3	13.3	32.2	15.3	15.8
Se ($\mu g.g^{-1}$)	0.2	0.0	0.2	0.1	0.1	0.0	0.3	0.0	0.3	0.1	0.1	0.1	0.1
Rb ($\mu g.g^{-1}$)	82.7	101.9	150.7	102.0	113.5	111.2	90.4	57.2	96.9	114.1	102.1	80.6	80.3
Sr ($mg.g^{-1}$)	0.3	0.2	0.2	0.2	0.2	0.2	0.3	0.3	0.2	0.2	0.2	0.2	0.2
Zr ($\mu g.g^{-1}$)	20.7	22.8	77.6	29.3	32.4	29.7	7.5	15.4	29.8	33.6	22.0	26.3	26.2
Nb ($\mu g.g^{-1}$)	4.5	4.9	11.4	7.2	6.5	5.5	6.6	3.7	3.3	6.2	7.4	6.5	8.4
Mo ($\mu g.g^{-1}$)	1.1	0.4	4.0	0.6	0.8	0.7	0.9	1.7	1.4	0.9	0.6	1.0	4.3

Table S2 (Extended, continued). Summary of the elemental composition of the borehole samples drilled at Vienne (Forum).

Sample ID	SC1-E +++	SC1-F ++	SC1-G **	SC1-I **	SC1-J **	SC1-K *	SC4-M ++	SC4-H ++	SC4-N +	SC4-O **	SC4-P **	SC4-Q *	SC4-R *
Ag ($\mu g.g^{-1}$)	5.6	2.8	2.4	1.6	5.1	0.3	5.4	10.8	17.4	7.6	16.7	3.0	2.9
Cd ($\mu g.g^{-1}$)	0.2	0.3	0.3	0.2	0.2	0.2	0.3	0.2	0.2	0.2	0.1	0.3	0.2
Sn ($\mu g.g^{-1}$)	72.8	14.0	8.8	5.4	6.2	2.3	13.9	4.5	11.2	14.7	20.0	7.5	10.3
Sb ($\mu g.g^{-1}$)	10.9	2.7	0.7	0.8	0.5	0.8	0.7	0.5	0.5	0.6	0.9	0.7	0.7
Nd ($\mu g.g^{-1}$)	12.2	15.4	25.4	20.1	16.9	16.2	21.2	9.8	13.7	17.0	24.4	18.6	17.8
Gd ($\mu g.g^{-1}$)	2.4	2.6	4.7	3.6	3.0	3.4	3.3	1.7	2.4	2.8	4.1	3.3	3.2
Hf ($\mu g.g^{-1}$)	0.6	0.7	2.3	0.9	0.9	0.8	0.2	0.4	0.8	1.0	0.6	0.7	0.8
W ($\mu g.g^{-1}$)	1.7	1.1	3.5	14.5	115.4	3.0	3.1	583.8	2194.7	116.4	14.7	8.1	9.3
Th ($\mu g.g^{-1}$)	4.2	5.7	14.4	6.8	6.1	5.5	10.1	3.6	5.3	7.2	8.2	6.1	5.5
U ($\mu g.g^{-1}$)	1.4	1.4	3.2	1.7	1.6	1.1	1.8	1.1	1.5	1.5	2.0	1.3	1.3

**: Iron Age; **: High Empire; $^{+}$: Late Antiquity; $^{++}$: Early Middle Ages; $^{+++}$: Early Modern*

Table S3. Summary of the analytical data of this study for local and regional Pb ores (Galena) samples analyzed in this study.

Location	Sample_ID	$^{206}Pb/^{204}Pb$	$^{207}Pb/^{204}Pb$	$^{208}Pb/^{204}Pb$	$^{207}Pb/^{206}Pb$	$^{208}Pb/^{206}Pb$	$^{204}Pb/^{206}Pb$	T_{mod} (MA)	μ	κ	Lat.	Lon.
ES	M1	18.610	15.686	38.710	0.843	2.080	0.05374	214.95	9.9033	3.9499	45.548367	4.852468
LP	M2	18.572	15.675	38.645	0.844	2.081	0.05385	222.66	9.8699	3.9372	45.490334	4.851110
LP	M4	18.562	15.675	38.639	0.845	2.082	0.05387	228.62	9.8693	3.9404	45.490334	4.851110
ES	M5	18.478	15.671	38.657	0.848	2.092	0.05412	283.55	9.8743	4.0039	45.548367	4.852468
LP	M7	18.586	15.667	38.650	0.843	2.080	0.05380	195.93	9.8335	3.9278	45.490334	4.851110
LP	M8	18.554	15.685	38.710	0.845	2.086	0.05390	253.64	9.9112	3.9861	45.490334	4.851110
LP	LP8	18.534	15.667	38.626	0.845	2.084	0.05395	233.99	9.8447	3.9490	45.490334	4.851110
LP	LP12	18.523	15.674	38.659	0.846	2.087	0.05399	256.51	9.8761	3.9762	45.490334	4.851110
BJ	M11	18.538	15.664	38.673	0.845	2.086	0.05394	226.98	9.8345	3.9704	46.200830	4.521390
BJ	B2	18.677	15.677	38.839	0.839	2.079	0.05354	147.57	9.8536	3.9682	46.200830	4.521390
BJ	B3	18.410	15.651	38.525	0.850	2.093	0.05432	296.81	9.8121	3.9737	46.186420	4.452840
SR	M9	18.415	15.680	38.612	0.852	2.097	0.05430	345.90	9.9237	4.0261	45.141773	4.828092
SR	S4	18.408	15.677	38.599	0.852	2.097	0.05432	344.85	9.9128	4.0227	45.141773	4.828092
SJMM	M6	18.570	15.674	38.688	0.844	2.083	0.05385	222.42	9.8668	3.9603	45.310988	4.660000
SJMM	M10	18.587	15.679	38.674	0.844	2.081	0.05380	218.55	9.8808	3.9436	45.309575	4.680817
SJMM	SJ4	18.600	15.667	38.652	0.842	2.078	0.05376	185.11	9.8301	3.9191	45.310988	4.660000
SJMM	SJ9	18.547	15.667	38.636	0.845	2.083	0.05392	225.94	9.8440	3.9460	45.310988	4.660000

Table S3 (continued). Summary of the analytical data of this study for local and regional Pb ores (Galena) samples analyzed in this study.

Location	Sample_ID	$^{206}Pb/^{204}Pb$	$^{207}Pb/^{204}Pb$	$^{208}Pb/^{204}Pb$	$^{207}Pb/^{206}Pb$	$^{208}Pb/^{206}Pb$	$^{204}Pb/^{206}Pb$	T_{mod} (MA)	μ	κ	Lat.	Lon.
SJMM	SJ11	18.555	15.664	38.669	0.844	2.084	0.05389	213.11	9.8284	3.9569	45.337659	4.627163
SJMM	SJ6	18.568	15.667	38.688	0.844	2.084	0.05386	209.02	9.8373	3.9586	45.341159	4.613361
SJMM	Mp1	18.538	15.675	38.659	0.846	2.086	0.05394	246.86	9.8765	3.9667	45.315769	4.665139
SJMM	SJ7	18.564	15.662	38.661	0.844	2.083	0.05387	202.91	9.8187	3.9461	45.356033	4.594482
SJMM	SJ8	18.590	15.665	38.640	0.843	2.079	0.05379	190.47	9.8276	3.9195	45.333111	4.699210
SJMM	SJ10	18.592	15.664	38.637	0.843	2.078	0.05379	185.56	9.8205	3.9160	45.308582	4.662758
VH	Ve1	18.410	15.678	38.683	0.852	2.101	0.05432	346.23	9.9177	4.0668	45.213024	4.207511
MSL	MS1	18.484	15.684	38.709	0.849	2.094	0.05410	303.95	9.9253	4.0321	45.276775	4.141367
SMLS	SM4	18.535	15.651	38.664	0.845	2.086	0.05395	202.86	9.7821	3.9624	45.875686	3.904969
SMLS	SM1	18.733	15.661	38.772	0.836	2.070	0.05338	74.58	9.7809	3.8925	45.865130	3.838527
SMLS	SM2	18.517	15.658	38.680	0.846	2.089	0.05401	230.25	9.8136	3.9858	45.844780	3.944021
VG	Va1	18.608	15.654	38.668	0.841	2.078	0.05374	155.27	9.7806	3.9181	45.745716	4.597834

ES = Estressin; LP = La Poype; BJ = Beaujolais; SJMM = Saint-Julien-Molin-Molette ; VH = Versilhac ; MSL = Monistrol-sur-Loire ; SMLS = Saint-Martin-La-Sauvauté; VG = Vaugneray

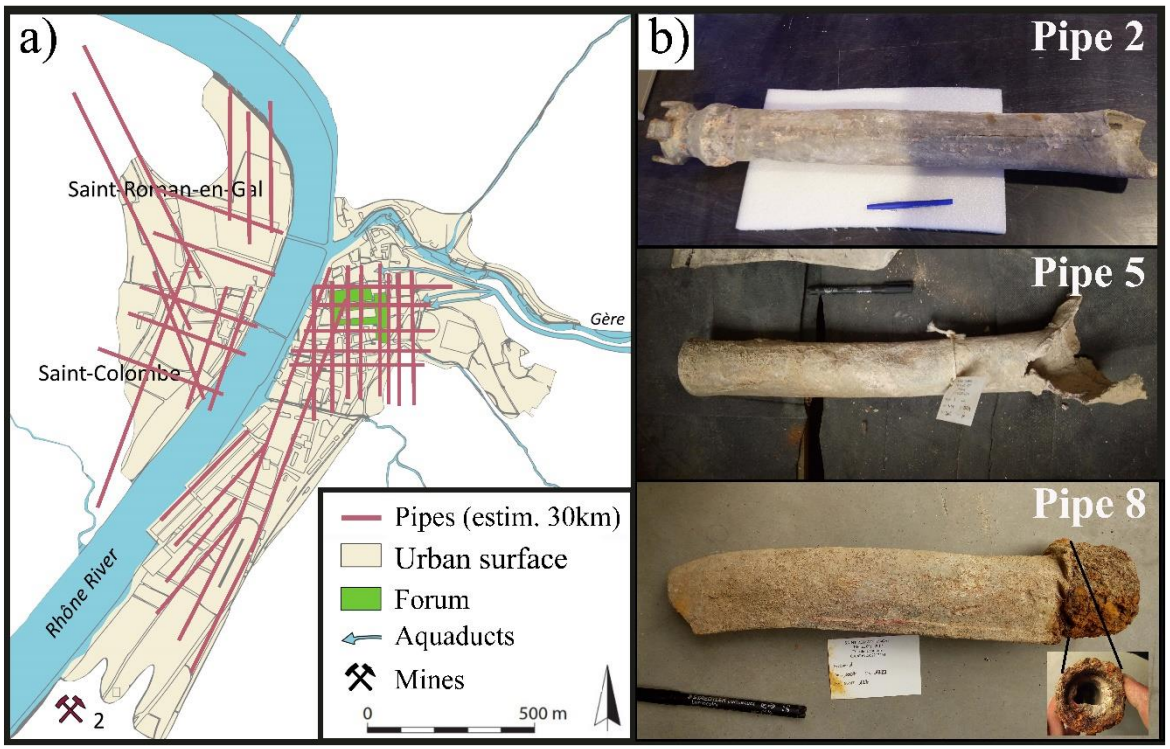

Figure S1. *a) Map of the ancient city of Vienne during the 1st century CE [adapted from (Adjajd and Lauxerois, 2014)] with location of the lead pipes network (red lines). Length estimation of the lead pipe network in Vienne is of 30 km (Helly, 2018). b) Photographs of sampled pipes number 2, 5, and 8. Pipe 8 average dimensions are one meter long, 8 cm of external average diameter, and 0.8 cm thickness, with a density of 11.3 g cm^{-3}. From these dimensions, the calculated lead volume for a one-meter pipe is expected to be 954.6 cm3, weighing around 10.8 kg. Hence, the total weight of lead used for 30km of lead water-pipe network in the city is estimated to be 323 tons.*

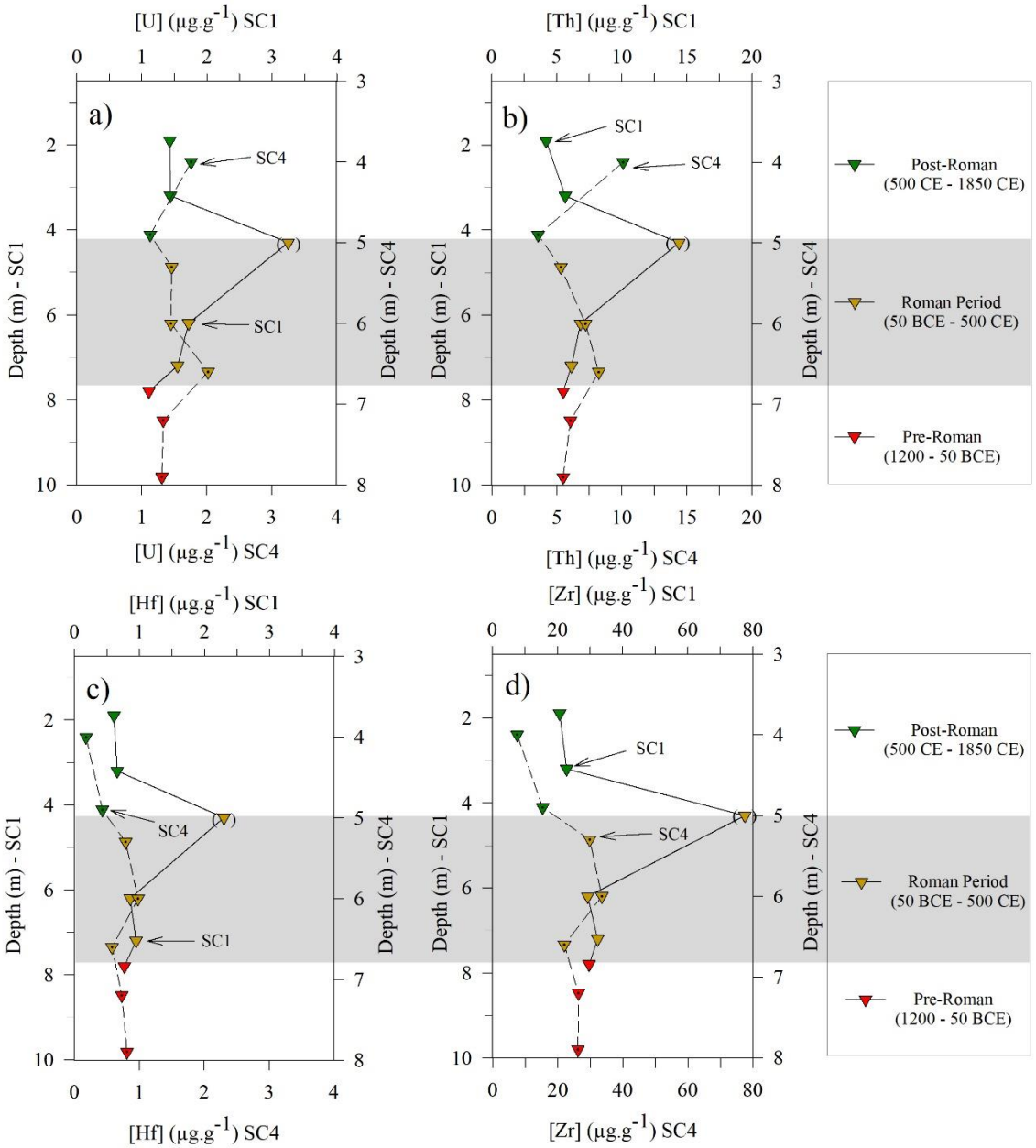

Figure S2. *Stratigraphic profile (down triangles) of a) uranium (U), b) thorium (Th) , c) hafnium (Hf), and d) zirconium (Zr) concentrations of boreholes SC1(straight line) and SC4 (dotted line) retrieved from Vienne's Forum. Scales between plots were adapted to match ages and periods. Symbol colors indicate their relative age obtained from ceramological dating of borehole layers by archeologists. Red colors refer to the pre-Roman period, dark yellow to the Roman Empire, and dark green to post-roman (i.e., Middle Age to Modern) periods. The sample in brackets for core SC1 (SC1-G, table S2) is considered an outlier due to a singular elemental composition characteristic of a backfill sample.*

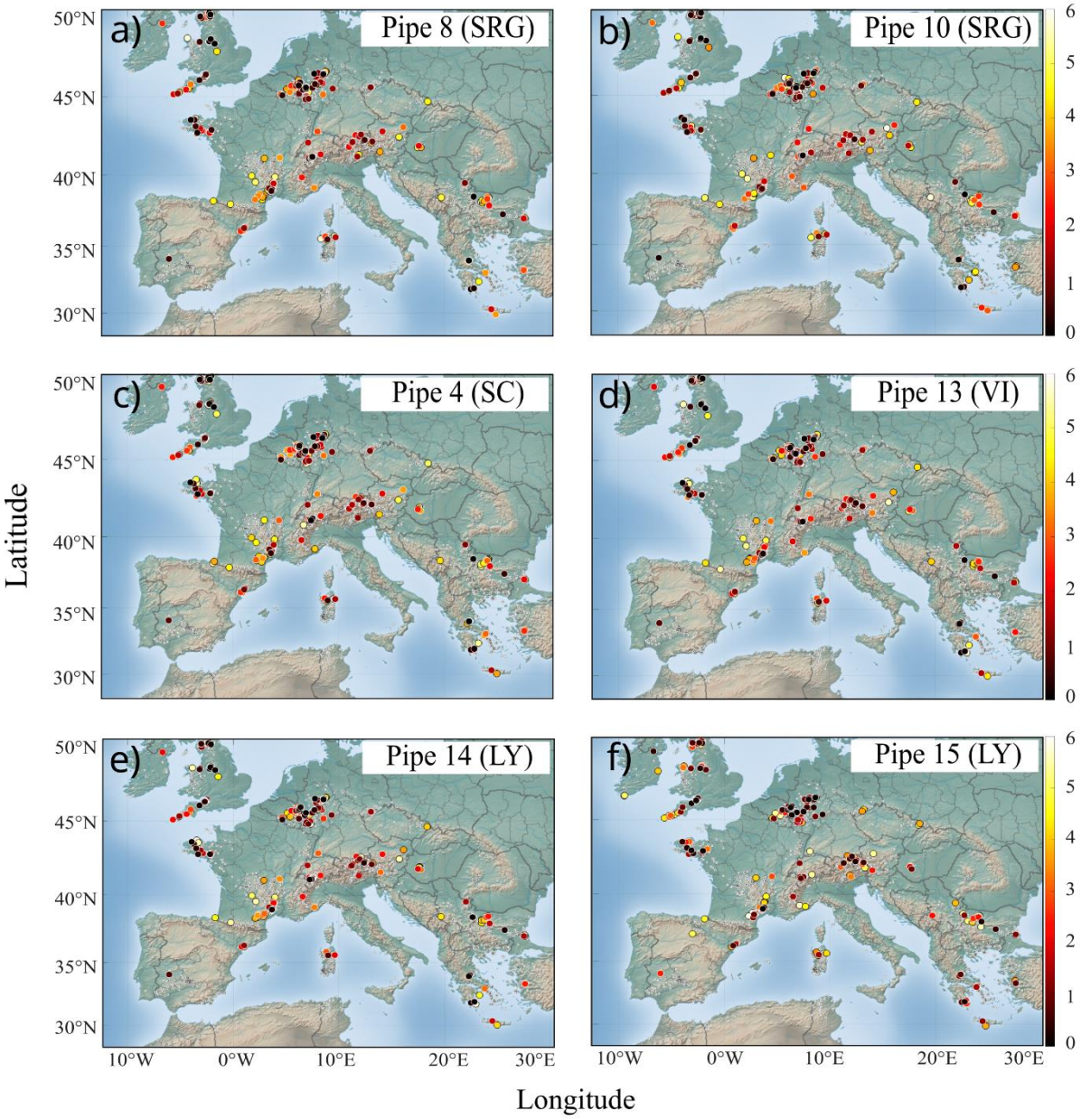
a)
Pipe 8 (SRG)
b)
Pipe 10 (SRG)
c)
Pipe 4 (SC)
d)
Pipe 13 (VI)
e)
Pipe 14 (LY)
f)
Pipe 15 (LY)
50°N
45°N
40°N
35°N
30°N
10°W
0°W
10°E
20°E
30°E
Latitude
Longitude
0
1
2
3
4
5
6

Figure S3. (1/3)

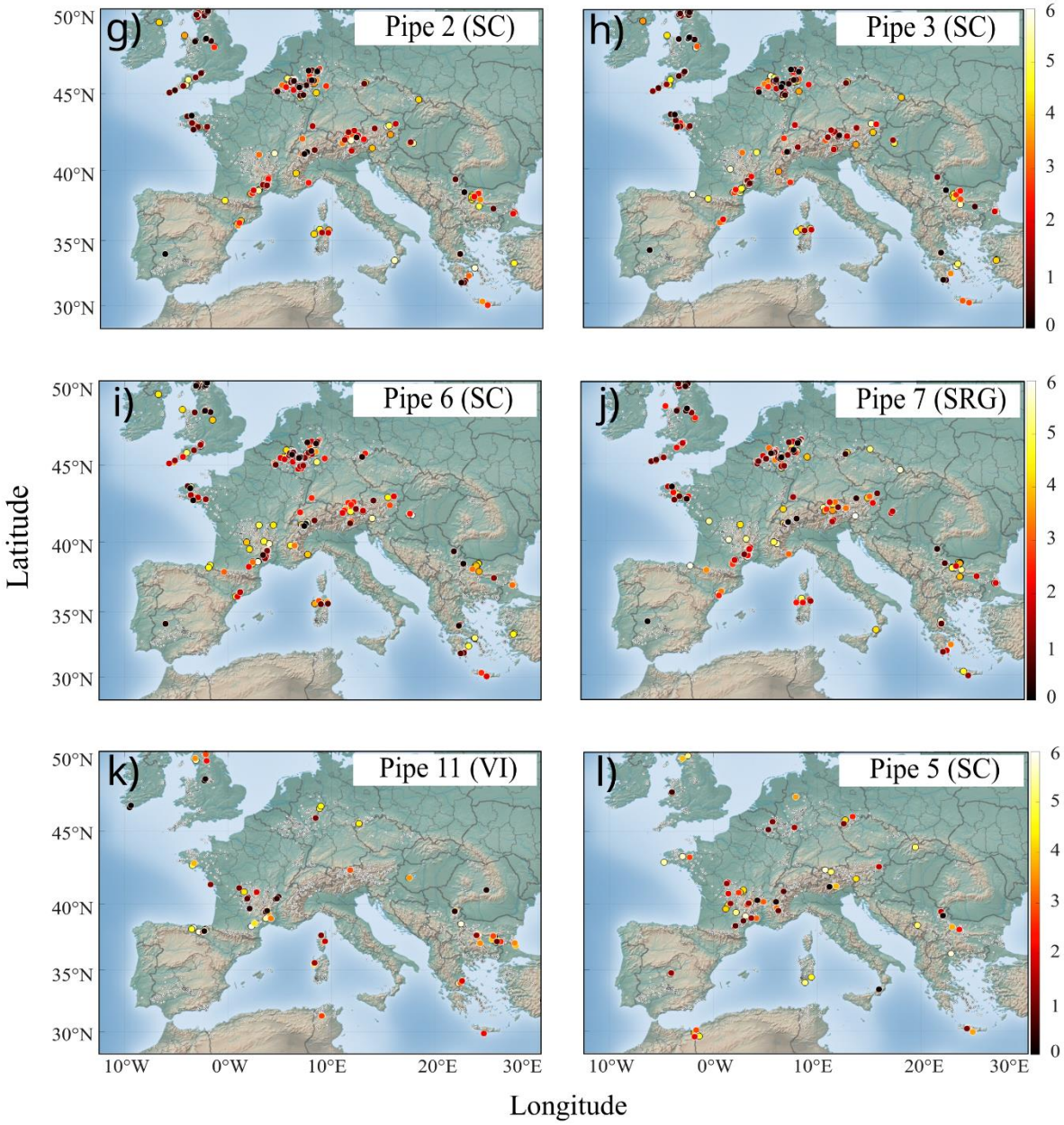
g)
Pipe 2 (SC)
h)
Pipe 3 (SC)
i)
Pipe 6 (SC)
j)
Pipe 7 (SRG)
k)
Pipe 11 (VI)
l)
Pipe 5 (SC)
50°N
45°N
40°N
35°N
30°N
10°W
0°W
10°E
20°E
30°E
0
1
2
3
4
5
6
Latitude
Longitude

Figure S3. (2/3)

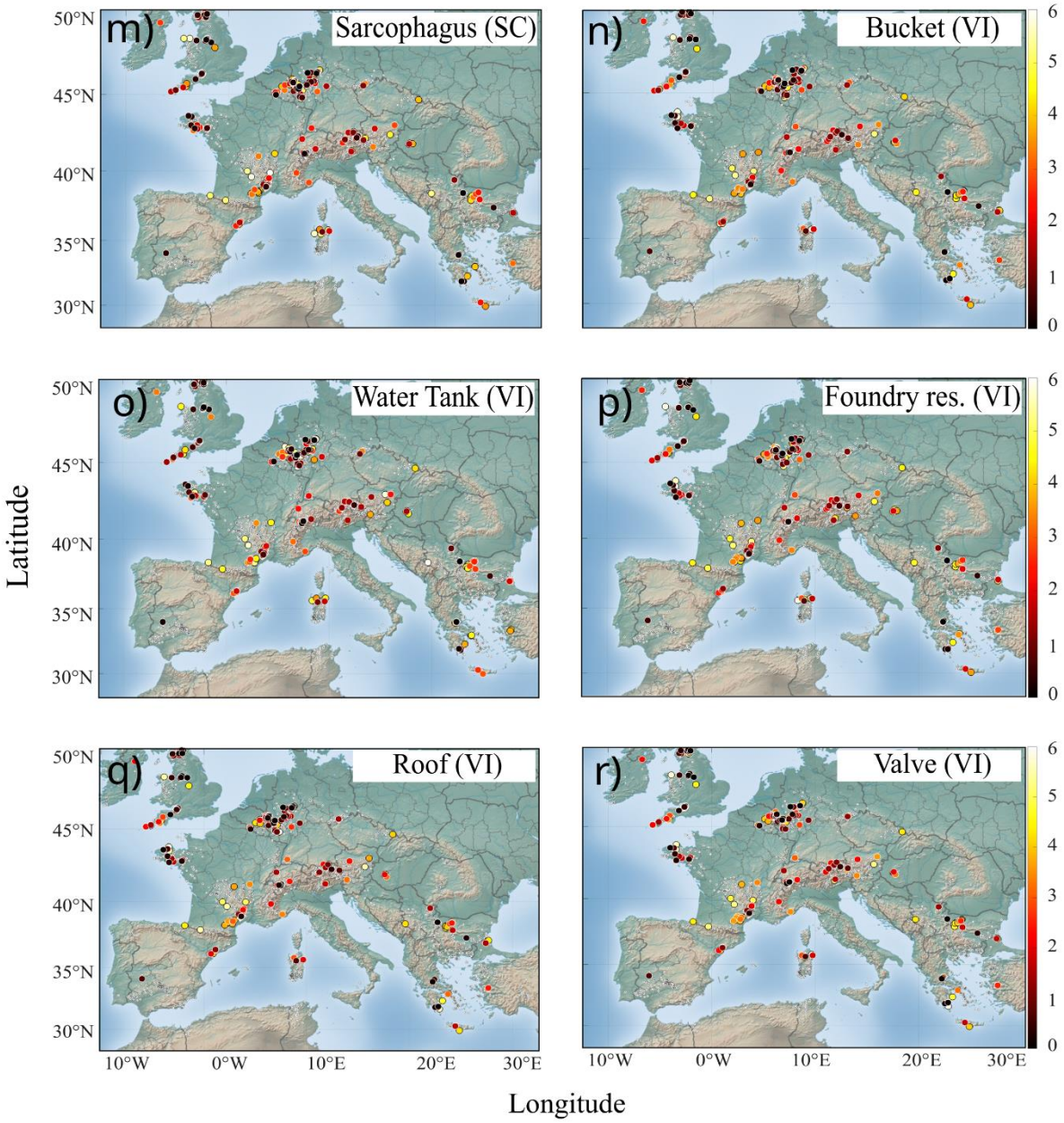

Figure S3. (3/3)

Figure S3. *Outputs of the data treatment obtained with the newly published algorithm (Albarede et al., 2024) showing the statistical probability of correspondence of Pb isotope compositions of artifacts from Vienne compared with the isotope compositions of end-members (ores) derived from a new database (Albarede et al., 2024b). From a to f (Fig. S2, 1/3): pipes 8 (a) and 10 (b) from St-Roman-en-Gal (SRG), pipe 4 (c) from Sainte Colombe (SC), pipe 13 (d) from Vienne (VI), and pipes 14 (g) and 15 (h) from Lyon (LY). From g to l (Fig. S2, 2/3): pipes 2 (g), 3 (h), 6 (i), and 7 (j) from Sainte Colombe (SC), pipe 11 (k) from Vienne (VI) and pipe 5 (l) from Sainte Colombe (SC). Note that these two latter pipes (5 and 11) do not match with Rhenish Massif, but match with regional ores, i.e., Wallis region and Cevennes, respectively. From m to r (Fig. S2, 3/3): a lead sarcophagus (m) from Sainte Colombe (SC), a bucket (n), a water tank (o), a foundry (p), a roof (q), and a valve (r) from Vienne (VI). The statistical probability of correspondence increases from white (value of 6) to black (value of 0).*

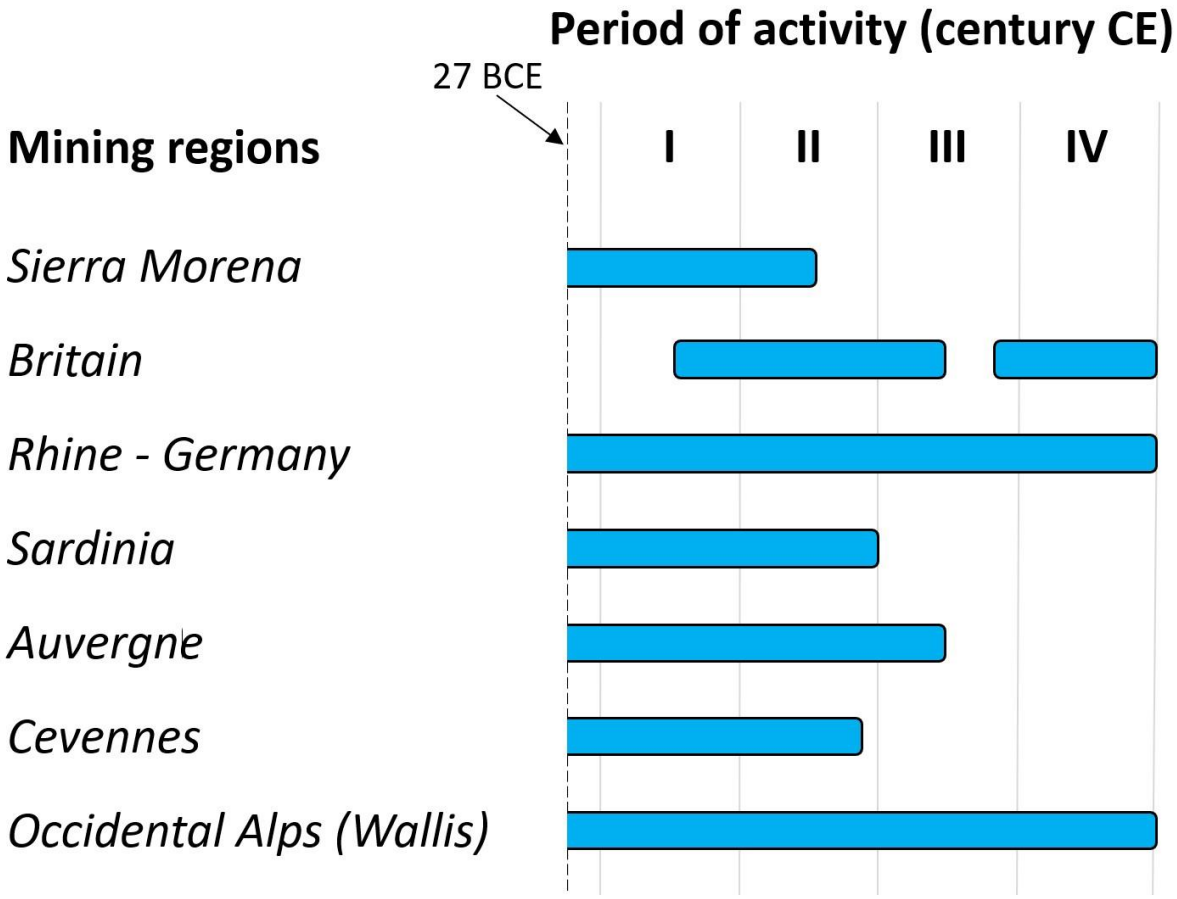

Figure S4. *The principal mining regions during the Roman Empire and the periods in which they were exploited (Adapted from Domergue 2010 and references within). The vertical dotted line represents the beginning of Imperial Rome (27 BCE).*

Annex 2:

Supplementary information for the research article entitled:

Copper and lead isotopes composition of ancient Roman human bones reveal health degradation due to lead poisoning (Vienne, France)

Table S1. *Anthropological information of bone samples from Vienne. Age groups are as follows: infant/juvenile (IJ, 0 – 20 years old), young adult (YA, 20 – 29 years old), mature adult (MA, 30 – 59 years old), old adult (OA, > 60 years old) and unknown (n.a.). Individuals in italics and with a * have been excluded and considered significantly affected by diagenesis.*

Material	Individual	Location	Archaeological site	sepultures	Sample_ID	Sex	Age	Datation
phalange	*human*	*Vienne*	*37 Vimaine st.*	*lead sarcophagus*	**HV1*	*female*	*young adult*	*Early 3rd CE*
phalange	*human*	*Vienne*	*37 Vimaine st.*	*wood trunk*	**HV2*	*female*	*30-50 y*	*Early 3rd CE*
phalange	human	Vienne	Charavel	nailed wood trunk	HV3	male	> 60y	High Empire
phalange	human	Vienne	Charavel	nailed wood trunk	HV4	male	30-59 y	High Empire
phalange	human	Vienne	Charavel	nailed wood trunk	HV5	male	30-59 y	High Empire
phalange	human	Vienne	Charavel	nailed wood trunk	HV6	male	> 60y	High Empire
phalange	human	Vienne	Ferré Boge	wood trunk	HV7	n.a.	n.a.	4th CE-5th CE
phalange	human	Vienne	Notre Dame d'outre Gère	n.a	HV8	n.a.	n.a.	5th - 6th CE
phalange	human	Vienne	Notre Dame d'outre Gère	masonry trunk	HV9	female	30-59 y	6th CE
phalange	human	Vienne	Nympheas	n.a	HV10	male	n.a.	4th CE
phalange	human	Vienne	Place d'Arpot	n.a	HV11	n.a.	n.a.	High Empire
phalange	human	Vienne	Place d'Arpot	n.a	HV12	n.a.	n.a.	High Empire
phalange	human	Vienne	St. Pierre St Georges	stone trunk	HV13	n.a.	n.a.	5th CE
phalange	human	Vienne	Vimaine II	n.a	HV14	n.a.	n.a.	late 3rd - early 4th CE
phalange	human	Saint-Roman-en-Gal	Thermes des lutteurs	pit	HSR1	male	20-29 y	4th CE
phalange	human	Saint-Colombe	289 Trenel	wood trunk	HSC1	female	young adult	3rd CE
phalange	*human*	*Saint-Colombe*	*289 Trenel*	*wood trunk*	**HSC1*	*n.a.*	*young adult*	*3rd CE*
phalange	human	Saint-Colombe	289 Trenel	wood trunk	HSC2	female	young adult	3rd CE
phalange	human	Saint-Colombe	289 Trenel	wood trunk	HSC3	male	adult	3rd CE
phalange	*human*	*Saint-Colombe*	*289 Trenel*	*trunk*	**HSC4*	*n.a.*	*immature*	*3rd CE*
phalange	human	Saint-Colombe	289 Trenel	wood trunk	HSC5	female	old	3rd CE
phalange	human	Saint-Colombe	289 Trenel	wood trunk	HSC6	n.a.	immature	5th - 6th CE
phalange	*human*	*Saint-Colombe*	*La Colombine*	*wood trunk*	**HSC7*	*n.a.*	*adult*	*4th CE*

Table S1 (continued). *Sample anthropological information of bone samples from Vienne.*

Material	Individual	Location	Archaeological site	sepultures	Sample_ID	Sex	Age	Datation
phalange	human	Saint-Colombe	Le Bourg	pit	HSC8	female	old	2nd - 3rd CE
phalange	human	Saint-Colombe	Le Bourg	pit with wooden covering	HSC9	male	mature/old	3rd - 4th CE
phalange	human	Saint-Colombe	Le Bourg	stone trunk wood cover	HSC10	n.a.	infant	middle 4th CE
phalange	human	Saint-Colombe	Le Bourg	stone trunk wood cover	HSC11	female	old	5th - 6th CE
phalange	human	Saint-Colombe	Le Bourg	pit with wooden covering	HSC12	male	young adult	5th - 6th CE
phalange	human	Saint-Colombe	Le Bourg	wood trunk	HSC13	male	adult	7th CE
phalange	human	Saint-Colombe	Le Bourg	stone trunk wood cover	HSC14	n.a.	immature	7th - 8th CE
phalange	human	Saint-Colombe	Le Bourg	stone trunk wood cover	HSC15	female	old	7th - 8th CE
phalange	*human*	*Saint-Colombe*	*Le Bourg*	*stone trunk wood cover*	**HSC16*	*n.a.*	*adult*	*3rd - 4th CE*
phalange	human	Saint-Colombe	Place de l'Egalité	pit	HSC17	male	30-59 y	4th CE
phalange	human	Saint-Colombe	Place de l'Egalité	wood trunk	HSC18	male	30-59 y	late 3rd - early 4th CE
phalange	human	Saint-Colombe	Place de l'Egalité	wood trunk	HSC19	male	30-59 y	late 3rd - early 4th CE
phalange	cow (Bovineae)	Saint-Colombe	Le Bourg	n.a.	ASC1	n.a.	n.a.	2nd CE
calcaneus	goat (Caprineae)	Saint-Colombe	Le Bourg	n.a.	ASC2	n.a.	n.a.	1st CE
tibio-tarsus	hen (Gallinaceae)	Saint-Colombe	Le Bourg	n.a.	ASC3	n.a.	n.a.	2nd CE
tibia	cat (Felidae)	Saint-Colombe	Le Bourg	n.a.	ASC4	n.a.	n.a.	2nd CE
calcaneus	Pig (Suidae)	Saint-Colombe	Le Bourg	n.a.	ASC5	n.a.	n.a.	1st CE
femur	Hare (Leporidae)	Saint-Colombe	Le Bourg	n.a.	ASC6	n.a.	n.a.	1st CE

Table S2. Lead (Pb) and copper (Cu) isotope composition of bone samples from Vienne. The three geochemically informed parameters (model age T_{mod}, $\mu = {}^{238}U/{}^{204}Pb$, and $k = {}^{232}Th/{}^{238}U$) were obtained with the equations given by Albarède et al. (2012) and using the Matlab code found in Delile et al. (2015). Individuals in *italics* and with a * have been excluded and considered significantly affected by diagenesis.

Sample_ID	$^{206}Pb/^{204}Pb$	$^{207}Pb/^{204}Pb$	$^{208}Pb/^{204}Pb$	$^{207}Pb/^{206}Pb$	$^{208}Pb/^{206}Pb$	$^{204}Pb/^{206}Pb$	$^{206}Pb/^{207}Pb$	T_{mod} (MA)	μ	κ	$\delta^{65}Cu$ (‰)
**HV1*	*n.a.*	*n.a.*	*n.a.*	*n.a.*	*n.a.*	*n.a.*	*n.a.*	*n.a.*	*n.a.*	*n.a.*	*n.a.*
**HV2*	*n.a.*	*n.a.*	*n.a.*	*n.a.*	*n.a.*	*n.a.*	*n.a.*	*n.a.*	*n.a.*	*n.a.*	*n.a.*
HV3	18.437	15.633	38.451	0.848	2.086	0.05424	1.179	229	9.70	3.92	n.a.
HV4	18.485	15.655	38.629	0.847	2.090	0.05410	1.181	220	9.73	3.97	n.a.
HV5	18.454	15.638	38.495	0.847	2.086	0.05419	1.180	222	9.70	3.93	n.a.
HV6	18.459	15.635	38.462	0.847	2.084	0.05417	1.181	215	9.70	3.91	-0.17
HV7	18.425	15.640	38.460	0.849	2.087	0.05427	1.178	245	9.71	3.93	-0.605
HV8	18.454	15.627	38.453	0.847	2.084	0.05419	1.181	209	9.68	3.91	n.a.
HV9	18.456	15.630	38.455	0.847	2.084	0.05418	1.181	211	9.69	3.91	-0.45
HV10	18.432	15.641	38.470	0.849	2.087	0.05425	1.178	242	9.71	3.93	-0.41
HV11	18.458	15.644	38.469	0.848	2.084	0.05418	1.180	226	9.72	3.91	-0.56
HV12	18.442	15.639	38.449	0.848	2.085	0.05422	1.179	232	9.71	3.91	-0.59
HV13	18.410	15.636	38.432	0.849	2.088	0.05432	1.177	250	9.70	3.92	n.a.
HV14	18.453	15.641	38.499	0.848	2.086	0.05419	1.180	227	9.71	3.93	0.14
HSR1	n.a.	n.a.	n.a.	n.a.	n.a.	n.a.	n.a.	n.a.	n.a.	n.a.	n.a.
HSC1	18.420	15.641	38.456	0.849	2.088	0.05429	1.178	250	9.71	3.93	-0.51
**HSC1*	*18.437*	*15.642*	*38.481*	*0.848*	*2.087*	*0.05424*	*1.179*	*239*	*9.72*	*3.93*	*-0.24*
HSC2	18.428	15.638	38.464	0.849	2.087	0.05427	1.178	241	9.71	3.93	-0.42
HSC3	18.423	15.639	38.458	0.849	2.088	0.05428	1.178	245	9.71	3.93	-0.42
**HSC4*	*18.416*	*15.642*	*38.457*	*0.849*	*2.088*	*0.05430*	*1.177*	*254*	*9.72*	*3.93*	*-0.68*
HSC5	18.388	15.638	38.448	0.850	2.091	0.05438	1.176	269	9.71	3.94	-0.51
HSC6	18.428	15.655	38.515	0.850	2.090	0.05427	1.177	261	9.74	3.95	-0.63
**HSC7*	*18.457*	*15.644*	*38.505*	*0.848*	*2.086*	*0.05418*	*1.180*	*227*	*9.72*	*3.93*	*-0.225*

Table S2 (continued). Lead (Pb) and copper (Cu) isotope composition of bone samples from Vienne.

Sample_ID	$^{206}Pb/^{204}Pb$	$^{207}Pb/^{204}Pb$	$^{208}Pb/^{204}Pb$	$^{207}Pb/^{206}Pb$	$^{208}Pb/^{206}Pb$	$^{204}Pb/^{206}Pb$	$^{206}Pb/^{207}Pb$	T_{mod} (MA)	μ	κ	$\delta^{65}Cu$ (‰)
HSC8	18.410	15.637	38.460	0.849	2.089	0.05432	1.177	251	9.71	3.94	-0.45
HSC9	18.411	15.633	38.428	0.849	2.087	0.05432	1.178	247	9.70	3.92	-0.65
HSC10	18.419	15.641	38.454	0.849	2.088	0.05429	1.178	251	9.71	3.93	-0.65
HSC11	18.426	15.639	38.456	0.849	2.087	0.05427	1.178	243	9.71	3.93	-0.805
HSC12	18.421	15.637	38.455	0.849	2.088	0.05429	1.178	244	9.71	3.93	-0.71
HSC13	18.424	15.640	38.474	0.849	2.088	0.05428	1.178	246	9.71	3.93	n.a.
HSC14	18.430	15.643	38.468	0.849	2.087	0.05426	1.178	244	9.72	3.93	-0.81
HSC15	18.419	15.643	38.461	0.849	2.088	0.05429	1.177	253	9.72	3.93	-0.86
**HSC16*	*n.a.*	*n.a.*	*n.a.*	*n.a.*	*n.a.*	*n.a.*	*n.a.*	*n.a.*	*n.a.*	*n.a.*	*n.a.*
HSC17	18.421	15.638	38.453	0.849	2.087	0.05429	1.178	245	9.71	3.93	-0.21
HSC18	n.a.	n.a.	n.a.	n.a.	n.a.	n.a.	n.a.	n.a.	n.a.	n.a.	n.a.
HSC19	n.a.	n.a.	n.a.	n.a.	n.a.	n.a.	n.a.	n.a.	n.a.	n.a.	n.a.
ASC1	n.a.	n.a.	n.a.	n.a.	n.a.	n.a.	n.a.	n.a.	n.a.	n.a.	n.a.
ASC2	n.a.	n.a.	n.a.	n.a.	n.a.	n.a.	n.a.	n.a.	n.a.	n.a.	n.a.
ASC3	n.a.	n.a.	n.a.	n.a.	n.a.	n.a.	n.a.	n.a.	n.a.	n.a.	n.a.
ASC4	n.a.	n.a.	n.a.	n.a.	n.a.	n.a.	n.a.	n.a.	n.a.	n.a.	n.a.
ASC5	n.a.	n.a.	n.a.	n.a.	n.a.	n.a.	n.a.	n.a.	n.a.	n.a.	n.a.
ASC6	n.a.	n.a.	n.a.	n.a.	n.a.	n.a.	n.a.	n.a.	n.a.	n.a.	n.a.

Table S3. Summary of the trace elemental content of cortical human bones from Vienne. Individuals in *italics* and with a * have been excluded and considered significantly affected by diagenesis. Hg is reported in $ng.g^{-1}$. All the other elements are reported in $ug.g^{-1}$.

Sample_ID	Hg ($ng.g^{-1}$)	Pb ($\mu g.g^{-1}$)	Mn ($\mu g.g^{-1}$)	Fe ($\mu g.g^{-1}$)	Co ($\mu g.g^{-1}$)	Ni ($\mu g.g^{-1}$)	Cu ($\mu g.g^{-1}$)	Zn ($\mu g.g^{-1}$)	Sr ($\mu g.g^{-1}$)
**HV1*	*n.a.*	*133914.18*	*1157.60*	*5911.56*	*11.03*	*8.22*	*213.00*	*221.92*	*1201.01*
**HV2*	*n.a.*	*65200.85*	*2274.66*	*2267.15*	*14.63*	*12.46*	*151.18*	*211.64*	*1550.42*
HV3	47.38	13.96	29.41	86.39	0.33	1.72	3.47	90.00	113.39
HV4	176.97	14.50	170.80	37.07	0.17	< LD	2.03	68.66	127.09
HV5	56.13	n.a.	n.a.	n.a.	n.a.	n.a.	n.a.	n.a.	n.a.
HV6	87.81	10.14	25.16	225.47	0.48	2.42	9.33	95.09	147.43
HV7	54.13	n.a.	n.a.	n.a.	n.a.	n.a.	n.a.	n.a.	n.a.
HV8	100.70	6.90	18.62	122.66	0.29	1.95	14.42	150.40	170.41
HV9	62.37	8.35	21.50	96.03	0.25	0.65	12.03	161.20	173.98
HV10	99.51	75.83	85.25	171.56	0.27	< LD	33.45	117.57	242.07
HV11	235.35	43.23	46.19	633.96	0.62	3.32	67.35	176.52	173.19
HV12	221.92	247.30	94.93	1906.13	1.74	3.95	56.11	252.73	217.17
HV13	222.07	73.09	59.38	52.91	0.16	3.21	16.61	200.72	210.78
HV14	88.87	43.39	55.95	247.29	0.34	3.25	21.37	231.83	141.38
HSR1	n.a.	42.87	8.96	278.18	0.59	0.78	28.77	96.95	163.61
HSC1	20.17	n.a.	n.a.	n.a.	n.a.	n.a.	n.a.	n.a.	n.a.
**HSC1*	*12.77*	*103.75*	*305.68*	*556.81*	*0.83*	*2.23*	*99.09*	*342.96*	*667.27*
HSC2	35.39	115.18	195.68	619.57	0.59	1.53	52.86	116.14	170.23
HSC3	18.10	n.a.	n.a.	n.a.	n.a.	n.a.	n.a.	n.a.	n.a.
**HSC4*	*17.45*	*1681.78*	*178.99*	*691.80*	*0.77*	*2.15*	*42.77*	*296.23*	*175.91*
HSC5	32.55	624.41	65.82	1902.05	1.00	1.53	62.72	138.72	217.90
HSC6	17.07	76.35	207.47	279.12	0.50	1.08	52.32	142.28	225.17
**HSC7*	*78.80*	*134.80*	*154.08*	*2831.34*	*1.39*	*3.96*	*16.10*	*183.08*	*154.21*

Table S3 (continued). Summary of the trace elemental content of cortical human bones from Vienne.

Sample_ID	Hg (ng.g^{-1})	Pb (µg.g^{-1})	Mn (µg.g^{-1})	Fe (µg.g^{-1})	Co (µg.g^{-1})	Ni (µg.g^{-1})	Cu (µg.g^{-1})	Zn (µg.g^{-1})	Sr (µg.g^{-1})
HSC8	543.45	165.33	17.62	142.29	0.33	1.55	70.70	82.06	242.17
HSC9	40.65	207.28	132.43	130.73	0.44	1.33	36.73	133.46	186.66
HSC10	n.a.	114.77	57.82	635.88	0.29	1.73	50.41	153.53	241.17
HSC11	35.47	167.48	144.01	381.58	0.30	2.33	37.29	168.48	168.75
HSC12	65.53	156.91	39.18	59.52	0.16	0.84	4.60	158.47	238.92
HSC13	8.63	85.16	110.18	88.72	0.21	2.40	69.47	134.42	130.98
HSC14	n.a.	141.85	510.67	855.86	0.66	5.83	83.91	215.77	191.03
HSC15	30.18	46.23	32.92	83.38	0.12	1.53	19.74	95.15	169.05
**HSC16*	*n.a.*	*289.67*	*0.13*	*5071.88*	*0.26*	*0.22*	*< LD*	*2.28*	*0.11*
HSC17	118.60	n.a.	n.a.	n.a.	n.a.	n.a.	n.a.	n.a.	n.a.
HSC18	n.a.	167.16	92.95	107.36	0.30	1.92	31.60	120.89	244.39
HSC19	n.a.	524.25	18.53	131.48	0.18	1.54	25.57	78.63	133.15
ASC1	139.53	31.24	648.66	1075.59	4.01	9.21	87.14	115.29	303.76
ASC2	90.05	46.22	37.65	149.74	0.47	1.42	115.52	299.78	381.25
ASC3	583.78	36.03	288.96	78.67	n.a.	1.65	48.49	187.53	291.20
ASC4	232.20	152.52	45.06	188.00	0.53	1.25	94.00	141.68	365.75
ASC5	102.76	20.46	22.82	82.06	0.52	0.68	73.22	124.85	231.71
ASC6	196.17	24.17	22.91	86.91	0.28	0.79	67.51	191.86	221.70

Table S4. Summary of the major elemental content of cortical human bones from Vienne. Individuals in *italics* and with a * have been excluded and considered significantly affected by diagenesis. All major elements are reported in ug.g^{-1} and wt. %.

Sample_ID	Na (µg.g^{-1})	Na wt. %	K (µg.g^{-1})	Mg (µg.g^{-1})	Mg wt. %	Al (µg.g^{-1})	Ba (µg.g^{-1})	Ca (µg.g^{-1})	Ca wt. %	P (µg.g^{-1})	P wt. %
**HV1*	*2455*	*0.25*	*461.96*	*1003*	*0.10*	*4017*	*58.7*	*232600*	*23.26*	*103835*	*10.38*
**HV2*	*1195*	*0.12*	*63.41*	*457*	*0.05*	*339*	*90.8*	*328506*	*32.85*	*83187*	*8.32*
HV3	3178	0.32	41.44	740	0.07	111	27.9	334791	33.48	124646	12.46
HV4	2192	0.22	20.88	608	0.06	49	33.7	232605	23.26	93513	9.35
HV5	n.a.	n.a.	n.a.	n.a.	n.a.	n.a.	n.a.	n.a.	n.a.	n.a.	n.a.
HV6	2348	0.23	61.25	647	0.06	237	44.3	352234	35.22	143424	14.34
HV7	n.a.	n.a.	n.a.	n.a.	n.a.	n.a.	n.a.	n.a.	n.a.	n.a.	n.a.
HV8	2290	0.23	72.76	941	0.09	128	61.6	326373	32.64	135393	13.54
HV9	2058	0.21	119.36	774	0.08	116	34.4	339485	33.95	144334	14.43
HV10	2014	0.20	56.63	756	0.08	231	280.9	306627	30.66	120923	12.09
HV11	1911	0.19	161.88	736	0.07	791	88.7	343014	34.30	143548	14.35
HV12	1821	0.18	413.07	919	0.09	2555	72.7	335235	33.52	141867	14.19
HV13	2822	0.28	118.26	794	0.08	99	35.1	346256	34.63	146686	14.67
HV14	2947	0.29	80.47	766	0.08	280	67.6	299348	29.93	121776	12.18
HSR1	2247	0.22	117.29	850	0.09	571	55.9	315069	31.51	126686	12.67
HSC1	n.a.	n.a.	n.a.	n.a.	n.a.	n.a.	n.a.	n.a.	n.a.	n.a.	n.a.
**HSC1*	*2593*	*0.26*	*104.37*	*701*	*0.07*	*514*	*151.7*	*330335*	*33.03*	*120983*	*12.10*
HSC2	2072	0.21	120.32	658	0.07	661	95.6	305276	30.53	109001	10.90
HSC3	n.a.	n.a.	n.a.	n.a.	n.a.	n.a.	n.a.	n.a.	n.a.	n.a.	n.a.
**HSC4*	*2871*	*0.29*	*124.52*	*732*	*0.07*	*821*	*130.5*	*289675*	*28.97*	*118419*	*11.84*
HSC5	2714	0.27	408.44	1245	0.12	2180	143.5	311475	31.15	120149	12.01
HSC6	2005	0.20	69.85	609	0.06	437	105.1	303001	30.30	125173	12.52
**HSC7*	*2454*	*0.25*	*533.56*	*1169*	*0.12*	*3416*	*55.4*	*293249*	*29.32*	*115011*	*11.50*

Table S4 (continued). Summary of the major elemental content of cortical human bones from Vienne.

Sample_ID	Na (µg.g^{-1})	Na wt. %	K (µg.g^{-1})	Mg (µg.g^{-1})	Mg wt. %	Al (µg.g^{-1})	Ba (µg.g^{-1})	Ca (µg.g^{-1})	Ca wt. %	P (µg.g^{-1})	P wt. %
HSC8	2267	0.23	226.32	1123	0.11	162	280.6	337431	33.74	133574	13.36
HSC9	2426	0.24	59.32	770	0.08	173	118.1	334908	33.49	136486	13.65
HSC10	2544	0.25	137.17	895	0.09	508	106.9	276949	27.69	113457	11.35
HSC11	2386	0.24	94.67	728	0.07	383	152.3	296720	29.67	119026	11.90
HSC12	4810	0.48	43.20	1315	0.13	69	48.9	405237	40.52	159259	15.93
HSC13	1361	0.14	43.80	568	0.06	120	110.5	241874	24.19	101503	10.15
HSC14	2032	0.20	205.90	738	0.07	971	168.8	274291	27.43	112661	11.27
HSC15	3273	0.33	42.26	1072	0.11	104	132.9	278177	27.82	114364	11.44
**HSC16*	*2476*	*0.25*	*876.51*	*1714*	*0.17*	*3973*	*317.4*	*262935*	*26.29*	*103535*	*10.35*
HSC17	n.a.	n.a.	n.a.	n.a.	n.a.	n.a.	n.a.	n.a.	n.a.	n.a.	n.a.
HSC18	2460	0.25	53.54	893	0.09	177	123.0	297652	29.77	100825	10.08
HSC19	3474	0.35	51.80	844	0.08	195	416.6	345563	34.56	136522	13.65
ASC1	4062	0.41	435.22	1801	0.18	319	313.9	337505	33.75	126072	12.61
ASC2	2973	0.30	243.25	1211	0.12	240	202.6	350654	35.07	132647	13.26
ASC3	3837	0.38	78.14	1084	0.11	207	298.8	457601	45.76	191814	19.18
ASC4	2074	0.21	76.80	616	0.06	207	230.9	351225	35.12	137946	13.79
ASC5	2671	0.27	29.08	811	0.08	187	179.8	338150	33.82	136481	13.65
ASC6	1655	0.17	45.01	621	0.06	185	175.7	270954	27.10	111853	11.19

Table S5. Summary of the elemental ratios (Ca/P, Sr/Ca, Ba/Ca, Pb/Ca) of cortical human bones from Vienne. Individuals in *italics* and with a * have been excluded and considered significantly affected by diagenesis.

Sample_ID	Ca/P	log_{10} (Sr/Ca)	log_{10} (Ba/Ca)	log_{10} (Pb/Ca)
**HV1*	*2.24*	*-2.29*	*-3.60*	*-0.24*
**HV2*	*3.95*	*-2.33*	*-3.56*	*-0.70*
HV3	2.69	-3.47	-4.08	-4.38
HV4	2.49	-3.26	-3.84	-4.21
HV5	n.a.	n.a.	n.a.	n.a.
HV6	2.46	-3.38	-3.90	-4.54
HV7	n.a.	n.a.	n.a.	n.a.
HV8	2.41	-3.28	-3.72	-4.67
HV9	2.35	-3.29	-3.99	-4.61
HV10	2.54	-3.10	-3.04	-3.61
HV11	2.39	-3.30	-3.59	-3.90
HV12	2.36	-3.19	-3.66	-3.13
HV13	2.36	-3.22	-3.99	-3.68
HV14	2.46	-3.33	-3.65	-3.84
HSR1	2.49	-3.28	-3.75	-3.87
HSC1	n.a.	n.a.	n.a.	n.a.
**HSC1*	*2.73*	*-2.69*	*-3.34*	*-3.50*
HSC2	2.80	-3.25	-3.50	-3.42
HSC3	n.a.	n.a.	n.a.	n.a.
**HSC4*	*2.45*	*-3.22*	*-3.35*	*-2.24*
HSC5	2.59	-3.16	-3.34	-2.70
HSC6	2.42	-3.13	-3.46	-3.60
**HSC7*	*2.55*	*-3.28*	*-3.72*	*-3.34*

Table S5 (continued). Summary of the elemental ratios (Ca/P, Sr/Ca, Ba/Ca, Pb/Ca) of cortical human bones from Vienne.

Sample_ID	Ca/P	log_{10} (Sr/Ca)	log_{10} (Ba/Ca)	log_{10} (Pb/Ca)
HSC8	2.53	-3.14	-3.08	-3.31
HSC9	2.45	-3.25	-3.45	-3.21
HSC10	2.44	-3.06	-3.41	-3.38
HSC11	2.49	-3.25	-3.29	-3.25
HSC12	2.54	-3.23	-3.92	-3.41
HSC13	2.38	-3.27	-3.34	-3.45
HSC14	2.43	-3.16	-3.21	-3.29
HSC15	2.43	-3.22	-3.32	-3.78
**HSC16*	*2.54*	*-6.39*	*-2.92*	*-2.96*
HSC17	n.a.	n.a.	n.a.	n.a.
HSC18	2.95	-3.09	-3.38	-3.25
HSC19	2.53	-3.41	-2.92	-2.82
ASC1	2.68	-3.05	-3.03	-4.03
ASC2	2.64	-2.96	-3.24	-3.88
ASC3	2.39	-3.20	-3.19	-4.10
ASC4	2.55	-2.98	-3.18	-3.36
ASC5	2.48	-3.16	-3.27	-4.22
ASC6	2.42	-3.09	-3.19	-4.05

Table S6 *Correlation coefficients and associated p values between concentrations and isotopic ratios. Significant p values (< 0.05) are in bold.*

	[Pb]		**[Hg]**		**[Cu]**		**[Fe]**		**[Mn]**		**[Sr]**		**[Ba]**		**[Al]**	
	R^2	*p*	R^2	*p*	R^2	*p*	R^2	*p*	R^2	*p*	R^2	*p*	R^2	*p*	R^2	*p*
$^{206}Pb/^{204}Pb$	0.405	**0.001**	0.00	0.78	0.14	0.08	0.00	0.9	0.00	0.9	0.03	0.44	0.2	**0.02**	0.000	0.9
$^{207}Pb/^{204}Pb$	0.002	0.86	0.00	0.81	0.05	0.3	0.02	0.52	0.20	**0.04**	0.007	0.7	0.01	0.6	0.020	0.5
$^{208}Pb/^{204}Pb$	0.07	0.2	0.00	0.8	0.03	0.5	0.00	0.95	0.06	0.3	0.006	0.7	0.03	0.4	0.000	0.9
$^{207}Pb/^{206}Pb$	0.4	**0.001**	0.01	0.7	0.20	**0.03**	0.05	0.7	0.02	0.5	0.04	0.4	0.3	**0.01**	0.003	0.8
$^{208}Pb/^{206}Pb$	0.2	**0.02**	0.00	0.9	0.08	0.2	0.00	0.9	0.07	0.2	0.01	0.6	0.2	0.06	0.000	0.9
$\delta^{65}Cu$ (‰)	0.04	0.4	0.01	0.7	0.02	0.6	0.02	0.6	0.04	0.42	0.02	0.6	0.03	0.45	0.010	0.6
[Pb]			0.01	0.7	0.01	0.6	0.20	**0.02**	0.01	0.56	0.01	0.6	0.15	**0.03**	0.200	**0.01**
[Hg]	0.007	0.7			0.02	0.42	0.01	0.6	0.00	0.9	0.01	0.6	0.2	**0.01**	0.006	0.7
[Cu]	0.007	0.6	0.03	0.4			0.02	0.5	0.14	**0.03**	0.42	**0.001**	0.2	**0.004**	0.004	0.7

Table S7. *Statistical summary of the elemental concentrations and ratios in cortical human bones (phalanges) from Vienne (this study) and from modern individuals* (Harkness and Darrah, 2019; Lyengar and Tandom, 1999; Martínez-García et al., 2005; Reiche et al., 2003; Zioła-Frankowska et al., 2017, 2015). *Trace elements are reported in µg.g^{-1}, Hg is reported in ng.g^{-1} and major elements are reported in mg.g^{-1} and wt. %.*

	elemental concentrations (*this study*)					*Ziola-Frankowska et al. 2015, 2017*	*Martinez-Garcia et al., (2005)*	*Harkness & Darrah (2005)*	*Lyengar et al., (1978)*	*Reiche et al., (2003)*
	mean	median	SD	min	max	range				
Hg (ng.g^{-1})	100.8	59.2	116.1	8.6	543.4	2 - 177	n.a.	n.a.	n.a.	n.a.
Pb (µg.g^{-1})	132.2	80.8	152.8	6.9	624.4	0.3 - 7.5	22.5 - 56	0.07 - 10	n.a.	n.a.
Mn (µg.g^{-1})	93.4	58.6	106.2	9.0	510.7	n.a.	n.a.	0.01 - 0.2	n.a.	n.a.
Fe (µg.g^{-1})	386.5	156.9	517.2	37.1	1906.1	20.6 - 840	439.6 - 1537	102 - 110	100 - 2000	n.a.
Co (µg.g^{-1})	0.4	0.3	0.3	0.1	1.7	n.a.	n.a.	0.1 - 0.3	n.a.	n.a.
Ni (µg.g^{-1})	2.1	1.7	1.2	0.7	5.8	0.03 - 15	n.a.	n.a.	n.a.	n.a.
Cu (µg.g^{-1})	36.0	32.5	24.2	2.0	83.9	0.04 - 7	16 - 43	0.04 - 31	1.1 - 50	n.a.
Zn (µg.g^{-1})	140.8	136.6	49.3	68.7	252.7	43.1 - 108	205.5 - 414	58 - 166	50 - 400	120 - 140
Sr (µg.g^{-1})	185.0	173.6	41.5	113.4	244.4	16.3 - 138	n.a.	21 - 115	n.a.	180 - 280
Na (mg.g^{-1})	2.5	2.3	0.7	1.4	4.8	2.2 - 6.6	n.a.	9.5 - 15	n.a.	7.6 - 9.1
Na wt. %	0.25	0.23	0.07	0.1	0.5	0.2 - 0.7	n.a.	1.16 - 1.6	n.a.	n.a.
K (mg.g^{-1})	0.12	0.08	0.10	20.9	413.1	0.3 - 9.3	n.a.	2 - 2.5	n.a.	n.a.
Mg (mg.g^{-1})	0.83	0.77	0.19	0.6	1.3	0.8 - 2.2	n.a.	1.6 - 2.3	n.a.	7.2 - 9
Mg wt. %	0.08	0.08	0.02	0.1	0.1	0.08 - 0.2	n.a.	7.8 - 8.1	n.a.	n.a.
Al (µg.g^{-1})	471.1	213.1	635.2	48.6	2555.1	n.a.	n.a.	0.2 - 3.5	n.a.	n.a.
Ba (µg.g^{-1})	116.9	100.4	93.1	27.9	416.6	0.24 - 7	n.a.	0.5 - 9	n.a.	n.a.
Ca (mg.g^{-1})	314.1	313.3	37.6	232.6	405.2	65.5 - 252	n.a.	358 - 411	n.a.	n.a.
Ca wt. %	31.4	31.3	3.8	23.3	40.5	6.6 - 25	n.a.	36 - 41.1	n.a.	38.2 - 38.6
P (mg.g^{-1})	126.0	124.9	16.5	93.5	159.3	29.5 - 109.2	n.a.	n.a.	n.a.	n.a.
P wt. %	12.6	12.5	1.7	9.4	15.9	2.9 - 11	n.a.	n.a.	n.a.	17.8 - 18

Table S8. *Statistical results (p values) for the Kruskal-Wallis test performed on the age groups and the time periods, and Mann-Whitney U tests performed for sex (Men - Women), individual (human - animal), sites (Vienna – Saint Colombe) and also contrasting Vienna (this study) with A Lanzada [Iberia, Spain, (López-Costas et al., 2020)] and Saint Laurent [Grenoble, France, (Jaouen et al., 2012)]. Significant values are in bolt and italics.*

	∂^{65}Cu (‰)	Hg (ng.g^{-1})	Pb (µg.g^{-1})	Cu (µg.g^{-1})	Zn (µg.g^{-1})	Fe (µg.g^{-1})	Mn (µg.g^{-1})	Sr (µg.g^{-1})	Ba (µg.g^{-1})	Al (µg.g^{-1})
this study										
Humans - animals	n.a.	***0.01***	0.15	***0.002***	0.25	0.47	0.92	***0.002***	***0.003***	0.88
Period										
HE - LA	***0.04***	***0.04***	0.73	0.5	0.08	0.43	0.38	0.500	0.35	0.44
EMA - LA	***0.01***	0.88	0.17	0.71	0.13	0.11	0.71	0.710	0.27	0.06
EMA - HE	0.99	0.05	0.12	0.32	0.69	0.51	0.55	0.320	0.05	0.37
Age group										
IJ - MA	0.06	0.17	0.96	0.09	0.06	***0.01***	0.15	0.09	0.61	0.03
IJ - OA	0.5	0.18	0.7	0.16	0.06	0.13	0.08	0.16	0.93	0.12
IJ - YA	0.44	0.23	1	0.36	0.25	0.19	0.15	0.36	0.25	0.40
MA - OA	0.13	0.96	0.6	0.64	0.91	0.19	0.78	0.64	0.58	0.37
MA - YA	0.35	1	0.96	0.5	0.57	0.30	0.86	0.50	0.44	0.22
OA - YA	0.79	0.97	0.7	0.76	0.61	1.00	0.96	0.76	0.20	0.59
Sex										
Men - Women	0.13	0.45	0.59	0.28	0.28	0.16	0.91	0.280	0.330	0.38
Sites										
(Vienne - St. Colombe)	0.05	< ***0.001***	***0.001***	0.19	0.42	0.45	0.19	0.190	***0.002***	0.46
Jaouen et al. (2012)										
Vienne - St. Laurent	< ***0.001***	n.a	n.a	***0.016***	***0.03***	***0.03***	< ***0.001***	n.a	n.a	n.a
Lopez-Costas et al. (2020)										
Vienne - A Lanzada	n.a	0.54	< ***0.001***	n.a.	n.a.	n.a.	n.a.	n.a.	n.a.	n.a.

Annex 3:

Supplementary information for the research article entitled:

Human bones from a medieval alpine miners' cemetery reveal post-mortem polymetallic contamination (Brandes, France)

Table S1. *Summary of the major and trace elemental content of cortical human bones (femur and phalanges) from the Saint-Nicolas church (Brandes), Saint-Ferreol church (Huez), and Saint-Pierre church (La Garde). All the elements are reported in ug.g^{-1} and wt. %. (Ca).*

	La Garde		Huez		Brandes							
	femur + phalange		femur + phalange		femur + phalange		femur		phalange		animals	
	med	SD	med	SD	med	SD	med	SD	med	SD	med	SD
Al (µg/g)	16.59	29.17	59.86	55.56	142.33	171.49	83.31	122.66	302.17	173.19	93.54	851.40
Cr (µg/g)	1.27	0.92	0.78	0.69	0.99	1.44	0.86	0.79	1.26	1.83	0.29	0.74
Mn (µg/g)	20.68	17.30	29.62	425.56	59.09	789.58	55.20	292.03	59.09	1076.49	75.13	1012
Co (µg/g)	0.05	0.06	0.20	0.49	0.22	1.18	0.22	0.69	0.28	1.52	0.72	12.40
Ni (µg/g)	0.87	0.37	1.14	1.12	1.06	3.00	0.97	1.51	1.18	3.86	13.72	10.96
Cu (µg/g)	5.09	3.10	3.05	14.02	81.89	112.24	53.94	94.68	136.15	114.93	1272.85	19041
Zn (µg/g)	127.27	64.84	121.89	54.33	170.10	530.77	170.10	157.10	188.12	735.15	4308.08	2385
As (µg/g)	1.71	0.56	2.23	0.52	12.45	13.14	9.83	9.04	16.25	15.88	14.81	745.98
Sr (µg/g)	451.26	188.61	272.78	213.89	516.80	141.88	595.46	152.98	479.68	105.34	601.12	158.33
Ag (µg/g)	0.13	0.16	< LOD	< LOD	0.99	2.82	0.29	1.02	2.08	3.46	18.45	301.77
Cd (µg/g)	0.06	0.07	0.09	0.28	1.01	3.04	0.38	0.87	2.06	3.90	20.66	71.97
Sn (µg/g)	0.06	0.19	0.06	0.08	0.04	0.05	0.04	0.06	0.05	0.04	0.04	0.02
Sb (µg/g)	1.87	2.23	0.87	38.60	109.26	63.96	135.61	63.72	95.95	64.48	386.53	718.37
Ba (µg/g)	138.36	84.18	139.11	376.62	376.88	448.01	347.53	454.96	523.79	444.35	1101.06	2074
Au (µg/g)	0.00	0.00	0.00	0.00	0.00	0.00	0.00	0.00	0.00	0.00	0.01	0.00
Pb (µg/g)	39.49	14.48	28.47	26.65	210.95	525.51	152.21	148.30	526.22	612.33	1220.46	68255
Th (µg/g)	0.01	0.01	0.01	0.01	0.04	0.04	0.02	0.03	0.06	0.04	0.02	0.07
U (µg/g)	0.88	0.53	0.60	0.41	10.57	11.34	8.64	11.83	12.02	11.14	0.31	2.80

Table S1. (continued) *Summary of the major and trace elemental content of cortical human bones (femur and phalanges) from the Saint-Nicolas church (Brandes), Saint-Ferreol church (Huez), and Saint-Pierre church (La Garde).*

	La Garde		Huez		Brandes							
	femur + phalange		femur + phalange		femur + phalange		femur		phalange		animals	
	med	SD	med	SD	med	SD	med	SD	med	SD	med	SD
Ca (wt. %)	32.73	3.25	27.81	3.46	31.80	3.36	33.86	2.46	29.66	3.06	29.76	8.51
Ca (µg/g)	327323	32532	278130	34576	318018	33644	338600	24623	296607	30575	297598	85098
Na (µg/g)	3577.29	322.84	2750.70	964.51	2429.73	654.24	2083.07	692.34	2654.95	534.02	2134.11	452
Fe (µg/g)	11.84	54.12	36.98	66.88	50.58	138.44	30.55	70.56	80.34	167.66	41.54	8255
Mg (µg/g)	1246	976	1974	968	784	319	806	394	753	218	913	664
K (µg/g)	60.82	7.04	35.24	22.45	61.40	19.64	56.69	16.60	65.73	21.88	36.67	14.55
P (µg/g)	134432	6906	128055	17361	131120	15498	141238	11546	122857	12133	133879	27415
P (wt. %)	13.44	0.69	12.81	1.74	13.11	1.55	14.12	1.15	12.29	1.21	13.39	2.74

Table S2. *Statistical results (p values) for the Kruskal-Wallis test performed on the type of bone (femur and phalange).*

	∂^{65}Cu (‰)	Pb (µg.g^{-1})	As (µg.g^{-1})	Sb (µg.g^{-1})	Cd (ug.g^{-1})	Mn (µg.g^{-1})	Al (µg.g^{-1})	Fe (µg.g^{-1})	Cu (ug.g^{-1})	Zn (ug.g^{-1})	Sr (ug.g^{-1})
femur-phalange (Brandes only)	0.07	< ***0.001***	0.19	0.32	< ***0.001***	0.4	***0.002***	***0.002***	***0.008***	0.84	***0.02***

Table S3. *Statistical summary of the elemental ratios (Sr/Ca, Ba/Ca, Ca/P) of cortical human bones from La Garde, Huez and Brandes*

	La Garde		Huez		Brandes							
	femur + phalange		femur + phalange		femur + phalange		femur		phalange		animals	
	avr	SD	avr	SD	avr	SD	avr	SD	avr	SD	avr	SD
$\log_{10}$(Sr/Ca)	-3.03	0.27	-2.98	0.20	-2.79	0.09	-2.77	0.11	-2.81	0.08	-2.59	0.07
$\log_{10}$(Ba/Ca)	-3.91	0.96	-3.36	0.59	-2.86	0.35	-2.95	0.35	-2.77	0.33	-2.22	0.54
Ca/P	2.36	0.13	2.23	0.08	2.39	0.14	2.36	0.08	2.43	0.17	1.98	0.30

Table S4. *Anthropological information of bone samples from Brandes, Huez, and La Garde. Age groups are as follows: infant/juvenile (IJ, 0 – 20 years old), young adult (YA, 20 – 29 years old), mature adult (MA, 30 – 59 years old), old adult (OA, > 60 years old) and unknown (n.a.).*

lab ID	sample ID	article ID	Site	Bone type	Sex	Age
C-S3	S03	B1	Brandes	femur	male	IJ
C-S4b	S04	B2	Brandes	phalange	inmature	IJ
C-FS4b		B2	Brandes	femur		
C-S9	S09b	B3	Brandes	femur	inmature	IJ
C-S23	S23	B4	Brandes	phalange	male	YA
C-FS23		B4	Brandes	femur		
C-S26	S26	B5	Brandes	phalange	female	YA
C-FS26		B5	Brandes	femur		
C-S3b	S03b	B6	Brandes	phalange	male	YA/MA
C-FS3b		B6	Brandes	femur		
C-S7b	S07b	B7	Brandes	phalange	female	YA/MA
C-FS7b		B7	Brandes	femur		
C-S16	S16	B8	Brandes	phalange	male	YA/MA
C-FS16		B8	Brandes	femur		
C-S17	S17	B9	Brandes	phalange	male	YA/MA
C-FS17		B9	Brandes	femur		
C-S18	S18	B10	Brandes	phalange	male	YA/MA
C-FS18		B10	Brandes	femur		
C-S8b	S08b	B11	Brandes	phalange	male	MA/OA
C-FS8b		B11	Brandes	femur		
C-S2	S02	B12	Brandes	phalange	male	MA
C-FS2		B12	Brandes	femur		
C-GOS2	S02	B13	Brandes	phalange?	male	MA
C-S7	S07	B14	Brandes	phalange	male	MA
C-FS7		B14	Brandes	femur		
C-S8	S08	B15	Brandes	phalange	female	MA
C-FS8		B15	Brandes	femur		
C-S9,2	S09	B16	Brandes	phalange	male	OA
C-FS9,2		B16	Brandes	femur		
C-S11b	S11	B17	Brandes	phalange	male	OA
C-FS11b		B17	Brandes	femur		
C-S20	S20	B18	Brandes	phalange	female	MA
C-FS20		B18	Brandes	femur		
C-B34	S34	B19	Brandes	phalange	male	OA
C-FB34		B19	Brandes	femur		
C-GOB34	S34	B20	Brandes	phalange	male	OA
C-FSF1	Huez	HU1	Huez	femur	n.a.	n.a.
C-FSF2	Huez	HU2	Huez	femur	n.a.	n.a.
C-FSF3	Huez	HU3	Huez	femur	n.a.	n.a.
C-SFMD	Huez	HU4	Huez	phalange	n.a.	n.a.
C-SFMTTD	Huez	HU5	Huez	phalange	n.a.	n.a.

Table S4. (continued). *Anthropological information of bone samples from Brandes, Huez, and La Garde. Age groups are as follows: infant/juvenile (IJ, 0 – 20 years old), young adult (YA, 20 – 29 years old), mature adult (MA, 30 – 59 years old), old adult (OA, > 60 years old) and unknown (n.a.).*

lab ID	sample ID	article ID	Site	Bone type	Sex	Age
C-FG1	La Garde 1	LG1	La Garde	femur	n.a.	n.a.
C-G2	La Garde S	LG2	La Garde	phalange	n.a.	n.a.
C-FG2	La Garde 2	LG2	La Garde	femur	n.a.	n.a.
C-+W+27	animal	A1	Brandes		n.a.	n.a.
C-+M+N	animal	A2	Brandes		n.a.	n.a.
C-+E-10	animal	A3	Brandes		n.a.	n.a.
C-+F-9	animal	A4	Brandes		n.a.	n.a.
C-+G-9	animal	A5	Brandes		n.a.	n.a.

Table S5. *Summary of the Cu isotope composition ($^{65}Cu/^{63}Cu$, in ‰) and elemental ratios (Sr/Ca, Ba/Ca, Ca/P) of cortical bones from Brandes, Huez, and La Garde*

article ID	Bone type	$^{65}Cu/^{63}Cu$ (‰)	log_{10}(Sr/Ca)	log_{10}(Ba/Ca)	Ca/P
B1	femur		-2.86	-2.49	2.23
B2	phalange	0.172	-2.80	-2.40	2.40
B2	femur	0.108	-2.70	-3.18	2.40
B3	femur		-2.54	-2.98	2.47
B4	phalange		-2.88	-2.49	2.40
B4	femur		-2.76	-2.56	2.32
B5	phalange		-2.81	-2.53	2.35
B5	femur		-2.75	-2.70	2.40
B6	phalange		-2.74	-3.23	2.56
B6	femur		-2.72	-3.20	2.37
B7	phalange		-2.80	-2.99	2.41
B7	femur		-2.79	-2.97	2.28
B8	phalange		-2.76	-2.68	2.38
B8	femur		-2.85	-3.26	2.35
B9	phalange	-0.045	-2.92	-3.28	2.44
B9	femur	0.241	-2.68	-3.08	2.44
B10	phalange	-0.092	-2.74	-2.38	2.40
B10	femur	-0.049	-2.82	-2.23	2.34
B11	phalange		-2.82	-3.03	2.40
B11	femur		-2.73	-3.31	2.38
B12	phalange		-2.99	-2.86	2.23
B12	femur		-2.89	-2.93	2.22
B13	phalange?		-2.82	-2.48	2.21
B14	phalange	0.011	-2.74	-2.38	2.33
B14	femur	0.103	-2.79	-2.57	2.38
B15	phalange		-2.86	-2.56	2.27
B15	femur		-2.83	-2.80	2.25
B16	phalange	-0.111	-2.81	-2.93	2.41
B16	femur	0.021	-2.71	-3.30	2.44
B17	phalange		-2.76	-3.06	2.88
B17	femur		-2.82	-3.33	2.42
B18	phalange	0.026	-2.92	-3.31	2.82
B18	femur	0.060	-3.03	-3.52	2.34
B19	phalange	-0.223	-2.72	-2.93	2.46
B19	femur	0.015	-2.65	-2.77	2.43
B20	phalange	-0.016	-2.70	-2.42	2.43
HU1	femur	0.034	-2.90	-3.59	2.17
HU2	femur	-0.094	-3.22	-4.18	2.16
HU3	femur		-2.69	-2.57	2.24
HU4	phalange	-0.215	-2.98	-3.17	2.36
HU5	phalange		-3.11	-3.30	2.24

Table S5. (continued). *Summary of the Cu isotope composition ($^{65}Cu/^{63}Cu$, in ‰) and elemental ratios (Sr/Ca, Ba/Ca, Ca/P) of cortical bones from Brandes, Huez, and La Garde*

article ID	Bone type	$^{65}Cu/^{63}Cu$ (‰)	log_{10}(Sr/Ca)	log_{10}(Ba/Ca)	Ca/P
LG1	femur		-3.34	-5.02	2.21
LG2	phalange	-0.205	-2.87	-3.34	2.44
LG2	femur	-0.258	-2.86	-3.37	2.43
A1			-2.70	-2.43	2.24
A2			-2.59	-2.74	2.15
A3			-2.50	-2.02	1.79
A4			-2.55	-1.38	1.54
A5			-2.63	-2.51	2.17

Table S6. *Summary of the major elemental content of cortical human bones from Brandes, Huez, and La Garde. All elements are reported in µg.g^{-1}*

article ID	Bone type	Ca (wt. %)	Ca (µg/g)	Na (µg/g)	Fe (µg/g)	Mg (µg/g)	K (µg/g)	P (µg/g)	P (wt. %)
B1	femur	34.6	346482.8	1618.0	238.3	315.7	68.5	155241.5	15.5
B2	phalange	37.5	374972.0	1791.8	36.4	832.6	59.8	155977.3	15.6
B2	femur	34.6	346113.4	1412.7	41.2	602.5	54.7	144445.1	14.4
B3	femur	34.0	339662.5	1288.7	68.7	661.9	86.8	137287.9	13.7
B4	phalange	25.9	259274.3	2655.2	111.2	761.0	67.0	107931.8	10.8
B4	femur	33.2	332362.6	1977.6	8.7	981.3	61.0	143465.3	14.3
B5	phalange	27.6	276241.0	2622.2	45.8	874.9	63.6	117564.0	11.8
B5	femur	34.3	342875.5	1738.2	24.3	794.1	49.2	143159.6	14.3
B6	phalange	27.1	271066.4	2506.8	559.7	473.9	26.2	105708.8	10.6
B6	femur	33.4	334410.1	1659.0	75.5	660.2	40.0	141355.8	14.1
B7	phalange	30.9	309197.4	2746.1	50.6	613.9	36.5	128439.9	12.8
B7	femur	32.1	321251.4	2700.5	16.8	921.4	56.9	141121.0	14.1
B8	phalange	31.1	311255.5	2294.3	199.1	672.7	89.8	130856.2	13.1
B8	femur	34.1	340864.5	2173.7	n.a.	775.2	32.8	145330.5	14.5
B9	phalange	27.9	278606.5	3810.1	7.2	1184.9	50.3	114245.0	11.4
B9	femur	34.3	342680.0	2171.4	5.6	903.1	55.2	140237.4	14.0
B10	phalange	30.4	303532.6	2839.7	254.6	736.9	80.3	126466.6	12.6
B10	femur	30.6	306067.3	2863.5	233.0	922.6	94.9	130872.1	13.1
B11	phalange	27.6	275824.9	3405.6	21.0	831.9	95.3	115114.0	11.5
B11	femur	33.2	332058.7	2352.7	27.2	1063.6	80.4	139414.1	13.9
B12	phalange	29.0	289603.1	2737.0	52.4	370.6	74.5	129858.6	13.0
B12	femur	34.6	345644.5	1911.1	35.8	382.6	61.8	155558.2	15.6
B13	phalange?	27.2	272084.3	2542.4	499.8	462.4	81.7	123092.0	12.3
B14	phalange	31.3	312751.5	2215.5	216.9	869.5	50.8	134201.2	13.4
B14	femur	41.1	411377.9	3074.8	22.8	1169.6	49.0	172763.5	17.3
B15	phalange	25.8	258334.9	3186.0	53.9	1028.3	53.7	113898.4	11.4
B15	femur	35.1	351119.9	1994.8	12.4	714.3	42.3	156343.8	15.6

Table S6. (continued). *Summary of the major elemental content of cortical human bones from Brandes, Huez, and La Garde. All elements reported in µg.g^{-1}*

article ID	Bone type	Ca (wt. %)	Ca (µg/g)	Na (µg/g)	Fe (µg/g)	Mg (µg/g)	K (µg/g)	P (µg/g)	P (wt. %)
B16	phalange	30.3	302920.1	2654.7	21.8	860.1	87.9	125852.6	12.6
B16	femur	33.8	337538.3	1939.9	42.3	925.0	76.6	138367.1	13.8
B17	phalange	35.3	353279.5	1811.7	106.1	498.0	55.6	122622.4	12.3
B17	femur	31.8	317525.4	2871.7	11.8	819.8	56.5	131136.6	13.1
B18	phalange	30.0	300002.1	3278.0	54.5	1038.1	64.5	106571.8	10.7
B18	femur	28.9	289392.7	4121.4	30.6	2183.0	49.1	123567.0	12.4
B19	phalange	29.3	293212.1	3185.5	214.3	640.6	94.1	119092.6	11.9
B19	femur	31.9	318512.4	2210.9	58.2	694.0	69.7	131103.6	13.1
B20	phalange	31.9	318736.5	2248.9	371.3	745.9	108.9	131373.8	13.1
HU1	femur	31.3	313262.0	2460.2	24.1	2724.0	43.5	144355.2	14.4
HU2	femur	27.7	276676.7	2891.3	5.1	3157.7	35.2	128055.2	12.8
HU3	femur	34.8	347511.3	1477.5	37.0	668.7	19.7	155179.3	15.5
HU4	phalange	26.2	262253.2	4163.5	72.9	1974.2	77.0	110916.8	11.1
HU5	phalange	27.8	278130.4	2750.7	173.7	1651.5	26.0	124421.5	12.4
LG1	femur	28.0	279613.0	3577.3	4.5	1246.8	57.8	126476.6	12.6
LG2	phalange	34.2	341780.9	3433.0	101.7	989.2	60.8	140233.3	14.0
LG2	femur	32.7	327323.7	4050.2	11.8	2793.8	71.2	134433.0	13.4
A1		29.9	299338.9	2646.5	28.7	2159.7	36.7	133879.5	13.4
A2		29.8	297598.6	2145.3	131.9	685.2	23.7	138583.1	13.9
A3		16.0	160046.8	1439.2	41.5	442.8	26.9	89272.9	8.9
A4		13.4	133680.4	1771.3	18518.7	913.8	56.0	87018.5	8.7
A5		30.7	306583.8	2134.1	37.6	1194.8	52.2	141358.3	14.1

Table S7. *Summary of the trace elemental content of cortical human bones from Brandes, Huez, and La Garde. All elements reported in µg.g^{-1}*

article ID	Bone type	Al (µg/g)	Cr (µg/g)	Mn (µg/g)	Co (µg/g)	Ni (µg/g)	Cu (µg/g)	Zn (µg/g)	As (µg/g)
B1	femur	213.6	0.9	32.8	0.2	2.8	47.1	190.8	1.4
B2	phalange	322.5	1.9	13.4	0.2	0.6	94.3	137.4	13.3
B2	femur	51.5	0.9	514.0	0.9	2.2	80.1	168.2	27.1
B3	femur	179.9	1.5	72.9	0.2	1.9	94.5	172.0	19.9
B4	phalange	131.1	1.2	88.5	0.1	1.1	64.4	107.7	9.6
B4	femur	31.3	0.8	14.9	0.1	0.3	20.7	149.6	3.8
B5	phalange	210.2	1.6	11.2	0.1	0.5	79.6	130.3	5.0
B5	femur	61.4	1.3	2.6	0.1	0.6	43.4	132.8	4.6
B6	phalange	272.1	0.7	4601.7	6.5	7.7	258.6	3296.4	65.5
B6	femur	153.6	0.7	1135.2	2.8	5.2	109.7	761.1	15.0
B7	phalange	331.3	1.3	26.9	0.2	0.3	228.3	152.2	21.4
B7	femur	85.3	0.3	37.5	0.1	0.5	24.4	185.4	3.6
B8	phalange	669.8	2.3	66.6	0.4	1.3	396.5	428.4	15.4
B8	femur	8.0	0.2	0.3	0.0	0.3	9.0	107.6	11.5
B9	phalange	68.0	0.5	51.5	0.2	0.4	26.6	107.7	17.1
B9	femur	40.8	1.6	11.1	0.1	0.4	47.0	106.0	25.1
B10	phalange	541.9	3.0	263.1	0.4	2.1	200.4	224.0	6.5
B10	femur	367.1	3.5	7.3	0.2	1.8	215.9	184.0	2.1
B11	phalange	281.9	0.5	886.2	1.3	6.9	74.5	291.1	17.6
B11	femur	85.9	0.6	140.3	0.3	0.9	16.3	142.2	11.6
B12	phalange	86.5	0.8	161.2	0.3	3.9	191.0	420.3	0.9
B12	femur	61.8	0.8	76.7	0.2	2.9	76.1	209.1	1.0
B13	phalange?	438.0	8.4	42.4	0.4	13.7	160.8	249.4	1.5
B14	phalange	353.6	2.6	41.3	0.2	1.1	97.1	123.1	3.6
B14	femur	76.7	1.1	80.2	0.2	0.7	69.3	432.9	2.7
B15	phalange	75.6	0.9	12.7	0.1	0.4	23.2	93.2	5.0
B15	femur	15.3	0.1	4.1	0.0	0.3	8.8	134.9	1.4

Table S7. (continued). *Summary of the trace elemental content of cortical human bones from Brandes, Huez, and La Garde. All elements reported in ug.g^{-1}*

article ID	Bone type	Al (µg/g)	Cr (µg/g)	Mn (µg/g)	Co (µg/g)	Ni (µg/g)	Cu (µg/g)	Zn (µg/g)	As (µg/g)
B16	phalange	123.9	0.4	342.2	0.4	1.7	83.7	370.4	18.4
B16	femur	127.3	1.9	185.5	0.3	2.1	133.4	121.4	18.0
B17	phalange	346.7	2.1	13.5	0.3	0.4	237.2	135.9	40.4
B17	femur	103.4	0.6	264.5	0.5	1.0	50.0	293.2	15.4
B18	phalange	171.7	0.5	18.0	0.2	0.8	111.5	118.3	20.3
B18	femur	81.3	0.4	24.2	0.1	0.9	57.8	141.9	8.1
B19	phalange	346.2	1.0	488.1	1.9	5.9	338.2	272.0	31.5
B19	femur	475.3	1.3	552.5	1.4	4.8	403.1	247.6	24.3
B20	phalange	529.2	2.3	941.8	1.4	9.0	358.1	239.5	18.7
HU1	femur	12.7	2.0	29.6	0.7	1.1	2.3	121.9	2.4
HU2	femur	2.0	0.1	16.8	0.2	0.7	3.0	80.5	1.5
HU3	femur	59.9	0.5	13.6	0.1	0.5	34.7	127.4	2.2
HU4	phalange	63.2	0.8	56.5	0.1	1.8	1.8	96.4	1.3
HU5	phalange	142.5	0.8	980.0	1.2	3.3	7.9	220.3	2.4
LG1	femur	14.2	0.0	48.1	0.0	0.4	3.9	224.5	1.2
LG2	phalange	65.9	1.3	20.7	0.1	1.2	5.1	101.5	2.3
LG2	femur	16.6	1.8	16.1	0.1	0.9	9.8	127.3	1.7
A1		44.7	0.3	6.6	0.1	13.7	416.1	235.8	4.4
A2		236.5	0.4	66.3	0.7	18.3	867.4	4308.1	3.7
A3		93.5	0.2	449.3	20.8	2.7	41476.0	4683.4	201.0
A4		1992.3	1.9	2378.5	24.8	1.2	27296.6	1592.0	1713.5
A5		16.8	0.2	75.1	0.2	27.4	1272.8	6047.3	14.8

Table S8. *Summary of the trace elemental content of cortical human bones from Brandes, Huez, and La Garde. All elements are reported in ug.g^{-1}*

article ID	Bone type	Sr (µg/g)	Ag (µg/g)	Cd (µg/g)	Sn (µg/g)	Sb (µg/g)	Ba (µg/g)	Pb (µg/g)	Th (µg/g)	U (µg/g)
B1	femur	477.9	2.0	0.4	0.0	60.7	1126.0	127.7	0.1	0.2
B2	phalange	594.0	1.7	2.2	0.0	103.9	1506.0	509.2	0.0	12.7
B2	femur	688.4	3.6	0.5	0.0	251.5	229.7	310.0	0.0	16.4
B3	femur	984.5	0.1	0.4	0.3	202.3	354.4	168.3	0.0	20.6
B4	phalange	341.0	1.0	0.7	0.0	33.6	839.6	174.0	0.0	17.2
B4	femur	579.9	0.2	0.1	0.0	54.0	919.5	38.7	0.0	1.7
B5	phalange	428.3	2.5	1.1	0.1	96.0	818.5	533.1	0.0	9.1
B5	femur	611.0	0.2	0.1	0.0	133.3	680.5	38.8	0.0	7.3
B6	phalange	497.9	11.3	15.2	0.1	251.5	160.2	903.2	0.1	19.3
B6	femur	642.9	1.7	3.8	0.0	217.2	211.3	622.9	0.0	32.4
B7	phalange	485.5	1.7	4.7	0.0	156.3	315.3	1125.5	0.0	14.1
B7	femur	515.8	0.1	0.9	0.0	111.5	340.6	153.5	0.0	7.0
B8	phalange	536.0	6.4	11.1	0.0	150.0	648.3	1907.1	0.1	40.7
B8	femur	484.0	0.2	0.1	0.0	176.3	189.4	11.2	0.0	3.7
B9	phalange	338.6	0.2	0.3	0.2	73.8	145.4	204.1	0.0	8.9
B9	femur	716.8	0.1	0.1	0.0	219.3	282.7	217.8	0.0	37.2
B10	phalange	549.3	3.1	2.2	0.1	42.9	1267.6	614.3	0.1	34.4
B10	femur	460.8	2.4	1.1	0.0	40.5	1799.9	66.9	0.1	14.4
B11	phalange	417.9	0.6	1.6	0.1	92.5	257.1	132.8	0.0	6.9
B11	femur	617.3	0.2	0.4	0.0	137.9	161.0	125.3	0.0	4.3
B12	phalange	299.7	4.3	1.3	0.1	95.9	399.3	182.3	0.1	0.2
B12	femur	445.4	1.2	0.4	0.1	81.0	408.4	37.8	0.1	0.1
B13	phalange?	407.2	10.1	2.3	0.1	76.6	892.8	430.4	0.2	0.3
B14	phalange	570.6	3.1	1.3	0.1	80.7	1305.7	519.3	0.1	6.6
B14	femur	663.7	0.4	0.6	0.2	111.5	1096.9	150.9	0.0	11.2
B15	phalange	360.1	0.7	0.3	0.1	79.7	709.2	109.1	0.1	1.0
B15	femur	517.8	0.1	0.2	0.0	77.9	560.8	95.9	0.0	0.2

Table S8. (continued). *Summary of the trace elemental content of cortical human bones from Brandes, Huez, and La Garde. All elements are reported in ug.g^{-1}*

article ID	Bone type	Sr (µg/g)	Ag (µg/g)	Cd (µg/g)	Sn (µg/g)	Sb (µg/g)	Ba (µg/g)	Pb (µg/g)	Th (µg/g)	U (µg/g)
B16	phalange	473.8	0.2	2.2	0.1	133.8	353.2	404.2	0.1	11.4
B16	femur	655.3	0.4	0.2	0.1	167.5	170.4	175.1	0.1	26.4
B17	phalange	615.3	0.7	2.0	0.1	286.2	310.8	1253.9	0.0	17.7
B17	femur	484.8	1.0	1.3	0.0	181.1	149.2	311.6	0.0	10.0
B18	phalange	363.3	0.3	0.7	0.0	93.9	145.7	720.2	0.0	5.7
B18	femur	269.1	0.1	0.4	0.2	73.0	87.1	187.4	0.1	6.5
B19	phalange	559.2	7.0	3.4	0.1	128.3	345.4	1991.0	0.1	22.6
B19	femur	719.9	1.5	1.3	0.0	139.6	540.4	342.1	0.0	29.3
B20	phalange	636.3	6.3	3.3	0.1	107.1	1208.5	1716.5	0.1	22.8
HU1	femur	395.0	<0,000	0.0	0.1	0.4	81.0	28.5	0.0	0.3
HU2	femur	167.4	<0,000	0.0	0.0	0.4	18.3	6.3	0.0	0.0
HU3	femur	702.6	<0,000	0.4	0.0	87.0	935.4	71.6	0.0	0.8
HU4	phalange	272.8	<0,000	0.1	0.2	0.9	178.6	33.1	0.0	1.1
HU5	phalange	218.3	<0,000	0.6	0.1	1.1	139.1	6.8	0.0	0.6
LG1	femur	127.1	0.0	0.0	0.1	0.1	2.7	47.6	0.0	0.0
LG2	phalange	456.3	0.4	0.1	0.0	4.5	156.9	19.5	0.0	0.9
LG2	femur	451.3	0.1	0.2	0.4	1.9	138.4	39.5	0.0	1.0
A1		601.1	10.0	1.4	0.0	331.0	1101.1	176.8	0.0	1.0
A2		769.3	18.5	20.7	0.1	386.5	537.8	1220.5	0.1	0.1
A3		501.7	119.9	152.4	0.0	435.6	1541.8	41492.2	0.0	0.2
A4		378.0	708.5	133.6	0.1	1955.3	5601.3	158108.1	0.2	6.5
A5		713.7	17.2	16.3	0.0	267.4	951.3	75.7	0.0	0.3

Figure S1. *Photograph of a green-stained animal bone sample from the site of Brandes.*

Annex 4:

Lead and mercury mining pollution over the last 2500 years in Europe: deciphering the contribution of Central and Eastern regions from western ones

This paper is in preparation for submission in: *Science Advances*

Lead and mercury mining pollution over the last 2500 years in Europe: deciphering the contribution of Central and Eastern regions from western ones

C. Heredia[1], S. Guédron[1*], D. Veres[2*], P. Sabatier[3], J. Longman[4], C. Chauvel[5], C. G. Tamas[6], F. Gogaltan[7], S. Campillo[1], A.-L. Develle[3], P. Telouk[8], and A.T. Gourlan[1]

[1] Univ. Grenoble-Alpes, Univ. Savoie Mont Blanc, CNRS, IRD, IFSTTAR, ISTerre, 38000 Grenoble, France

[2] Romanian Academy, Institute of Speleology, Clinicilor 5, 400006 Cluj-Napoca, Romania.

[3] EDYTEM, Université Savoie Mont-Blanc, CNRS, Le Bourget du Lac, France.

[4] Department of Geography and Environmental Sciences, Northumbria University, NE1 8ST Newcastle-upon-Tyne, United Kingdom

[5] Université Paris Cité, Institut de Physique du Globe de Paris, CNRS, UMR 7154, F-75005 Paris, France

[6] University Babeş-Bolyai – Faculty of Biology and Geoology, 1, M. Kogălniceanu, 400084 Cluj-Napoca, Roumania.

[7] Institutul de Arheologie şi Istoria Artei Cluj-Napoca, Romania.

[8] Laboratoire de Géologie de Lyon (LGL-TPE), Ecole Normale Supérieure de Lyon, Lyon, France.

*Corresponding author:

Stéphane Guédron and Daniel Veres

Abstract

Published environmental records commonly attribute the North hemisphere lead (Pb) and mercury (Hg) pollution signals to western Europe. Recent studies have documented central-eastern Europe as an important mining and metallurgy region, which differed in chronology and intensity from Western Europe. Here, the combination of metal accumulation rates, enrichment factors, and isotopic fingerprinting in five new records from the Balkans and Carpathians clearly assess the contribution of these sources at the local and regional scales. Records from the Carpathians testify to almost continuous and intense mining activity over the past 2,000 years, with trends independent of the main mining periods known in Western Europe. Notably, major mining activities in the Carpathians (i.e. Early Middle Ages) are only recorded in the central and eastern Alps but not in the western Alps, likely masked by trade winds. This demonstrates that this often-ignored source has surely contributed significantly to hemispheric or global metal emissions.

Introduction

The mastery of mineral extraction and metallurgical techniques was fundamental in the development of ancient societies around the world (1, 2). Extractive metallurgy began with the cold processing of native metals such as copper (Cu) and lead (Pb) ores between the 11th and 8th millennia BCE) in Southwestern Eurasia, i.e., the Fertile Crescent and Anatolia (3, 4). The smelting of metal expended between the 6th and 5th millennium BCE throughout Southwest Asia and Southeast Europe (3), with earliest Cu, gold (Au), silver (Ag) and Pb metallurgy reported in the Balkans (1, 5, 6). Metallurgical technology progressively spread over central-western Europe culminating in the mid-third millennium BC (7, 8). Along this multi-millennial history, numerous technological

inventions and innovations in high-temperature metallurgical technologies have enabled the separation of metals from their ores, and the creation of new alloys (9).

Industrialization of metallurgy started from the end of the Bronze Age (first millennium BCE) onward with the Greek and Phoenician societies (10, 11), and reached their apogee throughout the Carthaginian and Roman Empires (12). Because of the heterogeneous distribution of ore deposits across Europe, the growing demand for metals in these Empires have resulted in the development of trading networks across the Mediterranean and over Europe to sustain the central power (13). Amongst non-ferrous metals, Au, Ag, Cu and tin (Sn) were exploited for coinage production or luxury artefacts (12, 14), whereas others like Pb were mainly used for the development of urban water distribution systems by lead pipes (15, 16). Along the last three millennia, the magnitude of metallurgical activities in Europe varied through space and time in relation with regional political, economic and social contexts (e.g., empire or state expansion, wars, invasions, and major plagues) together with climate oscillations.

Because ore extraction and metallurgical activities release gaseous and particulate trace metals (i.e., Pb, Hg, Sb…) to the atmosphere, it makes possible the detailed record of historical metallurgy imprints in environmental archives. Numerous records have documented past metal pollutions across the continent, including ice cores (17, 18), and sediment cores from lakes (19-21), seas (22-24), and mires (25-28). Most of these studies have been performed in western Europe, and provide a coherent understanding of the timing and intensity of mining and metallurgical activities. These records inform that for the last 3 millennia, major metallurgical centers in western Europe (i.e., Iberia, the Alps, Great Britain and Scandinavia) were principally exploited during the Roman Empire (ca. 200BCE to 200 CE), the Late Medieval period (900 to 1400 CE), and the Modern Period (1700 CE to the modern days).

In contrast, much less is known about the history of mining and metallurgy in major polymetallic ore fields of Central - Eastern Europe, such as the Carpathian and Balkan regions, two regions considered the birthplace of mineral resource exploitation and metalworking in Europe. For instance, the Metaliferi mining district in the Apuseni Mountains (Romania) is the largest known gold and silver (Au-Ag) deposit in Europe (29). Archaeological studies have documented Cu smelting (9) and lead ore processing (9) in the region since prehistoric times, followed by a great increase during the late Bronze Ages (ca. 1600 to 1100 BCE), and a bloom during the late Iron Age - Dacian period (650 BCE – 160 CE) and the Romans (106 – 272 CE) with an estimation of 498 tons of Au and 950 t Ag extracted in the Northern Apuseni Mountains (30). Although important productions of Pb ores rich in Au and Ag are reported for the 12^{th} and 13^{th} centuries, little is known about the length, duration, and intensity of the mining and metallurgical activities, whereas this type of information is better constrained in Western Europe for a long time. In the Balkans, a recent peat record from Serbia (28) showed evidences of large-scale and intense metallurgically derived Pb emissions from 600 BCE, through the Roman/Byzantine periods, and into the medieval period. The record also indicated punctual drops in Pb pollution attributed to the disruptive socioeconomic impact in significantly different periods to those recorded in western Europe.

Sedimentary archives are useful tools for reconstructing past trace metal deposition (31). Ombrotrophic peat bogs are preferentially used for the record of atmospherically-mediated deposition because they are hydrologically isolated from surface and groundwater influence (25, 32, 33). In contrast, lacustrine sediments record both atmospheric and catchment weathering signals (34). While trace metal accumulation rates (ARs) records provide information about the intensity of deposition during a given period, their isotopic composition can document their sources, and allow the apportionment of

several sources (35-37). In particular, the combination of Pb isotope fingerprinting techniques (i.e., comparison of raw isotope ratios) with geological age of the tectonic province in which the ores formed (i.e., U/Pb (m) and Th/U (k) ratios), allows tracking metal provenance even in the absence of isotopic data on reference ores (36). Complementarily, the comparison of an elemental ARs with a conservative crustal element allows to assess the contribution of anthropogenic relative to geogenic sources (20, 38).

In this study, we present two high-resolution ombrotrophic peat and one Lake records from the Carpathians (Romania) to reconstruct the past anthropogenic pollution associated with mineral exploitation in central-eastern Europe. In order to discriminate the local contribution from the regional ones coming from the west (westerlies) and the south (northerlies), we then compare these records with two new lake sediment records from north-western Balkans (Slovenia).

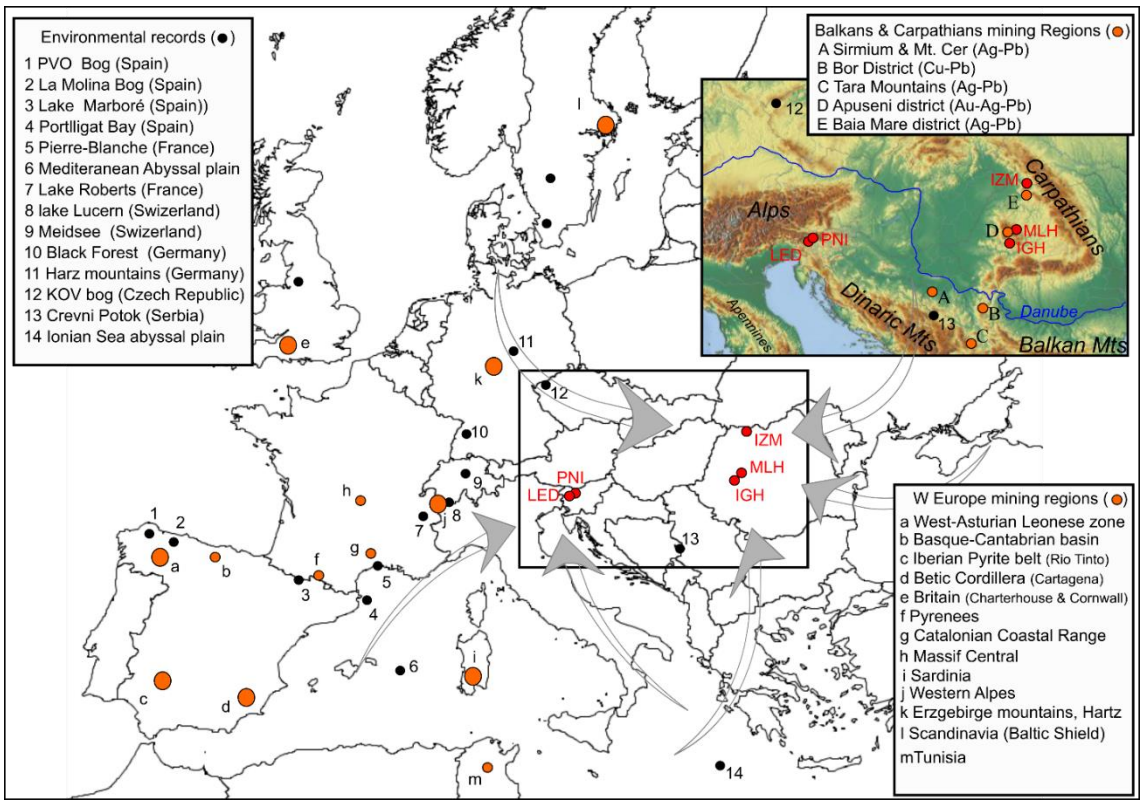

Figure 1. *Map of Europe indicating the location of the sites studied here (red dots), published records (black dots) from various remotes sites, and major documented*

historical mining districts/regions (orange dots). The arrows indicate the trade wind trajectoires flowing to the Balkans and Carpathians areas, i.e., air masses from the Mediterranean basin (SW/S and SE/S), the eastern continental Europe (E and SE), and the Northern Sea and Scandinavia (NW, during wintertime) (39). Top right panel shows the location of studied sites together with main mining areas reported for the last past 3000 years in central Europe.

Results and Discussion

Historical mining and metallurgy in the Carpathians

To document the history of mining and metallurgy in the Carpathians, three cores were collected at i) the Iezerul Mare (IZM) mire, i.e., near the Baia Mare mining field, ii) at the Mluha (MLH) mire, in the Apuseni (also called Metaliferi) Mountains near Roşia Montană, and iii) at lake Ighiel (IGH) a lake located downwind the main Au and Hg ore deposits exploited by the Romans, i.e., city of Ampellum (now called Zlatna) (Fig. 1). Ore deposits known in the Metalliferous Mountains districts consist of porphyry copper and Au-Ag epithermal deposits related to both Mezozoic and Neogene volcanism/magmatism (40, 41).

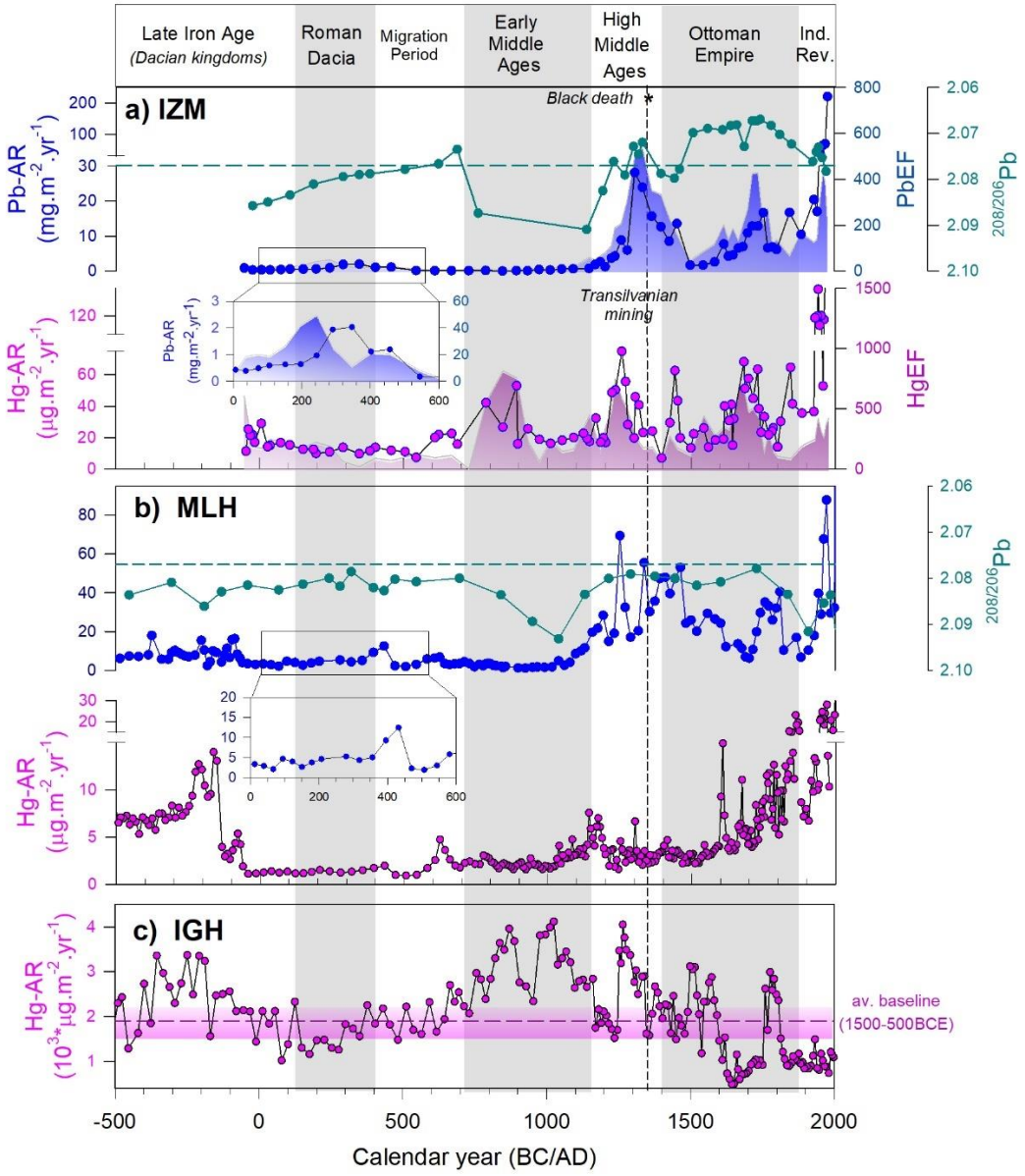

Figure 2. *Lead (Pb) and mercury (Hg) accumulation rates (AR, left Y axes), enrichment factors (EF, right Y axes) relative to background concentration normalized to Ti, and Pb isotopes ($^{208/206}$Pb) in the two Carpathian mires (axes reversed); A) Iezerul Mare mire (IZM), and Mluha (MLH), and C) Lake Ighiel (IGH) sediment records. Red dotted line shows the averaged $^{208/206}$Pb value [2.07787 ± 0.00148 (1σ)] reported for Au-Ag ores mined by the Roman in the Apuseni Mountains (41). Note that axes for $^{208/206}$Pb values are reversed.*

The three Carpathians records bear similarities in the timing of Pb and Hg signals when both elements are taken separately. However, Pb and Hg signals exhibit asynchronous increases, which are probably linked to ore extraction from distinct mining districts and metallurgical activities, or from external sources.

During the late Iron age (600 to 200 BCE), Pb accumulation rates (ARs) and enrichment factors (EFs) are low and stand around the geochemical background values (i.e., < 1 mg m-2 yr-1) reported over Europe (19, 42) with small peaks in PbARs in the MLH record suggesting several episodes of short duration Ag/Pb mining in the region. In contrast, HgARs depict sharp increases in both the MLH and IGH records between 300 and 100 BCE. This period coincident with the Dacian kingdoms, a period of extensive gold extraction in the "Golden Quadrangle" of the Apuseni Mountains (30, 43). Around 30 km south of Roşia Montană, the Zlatna district is the major local source of cinnabar ore of the region (44). Mercury accumulation rates in the Lake Ighiel (IGH) record, located few km from the Zlatna district, testify for major Hg release to the lake being an order of magnitude higher than reported Hg records in European lake sediment (19, 20, 45), but in the range of those reported for Almaden Hg district sediment (46). The significant ($p<0.05$) increase in HgARs at that time (2.5 ± 0.4 mg m-2 yr-1) compared to previous three centuries (1.9 ± 0.3 mg m-2 yr-1) corroborates historical studies that reported Hg extraction for Au amalgamation at Roşia Montană (47, 48).

From 160 to ca 300 CE, PbARs return to their baseline values until the 4th century CE where small but significant increases are found in both IZM (290-450 CE) and MLH (350- 450 CE) records (zooms in Fig. 2). In contrast, HgARs stand around their baseline values for the three records during this entire period. This period coincides with the Roman occupation of Dacia (106-276 CE), a period known for intense mining in the Apuseni Mountains with a total production estimated of about 498 t Au and 950 t Ag (30). Notably, extensive underground Roman mining has been reported in Roşia Montană during the 2nd and 3rd centuries CE (41). Such intense underground activities in the Metaliferi Mountains may explain the low amplitude of the Pb signal compared to the previous period at MLH. Consistently, changes in gold extraction and treatment (i.e.,

litharge and cupellation) by the Romans, also have probably reduced the use of Hg and its release to the atmosphere.

After the Roman retreat from the Dacia, from the 3rd century CE onward, the region became unstable during successive east and west-ward migrations. During this period, both Pb and Hg ARs remain around their respective baseline values, with the exception of moderate increases in HgARs, synchronous at IZM and MLH, followed by a rise at the end of this period (i.e., 5th and 7th century CE). This likely reflects a general cease in mining activities in the region with temporary occupation of the areas and mining activities (30). The following Early Middle Age, depict a similar trend for Pb, which stands on its baseline values. In contrast, Hg signal exhibits sharp increases with distinct periodicity and amplitude between the Northern and Southern Carpathians. To the north, a sharp increase in Hg ARs in the IZM record between ca. 650 and 900 CE is synchronous with the IGH one. In opposition, the signal remains low at MLH until 1000 CE followed by a gradual rise to the transition with the High Middle Ages period. The low Hg signal at MLH but high at IGH, hence suggests that Hg was extracted in the Zlatna district, and probably exported to other districts such as the Transylvanian basin for Au mining.

The main and synchronous rises in both Pb and Hg ARs and EFs are found for the three sites during the High middle Ages. All signals converge towards a general increase peaking during the 13th century CE. This period is known as the Transylvanian mining era, when the lead ores rich in Au and Ag where mined at Baia Mare and in the Rodna Massif (30). At that time, the mining of the non-metalliferous resources developed constantly and was stimulated by the more liberal policy towards the manufacturing activities. This period is interrupted by a sharp drop in both Pb and Hg ARs following of the black death event (1347 CE) in all records, peaking again during the middle of the following century before it gradually returns to baseline values at the onset of the Ottoman

occupation. The black plague pandemic period, i.e., from 1347 to 1352, also called "Black Death" originating from central Asia, killed between 25 and 30 million people (49). After entering Europe via the ports of Italy (50), it spread unchecked but spatially heterogeneous (51), and devastated more severely western medieval Europe than central Europe (52). Such massive deaths in western Europe resulted in breakdown of social structure and economy (including mining) of society. In central-eastern Europe, this period also coincides with the Mongol invasion (1240 – 1242 CE) that devastated the region, with strong economic and social consequences resulting in a major crisis (53, 54). The abrupt and synchronous declines recorded in the 3 records during this mining period therefore suggest that the Carpathian region has been significantly affected by the Mongol invasion and probably the pandemic too. Finally, all signals rebound at the end of the 17th century, during a period characterized by major technological progress allowing the extraction of deeper ore deposits and the building of metallurgical factories for Pb, Cu, Au, and Ag processing and separation (30). The annual Au production in Transylvania increased in the interval 1770-1841 from several hundred kilograms to 1,200 kg. Mining and metallurgy continuously increased from that time in the region and most mines for gold and salt were transferred in the state ownership between 1848-1918 CE.

Within both IZM and MLH records, Pb isotopes greatly document local mining. During mining periods (i.e., Dacian Kingdoms, Roman Dacia, Middle Age and Hungarian/Transylvanian mining epochs) sediments records exhibit shifts towards average $^{208/206}$Pb values for Carpathians ores (2.07787 ± 0.00148 (1σ)), whereas periods of reduced mining and metallurgical activities (i.e., Late Iron Age, Early Middle Ages, and onset and end of the Ottoman Empire), $^{208/206}$Pb rise to higher isotopic ratios around 2.09 ± 0.005 typical of the regional geological background. Hence, both Pb isotope records demonstrate that Pb signal is almost entirely originating from local mining, and

that extractive activities were intense and almost continuous during the last past 2500 years in the Carpathians.

Historical mining and metallurgy in the Balkans

In contrast to the Carpathian region, the lower Danube, i.e., the Balkan region, displays different political and mining/metallurgical histories. To complement a previous reconstruction performed in Serbia [Crveni Potok, eastern Balkans (28)], we here provide new data from Lakes Ledvicah (LED) and Planina pri jezeru (PNI) located in the Julian Alps (North-west Slovenia, Fig.1). Lakes LED (1850 m.a.s.l.) and PNI (1430 m.a.s.l.) are both relatively small and deep (2.2 ha, 14 max depth and 1.5 ha, 11 max depth, respectively), with respective catchment areas of 175 ha and 95 ha. The region receives annual rainfall between 2500 and 3000 mm through the alpine regime (55, 56).

From 500 BCE to 200 CE, both Lakes LED and PNI sediment records exhibit slight increases in Pb and Hg ARs and EFs (Fig. 3). Mining activities (Au, Pb and Fe) by both Illyrian and Celtic tribes such as the Tauriscans (57, 58) have been reported during the Late Iron Age, followed by the Romans who conquered the region during the 1st century BCE (59). Such Pb increase in the LED record thus reflect the extent of Roman mining and smelting throughout the Balkans consistently with the Crveni Potok record (28), as well as at the alpine scale (19, 20). The synchronous increase in Hg ARs in the LED record during this period suggests a common mining and metallurgical source for both metals during the Roman era.

From the decline of the western Roman empire (450 CE) to the early middle age, both Pb and Hg signals return to baseline values for at least 400 years. This period corresponds to the Late Antiquity crisis, a period of invasions (i.e., the Slavs) and warfare when populations living in the area either migrated to regions outside the borders or retreated to naturally well-protected peaks that were additionally fortified (60, 61). This low Pb

and Hg ARs period last until the 13th century with the exception of a gradual and small increase in Pb ARs recorded at LED during the Early Middle Age (EMA) to the onset of the Serbian kingdoms, i.e., between the 9th and the 12th centuries, whereas Hg only exhibit little variations. This Pb signal contrasts with the Serbian record of Crveni Potok, and suggests that increased mining Pb signal recorded in the eastern Balkans was probably local and not recorded in the western Balkans. This signal becomes, however, synchronous in the two regions from the onset of the Serbian Kingdom period.

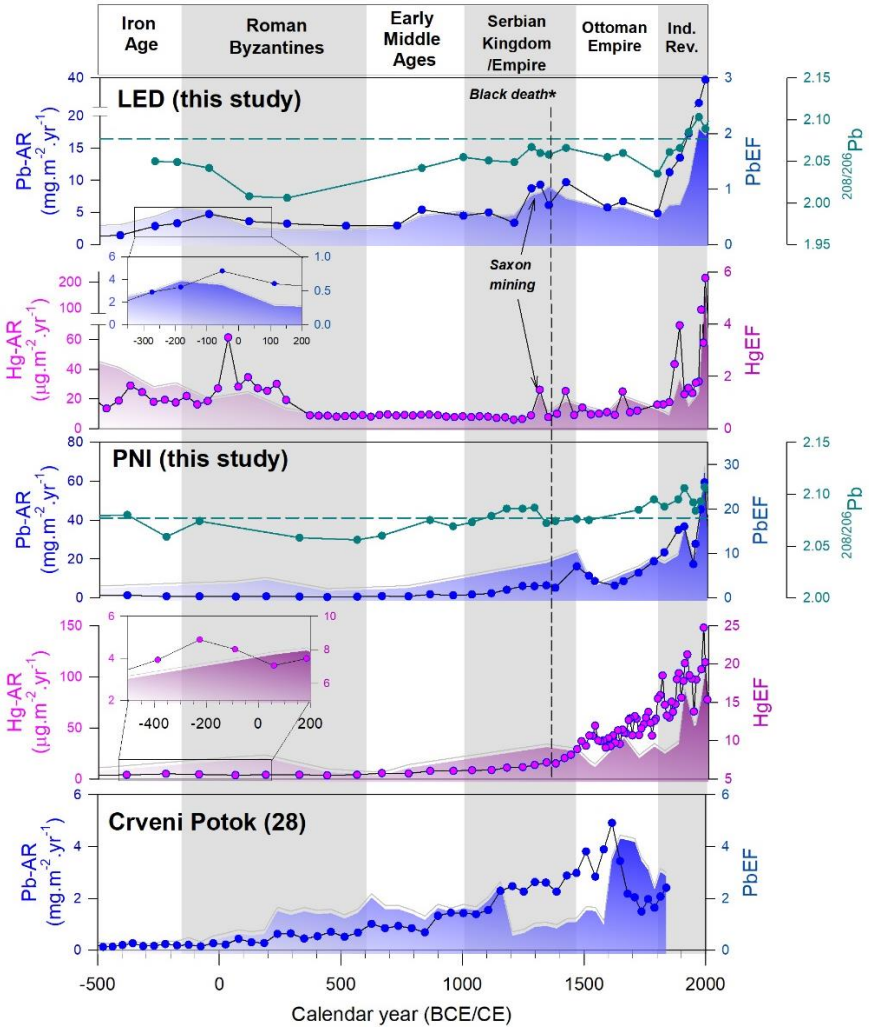

Figure 3. *Lead (Pb) and mercury (Hg) accumulation rates (AR, left Y axes), enrichment factors (EF, right Y axes) relative to background concentration normalized to Ti, and Pb isotopes ($^{208/206}$Pb) in the north- western Balkans lakes A) (LED), and B) (PNI). Bottom panel shows published Pb AR and EF record from Crveni Potok (Serbia) (28).*

From the 13th century onward, both Pb and Hg exhibit gradual and steady increases. From 1250 CE onward (i.e., during the Serbian Kingdom epoch), with the arrival of the Saxons miners (62), LED and PNI records exhibits a major and synchronous Pb and Hg ARs and EFs rises, which are abruptly interrupted around 1350 CE, coincident with the Black Death pandemic. Following a rebound after the pandemic, the Pb and Hg signal at LED and PNI again declines to baseline values during the 16th and 17th centuries. Same decline was observed in the Crveni Potok record, which was attributed to the decline of Ag production resulting from the restrictive impact of Ottoman laws and taxation system combined with the appearance of abundant and cheaper sources of Ag from the Americas (28, 63). Consistently, the steady increase in Hg ARs from the 16th century onward coincide with the rise in cinnabar extraction from the Idrija mine (64), which was extracted and exported to sustain Ag mining in the new world.

Both Pb and Hg records gradually increase from the 18th century onward, and exhibit major increases at the fall of the Ottoman empire (i.e., 1800 CE), indicating the onset of the industrial revolution in the Balkan region. This trend greatly resembles regional signals attributed to the "second and third mining bloom" of Ag in central-eastern Europe including the Ore Mountains, currently Czech Republic (65), and the eastern Balkans (28). Finally, both Pb and Hg ARs and EFs, steadily increase during the 19th and 20th centuries, highlighting the general increase in metal demand during the Industrial revolution in Europe.

Deciphering the source of historical mining signal in environmental records

Lead isotopes constitute a valuable tool for the identification of Pb sources, as Pb isotopes are supposed unaffected by weathering and metallurgical processes (36, 66). Lead (Pb) isotope signatures for historical peaks in mining and metallurgical activities recorded in

the Carpathians (IZM and MLH) and the Balkans (PNI and LED) records are similar to values reported for documented ores in these regions (43, 67).

Both Carpathian records fall within a narrow range of Pb isotope signatures values indicating a dominance of regional Pb signal (Fig. 4a). Only samples dated to the Late Iron Age and the Early Middle Ages, i.e., two periods of low Pb signal, exhibit the highest values typical of the geochemical background of the pre-anthropogenic period ($^{207/206}$Pb = 0.849 ± 0.007 and $^{208/206}$Pb = 2.087 ± 0.006, S.I. data). In contrast, all other samples are tightened within a narrow range similar to data reported for Apuseni ores [$^{207/206}$Pb = 0.819 ± 0.001 and $^{208/206}$Pb = 2.083 ± 0.001, (43)] indicating that the mining signal overwhelms all potential externals sources including the Industrial revolution lead gasoline signal along the 2500 years recorded.

In the Balkans, Pb isotope signatures exhibit a wider range of Pb isotope signatures with the highest values found during the last past 300 years (i.e., Ottoman Empire and industrial revolution) rising towards the lead gasoline signal (Fig. 4c). In contrast, Pb isotopes data from both the Middle Ages and the onset of the Roman empire, i.e., during the lowest Pb ARs and EFs signals, fall within the lowest isotopic values, likely reflecting the local geochemical background. Finally, the periods of high Pb ARs and EFs, i.e., from 1300 CE onward, and peaks at the apogee of the Byzantine Roman Empire, Pb isotopes data are clustered within the values reported for galena of the most productive Balkan mines, i.e., Kopaonik and Zletovo districts [$^{207/206}$Pb = 0.838 ± 0.001 and $^{208/206}$Pb = 2.077 ± 0.001, (67)].

The comparison of Pb and Hg ARs also reveals different trends between sites (Figs. 4c and 4d). The two Carpathians records highlight major rises in Pb AR during the last past 800 years (i.e., from the High Middle Ages to present), but show a mirrored trend regarding Pb versus Hg ARs biplots. For this latter period, without consideration of the

industrial revolution period, core MLH shows low Hg ARs independent of the Pb ARs levels, whereas in IZM exhibits higher Hg ARs with rising Pb ARs, which are of lower amplitude than MLH. This trend supports that intense Ag/Pb mining in the Apuseni as a major source of Pb for the archive (MLH), whereas underground Au extraction and ore treatment do not support extensive use and emission of Hg. In the northern Carpathians, gold or silver were likely extracted by Hg amalgamation in the Bahia Mare district or in the Transylvanian basin resulting in high Hg deposition recorded at IZM. In contrast, North-western Balkan records exhibits a covariation of both Pb and Hg ARs (R^2 = 0.89, p< 0.01) rising mainly from the HMA to the Ind. Rev. indicating a probable co-emission of these two elements during local and regional mining and metallurgical processes.

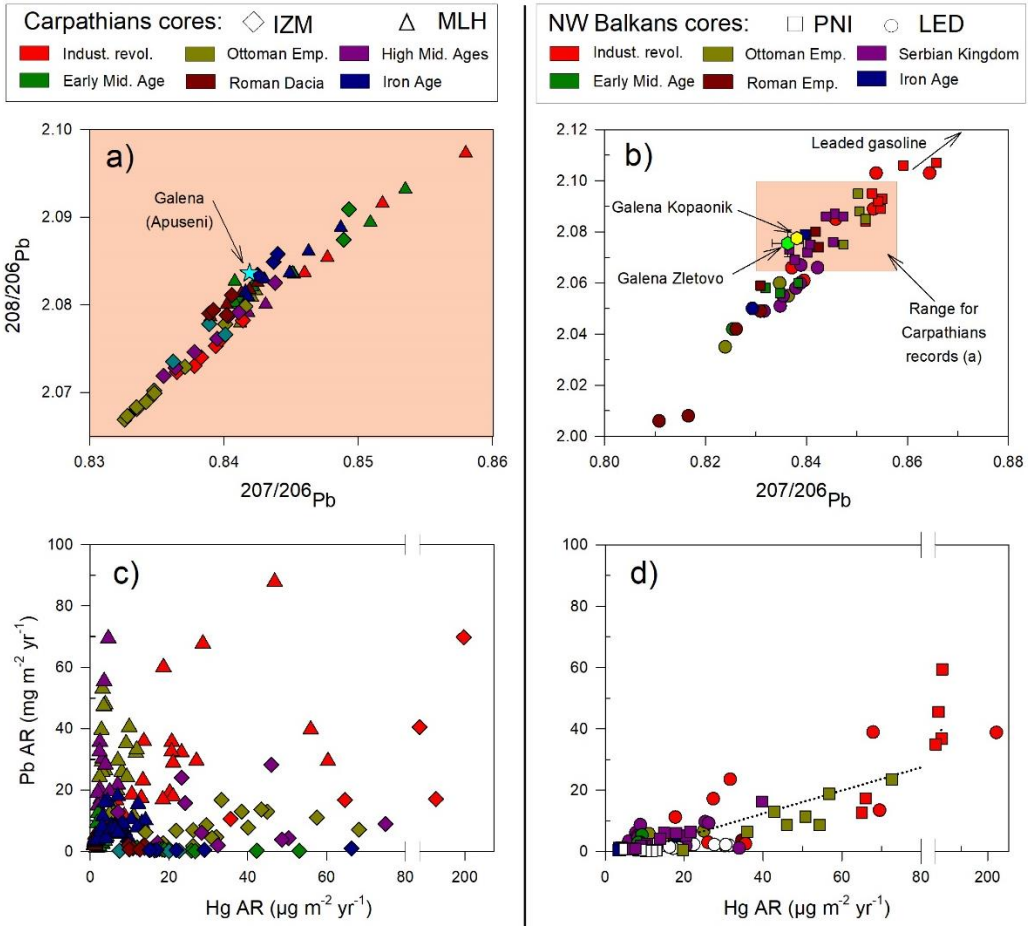

Figure 4. *Lead isotopes biplots of $^{207/206}$Pb versus $^{208/206}$Pb (panels a and c) and Lead versus Hg accumulation rates (panels b and d) for the two Carpathian mires; Izul mare mire (IZM, diamond), and Mlhua (MLH, triangle)), and the two north- western Balkans lakes; Lake Ledvicah (LED, circle) and Planina pri jezeru (PNI, square).*

Evidence of distinct timing and contribution of mining contamination through time

The timing and intensity of mining and metallurgical activities in Europe has varied along the last past 2500 years depending on mining and metallurgical processes, socio-political history (e.g., migrations, pandemics…), and climatic factors. The residence time of each considered metal of interest varies significantly according to its form (e.g., gaseous vs. particulate), which in turn depends on the extraction process (underground vs surface mining, fire abatement, etc.) and metallurgical process (e.g., combustion temperature and method). Contaminants such as Pb is mainly transported by aerosols and fine particles that have residence times of few days to weeks (68, 69) compared to elements such as Hg, which as a major gaseous component resulting in a global atmospheric lifetime estimated between 3 and 6 months (70). Hence, Hg contamination is likely to be spread of larger areas than Pb.

The atmospheric spreading of metal contamination over the continent depends however on major (i.e., westerlies) and regional trade winds. In central-eastern Europe, continental-type air masses originate mainly from 3 situation; i) Mediterranean Air (SW/S and SE/S), ii) eastern continental Europe (E and SE) and iii) Northern Sea and Scandinavia (NW, during wintertime) (39). In contrast, sources from Iberia (e.g. Almadén, Rio Tinto, Cartagena, Linares) are mainly transported by westerlies winds which follow through the Western Mediterranean and the Pyrenean routes (21). Hence, although simplistic, it can be assumed that western Europe records are almost unaffected by central - eastern Europe mining, whereas the western Alps region mainly records western (Iberia, France and western Mediterranean), and Northern region (Scandinavia, England and Germany) (71). In contrast, the eastern Alps are mainly under the influence of the eastern Mediterranean Sea (Saharan region, Greece …) and eastern Europa including the Carpathians (72). Finally, eastern Europe should be mainly affected by

northern (Scandinavia, Germany), eastern regions (Russia and middle east), and the eastern Mediterranean basin (e.g. south-eastern Balkans and Saharan region). It is worth mentioning that modern winds directions modelled through by back trajectories are influenced by a variety of local and long range transport processes (73) that might have change through time notably with historical changes in North Atlantic Oscillation (21). Hence, the comparison of Pb and Hg records in remote sites over Europe underlines both the trade-winds spreading and the amplitude of element dispersal.

The first major large-scale mining contamination is found during the Late Iron age / Roman empire period (250 BCE – 400 CE; phase I in Fig. 5). All records exhibit synchronous Pb and Hg ARs peaks indicating a co-emission of the two elements whose intensity likely depends on their respective content in mined ores and to the type of metallurgical process. Pb and Hg ARs peaks however show variable amplitude and timing between sites. The integrative Mediterranean Abyssal plain (22, 23) and the high altitude remote Lake Meidsee (20) records show evidence of the largest mining signal prior to the industrial revolution, and support a large-scale and almost synchronous Pb and Hg emission from various mining sites at the European scale. This mining signal in remote Spanish sites, i.e., PVO and Marboré (21, 25, 74), is found during the Roman Empire period (i.e., 50 BCE to ca 400 CE), whereas in the western Alps (i.e., Robert and Meidsee (19, 20)), and the Black forest (75), Hg and Pb contamination predates this period (i.e., 300 to 100 BCE) supporting a decline in mining activities in the western Alps during the Roman Empire. To the East, the western Balkan (LED) and the Carpathians (MLH) records, also exhibit Pb and Hg signal centered during the Late Iron Age and the Early Roman period (which is later in this region). Pb isotopes signals in Iberic, Alpine and Balkan records rise toward higher $^{208/206}$Pb values typical of the Hercynian massif, whereas Carpathians records tends to decrease towards lower $^{208/206}$Pb values typical of

signature of Neogene rocks of the Metaliferi mountains. Strikingly, both the Meidsee and PNI records highlight a mixed Pb isotopic signal with lower $^{208/206}$Pb values during the late Iron Age, which support depositions dominated by Carpathian inputs for the first part, followed by higher $^{208/206}$Pb values indicating a western Europe source for the Roman period. Hence, Pb isotope signals suggest that westerlies trade winds did not export Pb to central-eastern Europe or that this signal was masked by local signal, whereas in the central and eastern Alps, the pre-Roman Pb emission were transported to the Alps through eastern continental Europe air masses.

Following a general return to background Pb and Hg ARs, and close to geogenic Pb isotopic signatures in all the records during the Early Middle Ages (i.e., from ca. 400 to 750 CE, phase II in Fig. 5), Hg and Pb records rebound during the High Middle Ages (from 750 CE – 1300 CE, phase III in Fig. 5). This indicates a new mining epoch at the European scale during a period known for a general climate improvement over the continent (i.e., the Medieval Warm Period). As for phase I, major differences in the timing of peaks occurs between the records during the third phase. In western Europe, Pb and Hg signals in Iberian records show fine and high-amplitude ARs peaks centered around ca 800, and 1000 CE, whereas alpine ones are centered later, i.e. ca 1200 CE. In contrast, Balkans and Carpathians records show much later and wider peaks found between 1200 and 1450 CE (i.e. Saxon and Transylvanian mining epochs, phase IV in Fig. 5).

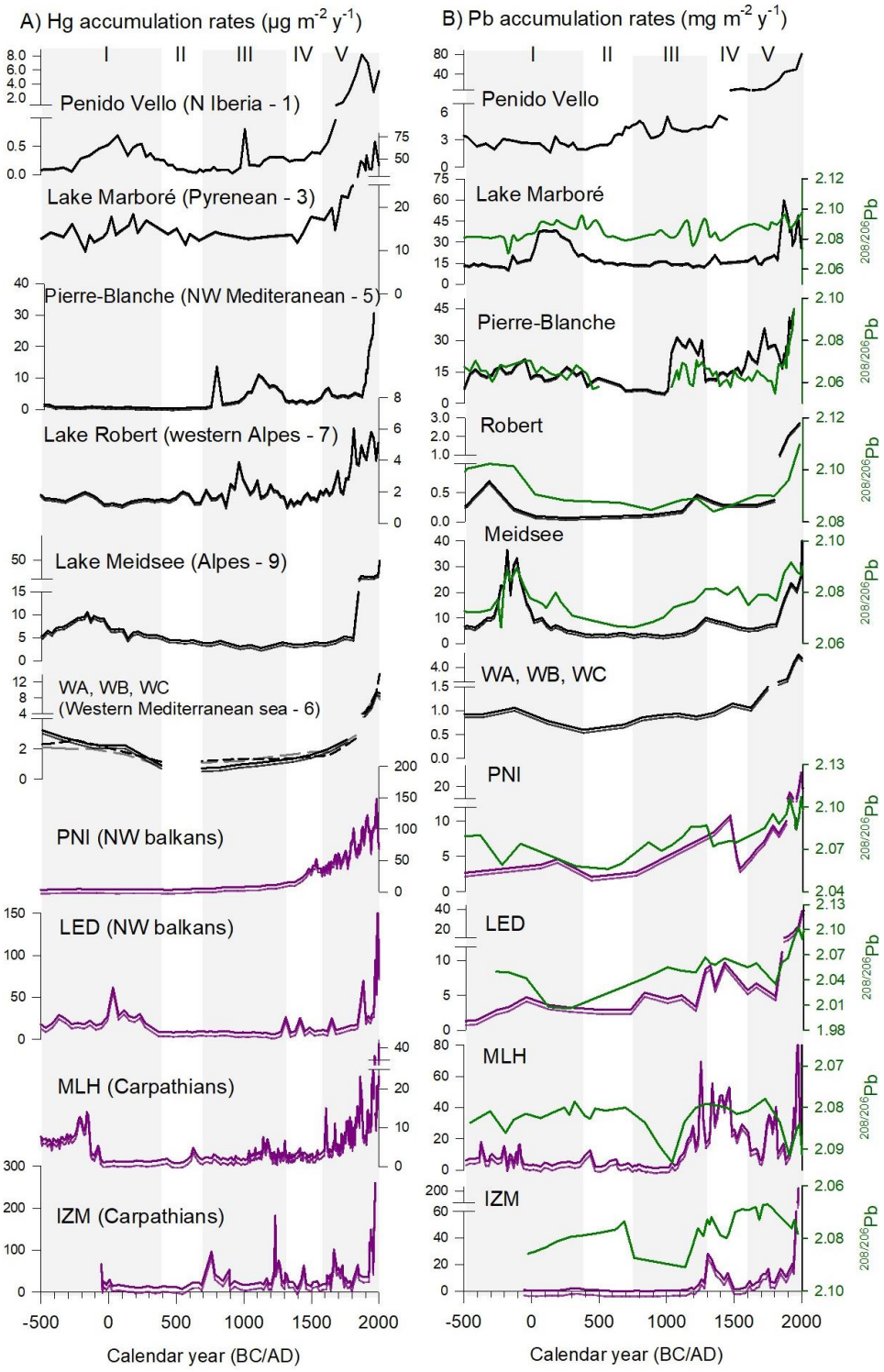

Figure 5. *Mercury (left panels) and lead (right panels) accumulation rates (AR, left ordinate axes) of remote environmental records from western to eastern Europe. The site number given after the name correspond to the location map (Fig. 1). Grey bands indicate broad cultural periods; Period I (Late Iron Age/Roman; Period II – Early Middle Ages, Period III – High Middle Ages, Period IV – Early Modern Period, and Period V – Industrial revolution.*

Another specificity of the Carpathians is the sharp Hg signal during both the early and high middle ages attributed to cinnabar extraction at Zlatna. As for the Late Iron Age - Roman Period, Pb ARs and isotope signatures exhibit asynchronous signal between western and central-eastern Europe, indicating distinct Pb sources and timing, and indistinguishable long-range transport of Pb deposition between these sites. At the transition between phases III and IV, central (Meidsee) and eastern Alpine (PNI and LED) records, again exhibit peaks overlapping these two distinct Pb ARs signals, with Pb isotopes signatures rising during the late phase III mining signal of western Europe, followed by a decline during the early phase IV coincident with the "mining boom" in central-Eastern Europe. One cannot exclude a similar "mining bloom" at the Ore Mountains (Erzgebirge, Germany) as another significant source for the central and eastern Alps. This "mining boom" in central-Eastern Europe ends with a major decline in Pb ARs during the 16th century, likely resulting from massive imports of Ag from the Americas which rapidly inundated the European market. Such extensive Ag extraction in the Americas required large exports of Hg from Almaden mines, consistent with increased Hg ARs in both Iberian records and all western Europe records including the Mediterranean Sea. In contrast, although Hg ARs in the Carpathians show a rising trend, the signal exhibits numerous fine and sharp peaks indicating discontinuous emissions and deposition in the region.

Finally, all records exhibit a decline in Hg and Pb ARs in the middle of the Little Ice Age period (i.e., 1400 to 1800 CE), followed by the global increase in both Pb and Hg ARs at the onset of Industrial revolution, highlighting a general increase metal demand and in mining and metallurgical activities across Europe.

Material and Methods

Core collection and analysis.

Cores from lakes LED (213 cm) and PNI (237 cm) were retrieved in 2014 using an Uwitec® gravity corer with hammer in the deepest part of their respective basins. All details and procedures for sediment sampling and lithological description of the sequences are described elsewhere (56). The IZM and MLH peat records were retrieved using a Russian peat corer All details and procedures for peat sampling and lithological description are described elsewhere (28). Sediment were collected via multiple overlapping and parallel cores. In the case of MLH, 620 cm of sediment was retrieved, covering the last 8000 years, while 800 cm of sediment was retrieved from IZM, covering the last 7000 years, but only the upper half (400 cm) is studied here.

Cores from lake LED and lake PNI were sliced with a vertical resolution of 1.5 cm. Cores from peat MLH and IZM were sliced contiguously over 1 cm intervals. For each subsample, water content was obtained from the difference in weight prior and post freeze-drying and then, dry bulk density (DBD) was calculated considering the subsample volume. Subsamples were finely ground (<63 μm) using an agate mortar before all chemical analyses.

X-Ray Fluorescence (XRF) analyses was performed at 1 mm steps on an Avaatech core scanner using different tube settings: at 10 kV–2 mA for Al, Si, S, K, Ca, Ti, Mn, Fe and at 30 kV–0.5 mA for Br, Sr, Rb, and Zr [26] (76).

All details for the chemical analyses QA/QC are given in supplementary material. All analytical procedures were conducted using ultra clean techniques and analyzed in a trace metal clean HEPA filtered laboratory (ISO 7), using high purity acids (Merck Suprapur quality) and ultrapure water (Milli-Q system).

Trace elements were measured by inductively coupled plasma mass spectrometry (Q-ICP-MS, Agilent 7900 CX) on samples digested with 10 mL of a mixture of pure acids ($HF/HCl/HNO_3$,1:6:2) following a microwave-assisted digestion (S.I.1). The digestion procedure was assessed using a certified material for soil (NIST 2709a and ERM-CC141) and lake sediment (LKSD1). All elements were within the satisfactory target recovery of 90 % and the analytical detection limits were well below the measurements of the samples analyzed.

Total Hg concentrations (THg) were determined by atomic absorption spectrometry (CV-AAS) after dry mineralization and amalgamation of the gold using an automatic mercury analyzer (Altec, model AMA 254). The relative error was around ±5% and always less than ±10%. The procedure was evaluated using a certified material for peat (ERM-CC-141).

Lead isotope analyses.

Lead isotopic analyses (^{204}Pb, ^{206}Pb, ^{207}Pb, ^{208}Pb) were obtained with a multi-collector inductively coupled plasma mass spectrometer (MC-ICP-MS, Nu Instruments, NuPlasma HR) at Ecole Normale Supérieure de Lyon for core IZM and ore minerals. Lead isotopic analyses (^{206}Pb, ^{207}Pb, ^{208}Pb) for cores MLH, LED and PNI were obtained with a quadrupol inductively coupled plasma mass spectrometer (QICP-MS, Agilent 7900) at ISTerre. All the analytical details can be found in (White et al., 2000). Dissolution of samples (about 50 mg) was achieved in closed Teflon® vessels using a mixture of 4.5 ml of concentrated HNO_3 (bi-distilled) and 0.5 ml of concentrated HF (Merck Suprapur quality). Samples were left on hot plates at 120 C for a minimum of 72h. Lead yield (~ 95%) was checked on an Agilent 7500 CX quadrupole ICP-MS within the analytical chemistry platform of ISTerre (OSUG-France). Lead was separated and purified from each sample in an HBr medium using anion-exchange columns loaded with AG1-X8 resin

(200–400 mesh, Acros Organics) according to a conventional method (Monna et al., 1997; Weeks et al., 2009). Thallium standard (Tl; NIST 997) was added to all samples to correct the instrument drift. Mass-fractionation effects were corrected by standard bracketing using the reference material of Pb (SRM 981).

The three geochemically informed parameters (Tmod, μ, and k) were obtained with the equations given by (Albarède et al., 2012) and using published Matlab code found in (77). Statistical analyses were performed using SigmaPlot version 12.5. P values *(p)* and correlation coefficients (R) are reported for linear regression analyses. In all cases, a p-value of 0.05 was chosen to indicate statistical significance.

Supplementary Information

S.I.1 Detailed protocols and QA/QC for chemical analysis

Trace elements were measured by inductively coupled plasma mass spectrometry (Agilent, 7500 CX quadrupole ICP-MS) within the analytical chemistry platform of ISTerre (OSUG-France) using a modified version of the method published by [33] (78). About 50 mg) was achieved following a microwave-assisted digestion with reverse aqua-regia, using concentrated bi-distilled HNO3 and HCl in a ratio of 3:1 [34] (79)(US EPA Method 3052; USEPA 1998). Samples were evaporated to dryness and re-dissolved in closed Teflon® vessels using a mixture of 3 ml of concentrated bi-distilled HNO_3 and 0.5 ml of concentrated HF (Merck Suprapur quality). Samples were left on hot plates at 120 C for a minimum of 72h. A weighted aliquot corresponding to 8 mg of starting powder sample was diluted in 2% (v/v) HNO_3 to obtain a dilution factor of about 5000 (in order to minimize matrix effects) before measurements on ICP-MS. Be, In, and, Bi was used as internal standards to correct for instrumental mass bias. The digestion procedure was assessed using a certified material for soil (NIST 2709a and ERM-CC141). All elements

were within the satisfactory target recovery of 90 % and the analytical detection limits were well below the measurements of the samples analyzed.

References

1. M. Radivojević, B. W. Roberts, Early balkan metallurgy: origins, evolution and society, 6200–3700 BC. *Journal of World Prehistory* **34**, 195-278 (2021).
2. N. Amzallag, From metallurgy to Bronze Age civilizations: the synthetic theory. *American Journal of Archaeology* **113**, 497-519 (2009).
3. B. W. Roberts, C. P. Thornton, V. C. Pigott, Development of metallurgy in Eurasia. *Antiquity* **83**, 1012-1022 (2009).
4. D. Killick, T. Fenn, Archaeometallurgy: the study of preindustrial mining and metallurgy. *Annu. Rev. Anthrop.* **41**, 559-575 (2012).
5. C. Renfrew, in *The Social Life of Things: Commodities in Cultural Perspective*, A. Apparadurai, Ed. (Cambridge University Press, Cambridge 1986), pp. 141-168.
6. T. Higham *et al.*, New perspectives on the Varna cemetery (Bulgaria)–AMS dates and social implications. *Antiquity* **81**, 640-654 (2007).
7. B. S. Ottaway, B. Roberts, The emergence of metalworking. *Prehistoric Europe: theory and practice*, 193-225 (2008).
8. W. O'Brien, *Prehistoric copper mining in Europe: 5500-500 BC.* (Oxford University Press, USA, 2015).
9. M. Radivojević *et al.*, On the origins of extractive metallurgy: new evidence from Europe. *J. Archaeol. Sci.* **37**, 2775-2787 (2010).
10. C. Giardino, in *The Etruscan World*. (Routledge, 2014), pp. 769-785.
11. J. G. Chamorro, Survey of archaeological research on Tartessos. *American Journal of Archaeology* **91**, 197-232 (1987).
12. J. C. Edmondson, Mining in the Later Roman Empire and beyond: Continuity or Disruption? *The Journal of Roman Studies* **79**, 84-102 (1989).
13. M. P. Charlesworth, *Trade-routes and Commerce of the Roman Empire*. (Cambridge University Press, 2016).
14. K. J. Westner *et al.*, Rome's Rise to Power. Geochemical Analysis of Silver Coinage from the Western Mediterranean (Fourth to Second Centuries BCE). *Archaeometry* **62**, 577-592 (2020).
15. H. Delile, J. Blichert-Toft, J.-P. Goiran, S. Keay, F. Albarède, Lead in ancient Rome's city waters. *Proceedings of the National Academy of Sciences* **111**, 6594-6599 (2014).
16. H. Delile *et al.*, A lead isotope perspective on urban development in ancient Naples. *Proceedings of the National Academy of Sciences* **113**, 6148-6153 (2016).
17. J. R. McConnell *et al.*, Lead pollution recorded in Greenland ice indicates European emissions tracked plagues, wars, and imperial expansion during antiquity. *Proceedings of the National Academy of Sciences*, (2018).
18. K. J. R. Rosman, W. Chisholm, S. Hong, J.-P. Candelone, C. F. Boutron, Lead from Carthaginian and Roman Spanish mines isotopically identified in Greenland ice dated from 600 BC to 300 AD. *Environ. Sci. Technol.* **31**, 3413-3416 (1997).
19. F. Elbaz-Poulichet *et al.*, A 10,000-year record of trace metal and metalloid (Cu, Hg, Sb, Pb) deposition in a western Alpine lake (Lake Robert, France): Deciphering local and regional mining contamination. *Quaternary Science Reviews* **228**, 106076 (2020).
20. F. Thevenon, S. Guédron, M. Chiaradia, J.-L. Loizeau, J. Poté, (Pre-) historic changes in natural and anthropogenic heavy metals deposition inferred from two contrasting Swiss Alpine lakes. *Quaternary Science Reviews* **30**, 224-233 (2011).

21. J. P. Corella *et al.*, Recent and historical pollution legacy in high altitude Lake Marboré (Central Pyrenees): A record of mining and smelting since pre-Roman times in the Iberian Peninsula. *Sci. Total Environ.* **751**, 141557 (2021).
22. D. Cossa *et al.*, Mercury deposition in the Eastern Mediterranean: Modern fluxes in the water column and Holocene accumulation rates in abyssal sediment. *Chem. Geol.*, 121652 (2023).
23. D. Cossa *et al.*, Mercury accumulation in the sediment of the Western Mediterranean abyssal plain: A reliable archive of the late Holocene. *Geochim. Cosmochim. Acta* **309**, 1-15 (2021).
24. M. Leblanc, J. A. Morales, J. Borrego, F. Elbaz-Poulichet, 4,500-year-old mining pollution in southwestern Spain: long-term implications for modern mining pollution. *Economic Geology* **95**, 655-662 (2000).
25. A. Martinez-Cortizas, X. Pontevedra-Pombal, E. Garcia-Rodeja, J. C. Novoa-Munoz, W. Shotyk, Mercury in a Spanish peat bog: archive of climate change and atmospheric metal deposition. *Science* **284**, 939-942 (1999).
26. A. Martínez Cortizas, L. López-Merino, R. Bindler, T. Mighall, M. Kylander, Atmospheric Pb pollution in N Iberia during the late Iron Age/Roman times reconstructed using the high-resolution record of La Molina mire (Asturias, Spain). *J. Paleolimnol.* **50**, 71-86 (2013).
27. R. Bindler, M. Klarqvist, J. Klaminder, J. Förster, Does within-bog spatial variability of mercury and lead constrain reconstructions of absolute deposition rates from single peat records? The example of Store Mosse, Sweden. *Global Biogeochem. Cycles* **18**, (2004).
28. J. Longman, D. Veres, W. Finsinger, V. Ersek, Exceptionally high levels of lead pollution in the Balkans from the Early Bronze Age to the Industrial Revolution. *Proceedings of the National Academy of Sciences* **115**, E5661-E5668 (2018).
29. P. Laznicka, *Giant metallic deposits: Future sources of industrial metals*. (Springer, 2006), vol. 1905.
30. M. Borcoş, G. Udubaşa, Chronology and characterisation of mining development in Romania. *Romanian Journal of Earth Sciences* **86**, 17-26 (2012).
31. P. M. Outridge, F. Wang, The stability of metal profiles in freshwater and marine sediments. *Environmental contaminants: using natural archives to track sources and long-term trends of pollution*, 35-60 (2015).
32. W. Shotyk, P. Blaser, A. Grünig, A. K. Cheburkin, A new approach for quantifying cumulative, anthropogenic, atmospheric lead deposition using peat cores from bogs: Pb in eight Swiss peat bog profiles. *Sci. Total Environ.* **249**, 281-295 (2000).
33. G. Le Roux *et al.*, Identifying the sources and timing of ancient and medieval atmospheric lead pollution in England using a peat profile from Lindow bog, Manchester. *J. Environ. Monit.* **6**, 502-510 (2004).
34. C. A. Cooke, R. Bindler, in *Environmental Contaminants*. (Springer, 2015), pp. 101-119.
35. J. Longman *et al.*, Quantitative assessment of Pb sources in isotopic mixtures using a Bayesian mixing model. *Scientific Reports* **8**, 6154 (2018).
36. F. Albarède, A. M. Desaulty, J. Blichert-Toft, A geological perspective on the use of Pb isotopes in archaeometry. *Archaeometry* **54**, 853-867 (2012).
37. S. Baron *et al.*, Geochemistry of Gold ores Mined During celtic times from the north-Western french Massif central. *Scientific Reports* **9**, 1-15 (2019).

38. S. Guédron, C. Grimaldi, C. Chauvel, C. Spadini, M. Grimaldi, Weathering versus atmospheric contributions to mercury concentrations in French Guiana soils. *Appl. Geochem.* **21**, 2010-2022 (2006).
39. W. Birmili, A. Wiedensohler, J. Heintzenberg, K. Lehmann, Atmospheric particle number size distribution in central Europe: Statistical relations to air masses and meteorology. *Journal of Geophysical Research: Atmospheres* **106**, 32005-32018 (2001).
40. C. G. Tămaş, S. Baron, B. Cauuet, Minéralogie et signature isotopique du plomb des minerais auro-argentifères exploités durant l'époque romaine à Alburnus Maior (Rosia Montanà, Roumanie). *ArcheoSciences. Revue d'archéométrie*, 83-89 (2009).
41. S. Baron, C.-G. Tămas, B. Cauuet, M. Munoz, Lead isotope analyses of gold-silver ores from Rosia Montana (Romania): a first step of a metal provenance study of Roman mining activity in Alburnus Maior (Roman Dacia). *J. Archaeol. Sci.* **38**, 1090-1100 (2011).
42. M. E. Kylander *et al.*, Refining the pre-industrial atmospheric Pb isotope evolution curve in Europe using an 8000 year old peat core from NW Spain. *Earth. Planet. Sci. Lett.* **240**, 467-485 (2005).
43. S. Baron, C.-G. Tămaş, B. Cauuet, M. Munoz, Lead isotope analyses of gold–silver ores from Roşia Montană (Romania): a first step of a metal provenance study of Roman mining activity in Alburnus Maior (Roman Dacia). *J. Archaeol. Sci.* **38**, 1090-1100 (2011).
44. Ș.-N. Vlad, E. Orlandea, Metallogeny of the Gold Quadrilateral: style and characteristics of epithermal-subvolcanic mineralized structures, South Apuseni Mts., Romania. *Studia UBB Geologia* **49**, 15-31 (2004).
45. H. Biester, R. Bindler, A. Martinez-Cortizas, D. R. Engstrom, Modeling the Past Atmospheric Deposition of Mercury Using Natural Archives. *Environ. Sci. Tech.* **41**, 4851-4860 (2007).
46. M. Jiménez-Moreno *et al.*, Sources and fate of mercury pollution in Almadén mining district (Spain): Evidences from mercury isotopic compositions in sediments and lichens. *Chemosphere* **147**, 430-438 (2016).
47. E. Paşca, Gold Culture and the History of Industrial Heritage at Roşia Montană. *Review of Historical Geography and Toponomastics* **5**, 81-96 (2010).
48. I. Abrudeanu Rusu, *Romanian Gold*. (Napoca Star Printing House, Cluj-Napoca, Romania, 1933 (2006)).
49. W. L. Langer, The black death. *Sci. Am.* **210**, 114-121 (1964).
50. H. Ditrich, The transmission of the Black Death to western Europe: A critical review of the existing evidence. *Mediterranean Historical Review* **32**, 25-39 (2017).
51. D. C. Mengel, A Plague on Bohemia? Mapping the Black Death. *Past and Present* **211**, 3-34 (2011).
52. A. Izdebski *et al.*, Palaeoecological data indicates land-use changes across Europe linked to spatial heterogeneity in mortality during the Black Death pandemic. *Nature Ecology & Evolution* **6**, 297-306 (2022).
53. A. V. Maiorov, The first Mongol invasion of Europe: Goals and results. *J. R. Asiat. Soc.* **32**, 411-438 (2022).
54. M. Font, The crises of medieval society: the Mongol invasion in Eastern and Central Europe. *Україна: культурна спадщина, національна свідомість, державність*, (2011).

55. A. Brancelj, *Visokogorska jezera v vzhodnem delu Julijskih Alp / High-mountain Lakes in the Eastern Part of the Julian Alps*. A. Brancelj, Ed., (Založba ZRC, Ljubljana, Slovenia, 2002).
56. N. Caf *et al.*, Multi-proxy reconstruction of the Holocene vegetation and land use dynamics in the Julian Alps, north-west Slovenia. *Journal of Quaternary Science*, (2022).
57. E. Isayev, *Migration, mobility and place in ancient Italy*. (Cambridge University Press, 2017).
58. M. Š. Kos, The Tauriscan Gold Mine. Remarks Conceming the Settlement of the Taurisci. *TYCHE–Beiträge zur Alten Geschichte, Papyrologie und Epigraphik* **13**, 13-13 (1998).
59. G. Žibret, M. Gosar, M. Miler, J. Alijagić, Impacts of mining and smelting activities on environment and landscape degradation—Slovenian case studies. *Land Degradation & Development* **29**, 4457-4470 (2018).
60. M. Andrič *et al.*, 6600 years of human and climate impacts on lake-catchment and vegetation in the Julian Alps (Lake Bohinj, Slovenia). *Quaternary Science Reviews* **227**, 106043 (2020).
61. M. Turk *et al.*, in *The Geography of Slovenia: Small But Diverse*. (Springer, 2019), pp. 127-141.
62. J. V. Fine, J. V. A. Fine, *The late medieval Balkans: A critical survey from the late twelfth century to the Ottoman conquest*. (University of Michigan press, 1994).
63. S. Guédron *et al.*, Reconstructing two millennia of copper and silver metallurgy in the Lake Titicaca region (Bolivia/Peru) using trace metals and lead isotopic composition. *Anthropocene* **34**, 100288 (2021).
64. M. Gosar, S. Pirc, M. Bidovec, Mercury in the Idrijca River sediments as a reflection of mining and smelting activities of the Idrija mercury mine. *Journal of Geochemical Exploration* **58**, 125-131 (1997).
65. L. Bohdálková, P. Bohdálek, E. Břízová, P. Pacherová, A. A. Kuběna, Atmospheric metal pollution records in the Kovářská Bog (Czech Republic) as an indicator of anthropogenic activities over the last three millennia. *Sci. Total Environ.* **633**, 857-874 (2018).
66. F. Albarède *et al.*, A miner's perspective on Pb isotope provenances in the Western and Central Mediterranean. *J. Archaeol. Sci.* **121**, 105194 (2020).
67. K. J. Westner, M. Vaxevanopoulos, J. Blichert-Toft, G. Davis, F. Albarède, Isotope and trace element compositions of silver-bearing ores in the Balkans as possible metal sources in antiquity. *J. Archaeol. Sci.* **155**, 105791 (2023).
68. C. Papastefanou, Residence time of tropospheric aerosols in association with radioactive nuclides. *Appl. Radiat. Isot.* **64**, 93-100 (2006).
69. M. Baskaran, G. E. Shaw, Residence time of arctic haze aerosols using the concentrations and activity ratios of 210Po, 210Pb and 7Be. *J. Aerosol Sci* **32**, 443-452 (2001).
70. H. M. Horowitz *et al.*, A new mechanism for atmospheric mercury redox chemistry: implications for the global mercury budget. *Atmospheric Chemistry and Physics* **17**, (2017).
71. S. Dunlop, *A dictionary of weather*. (OUP Oxford, 2008).
72. D. N. Nicolae, C. L. Talianu, R.-E. Mamouri, Air mass modification processes over the Balkans area detected by aerosol Lidar techniques. *Optoelectronics and Advanced Materials, Rapid Communications*, (2008).

73. Z. L. Fleming, P. S. Monks, A. J. Manning, Untangling the influence of air-mass history in interpreting observed atmospheric composition. *Atmospheric Research* **104**, 1-39 (2012).
74. A. Martınez-Cortizas *et al.*, Atmospheric Pb deposition in Spain during the last 4600 years recorded by two ombrotrophic peat bogs and implications for the use of peat as archive. *Sci. Total Environ.* **292**, 33-44 (2002).
75. M. Schütze, G. Tserendorj, M. Pérez-Rodriguez, M. Rösch, H. Biester, Prediction of Holocene Mercury Accumulation Trends by Combining Palynological and Geochemical Records of Lake Sediments (Black Forest, Germany). *Geosciences* **8**, 358 (2018).
76. T. O. Richter *et al.*, in *New Techniques in Sediment Core Analysis*, R. G. Rothwell, Ed. (Geological Society, London, 2006), pp. 39-50.
77. H. Delile *et al.*, Demise of a harbor: A geochemical chronicle from Ephesus. *J. Archaeol. Sci.* **53**, 202-213 (2015).
78. C. Chauvel, S. Bureau, C. Poggi, Comprehensive Chemical and Isotopic Analyses of Basalt and Sediment Reference Materials. *Geostandards and Geoanalytical Research* **35**, 125-143 (2011).
79. EPA, in *Report on the Environment*. (1996).

Annex 5:

Anthropogenic eutrophication of Lake Titicaca (Bolivia) revealed by carbon and nitrogen stable isotopes fingerprinting

This article has been published in *Science of The Total Environment* and is referenced as follows:

Heredia, C., Guédron, S., Point, D., Perrot, V., Campillo, S., Verin, C., Espinoza, M.E., Fernandez, P., Duwig, C., Achá, D., 2022. Anthropogenic eutrophication of Lake Titicaca (Bolivia) revealed by carbon and nitrogen stable isotopes fingerprinting. Science of The Total Environment 845, 157286. https://doi.org/10.1016/j.scitotenv.2022.157286

Science of the Total Environment 845 (2022) 157286

Contents lists available at ScienceDirect

Science of the Total Environment

journal homepage: www.elsevier.com/locate/scitotenv

Anthropogenic eutrophication of Lake Titicaca (Bolivia) revealed by carbon and nitrogen stable isotopes fingerprinting

C. Heredia [a,b,*], S. Guédron [a,c], D. Point [b,d], V. Perrot [a], S. Campillo [a], C. Verin [a], M.E. Espinoza [b], P. Fernandez [b], C. Duwig [c,e], D. Achá [b]

[a] Université Grenoble Alpes, Université Savoie Mont Blanc, CNRS, IRD, IFSTAR, ISTerre, 38000 Grenoble, France.
[b] Instituto de Ecología, Unidad de Calidad Ambiental (UCA), Carrera de Biología, Universidad Mayor de San Andrés, Campus Universitario de Cota Cota, casilla 3161, La Paz, Bolivia.
[c] Laboratorio de Hidroquímica - Instituto de Investigaciones Químicas - Universidad Mayor de San Andrés, Campus Universitario de Cota-Cota, casilla 3161, La Paz, Bolivia.
[d] Géosciences Environnement Toulouse (GET) - Institut de Recherche pour le Développement (IRD), CNRS, Université de Toulouse, France
[e] Univ. Grenoble Alpes, Univ. Savoie Mont Blanc, CNRS, IRD, IFSTTAR, IGE, 38000 Grenoble, France.

HIGHLIGHTS

- C and N stable isotopes were measured in four compartments of Lake Titicaca.
- Anthropogenic discharge affects baseline C and N isotope signatures.
- C recycling from soil, anthropogenic and lacustrine sources affect the $\delta^{13}C$ signature.
- $\delta^{15}N$ signatures track anthropogenic contamination independently of plant type.
- Decreased anthropogenic contribution in the bay assessed by isotope mixing model.

GRAPHICAL ABSTRACT

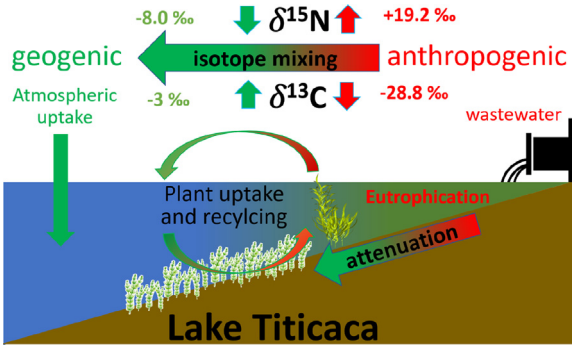

ARTICLE INFO

Editor: Jurgen Mahlknecht

Keywords:
Carbon stable isotopes
Nitrogen stable isotopes
Eutrophication
Lake Titicaca
Anthropogenic discharges

ABSTRACT

Cultural eutrophication is the leading cause of water quality degradation worldwide. The traditional monitoring of eutrophication is time-consuming and not integrative in space and time. Here, we examined the use of carbon ($\delta^{13}C$) and nitrogen ($\delta^{15}N$) isotopic composition to track the degree of eutrophication in a bay of Lake Titicaca impacted by anthropogenic (urban, industrial and agricultural wastewater) discharges. Our results show increasing $\delta^{13}C$ and decreasing $\delta^{15}N$ signatures in macrophytes and suspended particulate matter with distance to the wastewater source. In contrast to $\delta^{15}N$ and $\delta^{13}C$ signatures, in-between aquatic plants distributed along the slope were not only affected by anthropogenic discharges but also by the pathway of carbon uptake, i.e., atmospheric (emerged) vs aquatic (submerged). A binary mixing model elaborated from pristine and anthropogenic isotope end-members allowed the assessment of anthropogenically derived C and N incorporation in macrophytes with distance to the source. Higher anthropogenic contribution was observed during the wet season, attributed to enhanced wastewater discharges and leaching of agricultural areas. For both seasons, eutrophication was however found naturally attenuated within 6 to 8 km from the wastewater source. Here, we confirm that carbon and nitrogen stable isotopes are simple, integrative and time-saving tools to evaluate the degree of eutrophication (seasonally or annually) in anthropogenically impacted aquatic ecosystems.

1. Introduction

Human-induced eutrophication of surface waters has become a major concern of water quality impairment (Smith, 2003; Schindler, 2006). It is

* Corresponding author at: Université Grenoble Alpes, Université Savoie Mont Blanc, CNRS, IRD, IFSTAR, ISTerre, 38000 Grenoble, France
E-mail address: carlos.heredia-aguilar@univ-grenoble-alpes.fr (C. Heredia).

http://dx.doi.org/10.1016/j.scitotenv.2022.157286
Received 31 March 2022; Received in revised form 16 June 2022; Accepted 7 July 2022
Available online 12 July 2022

known to impact aquatic ecosystems (Backer and McGillicuddy, 2006; Paerl and Otten, 2013) with environmental and health-related costs estimated to several billions of dollars per year (Pretty et al., 2003; Dodds et al., 2009). The discharge of untreated wastewater in natural aquatic ecosystems induces a nutrient enrichment in the water column, affecting the trophic structure and composition of the in biological communities (Smith et al., 2006). A common response to the excess of nutrient inputs is the possible development of massive algal proliferation (i.e., blooms) which provokes oxygen depletion (i.e., hypoxia or anoxia) during the bacterial degradation of senescent blooms that can result in the death of benthic and pelagic biota (Diaz, 2001). Recurrence of such hypoxic events can cause the release of phosphorus from sediments (due to changing redox conditions), creating an internal feedback that amplifies eutrophication effects (Rosenmeier et al., 2004; Vahtera et al., 2007; Smith et al., 2015).

The monitoring of eutrophication generally includes cost and time-consuming in situ physicochemical analyses (pH, redox potential, total nutrient concentration, biochemical oxygen demand, etc.…) as well as macrophyte and algal species composition and biomass (Le Moal et al., 2018). In impermanently eutrophic ecosystems or those subject to occasional blooms, such traditional monitoring methods require a large number of measurements to obtain a significant spatial overview of the anthropogenic impacts, which are generally not constrained temporally. Therefore, the need for a different approach with sensitive techniques, providing a spatially and temporally integrative picture of eutrophication processes, is of high priority to understand the dissemination and triggering mechanisms of blooms. This latter information is key for the development of mitigation strategies before irreversible changes affect aquatic ecosystems.

Carbon ($\delta^{13}C$) and nitrogen ($\delta^{15}N$) stable isotope are good candidates to provide such level of information at the ecosystem scale (Fry, 2006; Dawson and Siegwolf, 2007; Glibert et al., 2018). Both C and N isotopic tracers provide information about the food web structures and are influenced by baseline changes and sources (Vander Zanden and Rasmussen, 1999; Liu et al., 2012). $\delta^{13}C$ allows the inference of energy sources (i.e., no significant fractionation of C isotopes during trophic transfer, resulting in isotopic ratios between consumers and their food almost identical), whereas $\delta^{15}N$ allows the determination of trophic levels (i.e., enrichment factor between consumers and their food is between 2 and 4 ‰) (Dawson et al., 2002; Michener and Lajtha, 2008; Middelburg, 2014). In addition, when a significant difference in isotopic signatures exists between natural and anthropogenic sources, it is possible to track and assess the magnitude of anthropogenic pollution (Glibert et al., 2018). On the one hand, carbon stable isotope ratios of organic matter ($\delta^{13}C_{org}$) can be used in freshwater ecosystems to distinguish between autochthonous and allochthonous sources of organic matter (Gu et al., 2006; Thevenon et al., 2012). $\delta^{13}C_{org}$ values of terrestrial primary productivity often differ from the $\delta^{13}C_{org}$ values of aquatic primary productivity (Fry, 2006). On the other hand, nitrogen stable isotope ratios ($\delta^{15}N$) can track anthropogenic nitrogen inputs (Glibert et al., 2018). The three primary sources of anthropogenically derived N in freshwater ecosystems are human and animal (e.g. septic and manure waste) sewage, synthetic fertilizers (from agricultural fields) and atmospheric deposition (Cole et al., 2006), with each of these sources often differing in their $\delta^{15}N$ signature. Sewage-derived N commonly presents $\delta^{15}N$ values enriched in heavier isotopes [$\geq$10 ‰, McClelland et al. (1997)] relative to the baseline value of atmospheric deposition (N_2), which is closer to 0 (Kendall et al., 2008; Holtgrieve et al., 2011). Once discharged in surface or ground water, anthropogenic N recycling (i.e., nitrification or denitrification) can cause large N isotope fractionation up to ±20 ‰ (Mariotti et al., 1988; Sebilo et al., 2003; Kendall et al., 2007). Changes in the isotopic composition of dissolved inorganic pools are reflected in the $\delta^{13}C_{org}$ and $\delta^{15}N$ of primary producers, which can assimilate dissolved nutrients from the water column and integrate the changes in isotopic sources over time (Schindler et al., 1997; Savage, 2005; Dawson and Siegwolf, 2007). Consequently, the $\delta^{13}C$ and $\delta^{15}N$ values of primary producers can alert the presence of anthropogenic nutrients before significant ecological changes occur in the environment (McClelland et al., 1997; Savage, 2005; Vermeulen et al., 2011). Enriched or depleted isotope ratios in relation to a "pristine" baseline can therefore be used as sensitive indicators of pollution (Costanzo et al., 2001).

In many developing countries, the demographic expansion and the development of urban centers and economic activities (e.g., mining, agriculture, industry) increase anthropogenic impacts on their surrounding ecosystems. This has been the case during the last few decades in the high-altitude Andean Altiplano (Mazurek, 2012), where the discharge of untreated wastewater from cities like Puno, Oruro, and La Paz/El Alto have led to the degradation of several water bodies. The most dramatic examples are the case of Lake Uru-Uru (Bolivia) (Alanoca et al., 2016; Guédron et al., 2017; Sarret et al., 2019), Puno Bay (Peru) in the northern basin of Lake Titicaca (Northcote, 1992), and Cohana Bay (Bolivia) in the southern basin of the Lake (Archundia et al., 2017a; Flores Avilés et al., 2022). Besides the permanent state of eutrophication in several shallow basins receiving untreated wastewater, punctual and sometimes massive bloom events have been reported at larger scales. For example, in 2015, Lake Titicaca suffered one of its major bloom event to date at the scale of its entire southern basin, triggered by an unusually intense rain episode that washed out large amounts of nutrients from the agricultural watershed and resulted in the massive death of birds and pelagic biota (Achá et al., 2018).

In this study, we examined $\delta^{13}C$ and $\delta^{15}N$ signatures in primary producers (macrophytes, periphyton), suspended particulate matter, and surface sediments along an eutrophication gradient in Lake Titicaca. The aim of this study is to test the efficiency of these tools for monitoring the dissemination and amplitude of anthropogenic discharges of wastewaters while considering the natural functioning of the ecosystem (trophic status and seasonality).

2. Material and methods

2.1. Study area

Lake Titicaca is the largest freshwater lake in South America. Located in the high tropical Andes (3809 m.a.s.l.) between Peru and Bolivia, it is divided into two separated basins: the northern great lake, namely Lago Mayor (7131 km^2; mean depth = 100 m; max depth = 285 m), and the southern small lake, namely Lago Menor (1428 km^2; mean depth = 10 m; max depth = 40 m) (Fig. 1a). Both basins are connected through the Strait of Tiquina (approx. 800 m wide). The only outlet of the system, the Desaguadero River, is located in the southern end of Lago Menor (Dejoux and Iltis, 1991). Its high elevation results in extreme hydro-climatic conditions, e.g., intense UV-radiation (Richerson et al., 1986; Villafae et al., 1999), lower dissolved oxygen (Achá et al., 2018), and large daily temperature variations which can overwhelm seasonal ones (Molina et al., 2014).

The climate of the Titicaca region is marked by a seasonal cycle of precipitation, and >70 % of the precipitation occurs during the austral summer (mean annual precipitation ~614 mm $year^{-1}$), concentrated between December and March, when moist air from the Amazon enters the Altiplano and discharges in the form of convective rainfalls (Guédron et al., 2018; Segura et al., 2019). Precipitation during the Austral summer produces intense and short duration floods of the lake's tributaries on the steep slopes of the lake (Roche et al., 1992).

This is the case for the Katari River, located in the southwestern part of Lake Titicaca, which exhibits water discharges up to 151 $m^3 \cdot s^{-1}$ during flood event, whereas its average annual discharge is 5.8 $m^3 \cdot s^{-1}$ (SENAMHI, 2020). The river drains a catchment area of >484 km^2, and is supplied by two perennial tributaries, i.e., Rio Seco (slope ~ 0.9 %) and Rio Pallina (slope ~ 0.03 %) and many ephemeral tributaries (Chudnoff, 2009). In its upstream part, the two perennial tributaries receive both treated and untreated wastewaters incoming from upstream cities [i.e., El Alto City (1.2 million habitants) and Viacha (80,000 habitants)] (Chudnoff, 2009; Archundia et al., 2017a,b). Downstream, the Katari river drains a flat agricultural areas where at least 65 % of the population is dedicated to agricultural and livestock practices (Flores Avilés et al., 2022).

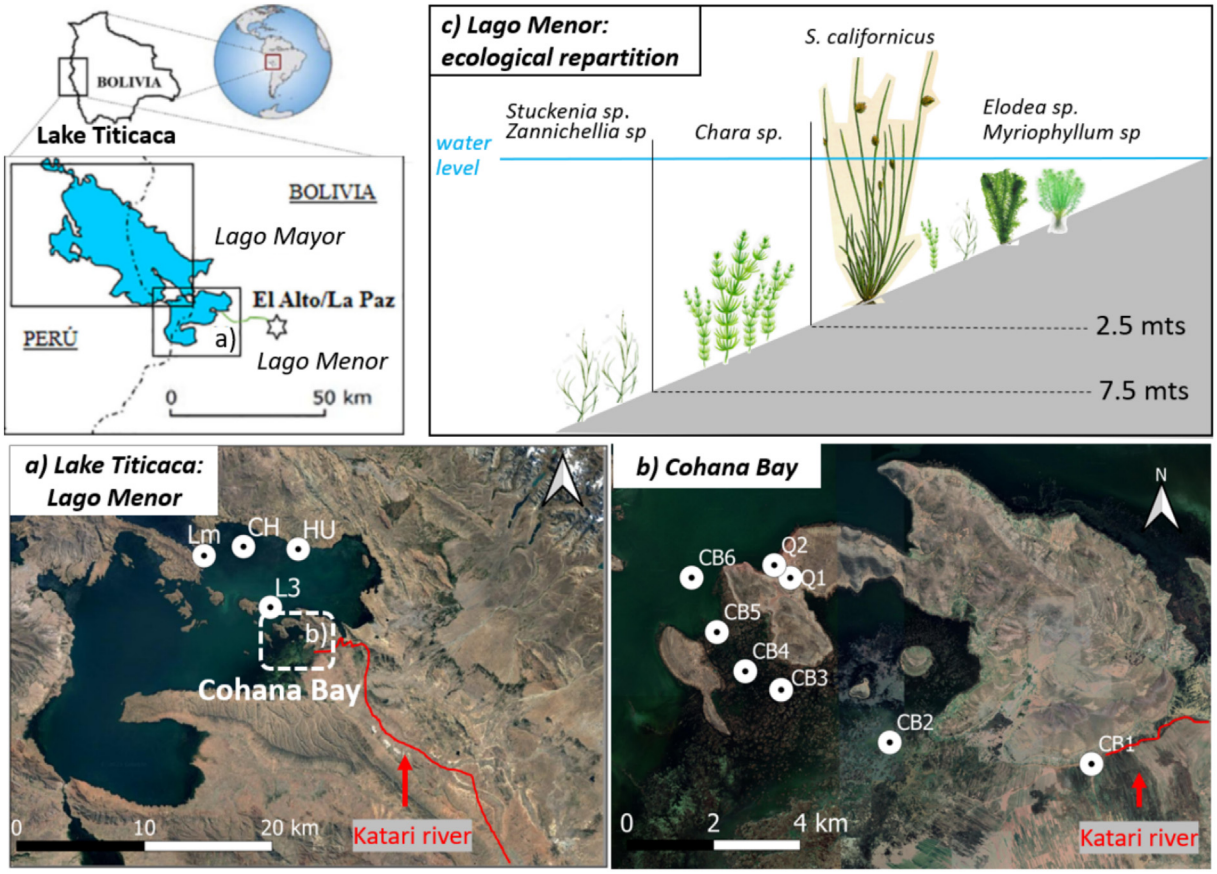

Fig. 1. Map of Lake Titicaca, presenting the sampling site location of a) control points in the coastal (CH = Chua, HU = Huatajata) and deep open waters (Lm and L3) of Lago Menor; b) the kilometric sampling points performed as a transect in the eutrophicated area of Cohana from the Katari River outlet (CB 1) to the open lake (CB 6) and from the weakly eutrophic Bay of Quehuaya (Q1 and Q2) for comparison and c) ecological repartition of the aquatic vegetation in Cohana Bay.

Currently, only small amounts of inorganic fertilizers are used in agricultural pratices (Martınez Gonzales et al., 2004; Aguilera et al., 2013). The Katari River flows into the Cohana Bay (Fig. 1b), a large (>86 km^2) and shallow area (average depth ~ 3 m) located in the southwestern part of the southern basin of Lake Titicaca. In the Bay, sediments are covered with totoras (*Schoenoplectus californicus*) in the inner margin (0–2 m depth) and by macrophytes (mostly *Characeae* spp.) in the photic zones (i.e., ~15 m depth) with maximum development between the depths of 4.5 and 7.5 m (Fig. 1c) (Collot et al., 1983; Dejoux and Iltis, 1991).

2.2. Sampling location and sample conditioning

Sampling was carried out in both April and September 2013, at the end of the wet and dry seasons, respectively. Six sampling sites were chosen within the Cohana Bay, starting from the confluence of the Katari River (KR) in the lake, and continuing towards the interior of the lake (CB 1 to CB 10.6) (Fig. 1c).

Sites were chosen following a eutrophication gradient previously determined by surface concentrations of dissolved organic carbon (DOC, Fig. 2). Two sampling zones outside Cohana Bay were chosen for comparison: i) the upper adjacent Bay of Quehuaya (Q1 and Q2) and Huatajata (HU) as representative of coastal sites exhibiting a weak eutrophication, and ii) three remote sites considered as non-impacted by anthropogenic activities: Chua (CH), the center of the open lake (L3) and just downstream of the Strait of Tiquina (Lm) which represents the water of the Lago Mayor (Fig. 1a).

All samples were obtained wearing nitrile gloves and collected in 50 ml polypropylene Falcon tubes to avoid cross-contamination. Macrophytes were collected manually or by dredging for the deep submerged ones. Five species belonging to four families were collected: *Schoenoplectus californicus* (Cyperaceae), Myriophyllum sp. (Haloagaceae), Elodea sp. (Hydrocharitaceae), Chara sp. (Characeae), and Stuckenia sp., Zannichellia sp. (Potamogetonaceae). Periphyton were collected manually by scraping them from the surface of substrate macrophytes. A Van Dorn bottle allowed the collection of water samples for SPM, then sieved and filtrated through pre-combusted glass microfiber filters (Whatman®, GF/F, 47 mm diameter, 0.7 μm mesh). Surface sediments were collected using a gravity corer.

Samples of macrophytes, periphyton, sediments (wet season only) and suspended particulate matter (SPM, dry season only) were collected at each site, except for the Chua, L3 and Lm sites where only POM was collected. Samples of superficial soil directly upstream of the Katari River inlet were also collected. All samples were stored at −20 °C and freeze-dried before laboratory analyses.

2.3. Chemical analysis

Physicochemical parameters (pH, redox potential, conductivity, dissolved oxygen, etc.…) of the water column at each site were measured with a HANNA HI-9828 submersible multiparameter probe (Hanna Instruments, Woonsocket, RI, USA).

Major anions concentrations were determined by ion chromatography (Dionex ICS 2000) and hydrogen sulfides by HPLC-UV following published procedures (Achá et al., 2018; Guedron et al., 2020).

Dissolved Organic Carbon (DOC) concentrations were determined by a Non-Dispersive Infra-Red (NDIR) CO_2 Shimadzu® (Model VCSN) spectrometer after humid oxidation in a sodium persulfate solution at 100 °C at the geochemistry-mineralogy platform of ISTerre (Grenoble, France).

Cavity Ring-Down Spectrometry (Picarro, Inc.®) coupled with Combustion Module (Costech, Inc.®) (CM-CRDS) allowed determination of

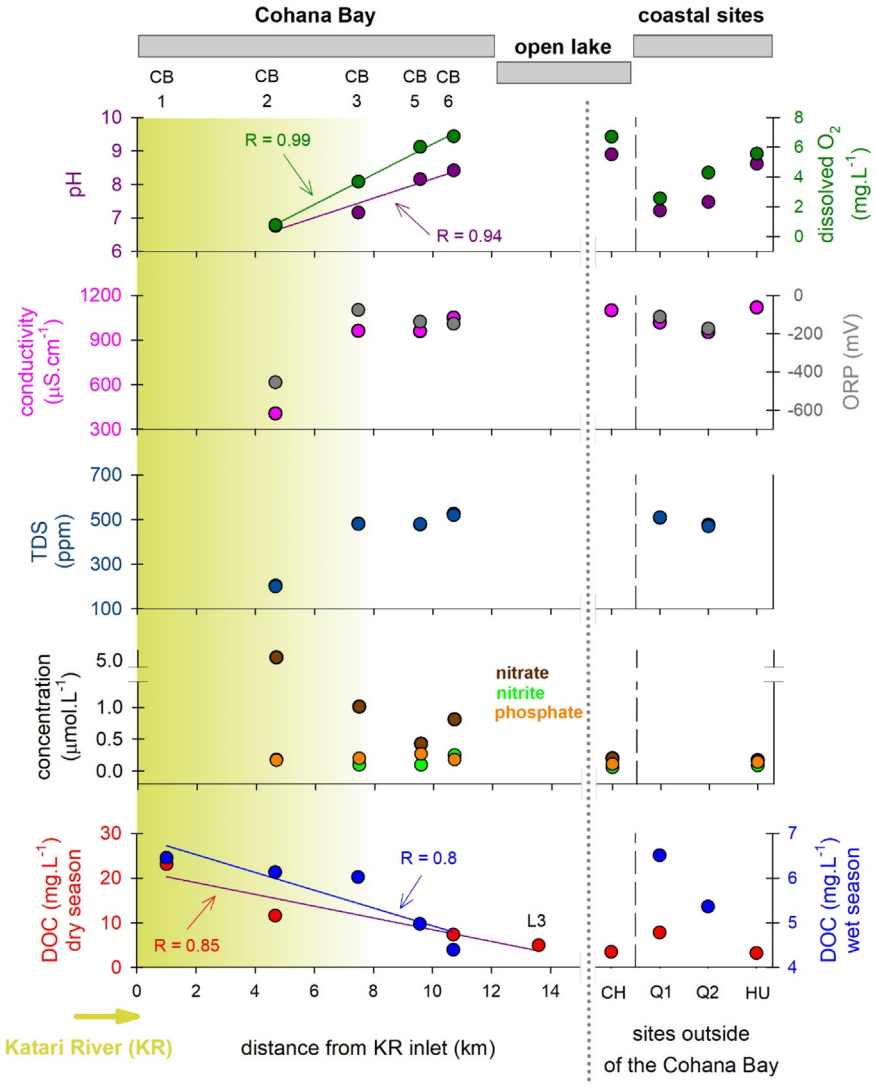

Fig. 2. Physicochemical parameters in surface water (1.5 m deep) of Cohana Bay (CB 1 to CB 6), the open lake (CH = Chua) and coastal sites (HU = Huatajata, Q1 and Q2 = Bay of Quehuaya) measured in April 2013. DOC was measured in April (wet season) and September (dry season) 2013. Regressions are plotted only for p values < 0.05. The colored area represents the wastewater input from the Katari River (KR). The three comparative sampling zones are indicated on the top of the figure with gray bands.

$\delta^{13}C_{bulk}$ of SPM as well as $\delta^{13}C_{org}$ of macrophytes, soils and sediments at the geochemistry-mineralogy platform of ISTerre of the University Grenoble-Alpes. Samples were calibrated against IAEA-603 standard. Analytical methods, calibration, and sample preparation (including decarbonatation) are detailed elsewhere (Paul et al., 2007; Balslev-Chausen et al., 2013; Cossa et al., 2021).

$\delta^{15}N$ of macrophytes, periphyton, SPM and sediment were measured using a Delta V Plus continuous flow isotope ratio mass spectrometer (CF-IRMS) (Thermo Scientific, Brême, Germany) with a ConFlo IV universal interface and ZeroBlank autosampler (Costech, Milan, Italy), after a complete combustion of samples on a Flash EA1112 Elemental Analyzer (EA) (Thermo Scientific, Milan, Italy) at the LIENSs laboratory of the University of La Rochelle (France). Samples were calibrated against IAEA-N1, -N2 and -N3 standards.

The analytical precision was ±0.11 ‰ (n = 27) for nitrogen (N_2) and ± 0.18 ‰ (n = 21) for carbon (CO_2). The isotopic composition was reported in relation to international standards for carbon (Vienna Pee Dee Belemnite - VPDB) and nitrogen (air) respectively. The data were expressed according to the deviation in parts per thousand (‰) from the respective standards, following the notation for isotopic composition (δ).

2.4. Statistical analysis

Statistical analyses were performed using SigmaPlot version 12.5. *P* values (p) and correlation coefficients (R) are reported for linear regression analyses. In all cases, a *p*-value of 0.05 was chosen to indicate statistical significance.

3. Results and discussions

3.1. Natural mitigation of anthropogenic wastewater discharge in the Cohana Bay

Physicochemical parameters along the Cohana Bay towards the open lake are presented in Fig. 2. The highest values of pH, conductivity (up to 1000 µS cm^{-1}), and total dissolved solids (TDS; up to 500 ppm) are found in the deepest part of the open Lake (i.e., Chua), which is consistent with its reported relatively saline and alkaline waters (Dejoux and Iltis, 1991) that result from the erosion of sulfate-rich minerals from the catchment (Banks et al., 2004; Ramos Ramos et al., 2014). Dissolved oxygen content is also near oxygen saturation at both sites due to the daily mixing of

the water column (Dejoux and Iltis, 1991). Similar values observed in the coastal site of Huatajata supports that these sites can be considered a weakly impacted area.

In contrast to the open lake, the physicochemical parameters of Cohana Bay's surface waters depict major gradients along the transect, illustrating the change in water quality between the inlet of the Katari river and the open lake. Previous publications (Archundia et al., 2017a,b) have documented the quality of the Katari River network, showing that water arriving at the lake had high DOC and nutrient contents but low dissolved oxygen and slightly acidic to neutral pH. The physicochemical dataset obtained downstream the confluence of the Katari River (i.e., CB1 and CB 2), confirms the significant contribution of urban (i.e., El Alto City and Viacha City) and agricultural areas in the discharges of DOC to the downstream freshwater ecosystem, a common feature of human-impacted watersheds (Stanley et al., 2012; Aitkenhead-Peterson et al., 2009). Higher DOC concentrations were found in this area during the dry season compared to the wet one (e.g. 23.1 and 6.5 mg L^{-1} at CB 2 for the dry and wet season, respectively, Fig. 2), which illustrates the dilution of DOC in wastewater during the wet season (December to April).

High concentration of DOC (and its organic acids) produces water acidification (Kortelainen, 1999) and the depletion of dissolved oxygen (Lindell et al., 1995) as observed in the first 5 km downstream the Katari River inlet. Strikingly, DOC concentrations decreased gradually along the transect in parallel with the rise in pH, conductivity, TDS, and dissolved oxygen from the Katari River inlet site (CB 2) to the interior of the bay (CB 6). Hence, this illustrates the attenuation of eutrophication within the Cohana Bay, where the water quality changes from anoxic, highly reducing and moderately acidic in the first kilometers from the inlet (CB 2), to oxic and alkaline but still reducing waters at 7.4 km (CB 3), and finally reaching similar quality status as the open lake (i.e., HU and CH) at 10.7 km (CB 6). In contrast, nitrate (NO_3^-) concentrations decreased within the first 5 km (from 5.2 to 0.8 μmol L^{-1}) whereas no variation in nitrite (NO_2^-, average = 0.13 ± 0.07 μmol L^{-1}) nor phosphate (PO_4^{3-}, average = 0.18 ± 0.05 μmol L^{-1}) were observed along the bay. Based on the annual average Katari river discharge of 5.8 $m^3 \cdot s^{-1}$ (SENAMHI, 2020), and average nitrate (3.3 ± 2.1 mg·L^{-1}) and phosphate (5.6 ± 3.1 mg·L^{-1}) concentrations in the lower Katari catchment (Archundia et al., 2017a,b; Sarret et al., 2019); the annual nitrate and phosphate discharge to the bay are 0.6 ± 0.4 Mg·y^{-1} and 1.0 ± 0.6 Mg·y^{-1}. The low concentrations in nutrients at CB 2 are consistent with those reported by Achá et al. (2018) for the Cohana area, but at least three times lower for NO_3^- and > 600 times lower for PO_4^{3-} concentrations reported in the Katari River mouth (Duwig et al., 2014). This points towards a rapid assimilation of nutrients (especially phosphate) in just a few kilometers within the lake. The low concentration of nutrients along Cohana Bay, despite the anthropogenic contribution, is a clear indication of its rapid assimilation by microorganisms and algae, especially by the macrophyte-related periphyton, most of which is attached to *S. californicus* (totora) in the belts that this macrophyte forms inside the Cohana Bay.

The great capacity of nutrient absorption by periphyton has already been documented in previous studies in this bay (Sarret et al., 2019; Quiroga-Flores et al., 2021). Hence, the natural mitigation of this anthropogenic contamination in the Cohana Bay results from (i) the uptake of DOC and nutrient by aquatic vegetation and algae and (ii) its dilution with pristine freshwater from the center lake region.

In the coastal site of Bay of Quehuaya, an analog of Cohana Bay without wastewater discharge, water physicochemistry had intermediate values, similar to those found at CB 3. Such moderate eutrophication status is likely due to the low-intensity anthropogenic activities in the surrounding villages (i.e., domestic wastewater, subsistence livestock farming and agriculture).

3.2. Carbon and nitrogen isotopic composition of Lake Titicaca's ecological compartments

3.2.1. Macrophytes: indicators of ecotopes and anthropogenic impact

Aquatic plant distribution in Lake Titicaca has previously been described to depend on water column depth (Fig. 1c). About 60 % of the Lago Menor's surface bottom is covered by aquatic vegetation (Collot et al., 1983).

Along the Cohana Bay transect, $\delta^{13}C_{org}$ values of macrophytes (all species considered) rise with the distance to the source along the eutrophication gradient (Fig. 3, top panel). The most depleted values are in the very shallow areas near the Katari River outlet (CB 1; $\delta^{13}C_{org}$ = −29.0 ± 0.4 ‰ and −26.5 ± 0.2 ‰ for the wet and dry season, respectively) in the range of reported values for emerged macrophytes [$\delta^{13}C_{org}$ = −26 ‰ to −28 ‰, green-colored band in Fig. 3, Rowe et al. (2002), Miller et al. (2010)]. The highest ones are in deeper areas towards the open lake (CB 6; $\delta^{13}C_{org}$ = −7.5 ± 0.6 ‰ and −8.2 ‰ for the wet and dry season, respectively), typical of the range reported for submerged macrophytes (ca. −12 ± 4 ‰, Fig. 3, dark cyan colored band) of Lake Titicaca (Rowe et al., 2002; Miller et al., 2010; Guedron et al., 2020). Such patterns of $\delta^{13}C_{org}$ in macrophytes reflect the pathway of carbon uptake, which is related to the plant's ecological distribution with water depth (e.g., emerged vs. submerged macrophytes), as well as changes in the quality (trophic status) of the water column. In the very shallow coastal sites, the dense vegetation of emerged macrophytes (i.e., *S. californicus*) which belongs to the group of the helophytes, exhibit isotopic values (average: −26.4 ± 1.5 ‰) within the range of terrestrial plants (−32 to −22 ‰), because most of the carbon is captured from the atmosphere (i.e., CO_2; $\delta^{13}C$ = −8 ‰) by the leaves. In contrast, submerged macrophytes (i.e., *Myriophyllum* sp., *Elodea* sp., *Chara* sp., *Stuckenia* sp. and *Zannichellia* sp.) exhibit more positive $\delta^{13}C_{org}$ values (average: −13.21 ± 6.5 ‰) because the carbon source mainly originates from the dissolved inorganic carbon (DIC), which includes dissolved CO_2 and all its pH-dependent forms. Hence, the difference in $\delta^{13}C_{org}$ between these aquatic plants is mostly attributable to their inorganic carbon source. The boundary layer diffusion effects during atmospheric vs. aquatic photosynthesis decrease the discrimination against the heavy isotope, resulting in higher $\delta^{13}C_{org}$ values in submerged macrophytes (Finlay and Kendall, 2007).

Amongst the species present in the Bay, emerged macrophytes (*S. californicus*) show similar $\delta^{13}C_{org}$ values (average: −26.4 ± 1.5 ‰) regardless of their location and the season. In contrast, submerged macrophytes collected in the coastal (Q2 and HU) and deep sites near the open lake (CB 6 and L3) exhibited the highest $\delta^{13}C_{org}$ values, up to −7 ‰ (Fig. 3). Along the Cohana bay, $\delta^{13}C_{org}$ of the submerged macrophytes decrease with distance to the KR inlet (−27.4 ± 1.3 ‰ at CB 1 to −7.7 ± 0.5 ‰ at CB 6, seasonal average) likely resulting from changing sources in the DIC pool. In submerged macrophytes near the Katari River inlet, $\delta^{13}C_{org}$ values are similar to allochthonous inputs dominated by terrestrial organic matter (OM) from the catchment (ca. −23.8 ‰, dotted line, Fig. 3). This indicates that the source of DIC for submerged macrophytes close to the Katari mouth mainly originates from the recycling of mixed terrestrial or anthropogenic OM. In contrast, towards the open lake, it rather originates from locally produced carbonate dissolution and the decomposition of OM, mostly from *Characeae* [−8 to −16 ‰, Rowe et al. (2002), Miller et al. (2010)].

Strikingly, nitrogen stable isotopes signatures of macrophytes exhibit a reverse trend compared to C isotopes, with decreasing $\delta^{15}N$ values with distance. The highest $\delta^{15}N$ values are found in the very shallow areas near the Katari River outlet, with higher values during the wet season, i.e., between CB 1 ($\delta^{15}N_{wet}$ = +19.8 ± 1.8 ‰, $\delta^{15}N_{dry}$ = +8.9 ± 1.5 ‰) and CB 2 ($\delta^{15}N_{wet}$ = +21.4 ± 2.0 ‰, $\delta^{15}N_{dry}$ = +10.7 ± 2.0 ‰) which are typical of N-enriched systems [i.e., between +10 and +20 ‰ (McClelland et al., 1997), dark yellow band in Fig. 3]. The lowest $\delta^{15}N$ values are found towards the open lake and remains in a narrow range independent of the season (e.g., CB 10.7: $\delta^{15}N$ = −3.6 ‰ ± 0.5 ‰, seasonal average), similar to those reported by Miller et al. (2010), typical of N-depleted ecosystems [−1 to −3 ‰, cyan colored band; Zhang et al. (2014)]. The costal sites (Q1 = −0.51 ‰, Q2 = −0.2 ± 1.2 ‰, Hu = −4.2 ± 5.6 ‰), and relatively deep (L3 = −0.7 ± 1.1 ‰) sites show similar low values.

In contrast to carbon cycling and isotopic signature ($\delta^{13}C_{org}$), the differences in the signature of $\delta^{15}N$ between macrophytes is caused by a wide and combined range of factors, including the various metabolic pathways used for nitrogen assimilation, changes in the types of nitrogen assimilated,

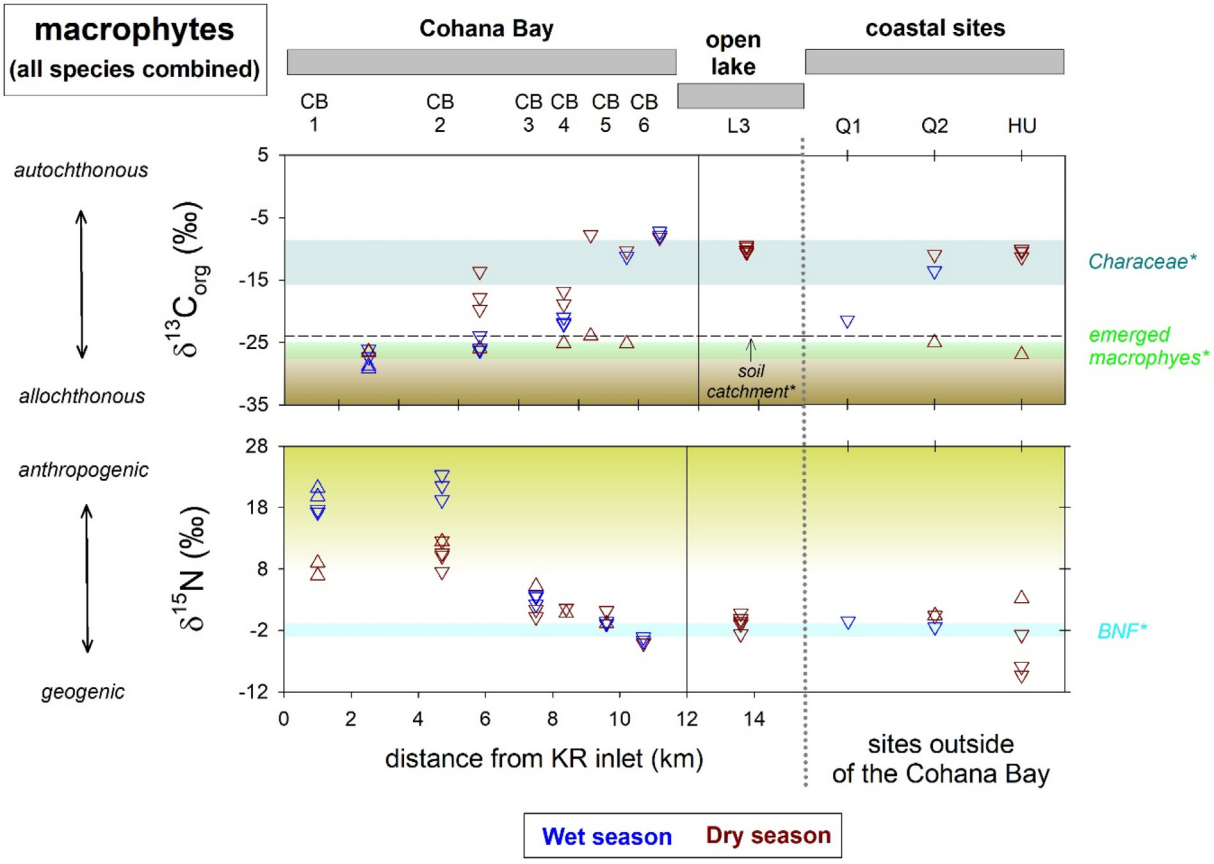

Fig. 3. $\delta^{13}C_{org}$ (top) and $\delta^{15}N$ (bottom) stable isotope composition of macrophytes (submerged: ∇, emerged: Δ) at Cohana Bay, the open lake and coastal sites (Q1 and Q2 = Bay of Quehuaya, HU = Huatajata). Colored triangles refer to wet (blue) and dry (red) season. Colored areas refer to: allochthonous terrestrial $\delta^{13}C$ (brown), anthropogenic $\delta^{15}N$ (yellow), submerged macrophyte $\delta^{13}C$ from lake shallows (dark cyan), emerged macrophyte $\delta^{13}C$ (green) and biological nitrogen fixation (BNF, cyan). Reference thresholds of colored areas are as follows: allochthonous $\delta^{13}C$ [−23 ‰, Finlay and Kendall (2007) and Chappuis et al. (2017)], anthropogenic $\delta^{15}N$ [+10 ‰, McClelland et al. (1997) and Finlay and Kendall (2007)], typical submerged macrophyte $\delta^{13}C$ [−8 to −16 ‰, Rowe et al. (2002)], typical emerged macrophyte $\delta^{13}C$ [−26 to −28 ‰, Rowe et al. (2002)] and BNF [−1 to −3 ‰, Zhang et al. (2014)]. $\delta^{13}C$ of the soil catchment (−23.8 ‰) is presented as a black dotted line. The three comparative sampling zones are indicated on the top of the figure with gray bands.

and the relative activity of nitrogen-fixing and denitrifying bacteria (Handley and Raven, 1992). Amongst these factors, the abundance of assimilated dissolved inorganic nitrogen (DIN) by plants, which can be in the form of nitrate (NO_3^-) and ammonium (NH_4^+), mainly depends on three major sources of supply; (i) the atmosphere (dry deposition and biological fixation), (ii) the catchment (i.e., mineralization of the OM), and (iii) fertilizers, animal or human waste (Finlay and Kendall, 2007).

In N-enriched ecosystems (e.g., human impacted environments), elevated $\delta^{15}N$ values (+10 to +20 ‰) are generally attributed to the removal of volatilized ammonia from human and animal wastes during early stages of wastewater degradation (McClelland et al., 1997) as well as the higher trophic level from which they have originated [i.e., consumers exhibit a 2 to 3 ‰ $\delta^{15}N$ enrichment relative to their diet, Kendall et al. (2007)]. In contrast, in N-limited ecosystems such as the open lake, nitrogen biological fixation (NBF) plays a major role in supplying bioavailable nitrogen (i.e., NH_3) to the N pool with $\delta^{15}N$ ratios [−1 to −3 ‰, Zhang et al. (2014)] that are close to those of atmospheric N_2 (ca. 0 ‰) (Chappuis et al., 2017).

The low N concentration in the entire Lake supports the hypothesis of a rapid N assimilation in the water column despite the high anthropogenic discharge into the Cohana Bay, and confirms that N and P are limiting factors for aquatic biota within the lake (Fig. 2, and Dejoux and Iltis, 1991). In N limited ecosystem, N uptake is expected to produce little net fractionation between the $\delta^{15}N$ of DIN and macrophyte (Finlay and Kendall, 2007). Therefore, $\delta^{15}N$ of macrophyte in Lake Titicaca likely integers the isotopic signature of the DIN source during the plant's life cycle. Although one cannot rule out significant fractionation of N associated with in situ growth and respiration (e.g., nitrification and denitrification) in the anoxic Katari river and the Cohana bay waters and sediment, high $\delta^{15}N$ values in macrophytes at the mouth of the Katari River (up to +21 ‰, Fig. 3) supports manure piles and septic waste as the main anthropogenic N source. These values are consistent with $\delta^{15}N_{NO3-}$ values reported for the lower Katari basin surface and ground waters (Flores Avilés et al., 2022). Hence, $\delta^{15}N$ values in macrophytes confirms physico-chemical observations (Fig. 2) and support anthropogenic inputs as the dominant N source within the first 5 km of the Cohana Bay, whereas depleted $\delta^{15}N$ values outside this area support the fixation of atmospheric N as the major supplier to the DIN pool.

In addition, the large seasonal variations in $\delta^{15}N$ observed within the first 5 km of the Cohana Bay reflect enhanced anthropogenic N inputs during the wet season, likely resulting from the leaching of urban and agricultural areas (Achá et al., 2018). In contrast, lower values $\delta^{15}N$ values in macrophytes at the mouth of the Katari River (+8.0 to 10.7 ‰, Fig. 3) during the dry season indicates an anthropogenic contribution mixed with a depleted ^{15}N source.

3.2.2. Periphyton: an integrator of macrophytes and water column signal

Periphyton is defined as a biofilm composed of an assemblage of organisms (e.g., algae, bacteria, fungi, microinvertebrates, prokaryotes, and protozoa), and organic and inorganic detritus held in a mucopolysaccharide matrix attached to macrophytes (Lowe, 1996). Several studies performed in Lakes Titicaca and Uru-Uru reported the periphyton to act as a trap for

suspended solids and dissolved elements, including nutrients (Alanoca et al., 2016; Lanza et al., 2017; Sarret et al., 2019; Guédron et al., 2020; Quiroga-Flores et al., 2021).

In the entire set of periphyton samples (Fig. 4, top), $\delta^{13}C_{bulk}$ did not exhibit any specific spatial distribution trend during the dry season, whereas a gradual increase of $\delta^{13}C$ values with distance was observed in the Cohana Bay during the wet season from CB 2 ($\delta^{13}C_{bulk} = -32.4$ ‰) to CB 5 ($\delta^{13}C_{bulk} = -18.15$ ‰). It is worth mentioning that samples collected during the wet season were exclusively associated with emerged macrophytes (i.e., *S. californicus*), whereas the ones collected during the dry season were associated with different macrophytes (Fig. 4). A previous study in shallow eutrophic lakes has reported that the $\delta^{13}C$ of the periphyton closely reflects the isotopic composition of the macrophyte that serves as substrate (De Kluijver et al., 2015). Accordingly, the high seasonal variation at coastal site Q2 (11.3 ‰) confirms this effect, where the ^{13}C-depleted value measured during the wet season is similar to that of the hosting macrophyte *S. californicus*, whereas the ^{13}C-enriched value measured during the dry season matches that of the submerged macrophytes (ca. -12 ± 4 ‰, dark cyan colored band in Fig. 4).

In the case of Cohana Bay, the lowest $\delta^{13}C_{bulk}$ values (average: -26.2 ± 5.4 ‰) were measured during the wet season and had similar values to those of the ^{13}C-depleted OM of emerged macrophytes, suggesting that the periphyton collected in the vicinity of the Katari outlet during the wet season have assimilated dominantly the OM of its hosting emerged macrophyte together with a contribution of entrapped or adsorbed allochthonous OM from the Katari River inlet. In contrast, periphyton collected towards the open lake (i.e., CB 5) and in Huatajata (HU) have assimilated the ^{13}C-enriched OM of the submerged macrophytes (ca. -12 ± 4 ‰, dark cyan colored band in Fig. 4) and algae [ca. -22.5 ‰, pink-colored band in Fig. 4; Rowe et al. (2002)]. The higher seasonal differences found for the shallow coastal sites at CB 2 (15.7 ‰) compared to that of CB 3 (6.3 ‰) supports a significant contribution of allochthonous OM during the wet season, which decreased with distance to the Katari outlet.

In contrast to $\delta^{13}C$ signatures, the $\delta^{15}N$ of periphyton exhibited a trend similar to their hosting macrophytes, with decreasing values from $+12$ ‰ at CB 2 to $+2.1$ ‰ at CB 5 during the wet season (10 ‰ difference) and from $+10.3 \pm 2.3$ ‰ at CB 2 to $+2.5 \pm 2$ ‰ at CB 3 during the dry season (7.8 ‰ difference, bottom panel in Fig. 4). Such ca. 7.8 ‰ drop in $\delta^{15}N$ in almost 3 km confirms the rapid assimilation of the anthropogenically-derived N followed by a dominance of DIN supplied by BNF. Amongst coastal sites, Huatajata exhibited $\delta^{15}N$ ratios ($+1.7 \pm 0.8$ ‰) typical of pristine or weakly polluted waters, whereas Bay of Quehuaya showed slightly higher $\delta^{15}N$ values (Q1 = 4.4 ‰, Q2 = 3.5 ‰) that could be attributed to a slight contribution of animal waste N inputs during the wet season.

3.2.3. Suspended particulate matter (SPM) and sediment: spatio-temporal indicators

Lake suspended particulate matter (SPM) is composed of both autochthonous (i.e., debris of primary producers and periphyton) and allochthonous

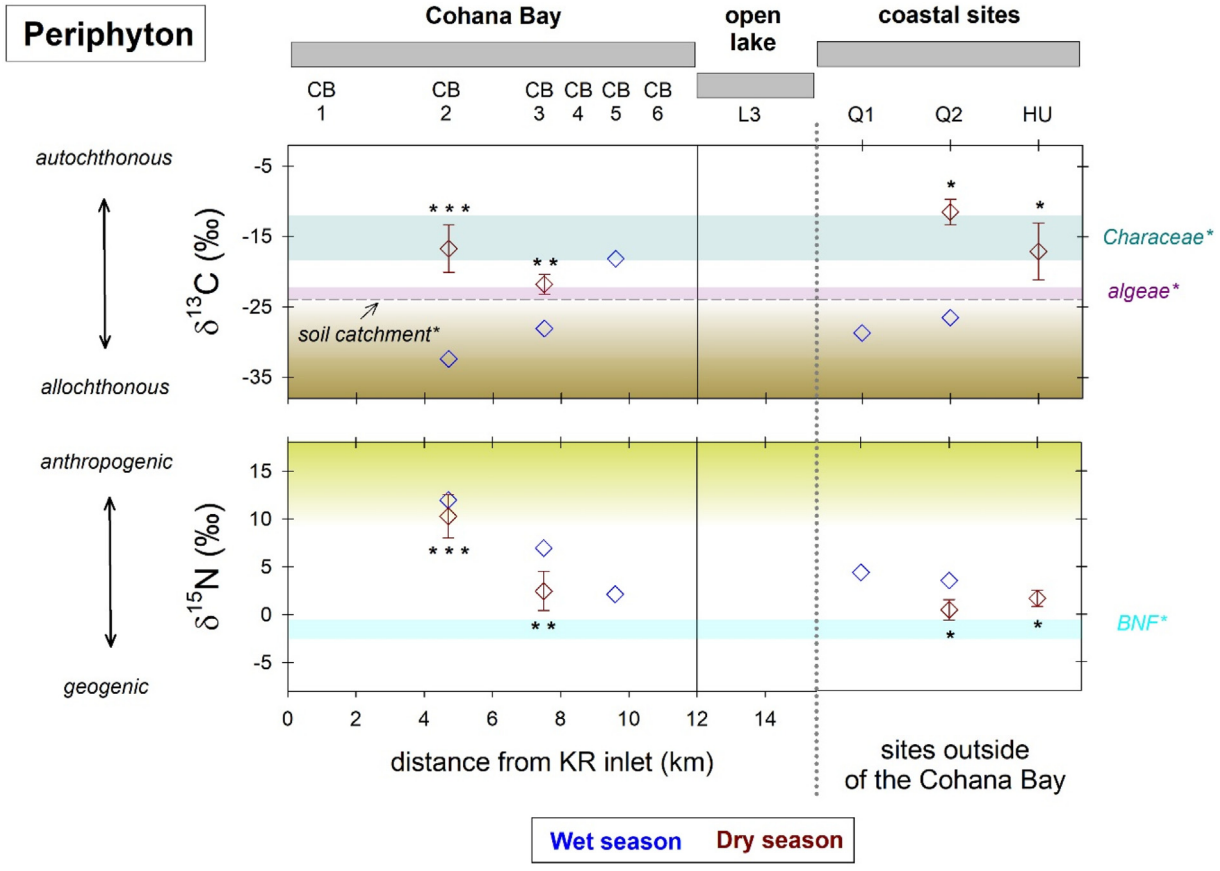

Fig. 4. $\delta^{13}C_{bulk}$ (top) and $\delta^{15}N$ (bottom) stable isotope composition of periphyton at Cohana Bay, the open lake and coastal sites (Q1 and Q2 = Bay of Quehuaya, HU = Huatajata). Colored diamonds refer to wet (blue) and dry (red) season. Error bars represent confidence intervals for data at each site. Colored areas refer to: allochthonous terrestrial $\delta^{13}C$ (brown), anthropogenic $\delta^{15}N$ (yellow), submerged macrophyte $\delta^{13}C$ from Lake Titicaca shallows (dark cyan), algae $\delta^{13}C$ (pink) and biological nitrogen fixation (BNF, cyan). Reference thresholds of colored areas are as follows: allochthonous $\delta^{13}C$ [-23 ‰, Finlay and Kendall (2007) and Chappuis et al. (2017)], anthropogenic $\delta^{15}N$ [$+10$ ‰, McClelland et al. (1997) and Finlay and Kendall (2007)], typical submerged macrophyte $\delta^{13}C$ [-8 to -16 ‰, Rowe et al. (2002)], local planktonic $\delta^{13}C$ [-22.5 ‰, Rowe et al. (2002)] and BNF [-1 to -3 ‰, (Zhang et al., 2014)]. $\delta^{13}C$ of the soil catchment (-23.8 ‰) is presented as a black dotted line. The three comparative sampling zones are indicated on the top of the figure with gray bands. The star symbols (*) indicate the hosting macrophytes from which periphyton was taken (*: Chara sp.; **: Elodea sp. - Stuckenia sp. – Zannichellia sp.; ***: S. californicus – Stuckenia sp. – Zannichellia sp.).

organic matter (i.e., terrestrial OM from the catchment) that settles to the bottom sediment. Therefore, both the SPM and sediment can be considered as an integrative picture of the lake productivity at short and longer temporal scale, respectively.

Similar to macrophytes, $\delta^{13}C_{bulk}$ values for SPM exhibited a linear increase with distance to the KR in the Cohana Bay of 11.2 ‰ (upper panel in Fig. 5). However, these values remained constant in the open lake and the coastal sites (average $\delta^{13}C_{bulk} = -17.7 \pm 0.8$ ‰ and -19.8 ± 0.9 ‰, for SPM and sediment respectively), and within the range of submerged macrophytes. These observations support our earlier findings that the contribution of allochthonous and anthropogenic OM inputs are significant within the first 8 km within the bay. They also imply a major anthropogenic OM contribution from upstream cities as the low $\delta^{13}C_{bulk}$ ratios found for SPM at CB1 (-29 ‰) is typical of sewage effluents and catchment runoff [average $\delta^{13}C_{org} = -24.2$ ‰, Gearing et al. (1991), Rosenmeier et al. (2004)]. Further in the bay and at other coastal sites, the decomposition of OM from submerged macrophytes (i.e., mostly Chara sp.) is the largest supplier to the DIC pool with a small contribution from pelagic primary productivity (i.e., algae).

Similar to SPM, $\delta^{13}C_{org}$ of sediment exhibit a gradual increase of 8.6 ‰ within the bay. However, whereas the SPM exhibit very negative values close to the KR outlet, the ones of sediment are in the typical range of soil and emerged macrophyte values and do not allow attributing a significant anthropogenic contribution. Then, the gradual rise of $\delta^{13}C_{org}$ within the bay can be attributed to the gradual change in dominant vegetation from emerged to submerged macrophytes. It is worth mentioning that collected sediments covered the ten first centimeters and have likely integrated the last 20 to 100 years of sedimentation. Indeed, the average sedimentation rate ranges between 0.1 and 0.5 cm per year in the coastal sites of Lake Titicaca (Guedron et al., 2020). Hence, the measured $\delta^{13}C_{org}$ signature integrates both the historical sediment signature and possible historical change in ecological distribution related to past lake-level changes (Guedron et al., 2021).

The $\delta^{15}N$ values of SPM also mirrored those of macrophytes, showing a linear decrease (11.1 ‰ difference between CB 1 and CB 6) with increasing distance to the Katari river. As for $\delta^{13}C$, the signatures of $\delta^{15}N$ remained constant in the open lake and at the coastal sites with depleted values (average: $\delta^{15}N_{SPM} = +1 \pm 1.2$ ‰). Again, these $\delta^{15}N$ values close to 0 in remote areas are indicative of nitrogen biological fixation [-1 to -3 ‰, Fig. 5, cyan colored band; Zhang et al., 2014], most likely due to insufficient NO_3^- in the DIN pool (Gu et al., 2006), contrasting with values near the Katari River outlet ($\delta^{15}N$; CB 1 = +9.5 ‰, CB 2 = 12.2 ‰) where wastewater-derived N is the main source.

In contrast, $\delta^{15}N$ values of the sediment did not show significant changes within the Cohana Bay, and remained in a narrow range of variation (2.6 ‰ difference) within the range of values of the BNF domain ($\delta^{15}N = -1.3 \pm 2.4$ ‰) as for the open lake and the coastal areas. Such a different trend found in $\delta^{15}N$ between SPM and sediment likely results, as for $\delta^{13}C_{org}$, from the large time period covered by the collected sediment cores. Hence, the recent anthropogenic signal has likely been smoothed or obliterated by the pristine historical signal of the sediment.

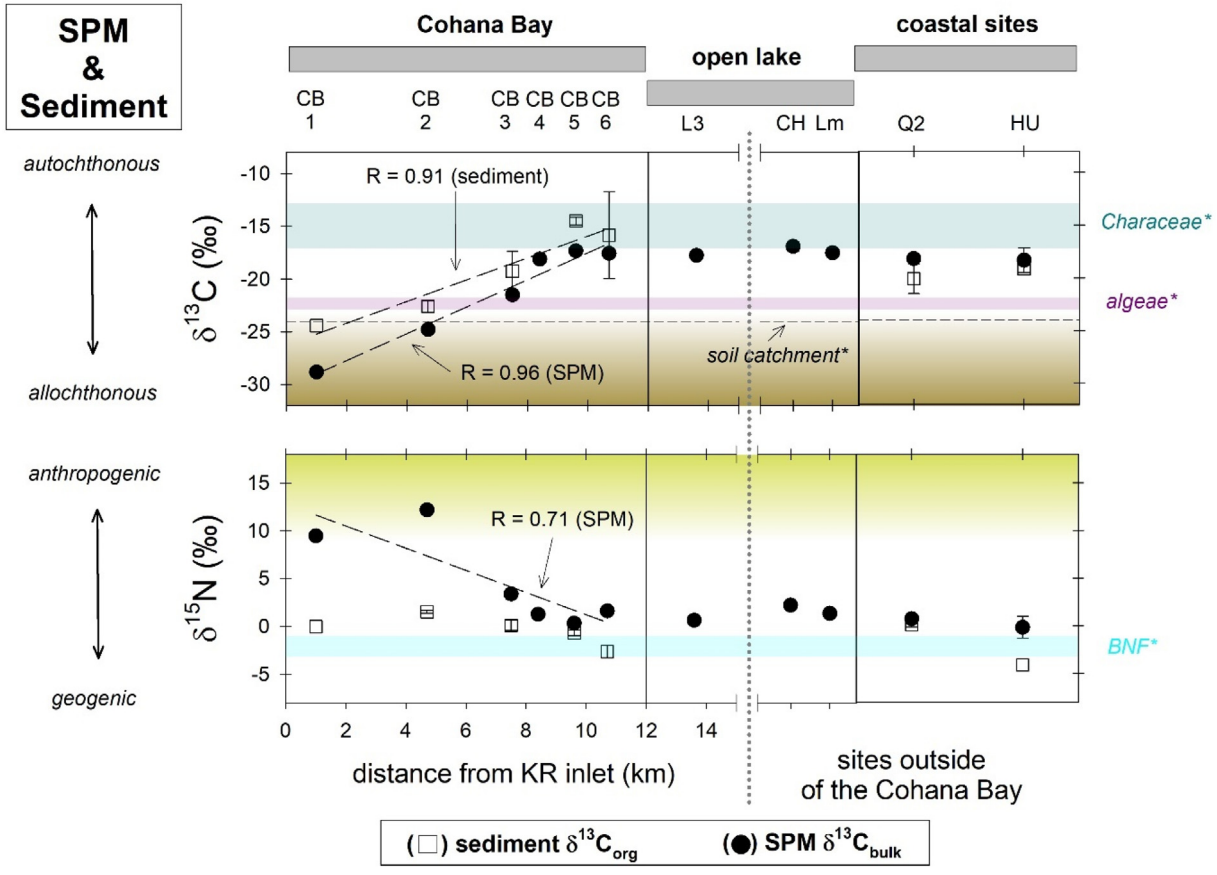

Fig. 5. $\delta^{13}C$ (top) and $\delta^{15}N$ (bottom) stable isotope composition of SPM (●, dry season) and sediment (□) at each sampling site for Cohana Bay, the open lake (CH = Chua, Lm = Lago mayor) and coastal sites (Q1 and Q2 = Bay of Quehuaya, HU = Huatajata). Error bars represent confidence intervals for data at each site. Regressions are plotted only for p values < 0.05. Colored areas refer to: allochthonous terrestrial $\delta^{13}C$ (brown), anthropogenic $\delta^{15}N$ (yellow), submerged macrophyte $\delta^{13}C$ from Lake Titicaca shallows (dark cyan), algae $\delta^{13}C$ (pink) and biological nitrogen fixation (BNF, cyan). Reference thresholds of colored areas are as follow: allochthonous $\delta^{13}C$ [-23 ‰, Finlay and Kendall (2007) and Chappuis et al. (2017)], anthropogenic $\delta^{15}N$ [+10 ‰, McClelland et al. (1997) and Finlay and Kendall (2007)], typically submerged macrophyte $\delta^{13}C$ [-8 to -16 ‰, Rowe et al. (2002)], local planktonic $\delta^{13}C$ [-22.5 ‰, Rowe et al. (2002)] and BNF [-1 to -3 ‰, Zhang et al. (2013)]. $\delta^{13}C$ of the soil catchment (-23.8 ‰) is presented as a black dotted line. The three comparative sampling zones are indicated on the top of the figure with gray bands.

3.2.4. Fingerprinting anthropogenic contamination with $\delta^{13}C$ vs $\delta^{15}N$

The spatial changes in both $\delta^{13}C$ and $\delta^{15}N$ signatures for macrophytes, SPM, and to a lesser extent for periphyton within the Cohana Bay, reveal that anthropogenic contamination is progressively attenuated within the bay. In contrast, other coastal sites (i.e., Quehuaya Bay and Huatajata) distant from the Katari Outlet only show a low contamination signal.

At the seasonal scale, both the macrophyte and periphyton show increased spreading of the anthropogenic contamination within the bay during the wet season, a period of enhanced catchment leaching (i.e., soils and urban area), river discharge, and transfer of dissolved and particulate C and N to the Lake. In addition, the significant inter-seasonal lake-level changes, up to 2 m (SENAMHI, 2021), also affect the ecotope distribution and the development of specific plant species aggregates more or less tolerant to high nutrient loads depending on the season and eutrophication status.

When using 2D isotopic graphs (Fig. 6), the differences are clearly noticeable for the spatial changes between $\delta^{13}C$ and $\delta^{15}N$ signatures within each compartment. Indeed, the absence of a significant correlation between $\delta^{13}C$ and $\delta^{15}N$ suggests that carbon and nitrogen recycling processes are significantly different inside the bay. Regardless of the season, the $\delta^{13}C$ of macrophytes (except *S. californicus*), periphyton and SPM within the first 8 km (i.e., between CB 3 and CB 4) exhibit lower values (Fig. 6) typical of allochthonous C (Finlay and Kendall, 2007; Chappuis et al., 2017).

In contrast, the $\delta^{15}N$ of the four lake compartments depict a clearer pattern of $\delta^{15}N$ depletion from anthropogenic $\delta^{15}N$-enriched values, to lower ones typical of N-biological fixation and/or atmospheric deposition around 5 km (Fig. 6). This rapid, close to the source, depletion of heavier N isotopes likely indicates a rapid consumption of anthropogenic N in this N-limited aquatic system, whereas the larger extension of the anthropogenic ^{13}C signal supports slower incorporation of anthropogenic C in the oligotrophic part of the system.

Hence, three zones can be identified in the Cohana Bay: (i) the first 5 km to the Katari River outlet where anthropogenic C and N inputs dominate, (ii) a transition zone between 7 and 8 km from the KR outlet that marks the mixing and dilution of urban and terrestrial OM, and (iii) a pristine zone in the deepest part of the bay dominated by N-fixation and autochthonous C similar to the rest of the open lake, providing the biogeochemical isotopic baseline signature of the ecosystem. The larger attenuation occurs within the belt of totoras which acts as a physical barrier where the biological pump (dominated by periphyton) consumes the discharged nutrients and entraps floating SPM.

Moreover, the 3 studied compartments showed substantial differences along the eutrophication gradient. Submerged macrophytes and SPM accurately illustrated the dilution between anthropogenic and natural OM sources. SPM illustrates greatly the two distinct anthropogenic and pristine pools, with few intermediates. For macrophytes, the ecological distribution along the bay shows the distinct ability of aquatic plant species to integrate the C signal depending on the plant type, water depth and quality. Indeed, whereas the emerged macrophyte (i.e., *S. californicus*, only found in very shallow areas) does not allow the C source identification because of its terrestrial-like behavior (i.e., atmospheric C incorporation), the submerged macrophytes, like Chara sp. and Elodea sp., which are relatively well

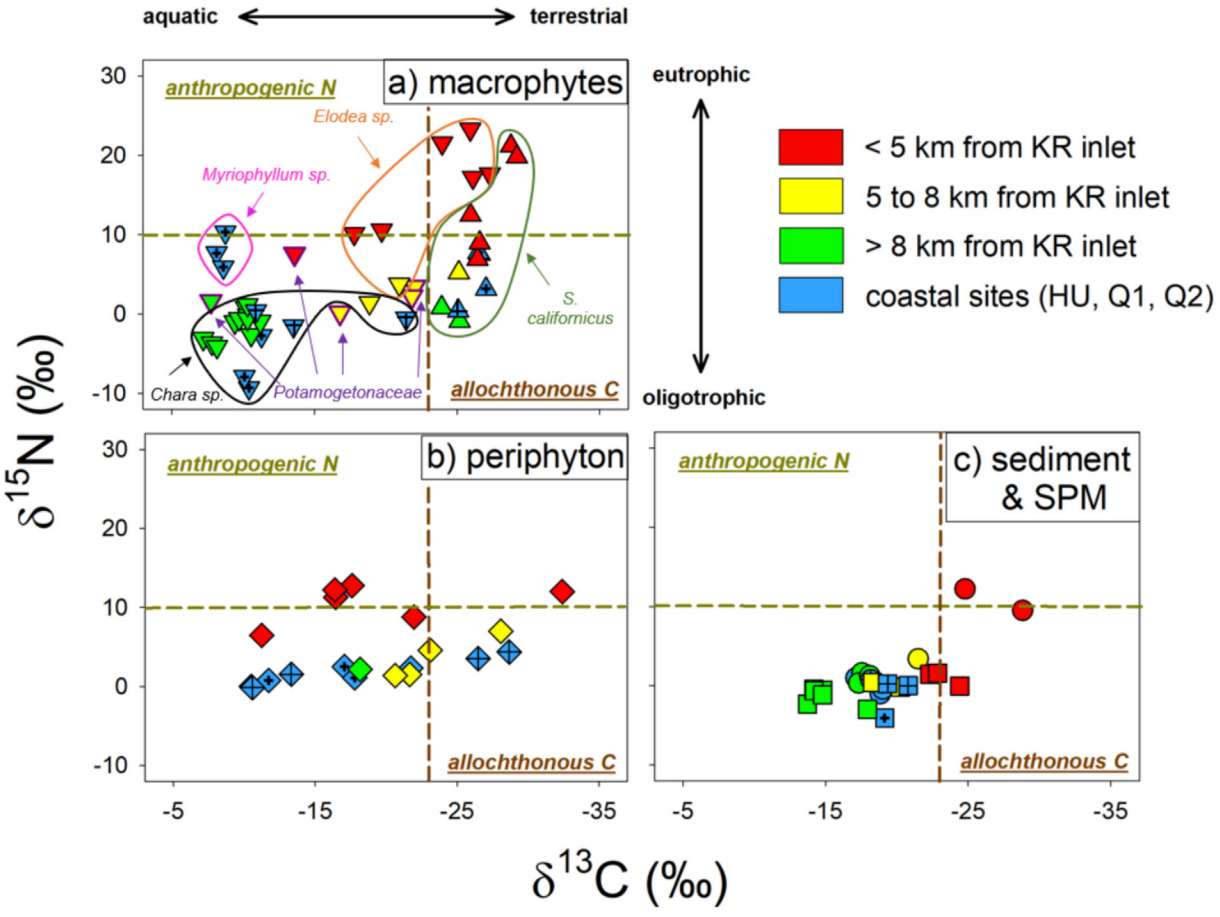

Fig. 6. $\delta^{13}C$ vs $\delta^{15}N$ biplots of: a) macrophytes (submerged: ∇, emerged: Δ), b) periphyton (◊), c) sediments and particulate organic matter (□ and ○, respectively) for Cohana Bay and the coastal sites (Huatajata and Bay of Quehuaya). Symbols represent individual values of each sample evaluated in this study. Colors refer to: the coastal sites (blue) and the polluted (red), transitioning (yellow) and pristine or weakly polluted areas (green) within Cohana Bay. Huatajata and Bay of Quehuaya are presented as x-hair and crossed symbols, respectively. Colored dotted lines refer to: allochthonous terrestrial $\delta^{13}C$ (brown) and anthropogenic $\delta^{15}N$ (dark yellow). Reference thresholds of colored areas are as follows: allochthonous $\delta^{13}C$ [−23 ‰, Finlay and Kendall (2007) and Chappuis et al. (2017)] and anthropogenic $\delta^{15}N$ [+10 ‰, McClelland et al. (1997) and Finlay and Kendall (2007)].

distributed along the transect, provide a large range of $\delta^{13}C_{org}$. This is not the case for myriophyllum sp., which is only encountered in the pristine coastal site and may indicate its sensitivity to eutrophication. In contrast, both macrophytes (emerged and submerged) exhibit high differences in $\delta^{15}N$ signatures as they integer DIN via the aqueous media.

Periphyton C and N isotope signatures range in between the ones of macrophytes and SPM. Their $\delta^{13}C$ values are however tightly related with those of their hosting plant (Fig. 6a and b), whereas their $\delta^{15}N$ is as narrow as the one of SPM (Fig. 6b and c) with all samples having an atmospheric N_2 source (i.e., close to 0) except for those located within the first 5 km from the KR.

Finally, for other shallow coastal sites away from Cohana Bay (i.e., Huatajata and Bay of Quehuaya), the absence of a significant pollution signal indicated by their $\delta^{13}C$ and $\delta^{15}N$ isotopic signatures reflects their overall intact status. However, some moderately higher values indicate that agricultural land leaching is the main source of allochthonous OM during the wet season.

3.3. Significance of lake ecological compartments as bioindicators of eutrophication

3.3.1. Mixing model with $\delta^{13}C$ vs $\delta^{15}N$

To estimate the contribution of wastewater effluent as a source of C and N to the ecosystem, we used a linear mixing model to calculate plant uptake of wastewater-derived carbon and nitrogen (Cecchetti et al., 2020). In the absence of precise isotopic data for each anthropogenic source (e.g., human and animal sewage, synthetic fertilizers…), a simplified two-source linear mixing model (taking into account a natural and an anthropogenic pool) was applied to our data according to Eqs. (1) and (2) for carbon, and Eqs. (3) and (4) for nitrogen:

$$\delta^{13}C_{Plants} = \left(\delta^{13}C_{prist}\right) * \left(f_{prist}\right) + \left(\delta^{13}C_{WW}\right) * \left(f_{WW}\right); \quad (1)$$

and

$$1 = f_{prist} + f_{WW} \quad (2)$$

$$\delta^{15}N_{Plants} = \left(\delta^{15}N_{atmos}\right) * \left(f_{atmos}\right) + \left(\delta^{15}N_{WW}\right) * \left(f_{WW}\right); \quad (3)$$

and

$$1 = f_{atmos} + f_{WW} \quad (4)$$

where $\delta^{13}C_{Plants}$, $\delta^{13}C_{prist}$, $\delta^{13}C_{WW}$ are the carbon isotope signatures of plants, pristine DIC and wastewater, and $\delta^{15}N_{Plants}$, $\delta^{15}N_{atmos}$, and $\delta^{15}N_{WW}$ are the nitrogen isotope signatures of plants, atmosphere and wastewater.

As mentioned previously, emerged and submerged macrophyte have different baseline $\delta^{13}C_{org}$ values because the fractionation of $^{13}C_{org}$ in macrophytes is plant-specific (i.e., pathway of DIC or atmospheric CO_2 uptake). Hence, to estimate the fraction of carbon uptaken without a single contribution of atmospheric CO_2, we only considered *Characeae* as their source of DIC may largely depend on the loading of DIC from the watershed (Bade et al., 2004), and because these submerged macrophytes have the largest distribution within the study sites. Carbon isotope endmember value for anthropogenic source ($\delta^{13}C_{WW}$) was taken from the one of SPM collected at the inlet of the Katari in Lake Titicaca (CB1; $\delta^{13}C = -28.8$ ‰). The pristine $\delta^{13}C$-DIC reference value ($\delta^{13}C_{prist}$) was taken from average values published for $\delta^{13}C$-DIC (-8.0 ‰) at the isotopic equilibrium with the atmosphere in alkaline and slightly positive pH (~8) lakes (Bade et al., 2004), which is similar to the values found in Characeae at site CB 6 and L3, and those reported for Characeae in Lake Wiñaymarca (Miller et al., 2010).

Nitrogen isotope endmember value for wastewater $\delta^{15}N$ was taken from Hydrocharitaceae samples collected during the most impacted wet season at the inlet of the KR (CB 1; $\delta^{15}N = 23.3$ ‰) which is in the range of reported $\delta^{15}N$ for wastewater (10 to 20 ‰), and to the one of $\delta^{15}N$ in nitrate of the Katari wastewater ($\delta^{15}N = 19.2$ ‰) from the upper part of the

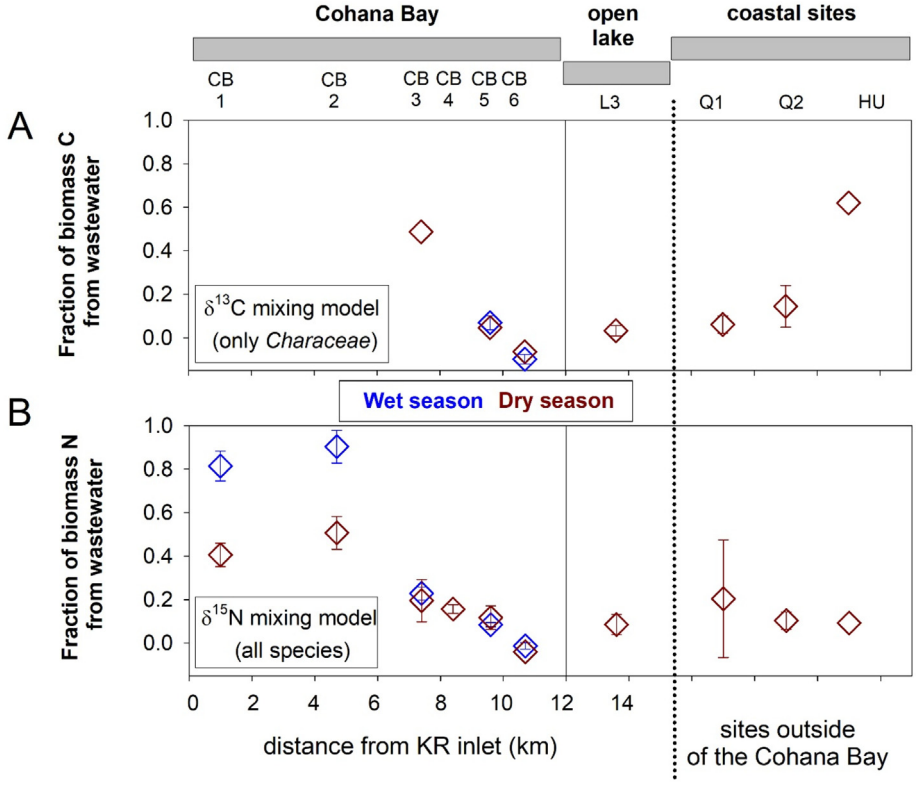

Fig. 7. δ^{13}Corg (top) and δ^{15}N (bottom) stable isotope mixing model of macrophytes at Cohana Bay, the open lake and coastal sites (Q1 and Q2 = Bay of Quehuaya, HU = Huatajata). Colored diamonds refer to wet (blue) and dry (red) season. Error bars represent confidence intervals for data at each site. The three comparative sampling zones are indicated on the top of the figure with gray bands.

catchment (Flores Avilés et al., 2022). The atmospheric endmember ($\delta^{15}N_{atmos}$) was taken from the average nitrogen biological fixation (NBF = −3 ‰) reference value (Zhang et al., 2014).

The fraction of Characeae biomass C contribution from wastewater to plants are represented in Fig. 7. Although the ^{13}C mixing model could not be applied within the first 5 km of the bay because of the absence of Characeae in this area, the model suggests that the wastewater contribution is still visible between 7 and 8 km, and in the coastal site of HU which also receives wastewater. In contrast, the anthropogenic contribution appears negligible after 8 km from the KR outlet as well as in the rural coastal sites of Q1 and Q2 (Fig. 7A). It must be considered that this model is imperfect as it doesn't take into account biological productivity and respiration, which could induce important changes in DIC carbon isotope ratios depending on the different levels of metabolism along the slopes of the lake.

The fractional contribution of biomass N from wastewater nitrogen to plants highlights a gradual decrease after the first 5 km from the shore, where the wastewater always exceeds 40 % to more distant areas where they drop to around 10 %, even at HU. The most striking feature illustrated by the model is the sharp uptake of wastewater N during the wet season which reaches up to 80 % within the first 5 km of the bay, whereas it stands between 40 and 50 % during the dry season (Fig. 7B).

4. Conclusions and perspectives

The study of $\delta^{13}C$ and $\delta^{15}N$ signatures within various baseline compartments of Lake Titicaca show the different trophic status of the lake with areas greatly impacted by anthropogenic discharges that have low $\delta^{13}C$ and high $\delta^{15}N$ signatures whereas pristine areas have high $\delta^{13}C$ and low $\delta^{15}N$ signatures. The gradual change in both $\delta^{13}C$ and $\delta^{15}N$ signatures along the Cohana Bay transect are thus essentially driven by the change of anthropogenic and background/biogeochemical natural sources. This change greatly illustrates the assimilation of anthropogenically derived OM in this ecosystem, mostly attributed to the strong fixation of nutrients by endemic macrophytes and their periphyton. The combined use of $\delta^{13}C$ and $\delta^{15}N$ brings complementary information, with $\delta^{13}C$ reporting about the C sources and recycling in the ecosystem, whereas $\delta^{15}N$ provides information about the N sources and ecological productivity.

SPM and macrophytes (except for the $\delta^{13}C$ of totoras) are the most suitable compartments for tracking the dissemination of anthropogenic discharges in the lake because their $\delta^{13}C$ and $\delta^{15}N$ compositions accurately reflects the trophic status of the water column. The $\delta^{15}N$ signature of the periphyton is also a suitable indicator of wastewater inputs, but their $\delta^{13}C$ signature shows limitations due to its closeness to the $\delta^{13}C$ values of the hosting macrophyte. As a large-time integrator, the sediment may also be a suitable indicator of trophic changes in the lake.

Hence both $\delta^{13}C$ and $\delta^{15}N$ signature in macrophytes and SPM, together with punctual physico-chemical measurements indicate that anthropogenically induced eutrophication is marked within the five first kilometers to the Katari river mouth, followed by a rapid attenuation or auto-epuration within the next 2 to 4 km resulting from the assimilation of discharged nutrients.

The results presented here bring new insights that are of great interest for pollution diagnostic studies and remediation strategies. For instance, filtering artificial wetlands that take advantage of the periphyton capabilities as a trap of organic matter, nutrients and heavy metals can be a much-needed alternative for preserving such a fragile ecosystem in front of the growing human pressure.

CRediT authorship contribution statement

Carlos Heredia (CH): Formal analysis, investigation, data curation, software, visualization, validation, writing – original draft.

Stéphane Guédron (SG): Conceptualization, methodology, supervision, formal analysis, investigation, resources, software, validation, data curation, visualization, writing – original draft.

David Point (DP): Conceptualization, methodology, funding acquisition, supervision, formal analysis, investigation, resources, writing – review & editing.

Vincent, Perrot (VP): Formal analysis, investigation, data curation, validation, writing – review & editing.

Sylvain Campillo (SC) and **Claire Verin (CV)**: Investigation, data curation, resources.

María Elena Espinoza (MES) and **Pablo Fernandez (PF)**: Investigation.

Celine Duwig (CD): Investigation, resources, writing – review & editing.

Darío Achá (DA): Project administration, conceptualization, methodology, funding acquisition, supervision, formal analysis, investigation, resources, validation, writing – review & editing.

Declaration of competing interest

The authors declare that they have no known competing financial interests or personal relationships that could have appeared to influence the work reported in this paper.

Acknowledgments

This work is a contribution to the EUTITICACA project (founded by the Impuestos Directos a los Hidrocarburos IDH administrated by the Universidad Mayor de San Andr_es, PI: D. Acha: darioacha@yahoo.ca), COMIBOL project (INSU CNRS/IRD EC2CO Program, PI: D. Point: david.point@ird.fr) and LA PACHAMAMA project (ANR CESA program, No ANR-13-CESA-0015-01, PI: D. Amouroux: david.amouroux@univ-pau.fr).

We wish to thank, J. Gardon, A. Terrazas, C. Gonzalez, N. Clavijo, L. Salvatierra, R. Rios, J.C. Salinas, A. Castillo, M. Claure, J. Tapia, J.L. Duprey (IRD Bolivia), la Familia Catari (Don Ramon, Don Maximo, Don Eric, Don Ruben and Donia Maria) and Don German Calizaya (Fishermen Association, Machacamarca, Bolivia) for their help and assistance during the field campaigns.

References

Achá, D., Guédron, S., Amouroux, D., Point, D., Lazzaro, X., Fernandez, P.E., et al., 2018. Algal bloom exacerbates hydrogen sulfide and methylmercury contamination in the emblematic high-altitude Lake Titicaca. Geosciences 8, 438.

Aguilera, J., Motavalli, P., Gonzales, M., Valdivia, C., 2013. Response of a potato-based cropping system to conventional and alternative fertilizers in the Andean highlands. Int. J. Plant Soil Sci. 3, 139–162.

Aitkenhead-Peterson, J.A., Steele, M.K., Nahar, N., Santhy, K., 2009. Dissolved organic carbon and nitrogen in urban and rural watersheds of south-central Texas: land use and land management influences. Biogeochemistry 96, 119–129.

Alanoca, L., Guedron, S., Amouroux, D., Audry, S., Monperrus, M., Tessier, E., et al., 2016. Synergistic effects of mining and urban effluents on the level and distribution of methylmercury in a shallow aquatic ecosystem of the Bolivian altiplano. Environ. Sci. Process. Impacts 18, 1550–1560.

Archundia, D., Duwig, C., Spadini, L., Uzu, G., Guedron, S., Morel, M.C., et al., 2017a. How uncontrolled urban expansion increases the contamination of the Titicaca Lake Basin (El alto, La Paz, Bolivia). Water Air Soil Pollut. 228, 1–17.

Archundia, D., Duwig, C., Lehembre, F., Chiron, S., Morel, M.C., Prado, B., et al., 2017b. Antibiotic pollution in the katari subcatchment of the Titicaca Lake: major transformation products and occurrence of resistance genes. Sci. Total Environ. 576, 671–682.

Backer, L.C., McGillicuddy Jr., D.J., 2006. Harmful algal blooms at the Interface between coastal oceanography and human health. Oceanography 19, 94–106.

Bade, D.L., Carpenter, S.R., Cole, J.J., Hanson, P., Hesslein, R.H., 2004. Controls of d13C-DIC in lakes: geochemistry, lake metabolism, and morphometry. Limnol. Oceanogr. 49, 1160–1172.

Balslev-Chausen, D., Dahl, T.W., Saad, N., Rosing, M.T., 2013. Precise and accurate δ13C analysis of rock samples using flash combustion-cavity ring down laser spectroscopy. J. Anal. At. Spectrom. 28, 516–523.

Banks, D., Markland, H., Smith, P.V., Mendez, C., Rodriguez, J., Huerta, A., et al., 2004. Distribution, salinity and pH dependence of elements in surface waters of the catchment areas of the Salars of Coipasa and Uyuni, Bolivian Altiplano. J. Geochem. Explor. 84, 141–166.

Cecchetti, A.R., Sytsma, A., Stiegler, A.N., Dawson, T.E., Sedlak, D.L., 2020. Use of stable nitrogen isotopes to track plant uptake of nitrogen in a nature-based treatment system. Water Res. X 9.

Chappuis, E., Seriñá, V., Martí, E., Ballesteros, E., Gacia, E., 2017. Decrypting stable-isotope (δ13C and δ15N) variability in aquatic plants. Freshw. Biol. 62, 1807–1818.

Chudnoff, S.M., 2009. A Water Quality Assessment of the Rio Katari River and its Principle Tributaries, Bolivia. Earth and Environmental Science. Master in Water Resources. The University of New Mexico, Albuquerque, New Mexico, p. 143.
Cole, M.L., Kroeger, K.D., Mcclelland, J.W., Valiela, I., 2006. Effects of watershed land use on nitrogen concentrations and δ15 nitrogen in groundwater. Biogeochemistry 77, 199–215.
Collot, D., Koriyama, F., García, E., 1983. Répartitions, biomasses et productions des macrophytes du lac Titicaca. Revue D'hydrobiologie Tropicale 16, 241–261.
Cossa, D., Mucci, A., Guédron, S., Coquery, M., Radakovitch, O., Escoube, R., et al., 2021. Mercury accumulation in the sediment of the Western Mediterranean abyssal plain: a reliable archive of the late holocene. Geochim. Cosmochim. Acta 309, 1–15.
Costanzo, S.D., O'Donohue, M.J., Dennison, W.C., Loneragan, N.R., Thomas, M., 2001. A new approach for detecting and mapping sewage impacts. Mar. Pollut. Bull. 42, 149–156.
Dawson, T.E., Mambelli, S., Plamboeck, A.H., Templer, P.H., Tu, K.P., 2002. Stable isotopes in plant ecology. Annu. Rev. Ecol. Syst. 33, 507–559.
Dawson, T.E., Siegwolf, R.T., 2007. Using stable isotopes as indicators, tracers, and recorders of ecological change: some context and background. Terrestrial Ecol. 1, 1–18.
De Kluijver, A., Ning, J., Liu, Z., Jeppesen, E., Gulati, R., Middelburg, J., 2015. Macrophytes and periphyton carbon subsidies to bacterioplankton and zooplankton in a shallow eutrophic lake in tropical China. Limnol. Oceanogr. 60, 375–385.
Dejoux, C., Iltis, A., 1991. Lake Titicaca: A synthesis of limnological knowledge. Monographie Biologicae. 68. Kluvier Academic Publisher, Dordrecht, p. 560.
Diaz, R.J., 2001. Overview of hypoxia around the world. J. Environ. Qual. 30, 275–281.
Dodds, W.K., Bouska, W.W., Eitzmann, J.L., Pilger, T.J., Pitts, K.L., Riley, A.J., et al., 2009. Eutrophication of U.S. freshwaters: analysis of potential economic damages. Environ. Sci. Technol. 43, 12–19.
Duwig, C., Archundia, D., Lehembre, F., Spadini, L., Morel, M.C., Uzu, G., et al., 2014. Impacts of anthropogenic activities on the contamination of a sub watershed of Lake Titicaca. Are antibiotics a concern in the Bolivian Altiplano? Procedia Earth Planet. Sci. 10, 370–375.
Finlay, J.C., Kendall, C., 2007. Stable isotope tracing of temporal and spatial variability in organic matter sources to freshwater ecosystems. In: Michener, R., Lajtha, K. (Eds.), Stable Isotopes in Ecology and Environmental Science. Blackwell Publishing, pp. 283–333.
Flores Avilés, G.P., Spadini, L., Sacchi, E., Rossier, Y., Savarino, J., Ramos, O.E., et al., 2022. Hydrogeochemical and nitrate isotopic evolution of a semiarid mountainous basin aquifer of glacial-fluvial and paleolacustrine origin (Lake Titicaca, Bolivia): the effects of natural processes and anthropogenic activities. Hydrogeol. J. 30, 181–201.
Fry, B., 2006. Stable Isotope EcologyVol 521. Springer, New York, NY.
Gearing, P.J., Gearing, J.N., Maughan, J.T., Oviatt, C.A., 1991. Isotopic distribution of carbon from sewage sludge and eutrophication in the sediments and food web of estuarine ecosystems. Environ. Sci. Technol. 25, 295–301.
Glibert, P.M., Middelburg, J.J., McClellan, J.W., Vander Zanden, M.J., 2018. Stable isotope tracers: enriching our perspectives and questions on sources, fates, rates, and pathways of major elements in aquatic systems. Limnol. Oceanogr. 64, 950–981.
Gu, B., Chapman, A.D., Schelske, C.L., 2006. Factors controlling seasonal variations in stable isotope composition of particulate organic matter in a softwater eutrophic lake. Limnol. Oceanogr. 51, 2837–2848.
Guedron, S., Audry, S., Achá, D., Bouchet, S., Point, D., Condom, T., et al., 2020. Diagenetic production, accumulation and sediment-water exchanges of methylmercury in contrasted sediment facies of Lake Titicaca (Bolivia). Sci. Total Environ. 723, 1–14.
Guedron, S., Tolu, J., Delaere, C., Sabatier, P., Barre, J., Heredia, C., et al., 2021. Reconstructing two millennia of copper and silver metallurgy in the Lake Titicaca region (Bolivia/Peru) using trace metals and lead isotopic composition. Anthropocene 34, 100288.
Guédron, S., Point, D., Acha, D., Bouchet, S., Baya, P.A., Molina, C.I., et al., 2017. Mercury contamination level and speciation inventory in the hydrosystem of Lake Titicaca: current status and future trends. Environ. Pollut. 231, 262–270.
Guédron, S., Ledru, M.P., Escobar-Torrez, K., Develle, A.L., Brisset, E., 2018. Enhanced mercury deposition by amazonian orographic precipitation: evidence from high-elevation Holocene records of the Lake Titicaca region (Bolivia). Palaeogeogr. Palaeoclimatol. Palaeoecol. 511, 577–587.
Guédron, S., Achá, D., Bouchet, S., Point, D., Tessier, E., Heredia, C., et al., 2020. Accumulation of methylmercury in the high-altitude Lake Uru Uru (3686 m asl, Bolivia) controlled by sediment efflux and photodegradation. Appl. Sci. 10, 7936.
Handley, L.L., Raven, J.A., 1992. The use of natural abundance of nitrogen isotopes in plant physiology and ecology. PlantCell Environ. 15, 965–985.
Holtgrieve, G.W., Schindler, D.E., Hobbs, W.O., Leavitt, P.R., Ward, E.J., Bunting, L., et al., 2011. A coherent signature of anthropogenic nitrogen deposition to remote watersheds of the northern hemisphere. Science 334, 1545–1548.
Kendall, C., Elliott, E.M., Wankel, S.D., 2007. Tracing Anthropogenic Inputs of Nitrogen to Ecosystems. Stable Isotopes in Ecology and Environmental Science, pp. 375–449.
Kendall, C., Elliott, E.M., Wankel, S.D., 2008. Tracing anthropogenic inputs of nitrogen to ecosystems. Stable Isotopes in Ecology and Environmental Science. Blackwell Publishing Ltd, pp. 375–449.
Kortelainen, P., 1999. Acidity and buffer capacity. In: Keskitalo, J., Eloranta, P. (Eds.), Limnology of Humic Waters. Backhuys, Leiden, pp. 95–115.
Lanza, W.G., Achá, D., Point, D., Masbou, J., Alanoca, L., Amouroux, D., et al., 2017. Association of a Specific Algal Group with methylmercury accumulation in periphyton of a tropical high-altitude andean Lake. Arch. Environ. Contam. Toxicol. 72, 1–10.
Le Moal, M., Gascuel-Odoux, C., Menesguen, A., Souchon, Y., Ettrillard, C., Levain, A., et al., 2018. Eutrophication: a new wine in and old bottle? Sci. Total Environ. 1–11.
Lindell, M.J., Granéli, W., Tranvik, L.J., 1995. Enhanced bacterial growth in response to photochemical transformation of dissolved organic matter. Limnol. Oceanogr. 40, 195–199.
Liu, B., Yan, H., Wang, C., Li, Q., Guédron, S., Spangenberg, J.E., et al., 2012. Insights into low fish mercury bioaccumulation in a mercury-contaminated reservoir, Guizhou, China. Environ. Pollut. 160, 109–117.
Lowe, R.L., 1996. Periphyton patterns in lakes. In: Stevenson, R.J., Bothwell, M.L., Lowe, R.L. (Eds.), Algal Ecology Freshwater Benthic Ecosystems. Academic Press, San Diego, p. 781.
Mariotti, A., Landreau, A., Simon, B., 1988. 15N isotope biogeochemistry and natural denitrification process in groundwater: application to the chalk aquifer of northern France. Geochim. Cosmochim. Acta 52, 1869–1878.
Martınez Gonzales, I., Roncal, R.Z., Miranda, A.P., Gotilla, J.S., 2004. Co-operation on the Lake Titicaca. UNESCO-IHP, Paris, France.
Mazurek, H., 2012. El censo en Bolivia, una herramienta de desarrollo. T'inkasos 15.
McClelland, J.W., Valiela, I., Michener, R.H., 1997. Nitrogen-stable isotope signatures in estuarine food webs: a record of increasing urbanization in coastal watersheds. Limnol. Oceanogr. 42, 930–937.
Michener, R., Lajtha, K., 2008. Stable Isotopes in Ecology and Environmental Science. John Wiley & Sons.
Middelburg, J.J., 2014. Stable isotopes dissect aquatic food webs from the top to the bottom. Biogeosciences 11, 2357–2371.
Miller, M., Capriles, J., Hastorf, C.A., 2010. The fish of Lake Titicaca: implications for archaeology and changing ecology through stable isotope analysis. J. Archaeol. Sci. 37, 317–327.
Molina, J., Satge, F., Pillco, R., 2014. Los recursos hidricos del TDPS. In: Puilly, M., Lazzaro, X., Point, D., Aguirre, M. (Eds.), Linea Base de Conocimientos Sobre los Recursos Hidrologicos en el Sistema TDPS Con Enfoque en la Cuenca del Lago Titicaca. IRD-UICN, Quito, Ecuador.
Northcote, T.G., 1992. Contamination. In: Dejoux, C., Iltis, A. (Eds.), Lake Titicaca: A Synthesis of Limnological Knowledge. Springer, Netherlands, Dordrecht, pp. 551–561.
Paerl, H.W., Otten, T.G., 2013. Harmful cyanobacterial blooms: causes, consequences, and controls. Microb. Ecol. 65, 995–1010.
Paul, D., Skrzypek, G., Fórizs, I., 2007. Normalization of measured stable isotopic compositions to isotope reference scales – a review. Rapid Commun. Mass Spectrom. 21, 3006–3014.
Pretty, J.N., Mason, C.F., Nedwell, D.B., Hine, R.E., Leaf, S., Dils, R., 2003. Environmental costs of freshwater eutrophication in England and Wales. Environ. Sci. Technol. 37, 201–208.
Quiroga-Flores, R., Guédron, S., Acha, D., 2021. High methylmercury uptake by green algae in Lake Titicaca: potential implications for remediation. Ecotoxicol. Environ. Saf. 207, 111256.
Ramos Ramos, O., Rotting, T.S., French, M., Sracek, O., Bundschuh, J., Quintanilla, J., et al., 2014. Geochemical processes controlling mobilization of arsenic and trace elements in shallow aquifers and surface waters in the Antequera and Poopó mining regions, Bolivian altiplano. J. Hydrol. 518, 421–433.
Richerson, P.J., Neale, P.J., Wurstbaugh, W., Alfaro, R., Vincent, W.F., 1986. Patterns of temporal variation in primary production and other limnological variables in Lake Titicaca, a high-altutude torpical lake. Hydrobiologia 138, 205–220.
Roche, M.A., Bourges, J., Cortes, J., Mattos, R., 1992. IV.1. Climatology and hydrology of the Lake Titicaca basin. In: Dejoux, C., Iltis, A. (Eds.), Lake Titicaca - A Synthesis of Limnological Knowledge. 68. Kluwer Academic Publishers, Dordrecht/Boston/London, pp. 63–88.
Rosenmeier, M.F., Brenner, M., Kenney, W.F., Whitmore, T.J., Taylor, C.M., 2004. Recent eutrophication in the Southern Basin of Lake Petén Itzá, Guatemala: human impact on a large tropical Lake. Hydrobiologia 511, 161–172.
Rowe, H.D., Dunbar, R.B., Mucciarone, D.A., Seltzer, G.O., Baker, P.A., Fritz, S.C., 2002. Insolation, moisture balance and climate change on the South American Altiplano since the last glacial maximum. Clim. Chang. 52, 175–199.
Sarret, G., Guédron, S., Acha, D., Bureau, S., Arnaud-Godet, F., Tisserand, D., et al., 2019. Extreme arsenic bioaccumulation factor variability in Lake Titicaca, Bolivia. Sci. Reports 9, 10626.
Savage, C., 2005. Tracing the influence of sewage nitrogen in a coastal ecosystem using stable nitrogen isotopes. Ambio 34, 145–150.
Schindler, D.E., Carpenter, S.R., Cole, J.J., Kitchell, J.F., Pace, M.L., 1997. Influence of food web structure on carbon exchange between lakes and the atmosphere. Science 277, 248–251.
Schindler, D.W., 2006. Recent advances in the understanding and management of eutrophication. Limnol. Oceanogr. 51, 356–363.
Sebilo, M., Billen, G., Grably, M., Mariotti, A., 2003. Isotopic composition of nitrate-nitrogen as a marker of riparian and benthic denitrification at the scale of the whole Seine River system. Biogeochemistry 63, 35–51.
Segura, H., Junquas, C., Espinoza, J.C., Vuille, M., Jauregui, Y.R., Rabatel, A., et al., 2019. New insights into the rainfall variability in the tropical Andes on seasonal and interannual time scales. Clim. Dyn. 1, 1–22.
SENAMHI, 2021. Reporte Semanal Lago Titicaca Abril.
SENAMHI, B., 2020. Servicio Nacional de Meteorología de Hidrología. La Paz, Bolivia. http://www.senamhi.gob.bo.
Smith, R.S., King, K.W., Williams, M.R., 2015. What is causing the harmful algal blooms in Lake Erie? J. Soil Water Conserv. 70, 27–29.
Smith, V.H., 2003. Eutrophication of freshwater and coastal marine ecosystems a global problem. Environ. Sci. Pollut. Res. 10, 126–139.
Smith, V.H., Joye, S.B., Howarth, R.W., 2006. Eutrophication of freshwater and marine ecosystems. Limnol. Oceanogr. 51, 351–355.
Stanley, E.H., Powers, S.M., Lottig, N.R., Buffam, I., Crawford, J.T., 2012. Contemporary changes in dissolved organic carbon (DOC) in human dominated rivers: is there a role for DOC management? Freshw. Biol. 57, 26–42.
Thevenon, F., Adatte, T., Spangenberg, J.E., Anselmetti, F.S., 2012. Elemental (C/N ratios) and isotopic (d15Norg, d13Corg) compositions of sedimentary organic matter from a high-altitude mountain lake (Meidsee, 2661 m asl, Switzerland): implications for Lateglacial and Holocene alpine landscape evolution. The Holocene 22, 1135–1142.

Vahtera, E., Conley, D.J., Gustafsson, B.G., Kuosa, H., Pitkänen, H., Savchuk, O.P., et al., 2007. Internal ecosystem feedback enhance nitrogen-fixing cyanobacteria blooms and complicate Management in the Baltic SeaA. Ambio 36, 186–194.

Vander Zanden, M.J., Rasmussen, J.B., 1999. Primary consumer δ 13 C and δ 15 N and the trophic position of aquatic consumers. Ecology 1395–1404.

Vermeulen, S., Sturaro, N., Gobert, S., Bouquegneau, J.M., Lepoint, G., 2011. Potential early indicators of anthropogenically derived nutrients: a multiscale stable isotope analysis. Mar. Ecol. Prog. Ser. 422, 9–22.

Villafae, V.E., Andrade, M., Lairana, V., Zaratti, F., Helbling, E.W., 1999. Inhibition of phytoplankton photosynthesis by solar ultraviolet radiation: studies in Lake Titicaca, Bolivia. Freshw. Biol. 42, 215–224.

Zhang, X., Sigman, D.M., Morel, F.M.M., Kraepiel, A.M.L., 2014. Nitrogen isotope fractionation by alternative nitrogenases and past ocean anoxia. Proc. Natl. Acad. Sci. U. S. A. 111, 4782–4787.